Recycling of high temperature solid oxide electrolyzers or fuel cells and recovery of waste materials

Gudaysew Tsegaye Yenesew

DOCTORAT MATIERE BRETAGNE MOLECULES LOIRE ET MATERIAUX

Nantes Université

Thèse de doctorat de

NANTES UNIVERSITE

Ecole Doctorale n° 596
Matière, Molécules, Matériaux
Spécialité : *Science des Matériaux*

Par

« Gudaysew Tsegaye YENESEW»

«Recycling of high temperature solid oxide electrolyzers or fuel cells and recovery of waste materials»

Thèse présentée et soutenue à Nantes, le 16 décembre 2022
Unité de recherche : CNRS UMR 6502, Institut des Matériaux de Nantes Jean Rouxel (IMN)

Rapporteurs avant soutenance :

Jean-Marc BASSAT	Directeur de Recherche CNRS, ICMCB, Bordeaux
Armelle RINGUEDE	Directrice de recherche CNRS, IRCP, Paris

Composition du Jury :

Examinateurs :	Florent BOUCHER	Directeur de Recherche CNRS, IMN, Nantes
	Aurélie ROLLE	Maître de Conférences, Centrale Lille
	Olivier JOUBERT	Professeur, Nantes Université, IMN, Nantes
	Annie LE GAL LA SALLE	Chercheur CNRS HDR, IMN, Nantes
Invité(s)		
	Yves BOUSSANT-ROUX	Ingénieur PhD SAINT-GOBAIN, Cavaillon
	Raphaël IHRINGER	Ingénieur PhD Fiaxell,Lausanne, Suisse
	Eric QUAREZ	Chargé de Recherche CNRS, IMN, Nantes

Acknowledgement

This work was funded by the CNRS under the 80|Prime program and carried out at the Institut des Matériaux de Nantes Jean Rouxel (IMN). I would like to express my gratitude to the CNRS, and Nantes University, especially to the management of the IMN under Florent Boucher and to the leader of the ST2E team, Olivier Joubert for their warm reception and host.

I would like to express my sincere gratitude to all the jury members for agreeing to be part of my thesis jury and for making great efforts to come in person to IMN for my presentation. I would like to give special thanks to my two rapporteurs Jean-Marc BASSAT, Research Director at CNRS, ICMCB, Bordeaux, and Armelle RINGUEDE, Research Director at CNRS, IRCP, Paris, for taking their time to carefully read and assess the quality of my manuscript and for their pertinent remarks. I would also like to thank Florent Boucher, Aurélie ROLLE, Yves BOUSSANT-ROUX and Raphaël Ihringer for their effort to read my manuscripts and their genuine remarks.

I feel that my words are insufficient to my expressions about my respectable and worthy supervisor Professor Olivier Joubert, for his keen interest, exemplary guidance, monitoring and constant encouragement from the beginning to the end of this study. The courage, help and guidance he has given me from time to time shall carry me a long way in the path I am about to embark.

I would like to express my heartfelt gratitude and commitment to my outstanding co-supervisor, Dr. Annie Le Gal La Salle, for her kind behavior, unconditional love and smile, valuable suggestions and technical guidance to which this research has found its way to a successful conclusion. I would not like to miss your dedication and patience, especially in writing of this thesis. You worked on your holiday and at night. I will not forget to say thanks again.

I have no words to express my profound sense of gratitude and innumerable thanks to Eric Quarez for his contribution as my thesis jury member and for his scientific collaboration that made this work even more brilliant. Eric, I admire your willingness to share all your knowledge and let us benefit from your inventiveness. Your kindness and pedagogy encouraged me to ask

you for help in any question. You always knew how to remain positive and had the right words to encourage me.

I was fortunate to be accompanied by excellent and harmonizing person Nicollet Clement. Your good understanding provided me with a perfect scientific and relational framework and I am truly grateful. I thank you, Clement, for your inexhaustible dynamism, your numerous advices and your scrupulous eye in proofreading. You always made yourself available when I needed help.

I would like to acknowledge Rose-Noelle VANNIER and Gilles Taillades, who were members of my CSI (Individual Ph.D. Committee). They follow up my progress and give their comments every year.

I would also like to thank Thierry Brousse and Olivier CROSNIER, who warmly welcomed me for my internship at Polytech. It was a real pleasure to work with you. As technical supervisors, you gave me your trust and at the same time were very attentive to my progress.

My special thanks go to my colleague Nassima Kana for her continuous encouragement to work hard and have always been a precious help with all administrative and organizational problems. I will extend my special thanks to Amina MERABET. Amina you are a unique person who deserves to be known! Your strong character, caring and incredible kindness make you an unavoidable ally. I sincerely believe that every PhD student would need a person like you during their thesis.

My sincere thanks to my colleagues at IMN for the good atmosphere in the laboratory. I would like to thank Alexandre, Nusik, Insaf, Boluwatife, Lozane, Valentin, Amal, Louis, Mickel, Alia, Simon, Mohammed, Pablo, Morgan, Camille, Etienne, Lou, Chloé, Jianhan, Julio, Yao, Lucas... and many others.

I have great respect for the people who crossed my path during my education and thank them for helping me in their own way to grow and deepen my reflections to be the best version of myself. I extend my special respect to all my teachers at the different levels of academic. Dear my teachers, I truly appreciate your efforts to nourish wisdom, courage and love. I would like to

mention two teachers who had the greatest part in turning my life around: Mr. Bizualem Getaneh and Dr. Kalid Ahmed.

My genuine appreciation and thanks also goes to my husband Lealem Beza. This adventure would not have been possible without your support. You gave me the ideal freedom and autonomy that I desired. You did not hesitate to send me to other continents to continue my studies. Thank you so much for your coaching and constant support. Dear Lealem, you are my life mentor!

Finally, I would like to thank my parents and relatives from the bottom of my heart for their love, patience, dedication and constant support during my study period.

Abbreviations and symbols

ADP: Abiotic Depletion Potential

AFC: Alkaline fuel cell

AP: Acidification potential

APU: Auxiliary power unit

BET: Brunauer-Emmett-Teller surface area analysis

BSE: Backscattered electron

CBA: Cost-benefit analysis

CFC: Chlorofluorocarbon

CHP: Combined heat and power

CTUe: Comparative toxic units (ecotoxicity potential)

CTUh: Comparative Toxic Unit for human

DOE: Department of Energy

DMG: Dimethylglyoxime

EDS: Energy dispersive X-ray spectroscopy

EF: Environmental Footprint

EF: Environmental impact categories of the

EIS: Electrochemical Impedance Spectroscopy

EO: Electric-only

EOL: End-of-life

EP: Eutrophication potential

EPf.w.: Eutrophication, freshwater

EPmarine: Eutrophication, marine

EPR: Extended producer responsibility

ETf.w.: Ecotoxicity, freshwater

EU: European Union

FD: fossil depletion

GDC: Gadolinia doped ceria

GWP: Global warming potentials

HTPcancer: Human toxicity, cancer

IAEA: International atomic energy agency

ICP-MS: Inductively Coupled Plasma Mass Spectrometry

ICSD: Inorganic crystal structure database

IPP: Integrated Product Policy

ISO: International Organization for Standardization

ISO: International Standards Organization

IUPAC: International union of pure applied chemistry

kBq U-235 eq kilobecquerel

LCA: Life cycle assessment

LCA: Life cycle assessment

LCIA: impact assessment results

List of abbreviations

LSC: Strontium-doped Lanthanum cobaltite

LSM: Strontium-doped Lanthanum Manganite

MCFC: Molten carbonate fuel cell

NMVOC: Non-methane volatile organic compounds

ODP: Ozone Depletion Potential

ODP: Ozone depletion potential

PAFC: Phosphoric acid fuel cell

PED: Primary energy demand

PEMFC: Proton exchange membrane fuel Cell

PM: Particulate matter

POCP: Photochemical ozone creation potential

POCP: Photochemical ozone Formation

PSD: Particle size distribution

REE: Rare earth element

SE: Secondary electron

SEM: Scanning electron microscope

SOFC: Solid oxide electrolyzer cell

SOFC: Solid oxide fuel cell

TGA: Thermogravimetric analysis

WEEE: Waste electrical and electronic equipment

XRD: X-ray diffraction

YSZ: Yttria-stabilized zirconia

Contents

List of figures

List of tables

Résumé de Thèse

L'évolution de la société et le développement économique rapide de nombreux pays ont conduit à une utilisation excessive et accélérée des combustibles fossiles carbonés (pétrole, gaz naturel et charbon) au cours du siècle dernier, provoquant une crise énergétique mondiale. Actuellement, ces combustibles représentent plus de 80 % de la production mondiale d'énergie. Cependant, ces ressources sont limitées, non renouvelables et situées dans des pays à risque. Par conséquent, l'ère du pétrole bon marché touche à sa fin en raison de nombreux facteurs tels que la rareté et les problèmes géopolitiques.

De plus, l'exploitation et l'utilisation des combustibles fossiles entraînent une augmentation significative de la production de gaz à effet de serre et du réchauffement climatique, surtout depuis les années 1990. Plus récemment, la crise énergétique mondiale croissante et les préoccupations liées au changement climatique ont conduit à un changement de paradigme sociétal et économique. Par exemple, l'Accord de Paris sur le changement climatique (12 décembre 2015) appelle à limiter le réchauffement climatique en dessous de 2°C, de préférence à 1,5°C, et à réduire fortement les émissions de gaz à effet de serre (d'au moins 55 % d'ici à 2030 pour l'UE).

Par conséquent, le passage à des sources d'énergie renouvelables (notamment le solaire, l'éolien, l'hydraulique, la géothermie et la biomasse) semble être la seule alternative viable à long terme pour réduire le fardeau des combustibles fossiles et les impacts environnementaux. Bien que ces technologies de production renouvelable ne représentent encore qu'une part limitée du mix électrique mondial, leur part sur certains marchés de l'électricité sera importante dans les décennies à venir. Par exemple, selon la revue "Statistical Review of World Energy" (2022), la part des énergies renouvelables passera de 20 % en 2010 à 29 % en 2020, et l'agence américaine Bloomberg rapporte que la part des énergies renouvelables atteindra 62 % en 2050.

Toutefois, l'électricité décarbonée produite à partir de ces sources renouvelables présente l'inconvénient de n'être disponible que de manière intermittente et dans des endroits spécifiques. Elle doit être stockée pour être disponible en cas de besoin. Parmi les différents moyens de stocker cette électricité, le dihydrogène H_2 pourrait devenir un vecteur énergétique majeur. Cette petite molécule a une densité énergétique massique élevée et est transportable, stockable et peut

fournir une énergie propre par combustion ou par transformation en électricité via une pile à combustible. Produit à partir d'eau en utilisant de l'électricité décarbonée, ce vecteur d'énergie chimique jouera un rôle important dans la décarbonation des transports (principalement les véhicules lourds), des habitations et des bâtiments. Il permettra également de décarboner l'industrie en remplaçant l'hydrogène, issu de la transformation chimique de combustible carboné (gaz naturel ou charbon), utilisé comme matière première chimique. Compte tenu du large déploiement de l'hydrogène décarboné, une production massive d'électrolyseurs est nécessaire dans un avenir proche. Par exemple, 40 MW d'électrolyseurs sont déjà installés en France en 2021, tandis que 6,5 GW sont attendus en 2030.

L'hydrogène peut être à nouveau transformé en électricité, à tout moment et en tout lieu, et sans émission de CO_2, en utilisant des piles à combustible. Là encore, une production massive de piles à combustible est attendue afin de couvrir le déploiement des nouveaux usages de l'hydrogène notamment dans les véhicules lourds électriques (du véhicule utilitaire aux avions). Les électrolyseurs et piles à combustible sont des dispositifs électrochimiques où des réactions électrochimiques se produisent sur des électrodes séparées par un électrolyte conducteur ionique. En mode pile à combustible, un oxydant (par exemple l'oxygène de l'air ambiant) et un combustible (par exemple l'hydrogène) sont fournis séparément sur chaque électrode pour générer des électrons et de l'eau (si H_2 est le combustible), tandis qu'en mode électrolyseur, des électrons et de l'eau sont fournis et l'eau est séparée pour produire de l'hydrogène et de l'oxygène séparément sur les électrodes. Il existe différents types de dispositifs électrochimiques qui se distinguent par la nature de leurs composants et leurs températures de fonctionnement.

Parmi les différents types d'électrolyseurs et de piles à combustible, les électrolyseurs et les piles à combustible à base d'oxydes solides (en anglais Solid Oxide Fuel cell (SOFC) et Solid Oxide Electrolyser (SOEC)), fonctionnant à des températures élevées, sont des systèmes très prometteurs car ils ne nécessitent pas de catalyseurs coûteux comme le platine et présentent des rendements électriques élevés. Des systèmes de petite et grande taille sont déjà présents sur le marché. En France, la fabrication à grande échelle d'électrolyseurs à oxyde solide est déjà en route notamment du coté de Béziers dans la gigafactory Genvia. Cette coentreprise Schlumberger-CEA annonce une production de 300 systèmes SOEC (10kW) d'ici fin 2022 avec un objectif d'assemblage de modules au-delà du mégawatt d'ici 2023. Malgré tout, des

améliorations sont nécessaires, notamment en termes de durée de vie et de coût et de gros projets de recherche sont lancés en parallèle dans le cadre notamment du PEPR hydrogène.

Chaque cellule électrochimique individuelle contient des quantités importantes de matières premières critiques, telles que Ni, Co, La, Gd, Ce, Sr, Zr et Y et la production massive d'électrolyseurs devra relever le défi majeur de la production massive des matières premières. Comme dans tous les secteurs industriels, le recyclage et la réutilisation des déchets de production ou des produits en fin de vie doivent être encouragés. Le recyclage des électrolyseurs et piles à oxyde solide peut également être très intéressant d'un point de vue économique. Par exemple, les minéraux primaires riches en nickel ont une teneur chimique 25 à 40 fois inférieure à celle des déchets des cellules d'oxyde solide. Il est donc possible de dire que l'extraction de Ni à partir des déchets d'oxydes solides est plus économique que l'extraction de Ni à partir des matières premières.

Dans le but de favoriser l'émergence de nouveaux axes de recherche sociétale, le CNRS a lancé en 2019 un programme de thèse intitulé " 80 primes " et l'IMN (axe thématique "Pile à combustible et hydrogène") a pu bénéficier d'une bourse pour répondre à la problématique du recyclage des dispositifs de stockage d'énergie électrique à hydrogène et cela bien avant leur développement économique à grande échelle.

C'est le recyclage des oxydes contenus dans les cellules à oxyde solide (en anglais Solid Oxide Cells ou SOC) qui est l'objectif principal de cette thèse. Plus précisément, ce sont les méthodes de séparation et récupération des composants céramiques des déchets de SOFC ou SOEC et la caractérisation et réutilisation de ces produits récupérés, en tenant compte de la présence éventuelle d'impuretés, qui sont présentées.

Afin de répondre aux exigences économiques et environnementales liées à la criticité des matières premières, des techniques de recyclage et de caractérisation ont été étudiées à l'échelle du laboratoire.

Dans ce travail sont proposées des stratégies efficaces pour recycler les matériaux céramiques constitutifs des SOEC ou SOFC, c'est-à-dire de la cobaltite de lanthane de l'électrode à air (formulation $La_xSr_{1-x}CoO_3$), de l'oxyde de nickel (NiO) qui représente environ 50% du poids de la cellule et de la zircone stabilisée à l'yttrium (YSZ) provenant à la fois de l'électrode à

combustible et de l'électrolyte. Deux processus en plusieurs étapes impliquant le concassage et le broyage, la lixiviation assistée par acide et la précipitation des constituants sont mis en œuvre. Ces deux procédés sont principalement basé sur la très grande différence de stabilité des composés céramiques constituants les cellules SOFC ou SOFC en présence d'acide nitrique : la zircone stabilisée réputée pour sa stabilité chimique et les autres oxydes notamment de nickel facilement solubles. Deux types de cellules commerciales ont été testées, provenant des sociétés Fiaxell et Elcogen.

Deux voies ont été mise en place dans ce processus de recyclage. L'une est la voie "grattage mécanique", nommée ainsi vis-à-vis de la technique de récupération de l'électrode à air utilisée. L'autre voie est la "diméthylglyoxime (DMG)", qui met en avant l'utilisation du DMG comme réactif de complexation et de précipitation. Ces deux stratégies de recyclage étudiées dans la thèse peuvent être résumées comme suit :

Voie "grattage mécanique"

Un simple grattage mécanique a été utilisé pour récupérer les composants des matériaux d'électrode à air sous forme de poudres. Leur composition, déterminée par EDX et ICP-MS, a montré un bon accord avec les valeurs attendues: $La_{0.6}Sr_{0.4}CoO_{3-\delta}$. La phase LSC est pure à 99 %, ce qui correspond à une qualité commerciale. Ce, Gd, Y, Zr, Si et Fe, présents à l'état de traces, proviennent probablement des couches adjacentes de GDC et d'YSZ ou des matières premières utilisées pour synthétiser le composant de l'électrode à air. LSC recyclé peut être utilisé dans la production de nouvelles électrodes à air.

L'électrode à combustible et la couche d'électrolyte restantes sont ensuite réduites sous forme de poudres par broyage (broyeur planétaire pendant 5 heures). Une attaque acide par de l'acide nitrique concentré (65 % en poids) à 75°C pendant 24 heures permet de mettre en solution le nickel mais pas YSZ. Différents acides ont été testés, et l'acide nitrique s'est avéré être le meilleur solvant de lixiviation. Des étapes successives de centrifugation, filtration, lavage et séchage permettent la séparation et la récupération de NiO et d'YSZ.

Les rendements de récupération de NiO et d'YSZ à partir des deux produits commerciaux sont supérieurs à 90 %. Ce rendement pourrait être certainement augmenté par un recyclage à grande échelle.

Les produits de récupération ont été finement caractérisés par microscopie électronique à balayage, diffraction des rayons X, BET et électrochimie.

La pureté du NiO récupéré est supérieure à 99 % avec une faible teneur en Y et Si. Pour les deux produits (Fiaxell et Elcogen), l'oxyde de nickel récupéré montre une bonne surface spécifique par BET (respectivement 8.1 et 13.9 m^2/g) associée à une taille moyenne de particule submicronique. La poudre de NiO récupérée est une nouvelle matière première utilisable notamment pour l'industrie des piles ou des électrolyseurs à oxydes solides sans autre modification.

La diffraction des rayons X sur la poudre d'YSZ récupérée montre, à température ambiante, un mélange des différents polymorphes connus de ce type de composé (monoclinique, quadratique et cubique) en accord avec un faible taux en yttrium. L'étude XRD in situ à haute température montre une transformation successive des phases lors du chauffage et du refroidissement.

La surface spécifique par BET est proche de 4 m^2/g (pour les 2 types de cellules testées) associée à une taille de particule sub-micronique. Ces valeurs sont en accord avec celles attendues pour des poudres d'YSZ commerciales (comme par exemple Tosoh).

La spectroscopie d'impédance électrochimique (SIE) a permis de caractériser la conductivité ionique de YSZ récupéré (analyseur de réponse en fréquence Solartron 1260, gamme de fréquence de 10 MHz à 0,1 Hz, amplitude du signal 50 mV). Tout d'abord, de petites ($\oslash$ < 10mm) pastilles denses (> 95%) ont été obtenues après une étape de frittage à 1450°C pendant 10 heures. Ensuite des cellules symétriques LSM/YSZ/LSM ont été réalisées avec un manganite de lanthane comme électrode. Les diagrammes de Nyquist enregistrés à différentes températures (250°C à 750°C avec un pas de 50°C après un plateau de stabilisation de 30 min) ont été modélisés avec un circuit électrique équivalent composés de résistances et de capacités. Les conductivités de grains et de joints de grains ont pu être extraites, discutées notamment en comparaison avec les données de la littérature ou avec des mesures réalisées sur des poudres commerciales de référence.

Les niveaux de conductivité ionique total des composés YSZ récupérés (issu des cellules Fiaxell et Elcogen) sont similaires, de l'ordre de 5 10^{-3} $S.cm^{-1}$ à 700°C. Cependant, la conductivité de joints de grains de YSZ "Fiaxell" est légèrement inférieure à celle de YSZ "Elcogen". Ceci est dû à la présence de traces d'impuretés de silice ($ZrSiO_4$) révélées par EDX et distribuées aux limites des grains. La comparaison du niveau de conductivité et de l'énergie d'activation de YSZ recyclé

avec celle des composés de référence montre une forte proximité avec 3YSZ. Cette évaluation est confirmée par l'analyse EDX de YSZ recyclé : 4YSZ ($Zr_{0,92}Y_{0,08}O_{1,96}$). La composition 4YSZ est attendue puisque 8YSZ et 3YSZ sont utilisés respectivement dans les matériaux d'électrolyte et d'électrode à combustible avec une plus grande teneur en 3YSZ liée à l'épaisseur plus importante de l'électrode à hydrogène (les 2 cellules commerciales sont de type électrode support).

L'analyse des images MEB des surfaces frittées montre une structure dense, cristallisée et bien développée, séparée par des joints de grains visibles. Une taille moyenne de grain de 1,8 µm et 1 µm a été obtenue pour YSZ récupéré respectivement à partir des cellules Elcogen et Fiaxell. Quant à la couche barrière, l'oxyde de cérium dopé au gadolinium (GDC), les 2 cations Gd et Ce ont été détectés en très petites quantités (<1%) dans NiO et YSZ récupérés.

Comme prévu d'après leur composition, la conductivité de YSZ recyclé s'est avérée être supérieure mais proche de celle du 3YSZ commercial. Par conséquent, YSZ recyclé (qui est du 4YSZ) peut être utilisé pour remplacer le 3YSZ dans la fabrication d'une électrode à combustible. D'autres techniques devront être utilisées pour caractériser les propriétés mécaniques de ce matériau.

De nouvelles compositions plus riches en yttrium ont été obtenues à partir de la poudre recyclée 4YSZ mélangée à de l'oxyde d'yttrium commercial et traitée thermiquement. Ainsi des poudres de 6YSZ, 8YSZ et 10YSZ ont été synthétisées et entièrement caractérisées. L'étude électrochimique par EIS montre un ordre attendu de conductivité ionique 8YSZ > 10YSZ > 6YSZ > 4YSZ (tel que récupéré). De cette manière, nous avons montré que le 4YSZ récupéré peut être utilisé comme poudre de base pour produire d'autres compositions utilisées par exemple pour la fabrication d'électrolytes.

Une autre stratégie de recyclage qui utilise du Diméthylglyoxime a également été étudiée au cours de ce travail et les résultats peuvent être résumés comme suit :

Voie DMG (diméthylglyoxime)

Ce procédé est globalement assez proche du précédent mais permet d'éviter l'étape du grattage mécanique. En effet, un grattage mécanique cellule par cellule n'est pas facile à adapter à l'échelle industrielle surtout lorsque les cellules à recycler sont cassées en petits morceaux. Il est plus simple d'utiliser une approche de séparation chimique dès le départ. Ce procédé DMG combine

notamment un broyage des cellules à recycler, une attaque acide et une complexation organique. L'étape initiale consiste à broyer tous les composants céramiques des cellules, y compris l'électrolyte, l'électrode à combustible et les électrodes à air. L'analyse DRX de cette fine poudre noire montre un mélange constitué majoritairement de NiO (47 % en poids) et d'YSZ (51 % en poids) présent sous différentes formes, ainsi que de la phase de type LSC ($La_xSr_{1-x}CoO_3$). Ensuite, l'ensemble de la poudre subit une attaque avec de l'acide nitrique concentré. Le solide récupéré après centrifugation et filtration est de type YSZ. La partie liquide contenant les ions métalliques dissous par l'acide est mélangée avec du Dimethylglyoxime, DMG (de formule $C_2H_8N_2O_2$). Ce solide organique a la propriété de former un complexe stable sélectivement avec le nickel, qui précipite en phase solide. Par centrifugation et filtration, le complexe Ni-DMG et le filtrat ont été séparés.

Les paramètres principaux qui peuvent influencer la complexation sélective du nickel ont été affinés, le pH et la rapport Ni/DMG. La valeur optimale du pH doit se situer dans une gamme qui peut stabiliser le complexe Ni-DMG en évitant la précipitation d'hydroxydes. L'optimum est à pH ~5.5. Du NiO pur a été récupéré après un traitement thermique du complexe Ni-DMG à 500°C pendant 3 heures montrant des particules de type "nanoflakes". Après évaporation du solvant, le composé LSC a été récupéré. Même si des traces d'oxyde de nickel ont été détectées, le niveau de pureté de LSC est de qualité commerciale.

Ces deux procédés ont donc montré la possibilité de séparer aisément les constituants des cellules céramiques SOEC/SOFC. Cette thèse s'est aussi attachée à des aspects environnementaux et économiques. Il est en effet par exemple important de minimiser les quantités de produits nécessaires au recyclage, et même de pouvoir les réutiliser. C'est le cas par exemple de l'acide nitrique et du DMG. La récupération de l'acide HNO_3 est proposée grâce à un mécanisme de distillation. 88.0 % de cet acide initialement utilisé est récupéré. Le DMG peut être recyclé par traitement du complexe à l'acide chlorhydrique.

Afin de déterminer si la stratégie de récupération des matériaux décrite dans cette thèse est économiquement réalisable, une brève analyse coût-bénéfice a été effectuée en utilisant des paramètres de processus optimisés pour un recyclage à l'échelle du laboratoire basé sur 2,5 g de déchets de composants céramiques de cellules à oxyde solide. Cette analyse est réalisée en comparant les coûts estimés du recyclage (énergie électrique, équipements, produits hors coûts

humain) à ceux des produits récupérés. Les 2 voies ("grattage mécanique" et "DMG") ont été comparées. Il s'avère que le grattage mécanique est avantageux en termes de pureté du produit récupéré et de coût de recyclage. Sur la base de cette étude, le résultat montre que le coût de recyclage est environ 50% inférieur au produit recyclé. Cependant, le recyclage à grande échelle pourrait entraîner une forte demande de tri et de grattage manuel donc de temps "homme", ce qui alourdirait la facture globale de ce procédé. En revanche, les méthodes DMG sont avantageuses en termes de rendement et d'adoption à grande échelle du recyclage.

L'impact environnemental du recyclage des cellules céramiques a aussi étudié au cours de la thèse. Les données originales du laboratoire ont été utilisées pour l'inventaire de l'analyse du cycle de vie (ACV). La méthode traduit les émissions et les ressources matérielles et les convertit en indicateurs environnementaux sur la base de facteurs de caractérisation spécifiques. L'analyse du cycle de vie des phases de recyclage présente un niveau élevé d'incertitude. Dans certains cas, les variables n'ont pu être qu'estimées et les valeurs de produits similaires ont dû remplacer les données manquantes, ce qui affecte les résultats.

Si on compare seulement les 2 voies de recyclage, il apparait que le "grattage mécanique" montre un impact 16 fois plus faible (notamment sur les indicateurs tels que l'acidification, le changement climatique, l'écotoxicité, l'eutrophisation et le rayonnement ionisant.) que la voie "DMG". Sur cette base la voie "grattage mécanique" s'avère être le meilleur choix à l'échelle du laboratoire.

Au cours de cette thèse, deux processus en plusieurs étapes impliquant le concassage et le broyage, la lixiviation assistée par acide et la précipitation des constituants ont été mis en avant. Après le recyclage, les matériaux récupérés ont été soigneusement caractérisés en termes de propriétés structurales et morphologiques, de conductivité et de pureté chimique. Les premières analyses économiques montrent que ces procédés de recyclage sont rentables et directement applicables au niveau industriel ce qui pourrait ouvrir de nouvelles perspectives pour l'utilisation de ces matériaux récupérés et dans le retraitement des SOEC/SOFC. Le potentiel environnemental est évalué, soulignant les avantages significatifs du recyclage par rapport à l'utilisation de ressources minérales primaires.

Les efforts déployés pour développer des technologies à faible impact sur l'environnement et à faible coût restent un défi en termes de recyclage à grande échelle. Cette thèse s'est concentrée

sur le cœur des piles ou des électrolyseurs à oxydes solides, l'efficacité du recyclage doit aussi prendre en compte les autres composantes du stack notamment les matériaux d'interconnexion et les joints ainsi que les composantes du système.

General Introduction

The evolution of society and the rapid economic development of various regions have led to the excessive and accelerated use of fossil fuels (oil, gas, and coal) in the last century causing a global energy crisis. Currently, fossil fuels account for more than 80% of the world's energy production. However, these resources are limited and non-renewable. Therefore, the era of cheap oil is coming to an end due to many factors such as scarcity and geopolitical problems.

Moreover, the exploitation and use of fossil fuel leads to a significant increase in the production of greenhouse gases and in global warming, especially since the 1990s. More recently, the growing global energy crisis and concerns about climate change have led to a societal and economic paradigm shift. For example, the Paris Agreement on climate change (December 12, 2015) calls for limiting global warming below 2°C, preferably 1.5°C, and for targeting a net-zero emissions world.

Consequently, switching to renewable energy sources (e.g., solar, wind, hydro, geothermal, and biomass) appears to be the only viable long-term alternative to reduce fossil fuel burdens and environmental impacts. Although these renewable generation technologies still account for a limited share of the global electricity mix, their share in some electricity markets will be significant in the coming decades. For example, according to the Statistical Review of World Energy (2022), the share of renewables will increase from 20% in 2010 to 29% in 2020, and BloombergNEF reports that the share of renewables will increase to 62% by 2050 (Figure 1).

However, electricity from such renewable sources has the disadvantage of being available only intermittently and in specific locations. It must be stored to be available when needed. Among the different ways to store this decarbonized electricity there is hydrogen (H_2). This small molecule has a high energy density relative to its weight and is a clean, safe, transportable and storable. Produced from water using decarbonized electricity, this chemical energy carrier will play an important role in the decarbonization of transportation (mainly heavy vehicles), homes and buildings. It will also use to decarbonized industry by replacing carbonized Hydrogen used as chemical feedstock.

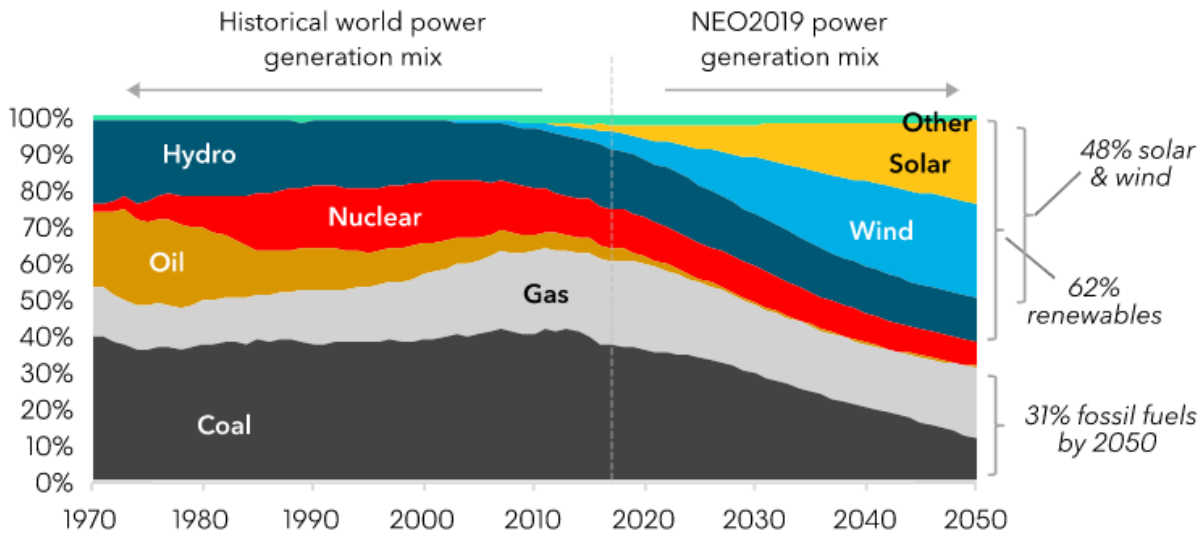

Figure 1. Global energy mix from 1970 to 2050 (Source: BloombergNEF).

Taking into account the large deployment of decarbonized Hydrogen, a massive production of electrolysers is necessary in a near future. For instance, 40 MW of electrolyzer is already installed in France in 2021 whereas 6.5 GW is expected in 2030. Hydrogen can be transformed again into electricity, at any time or anywhere, and without CO_2 emission, by using fuel cells. Again, a massive production of electrolyzers and fuel cells is also expected in order to cover the deployment of hydrogen based electric heavy vehicles.

There are several types of electrolysers and fuel cells operating either at (i) low temperature and based on a Polymer Electrolyte Membrane (PEMEC and PEMFC) or Phosphoric Acid electrolyte (PAFC) or Alkaline electrolyte (alkaline electrolyzer and fuel cell), or (ii) high temperature and based on a Molten Carbonate electrolyte (molten carbonate fuel cell, MCFC), or a ceramic electrolyte (Solid Oxide electrolyzer-SOEC or Solid oxide Fuel Cell-SOFC).

Both electrolyzer and fuel cell are electrochemical devices where electrochemical reactions occur on electrodes separated by an electrolyte which is a good ionic conductor. In the fuel cell mode, an oxidant (for instance oxygen from ambient air) and a fuel (for instance hydrogen) are provided separately on each electrode to generate electrons and water (if H_2 is the fuel) whereas in the electrolyser mode electrons and water are provided and the water is separated to produce Hydrogen and oxygen separately on the electrodes. The different type of electrochemical devices mentioned above differs by the nature of their components and their operating temperatures.

Among them solid oxide based electrolysers and fuel cells (SOEC and SOFC)s, operating at high temperatures, are very promising systems since they do not require expensive catalysts such as Platinum, and present high electrical efficiencies. Small and large systems are already present on the market even if improvement are needed, such as lifetime and cost. In France, the manufacturing of solid oxide electrolyzers will occur at the Genvia gigafactory, which is established in Béziers. The mass production of electrolysers is on the road. Genvia announce a production of 300 SOEC stacks (10 kW) by the end of 2022 with an objective to assemble modules beyond the megawatt level by 2023.

Research activities are also necessary in order to accelerate the development of the industrial sector in the hydrogen domain. Along the hydrogen value chain, all the sectors can be optimize and new systems could result from such a breakthrough. In the Solid Oxide area, increasing electrolyser outlet H_2 pressure, better reversibility, co-electrolysis, lifetime, SOFC stability when operating in carbonaceous gases, are the main common international research axis. At IMN, researchers from the ST2E team have a long experience in the field of ceramic materials for high temperature fuel cells and electrolysers (SOFC and SOEC). During the last 10 years, Kawther Thabet, Jean-Marie Doux, François Ricoul and Leonard Thommy worked for their thesis in this field with their know-how in synthesis and more generally in solid chemistry, they have developed new electrodes and electrolytes materials. With the objective of promoting the emergence of new axis of societal research, in 2019 the CNRS launched a thesis program entitled "80 primes" and the IMN Fuel-cell and hydrogen was able to benefit from a scholarship. This study responds to a societal demand related to the problem of recycling devices for hydrogen electric energy storage well before their large-scale economic development. It is the recycling of the oxides contained in the solid oxide cells which is the main objective of this thesis.

Each single cell contains significant amounts of critical raw materials. e.g Ni, Co, La , Gd, Ce, Sr, Zr and Y. In this regard, the technology will face the major challenge of mass production of feedstock. Moreover, as in all industry sectors, the recycling and reuse of production waste or end-of-life products should be encouraged. Recycling solid oxide cells can also be very interesting from an economic point of view, and not necessary for direct re-use in SOC. Indeed, for example, the primary nickel-bearing minerals have a chemical content 25 to 40 times lower than the waste products of the solid oxide cells. Therefore, it is possible to say that the extraction

of Ni from waste products is more economical than the extraction of Ni from primary nickel bearing minerals.

It is then necessary to develop practical methods for separating and recovering the ceramic components of SOFC or SOEC waste products, but it is also important to show the re-using of these recovered products, taking into account the possible presence of impurities

In this work, we propose effective strategies for recycling fuel electrode-supported SOFC ceramic materials, i.e. the air electrode ($La_{1-x}Sr_xCoO_3$), nickel oxide (NiO) which accounts for about 50% of the cell weight, and yttrium-stabilized zirconia ($Zr_{1-x}Y_xO_{2-x/2}$ called YSZ) coming from both the fuel electrode and the electrolyte. Multi-stage processes involving crushing and grinding, acid-assisted leaching, and precipitation of the constituents are carried out.

The work is organized as follows:

- The first chapter of this manuscript presents the concepts and state-of-the-art in hydrogen economy, and solid oxide fuel cells and electrolyzers with emphasis on issues linked to their end of life. It also describes the advantages of using recycled products over primary products in terms of economic and environmental impact.

- The second chapter presents experimental data, i.e. chemical reagents, procedures and characterization methods used during the thesis.

- In the third chapter, the recycling of component materials by mechanical scratching route are presented. The recovery of YSZ, NiO and $La_{1-x}Sr_xCoO_3$ are presented. The techniques of "mechanical scratching route", grinding and leaching to recover the products are discussed. The recovered materials are carefully analyzed for their structural and morphological properties, conductivity, and chemical purity. The recovery yield is also investigated. Upcycling of recovered YSZ by commercial Y_2O_3 to increase the yttrium content and in a way that can be used for electrolyte production is studied.

- The fourth chapter deals with an alternative recycling strategy addressing limitations associated with mechanical scratching which is named as "Dimethylglyoxime (DMG) route". This route uses Dimethylglyoxime (DMG) as a precipitating reagent for nickel that can be used, after YSZ precipitation, in order to separate nickel from the other elements constituting the air electrode. It is a cost effective recycling process that can be directly applied at the industrial level and could

open new perspectives for recovering solid oxide cells containing nickel. Throughout this thesis, different milling and leaching devices or leaching and precipitation chemicals are tested.

-The last chapter of this manuscript deals with their comparison, in terms of efficiency and cost-effectiveness. The final section addresses the cost benefit analysis and environmental impact assessment of the optimized protocols.

Chapter 1: Literature review

There is a large consensus in the world saying that green hydrogen will play an important role in the energy sector. Hydrogen can be also used in other various sectors of the economy, contributing to public health and global warming reduction. One way to produce green hydrogen is high temperature solid oxide electrolysis showing electric efficiencies up to 89% (lower heating value), well above alkaline (58%) and PEM water electrolysis (63%) [1].

The rapid growth of hydrogen during the next 5 years is linked to a necessary mass production of electrolysers such as SOE. In France, in 2024, there will be two gigafactories in the field of electrolyser production. One, Genvia, located in the south of France will produce massively SOE and the second, Symbio located in Lyon for PEM fuel cell production. Indeed, for both markets the size increase requires recycling and reuse of critical raw materials. Concerning low temperature PEMFC, 85% of PGM (platinum goup metal) particles can be recovered [2]. Recycling processes of Pt spent devices are numerous and are increasing in the last few years (>2000 for the 10 years) [3].

This chapter is devoted to the general data concerning hydrogen and SOC technology. The final section of this chapter addresses the issue of products and disposal sites, with an emphasis to the need for a circular economy through recycling and an overview of a possible life cycle concept for SOCs.

1.1 Hydrogen for decarbonizing economy

1.1.1 Hydrogen: some data

Hydrogen is a colorless and odorless gas. It is the lightest element (eight times lighter than methane) [4] [5]. It is then a powerful energy carrier that can deliver three times more energy per unit mass than gasoline and diesel did. Quantitatively, hydrogen, gasoline and diesel have an energy density of 120 MJ/Kg (33.6 kWh), 45.8 MJ/Kg, 45.5 MJ/Kg (12-14 kWh), respectively [6]. Hydrogen is a medium for storing clean and flexible energy obtained from primary energy sources, but is not itself an energy source.

Hydrogen is the most abundant element in the universe. However, it is not found in its purest dihydrogen form, and must be produced from fossil fuels or water. Hydrogen can be stored in large quantities and over a long period. In order to be stored, it can be liquefied or compressed in its standard state [7]. Liquid hydrogen requires a cryogenic tank with a temperature below the melting point of hydrogen (-253°C). Large quantities of hydrogen can also be stored in salt caverns. Hydrogen can also be stored in solids, in the form of metal hydrides and intermetallic alloys that absorb hydrogen, e.g. $LaNi_5$ or Na_3AlH_6.

Hydrogen is applicable in various sectors of the economy (Figure 1.1). The main applications of hydrogen includes ammonia and fertilizers production [8] [9] [10] [11] which covers 55% of the total hydrogen demand. The second biggest demand for hydrogen is associated with oil refiners, which accounts for 25% of the total hydrogen produced. The third application is methanol production[12] [13] [14] [15] [16]. Compared to conventional fuels, renewable methanol from green hydrogen reduces CO_2 emissions by up to 95%, nitrogen oxide emissions by up to 80%, and completely avoids sulfur oxide and particulate matter emissions [17].

Hydrogen can also be used in green iron and steel production. Hydrogen in pure form or in a mixture with other gases is used as a reducing agent to reduce iron oxide. Iron and steel production is the fourth sector with high hydrogen demand, along with oil refining, ammonia synthesis and methanol production [18] [19] [20] [21] [22] [23].

Hydrogen provides power generation without emitting greenhouse gases, fine particulate matter or Sulphur dioxide. It has also great opportunities in the energy sector as an energy carrier in clean mobility. It can be directly used in fuel cells or in internal combustion engines. If batteries are suitable for cars in urban transport, hydrogen, with its higher energy density, is better suited for heavy vehicles such as buses, trucks, trains, planes and cargo ships. The other application of hydrogen is building heating, since no harmful products are rejected when hydrogen is burned at home. The demand of hydrogen in different sectors is shown in Figure 1.1. There are many plans to increase the supply and acceptance of hydrogen use in many sectors, especially in the energy one.

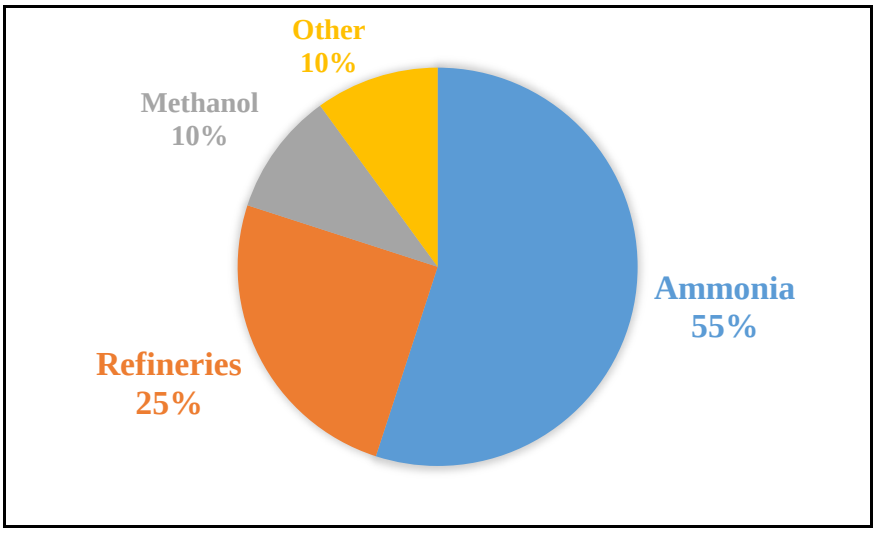

Figure 1.1 Hydrogen demand in different sectors (adapted from data from hydrogen Europe.eu/hydrogen-application) [24].

1.1.2 Hydrogen in the energy mix plan

Decarbonizing energy sector has a role of choice in making climate neutral economy. As shown in Figure 1.2, the energy sector constitutes about 73.2 % of greenhouse gas emission [25]. This shows how deep decarbonization of energy sector can mitigate the greenhouse gas emission. According to world metrological organization, climate change is 0.2°C per decade, and global temperature will rise by 3 °C to 4 °C per decade by 2100 if timely action is not taken [26]. Indeed, in order to follow the Paris Agreement agenda, with the aim to keep the Earth's temperature rise below 1.5-2.0 °C, new energy sources must be intensively developed.

Energy from hydrogen can also be used to regulate weekly and monthly demand and supply. It also serves to improve access to energy in isolated areas and can result in users being less dependent on specific energy sources. According to the 2050 net-zero plan, hydrogen has decisive role as energy carrier to power the world. The comparison of the energy supply chain by different energy carriers for 1990, 200, 2015, 2019, 2040 is shown in Figure 1.3 [27]. The renewable energy sources are the major contributors for global electricity mix.

Greenhouse gas emission emitted by different sectors:

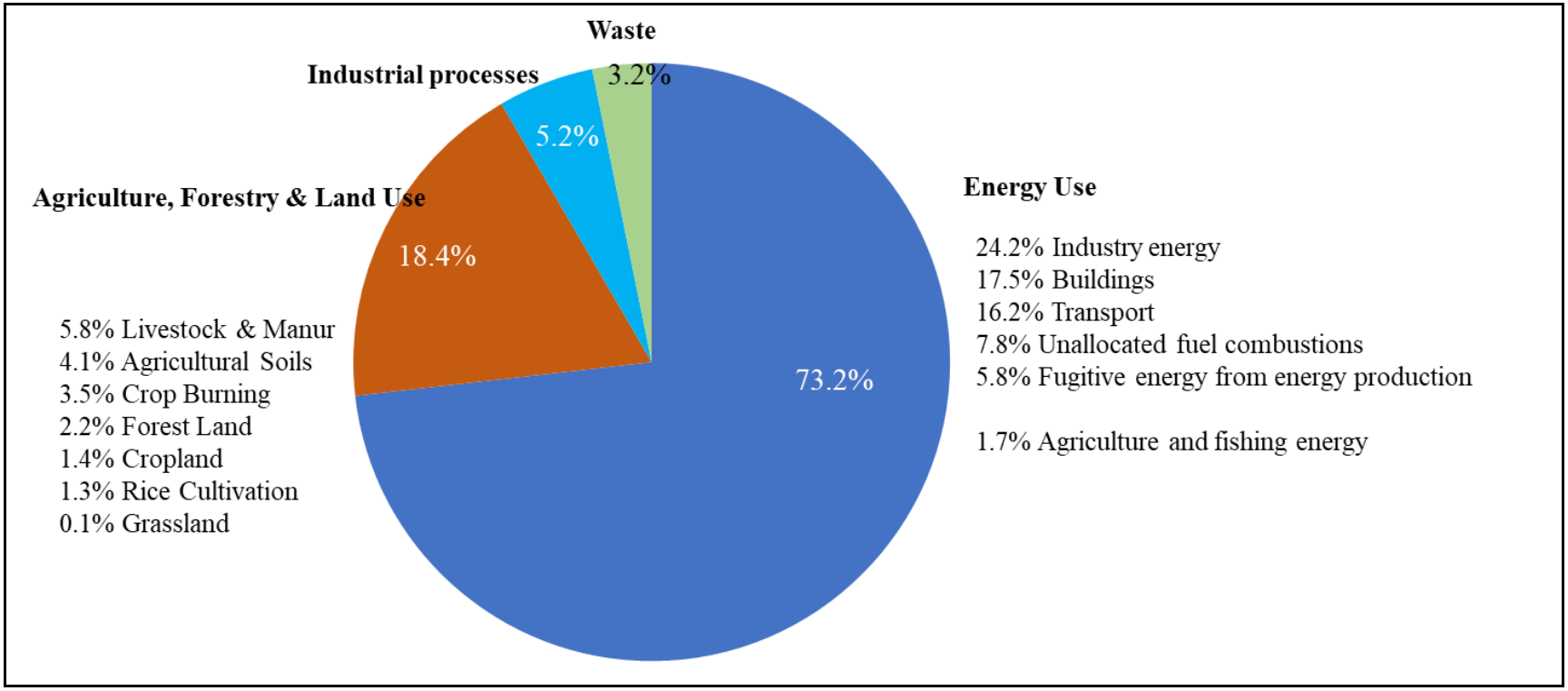

Figure 1.2. A Global Breakdown of Greenhouse Gas Emissions by Sector in 2016[25] [adapted from Visual capitalist/energy.

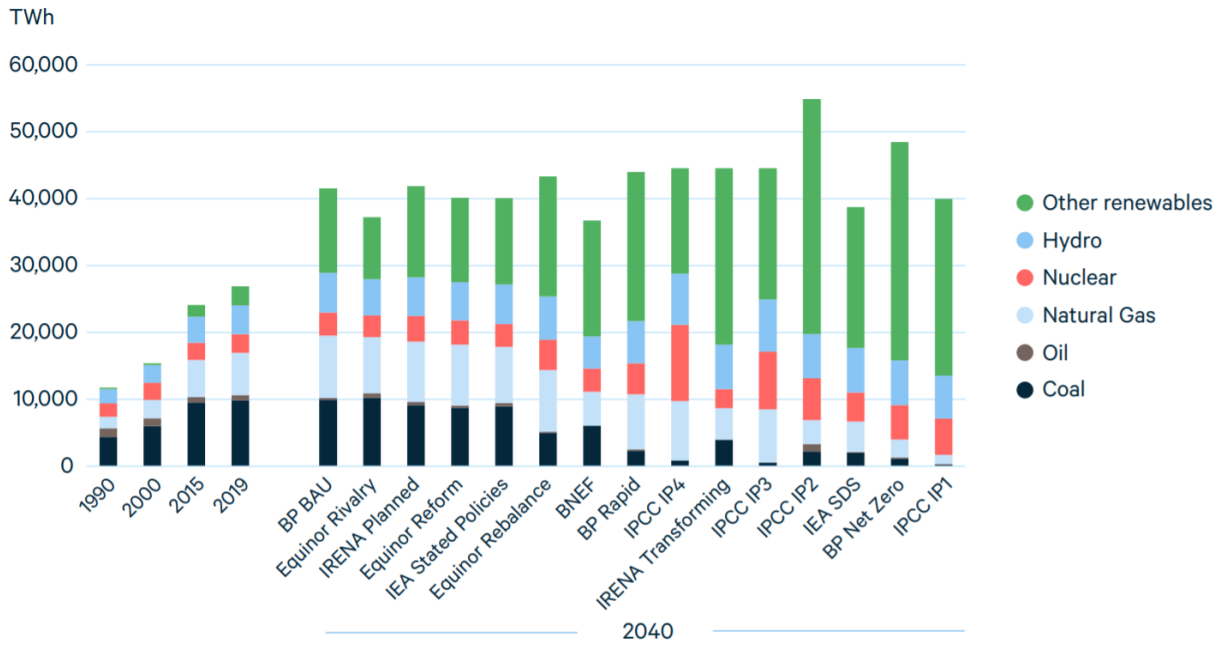

Figure 1.3. The global electricity mix for the 1990 to 2019 and different reports for global electricity mix in 20240 [27].

Currently, the consumption of green hydrogen in the industrial, transportation, energy, and building sectors is still limited. The power sector is expected to increase by 12 TWh in 2030, 301 TWh in 2040 and 626 TWh in 2050 [28]. Figure 1.4 [29] represents, hydrogen demand by sector in the Announced Pledges and Net zero Emissions scenarios from 2020 to 2050 (Figure 1.5) [27].

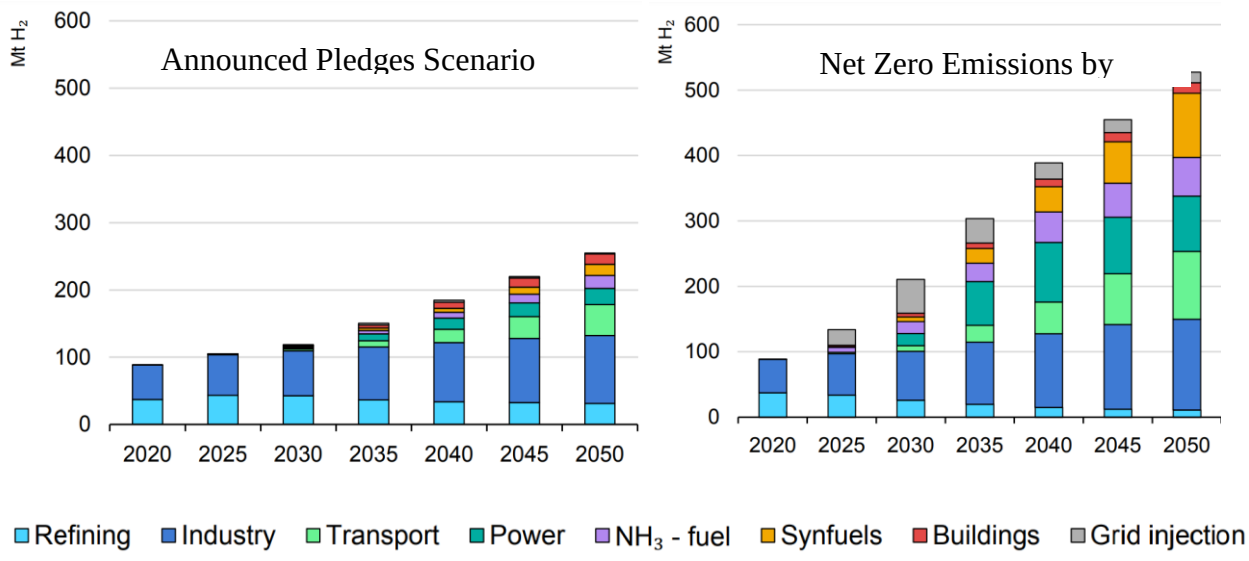

Figure 1.4. Hydrogen demand in different sectors by 2050 for the net zero emission scenario [29] [Adapted from Global Hydrogen Review 2021]. ***Notes:*** *"NH3 - fuel" refers to the use of*

hydrogen to produce ammonia for its use as a fuel. The use of hydrogen to produce ammonia as a feedstock in the chemical subsector is included within industry demand.

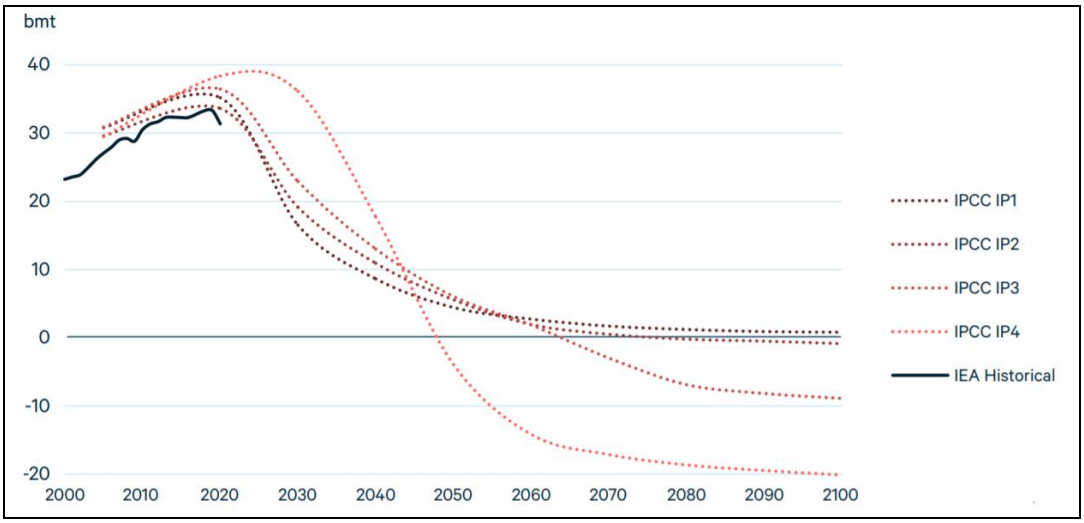

Figure 1.5. Global CO_2 emissions trends of the IPCC Illustrative Pathways [27] (International Energy Agency 2021).

Despite the potential and momentum of hydrogen, large-scale production and supply to meet future demand remains a challenge. This requires environmentally friendly production as well as large-scale and long-term storage.

1.1.3 Current status of hydrogen production

There are several ways to produce hydrogen. Currently, the primary hydrogen production is from fossil based, i.e. 48% of hydrogen produced from natural gas, 30% from coal (the second popular route), 18% from oil based (

Figure *1.6*). Out of the current hydrogen production only 4% is produced by electrolysis of water [30].

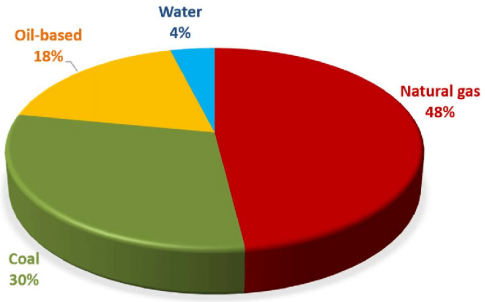

Figure 1.6. The current sources of hydrogen production [30]

Hydrogen can also be produced from biomass without combustion, by high temperature treatment of organic materials [31]. A brief outline of the hydrogen production from biomass is shown in the Figure 1.7.

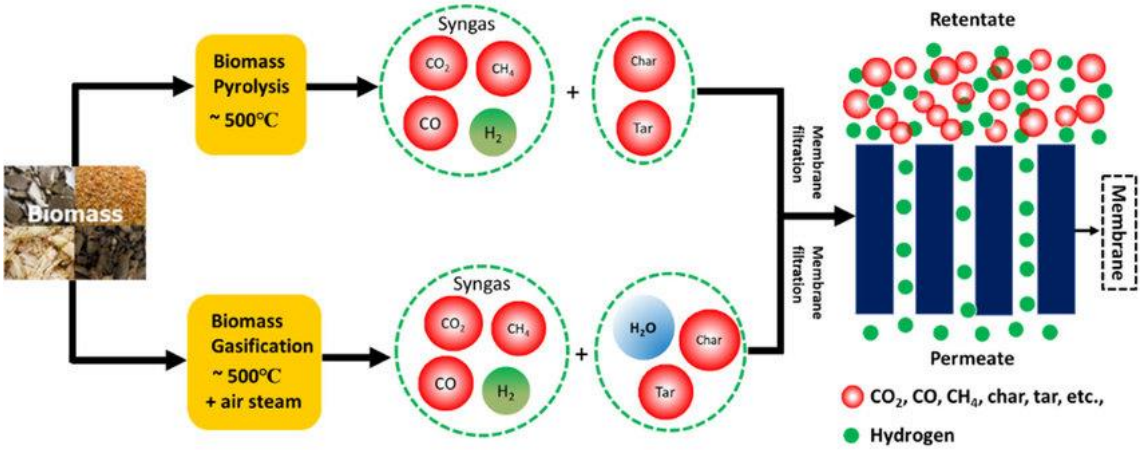

Figure 1.7. Hydrogen production diagram from biomass [31].

Up to now, different colors have been assigned to hydrogen, depending on its production source. Green color is used for hydrogen produced from electricity issued from renewable energy sources such as solar, wind, hydro, and geothermal, (e.g. Figure 1.8). On the opposite, Gray color is used for hydrogen issued from natural gas and coal through steam reforming. This is the most common technique used today to produce hydrogen, but it releases a lot of CO_2 into the atmosphere. Dark green color is hydrogen from bio methane plus carbon capture and storage. Blue color is hydrogen from natural gas, but the process is purified by carbon capture and storage. From all, the need for green hydrogen production is promoted. Recently, in France, hydrogen colors have been replaced by two denominations "decarbonized" and "carbonized". To be called

"decarbonized", hydrogen should be produced with a low CO_2 footprint. The limit was fixed to 3kg of CO_2 per kg of H_2 in order to include hydrogen produced by electrolysis using electricity coming from nuclear plant. The need for decarbonized or green hydrogen production is encouraged.

1.1.4 Hydrogen production via solid oxide electrolysis

Hydrogen production by electrolysis of water is an efficient way to produce pure hydrogen [32] [33] [34], according to reaction (Equation 1.1)

$$H_2O \rightarrow H_2 + \frac{1}{2}O_2 \qquad \text{Equation 1.1}$$

It can be produced in its purest form with up to 99.999 Vol% [35]. [36] [37] with an efficiency which can reach 90% [38].

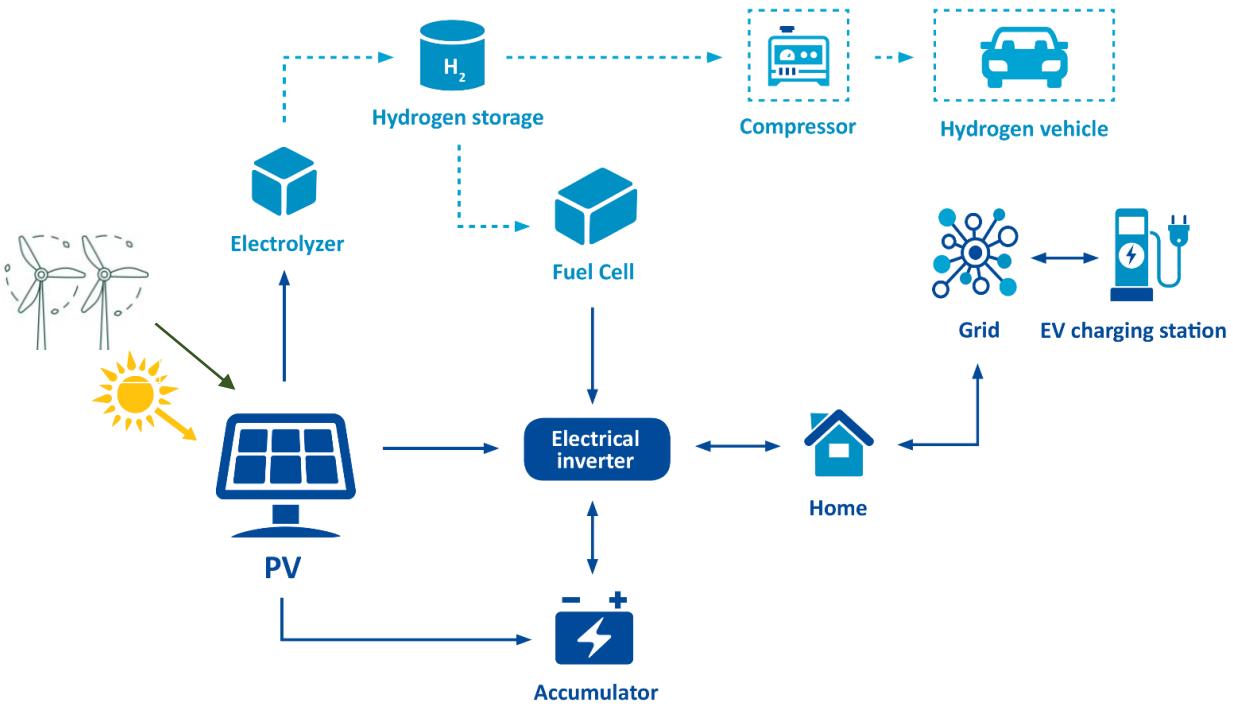

Figure 1.8. Green hydrogen production from solar panel and wind application.

1.2 Solid oxide fuel cell and electrolyzer technologies

Both solid oxide fuel and electrolyzer single cells consist of a dense ceramic electrolyte (a good ion conductor but electronically insulator), sandwiched between two porous electrodes (good electronic and ion conductors). The fuel electrode (also called negatrode or anode in fuel cell mode or cathode in electrolysis mode) is classically a metal-ceramic composite usually called cermet [39]. The air-electrode (also called positrode or cathode in fuel cell mode or anode in electrolysis mode) is a usually a mixed ion and electronic conductor (MIEC) ceramic oxide [40] [41] [42]. Interconnects and sealants complete the system [43] [44] [45] [46] [47]. The planner SOCs stack is illustrated in Figure 1.9. In fuel cell mode (SOFC mode), due to the oxygen partial pressure gradient between the surface of the air electrode and the fuel electrode, the oxygen, after being dissociated in O^{2-} ions, starts to transport through the dense electrolyte to react with hydrogen at the fuel electrode (anode).

The efficiency of conventional combustion with Carnot limitation is about 33-38% [48], but high temperature SOFCs have an electrical efficiency of more than 70% [49], and when the waste heat is used, it reaches more than 90% [50].

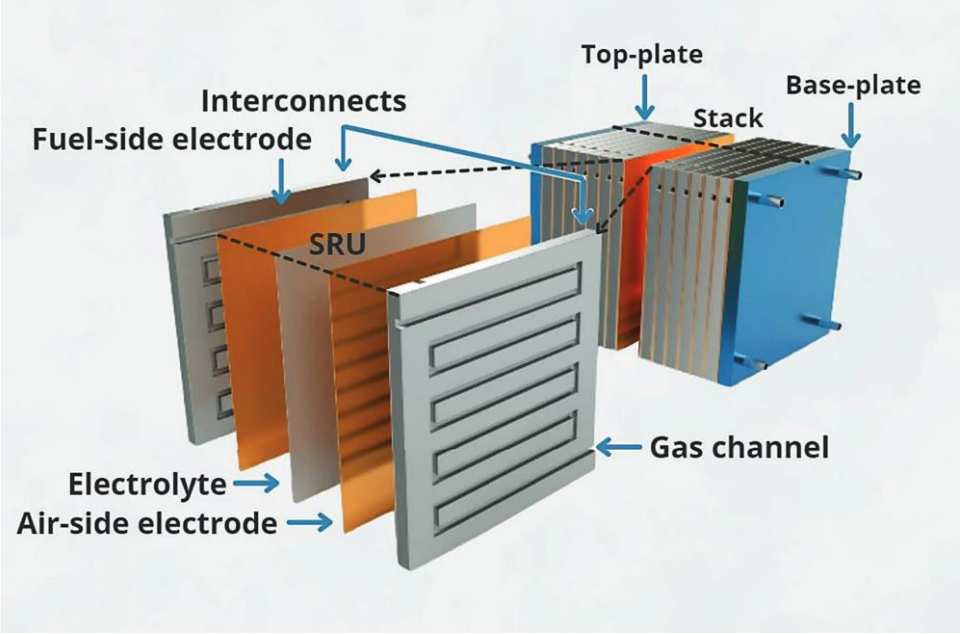

Figure 1.9. Functional core units and configuration of a planar SOC stack [50]

High-temperature Solid oxide cells can be reverse devices that operate as fuel cells (SOFC mode) to produce heat and electricity and, conversely, as electrolyser (SOE mode) cells to produce hydrogen (Figure 1.10). These SOECs are efficient and environmentally friendly ways to produce hydrogen [51] [52]. Solid oxide electrolysers are also capable of electrolyzing CO_2 to CO or co-electrolyzing steam/CO_2 to a H_2/ CO mixture.

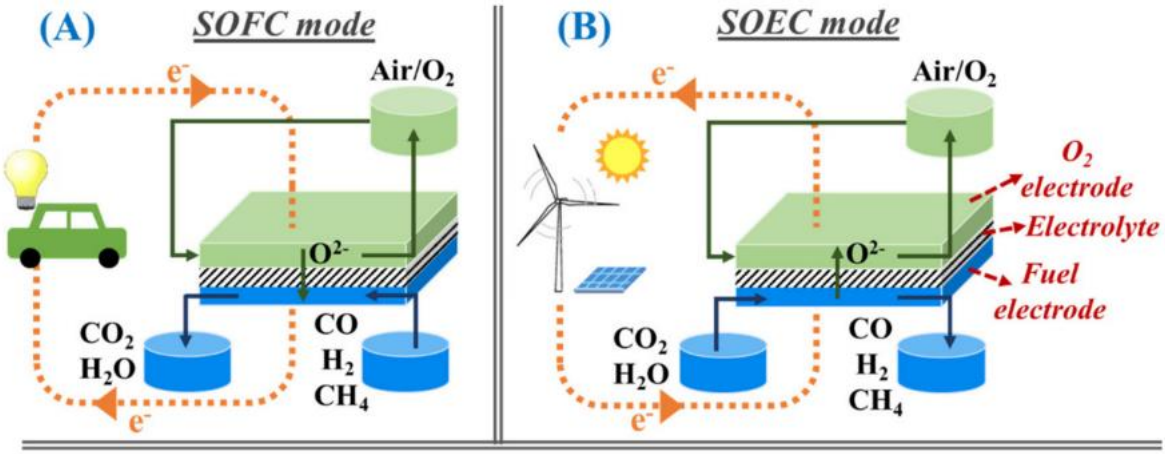

Figure 1.10 Solid oxide cell (SOC) operation in (A) fuel cell mode (B) electrolysis mode[53]

Compared to other fuel cell or electrolyzer technologies, SOFC and SOEC have the following advantages.

a) High electrical efficiency up to 90%.
b) Flexibility in fuel choice in SOFC mode: (e.g., H_2, CH_4, biogas and liquid fuel, natural gas, diesel, alcohol, and gasoline) [54].
c) Flexibility in electrolysis mode producing H2 using water, syngas (CO and H_2) using CO_2 and water, ammonia using N_2 and water.
d) Environmental respect, with minimal emissions during the manufacturing phase [55], and in SOFC mode producing only heat and H_2O when pure H_2 is used as fuel.
e) Good long-term stability, strong mechanical properties: SOFCs and SOEs have a potentially long life expectancy of more than 40000-80000 h [55] [56].
f) Low cost component materials, no expensive catalyst needed.

g) Completely solid structure yields low maintenance cost and difficulties associated to liquid electrolytes, especially corrosion.

1.2.1 History of solid oxide fuel cell and electrolyzer technologies

Hydrogen and energy have a common history for 200 years.

- 1800: Nicholson and Carlisle first demonstrated the process of electrolysis by producing hydrogen and oxygen when applying electric current to water[57].
- 1820, Mikael Faraday investigated and gave a quantitative expression to Nicholson and Carlisle's findings, which were introduced in 1833 as the laws of electrolysis [58].
- 1839: The first fuel cell is discovered and then designed by William R. Grove in 1842 [59]. Grove referred to this device as a gaseous voltaic battery [60].
- 1875: The book "The Mysterious Island" of Jules Verne contains a vision of the future and the aspiration to power the whole world through the energy of water molecules [61].
- 1889, Ludwig Mond and Carl Langer designed a diaphragm to avoid electrode flooding and prevent hydrogen and oxygen from mixing.
- 1897: Nernst developed high-temperature lamp made of 15% Y_2O_3-doped zirconia.
- 1902: Friedrich Wilhelm Ostwald associated the oxidation-reduction reactions to the electricity production [62]. Water electrolysis cells are commercialized by the Oerlikon Engineering Company [63].
- In 1937: Baur and Preis constructed solid oxide fuel cells from a mixture of the ceramics ZrO_2 and Y_2O_3 [64].
- 1943: Intensive investigations of SOFC was done by Wagner and his research group in Germany.
- After 1960, a rapidly growing number of patents and scientists worked on the different problems of SOFCs, and by 1970 the basis was established on which the broad technologically orientated development of SOFCs proceeds today.
- Since the 1975s, hydrogen and Fuel cells has sparked several waves of investment interest. Nowadays, low temperature electrolysis technologies (alkaline or polymer

exchange membranes electrolysers) are available with a large number of manufacturers. High temperature electrolysis (SOE) are less mature.

- Today, there are many solid oxide cell manufacturers. The current commercial status of solid oxide fuel cells are reviewed in section 1.2.4.

1.2.2 Operating principle of solid oxide fuel cells

Air flows into the air electrode and fuel flows into the anode/fuel electrode. The sandwiched electrolyte allows the passage of oxide ions or protons and acts as a gas diffusion mixing barrier [65]. Figure 1.11 shows a schematic diagram of the SOFC operating system, in which the conducting electrolyte is an anionic conductor.

When used in a fuel cell, the maximum power brought by fuel is limited by the thermodynamics and free enthalpy of the reaction of oxygen and hydrogen.

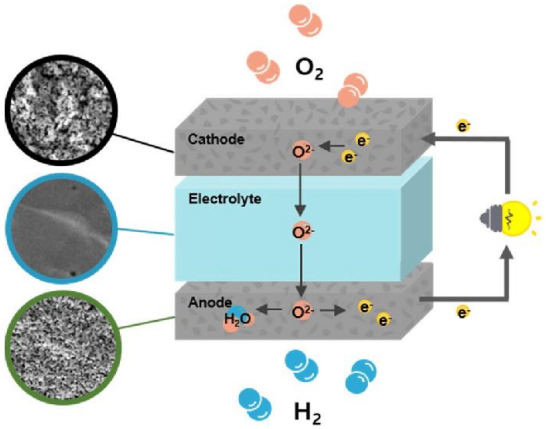

Figure 1.11. Schematic illustration of component of SOFCs

The thermodynamics is given in the following:

$$\Delta_r G(T,p) = -W_{max} = \Delta_r H(T,p) - T\Delta_r S(T,p) \qquad \text{Equation 1.2}$$

Where ΔG is the Gibbs free energy, Wmax is the maximum work a system can do, ΔH is the change in enthalpy, T is the temperature, and ΔS is the change in entropy for a reaction r as a function of temperature and pressure. The energy difference between the reaction enthalpy and Gibbs energy is the heat energy released during the reaction. Faraday's law gives the relation between the theoretical voltage between the two electrodes and the Gibbs energy:

$$E = -\frac{\Delta_r G(T,p)}{Z_e * F} = \frac{W}{Z_e * F}$$ Equation 1.3

Where z is the number of electrons involved in the reaction, e is the elementary charge, F is Faraday, and E is the cell potential.

For end-user, the produced heat and electrical power are the final requirements. Electrical efficiency is calculated by considering the ratio of amount of useful energy produced and used in terms of change of Gibbs free energy (ΔG), and enthalpy change (ΔH). On the other hand, the Voltage efficiency is calculated in terms of the ratio of the operating cell voltage to the ideal voltage. Typically, many cells (up to 100) must be connected in series to achieve the output voltage required for a particular application.

1.2.3 Components of SOCs

Currently there are different cell configurations, most common designs are shown in Figure 1.12 [50]. Each cell design has advantages and dis advantages. Electrolyte Supported Cell (ESC) design has the advantage of strong structural support based on thick dense electrolyte (≈200µm), fewer mechanical failures, resistance to oxidation and reduction changes at the fuel and air electrodes [66]. The problem associated with this design is a longer ionic path, resulting in a higher resistance due to ohmic loss. In this context, a high operating temperature is required for ionic conductivity, which in turn requires high temperature compatible materials.

The Fuel Electrode Supported (FESC) design is based on a thick porous electrode (≈ 400µm). It presents a lower overvoltage, and can be operated at lower temperatures (Ni-YSZ/YSZ/LSM 800°C) [67] using the same materials as ESC. This is the most common design type of SOFCs fabrication [68]. The disadvantage associated with anode-supported cells is their susceptibility to cracking during reduction and oxidation cycles, restriction of mass transport, high ohmic loss and deformation of internal cracks at high temperatures. On its side Air Electrode Supported (ASC) design can be operated at less than 800°C, but suffers from mass transport limitations and high ohmic loss [69]. Finally, substrate-supported design such as Metal Supported Cell's one (MSC) allows thin-cell components and can operate at lower temperatures but its realization remains today challenging. Interconnect supported cell can operate at lower temperatures and provides strong structural support, but has sintering complication and contact difficulties.

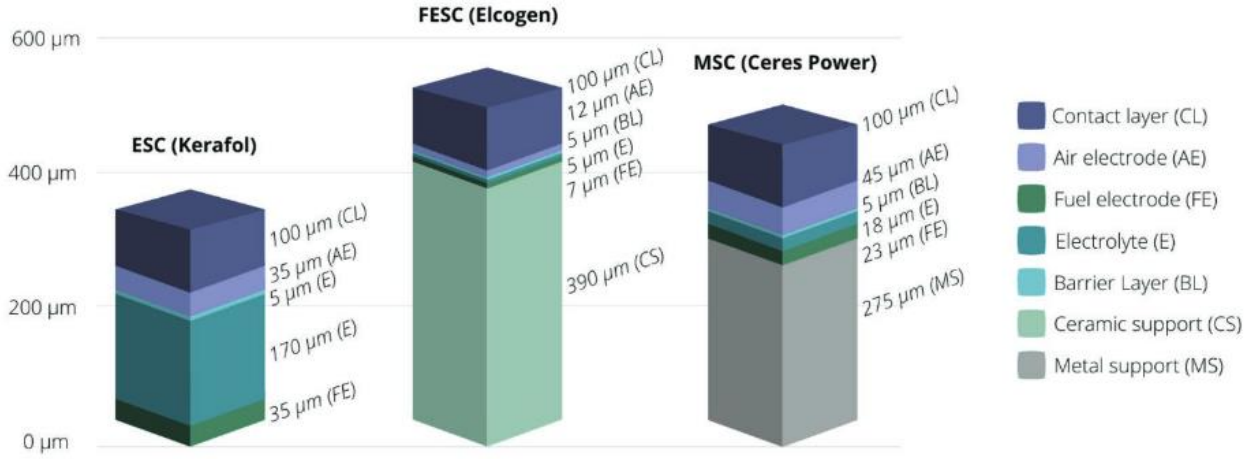

Figure 1.12. SOFCs components and cell design configurations. Approximations of SOC functional layer thicknesses, using the example of three industry-leading manufacturers[50].

1.2.3.1 Electrolyte

The electrolyte is placed between the fuel electrode and the air electrode (Figure 1.12), and has several roles. (1) It assures separation of fuel and air gases. For this purpose, it must have a high density of more than 95% of theoretical density and be free from cracks. (2) It acts as an electron diffusion block (as separator) and as a medium for ion transfer from one terminal to the other. For this purpose, the electrolyte materials should have a higher degree of oxide ion conduction, i.e., they should have a high ion transference number close to one. On the other hand, it should have very low electronic conductivity (electrically insulating) to avoid short circuits (leakage currents) [70]. (3) Since the electrolyte is in contact with both the anode and cathode, it should be chemically and mechanically stable in both reducing and oxidizing atmospheres. Its thermal expansion coefficient should match with the fuel and air electrodes' ones. Apart from intrinsic properties, it is also desirable to have a low-cost, simple and scalable manufacturing technology. The selection of electrolyte materials should also take into account the possibility of optimizing phase defects such as oxygen vacancies and sintering properties.

There are two different types of electrolytes depending on the type of ionic conduction: oxygen-conducting electrolytes and proton-conducting electrolytes. The state of the art materials are respectively Yttria stabilized Zirconia, called YSZ with the general composition $(ZrO_2)_{1-x},(Y_2O_3)_x$ and Barium Cerate substituted by Yttrium and zirconium (BZCY). Other materials less usual are

also good electrolyte e.g. calcium or Scandium stabilized zirconia and substituted ceria such as samarium, yttrium or gadolinium doped ceria (SDC, YDC or GDC) with a general formula $Ce_{1-x}M_xO_{2-\delta}$ (M = Sm, Y or Gd)

Yttria Stabilized Zirconia:

Zirconia (ZrO_2) is not a good ionic conductor due to the absence of intrinsic oxygen vacancy. Moreover, ZrO_2 shows three allotropes depending on the temperature (Figure 1.13). Monoclinic (Baddeleyite) is stable at temperatures below 1170℃[71]. Tetragonal (t-YSZ) is stable between 1170 and 2370℃ where as cubic is stable from 2370℃ to its melting point [72]. The transition from the tetragonal to the monoclinic phase is martensitic (diffusion less) [73] and is accompanied by a change in shape and an increase in volume of ~5% [74]. Consequently, using dense ZrO2 in a device where the temperature evolves in the range of these transitions, thermal and mechanical stresses are generated leading to the failure of the system. Other stimuli (Pressure) and different metal substitution such as yttrium on zirconium site can lead to the stabilization of one of the 3 allotropic types or a mixture [75] [76] [77].. For example, the cubic type "ZrO_2", with a crystal structure of Fm-3m in which metal atoms are coordinated by eight evenly spaced oxygen atoms, is stabilized at room temperature at sufficiently high yttrium substitution ratio ($Zr_{1-x}Y_xO_{2-x/2}$ with $x > 0.15$). The tetragonal zirconia exhibits elongation in the c-axis[78]. In addition, the oxygen ions are displaced in the c-axis direction from their high symmetry position $c=2\sqrt{a}$.

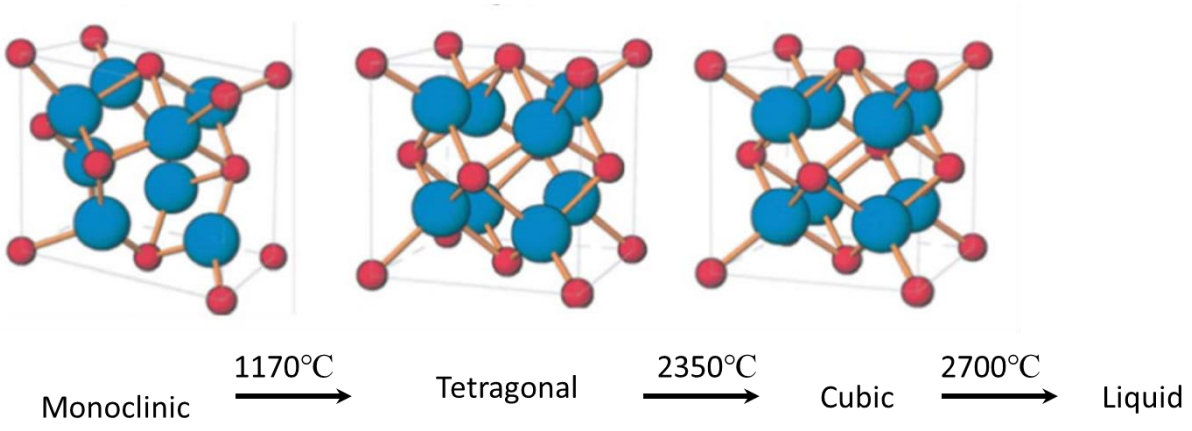

Figure 1.13. The Polymorphic transformation of ZrO_2 [79].

More generally, thermally assisted mechanical issues of ZrO_2 is resolved by partially replacing Zr^{4+} by an element that has a lower valence/oxidation number, often Y^{3+} but also scandium or calcium oxides are used in order to stabilize at room temperature a cubic phase. Together with this stabilization, the lower valence ion substitution produces oxygen ion vacancies [80] which allows oxide ion mobility and then its use in devices such as fuel and electrolyzers cells.

According to the Kronger-Vink notation, the substitution of Zr^{4+} by Y^{3+} and the creation of oxygen vacancies is modeled by the following reaction:

$$Y_2O_3 + 2Zr_{Zr}^{x} + O_O^{x} \rightarrow 2Y_{Zr}' + V_O^{\cdot\cdot} + 2ZrO_2 \quad \text{Equation 1.4}$$

Where $Y_{zr}^{\bullet}$ represents yttrium in the zirconium lattice and has a net positive charge, V_O'is the vacancy of oxygen and has a net negative charge, and Zr_{Zr}^{x} and O_O^{x} represent zirconium and oxygen in their regular lattice positions with net charge of zero. It is generally assume that an ionic conductivity level above $10^{-2}S.cm^{-1}$ is necessary for application as electrolyte in electrochemical devices (e.g. fuel cell, electrolyzer, batteries). Among usual electrolytes, ceramic materials such as YSZ reach this target (Figure 1.14).

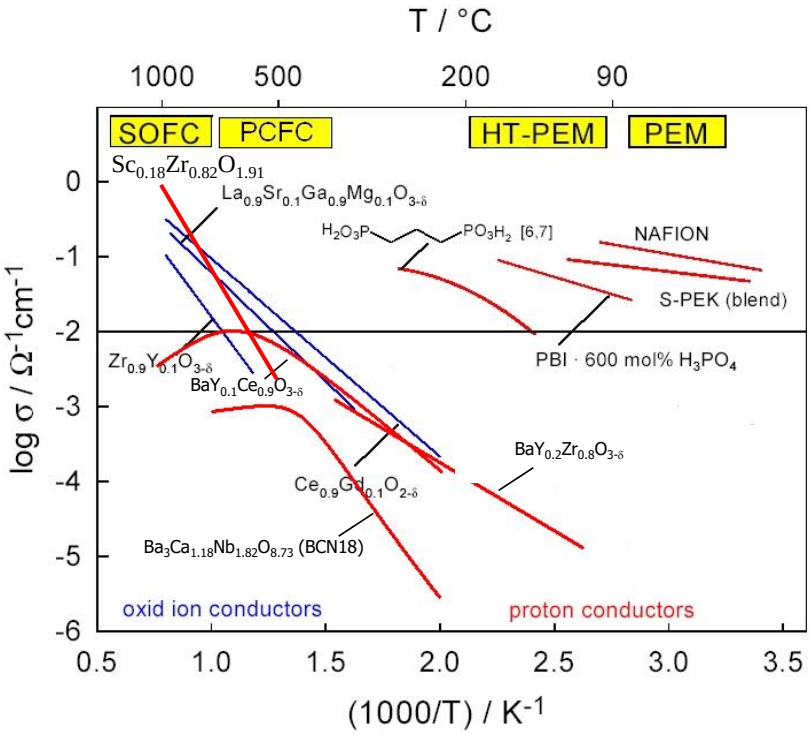

Figure 1.14. Comparison of different electrolyte materials

(YSZ conductivity is about 10^{-2} Scm^{-2} at 700°C [81]) whereas polymer based membrane (e.g. Nafion) shows good conductivity values at nearly room temperature (Figure 1.14). Therefore, electrochemical devices based on YSZ electrolyte operate necessarily at high temperature (600-1000 °C). On one side, this operating temperature range can lead to element diffusion [82] [83] which negatively affects the durability of these devices and on the other side it is increases the electrical efficiency and also avoid the use of costly catalysts [84]. Moreover, manufacturing processes of ceramics implying many high temperature steps are more costly.

As mentioned before, ceria doped materials such as CGO are also very interesting electrolyte showing $10^{-2}Scm^{-2}$ at 500°C only. The main issue of doped ceria restraining the operating range at low temperature is the appearance of a weak, but non negligible, electronic conductivity in reducing atmospheres. Although LSGM ($La_{0.9}Sr_{0.1}Ga_{0.9}Mg_{0.1}O_{3-d}$) (Figure 1.14) has a better conductivity than YSZ, its downside is the evaporation of La and the development of an insulating phase and a high reactivity with Ni at the fuel electrode.

1.2.3.2 Fuel electrode

The anode is a porous electrode allowing the electrochemical oxidation of the fuel [85] [39] [86]. The materials used to make fuel electrodes must have the following properties [87] [88]:

- Excellent catalytic activity to support electrochemical oxidation of various fuels, including a variety of hydrocarbon-based fuels.
- In addition to high electronic conductivity, the fuel electrode should also have good ionic conductivity to extend the Triple Phase Boundary (TPB) zone.
- The fuel electrode should have sufficient porosity to allow diffusion of incoming and produced gas.
- High chemical, microstructural, mechanical and thermal stability and compatibility with other components with very small TEC mismatch [89].
- Resistance to poisoning effect in case of utilization of carbonaceous fuel (sulfur[90] [91] or carbon deposition) and other impurities[92] coming from other components (chromium from stainless steel bipolar-plates).
- Performance durability[93]
- Simple, safe and low cost of manufacturing technology to scale up [94].

The cermet Ni-YSZ has met most of the above requirements and is selected as the most common candidate for commercialization.

Concerning the choice of Ni: it is well explained by T. Setoguchi et al. [95]. When a metal has a large negative heat of formation, such as Mn as shown in Figure 1.15a, reaction (5) (metal oxide reduction) proceeds easily and reaction (6) (metal oxidation) becomes the rate-determining step of the overall redox reaction. On the other hand, when there is a small negative heat of formation of the oxide, such as Au, the overall reaction is limited by reaction (6). As a compromise, a metal with an intermediate heat of oxide formation, such as Ni, would have the highest overall reactivity.

$$MO + H_2 = M + H_2O \qquad (5)$$

$$M + O^{2-} = MO + 2e^- \qquad (6)$$

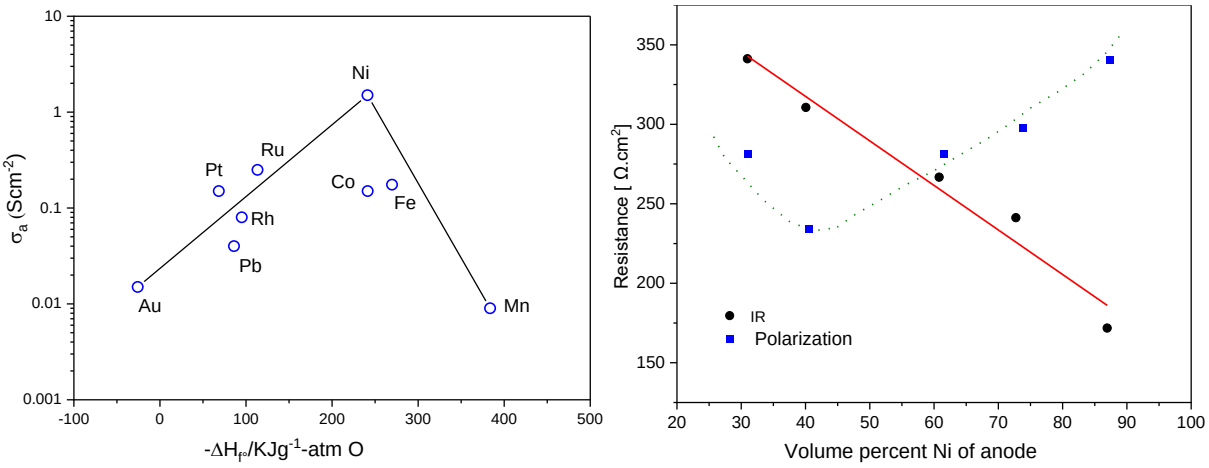

Figure 1.15. (a) The conductivity as a function of enthalpy of reaction of applicable transition metals in fuel electrode of SOFCs [95] (b) The effect of Ni content on the internal resistance (IR) and polarization resistance of fuel electrode [39].

Concerning Nickel/YSZ ratio: Since the electronic conductivity is given by Ni and the ionic conductivity by YSZ [96], optimization of the Ni:YSZ content, in the aim of increasing TPB volume while maintaining good percolation is required. The Ni quantity depends on the characteristics of initial powders on sintering temperature but also on operation conditions such as temperature, voltage, or incoming gas composition. According to the study of Kahlid et al. [97] in his Life cycle assessment, the fuel electrode must be prepared with 70 wt% NiO. Mostly fuel electrodes are prepared with 40-60 wt% NiO that results in a huge amount of Ni consumption for the production of SO single cells [39] [98] (Figure 1.15b).

Problems associated with Ni-based electrodes are coming from the small size of Nickel particles needed to optimize the catalysis activity of Nickel. During operation at high temperature, cell mechanical degradation is observed induced by nickel particles sintering. This effect is enhanced during redox or temperature cycling. Moreover, in case of operation with impure hydrogen, nickel catalyzes carbon deposition or reacts with H_2S leading to a decrease of their catalytic activities. .Other materials have been also tested (Table 1.1) presenting Mixed Ionic and electronic conductivity (e.g. LSCM) or by using other metal instead of Ni (e.g. Cu). However, they are not commercially used due to their cost of lower catalytic activity.

Table 1.1. Comparison of electrical and catalytic characteristics of main types of anode martials for SOFCs (adapted from Yu Liu)[87].

Fuel electrodes	Conductivity (Scm^{-1})	Working temperature °C	Catalytic activity	Resistance to carbon deposition	Tolerance to sulfur	cost
Ni cermet	High	500-1000	High	Low	Low	Low
Perovskite $(La,Sr)Co,Mn)O_3$	Low	500-1000	Low	High	High	High
Cu cermet	High	500-800	Low	High	moderate	low

1.2.3.3 Air electrode

The air electrode must favor the oxygen reduction. Indeed, the main requirements for the selection of air electrode materials are [42]:

- Good porosity to allow oxygen transport.
- High electronic and ionic conductivities, associated to a good catalytic activity for oxygen reduction reaction.
- High concentration of three-phase boundary (TPB) points.
- Thermal expansion coefficients compatible with the electrolyte and interconnects.
- Good chemical stability in an oxygen-rich environment under operating conditions.
- Chemical stability towards adjacent materials, in order to avoid the formation of an insulated layer, as it is the case when Strontium based materials reacts with YSZ [82].
- Low cost and simple fabrication.

Mixed ion and electronic conductor materials belonging to the perovskite family, and especially lanthanum-cobaltite and ferrite, are the most common air electrode materials [99] for an operating temperature around 700-800°C. These are manly LSC ($(La,Sr)CoO_3$), LSF ($(La,Sr)(Fe)O_3$), LSCF ($(La,Sr)(Co,Fe)O_3$))[100] and LCCF ($(La,Ca)(Co,Fe)O_3$). Samarium-Strontium-Cobaltite (SSC), $(Sm,Sr)CoO_3$ is also used. Lanthanum Manganite based electrodes are also very well-known but their utilization is usually restricted to higher operating temperatures (1000°C). Lanthanum-Strontium-Manganite Ferrite (LSMF),

(La,Sr),(Mn,Fe)O_3 [101], Praseodymium-Strontium-Manganite (PSM), (PrSr)MnO3 and Praseodymium-Strontium-Manganite Ferrite (PSMF), (Pr,Sr)(Mn,Fe)O_3, [102].

The most common challenge with air electrodes is mechanical delamination from the electrolyte due to TEC mismatch and the formation of an intermediate layer. The TEC of the most employed fuel electrode materials are given Table 1.2.

Table 1.2.Perovskite-type oxide materials: thermal expansion coefficient (TEC), electronic (σ_e), and ionic conductivities (σ_i) in air [42]

Composition	TEC ($\times 10^{-6} K^{-1}$)	T (°C)	σ_e (Scm^{-1})	σ_i (Scm^{-1})
$La_{0.8}Sr_{0.2}MnO_3$	11.8	900	300	5.93×10^{-7}
$La_{0.6}Sr_{0.4}CoO_3$	20.5	800	1,600	0.22
$La_{0.6}Sr_{0.4}FeO_3$	16.3	800	129	5.6×10^{-3}
$La_{0.6}Sr_{0.4}Co_{0.8}Fe_{0.2}O_3$	21.4	800	269	0.058
$Pr_{0.7}Sr_{0.3}Co_{0.2}Mn_{0.8}O_3$	11.1	800	200	4.4×10^{-5}
$Pr_{0.8}Sr_{0.2}Co_{0.2}Fe_{0.8}O_3$	12.8	800	76	1.5×10^{-3}

1.2.3.4 Interconnect and sealing materials

The main function of interconnect is to conduct electrons to the external circuit. The interconnect material should have high electronic conductivity, be thermally stable at the high SOFC operating temperatures, and be chemically stable at extreme partial pressures. Cr alloys, $LaSrCrO_3$ or nickel, stainless steel or Inconel are the most commonly used interconnect material [103] [104] [105].

A good seal is required to prevent mixing of fuels and air, and gas leaks. Sealing techniques are more difficult for planar cells than for tubular cells because all surfaces must be sealed. Glassy materials are used for sealing to be able to compensate for the comparison in gas flow. Rigid materials must have the same coefficient of thermal expansion.

1.2.4 Commercial status of solid oxide fuel/electrolyzer cells

Currently, many companies around the world are manufacturing SOFC or SOEC systems, stacks or cells, for instance Ceres power (U.K.), Bloom Energy (U.S.), Convion (Finland), AVI (Austria), AISIN (Japan), SOLIDpower (Italy), Bosch (Germany), Fuelcell Energy, Inc (U.S.), Elcogen (Estonia), Sunfire GmbH (Germany) [106], Fiaxell (Switzerland), Sylfen (France), SRT microcéramique (France) [107]. As shown in the Figure 1.17 and Figure *1.18*, the market of SOFCs is progressing exponentially.

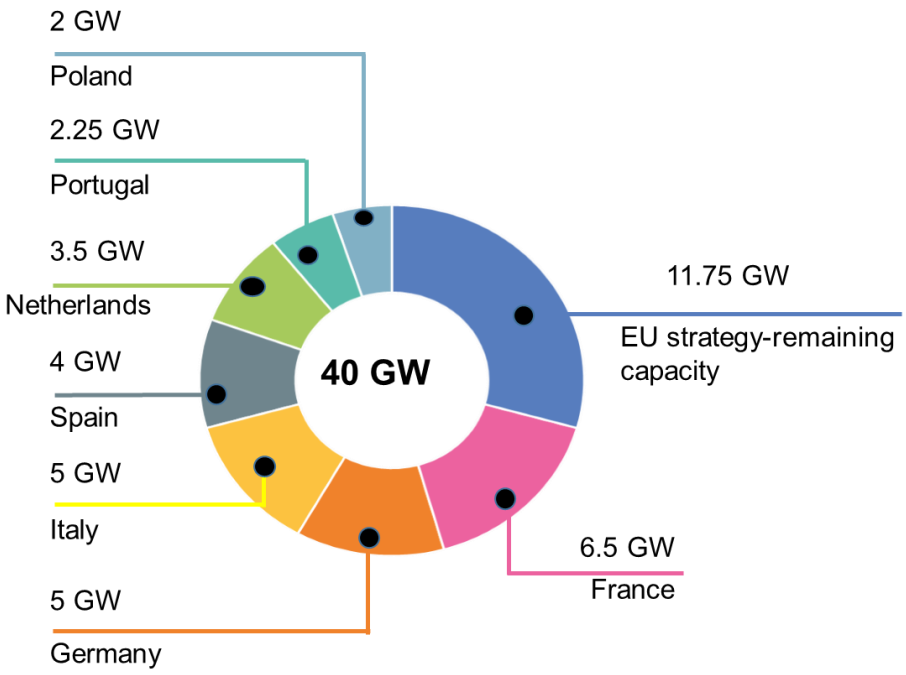

Figure 1.16. Expected electrolyzer installation of highest hydrogen investor countries (adapted from IRENA 2021) [34]. France, Germany, Italy, Spain Netherlands account for the largest hydrogen production.

The market share at this time is mainly used for commercial, military, and spacecraft applications, and is developing quickly. With the European hydrogen strategy , the plan is install 40 GW of electrolyzers by 2030 [34] (Figure 1.16). Worldwide installed hydrogen electrolyzer capacity is expected to increase from 20 GW in 2020 (IRENA, 2020)[108] to 80 GW in 2030 (Hydrogen Council, 2021) and 1–3 TW in 2050 if a CO_2 net-zero emission scenario is targeted [50].

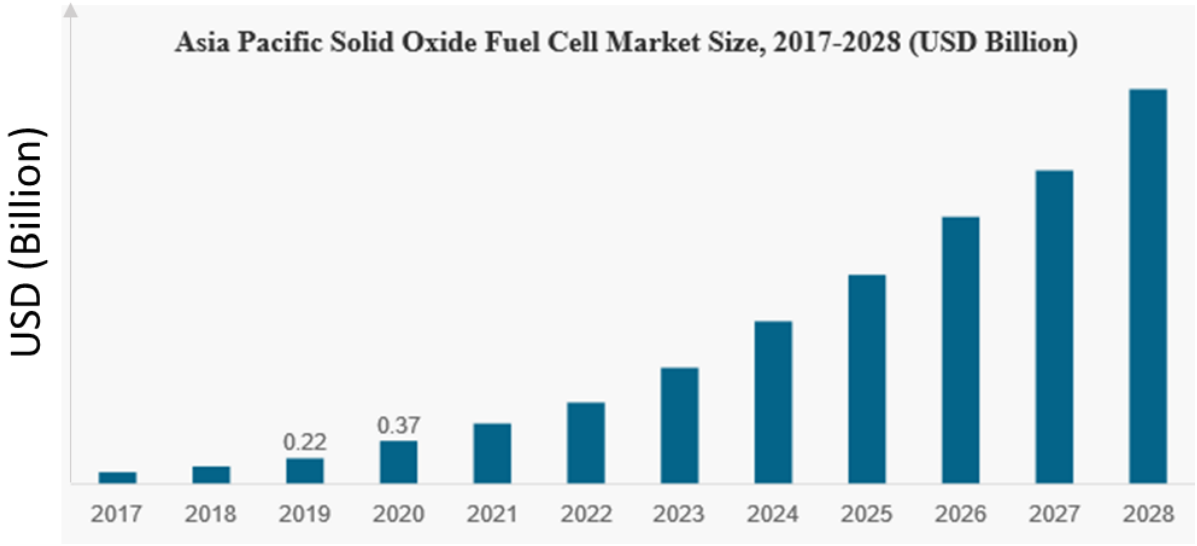

Figure 1.17. The investment progress of Solid oxide fuel cell from 2017 up to 2028[106].

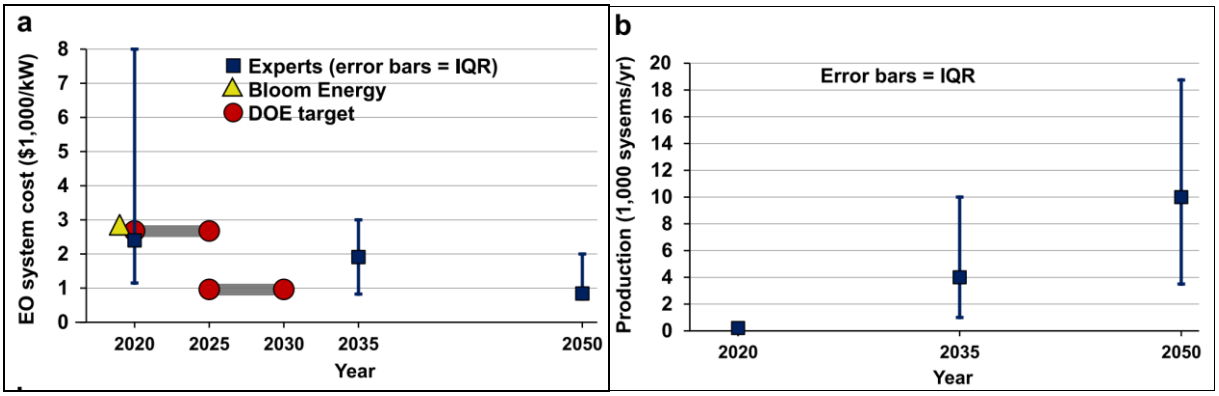

Figure 1.18 Experts' assessments of 250 kW EO system cost (2018 USD/kW) and production volume. Squares and error bars represent medians and IQRs, respectively, of best estimates. (a) Equipment cost. DOE's 2020–2025 and 2025–2030 targets are $2,676/kW and $963/kW, respectively. (b) Production volume (taken from [109].

1.3 End of life management of SO systems and product life cycle concept

As a result of population growth and advanced technology, the demand for natural resources has quadrupled in the last 50 years. However, our resources are limited [110]. We must use them properly and keep the next generation in mind [110]. In order to meet the increasing demand for economic, environmental and social benefits, the implementation of wise treatment of end of life

products is urgently needed. The ultimate solution for the wise use of these elements is to recycle and reuse them. Root of failure and waste generation for SOCs system are presented below.

1.3.1 Challenges in component materials degradation

A high operating temperature of an SOFC is required to have good electrode reaction kinetics and electrolyte conductivity. However, it faces an accelerated chemical and mechanical degradation of materials [111] [112] due to inter diffusion and formation of insulating phase ($SrZrO_3$ layer at the air electrode/electrolyte interface). Nickel grain coarsening leading to formation of micro cracks between Ni/YSZ particles air electrode and GDC delamination are also an other causes of failurity [113].

In addition, evaporation of chromium oxide from the stainless steel components are then act as a catalytic poison on the air electrodes. Theses degradations cause the overall reduction of electrochemical reactive sites or even the complete failure of the cell [114] [115] [83] [116] (Figure 1.19 and Figure *1.20*) which has immediate consequences for the consumption of critical raw materials and waste landfills.

The critical goal for commercializing solid oxide systems is ensuring that they are competitive with other electrolyser/power generation technologies. For instance, under the legislation for stationary power generation products, the operating time must be 100,000 hours[56] or more, with a degradation rate of less than 0.2 % per 1,000 hours (equivalent to 20% of performance decrease at the end of life). J. Schefold et al. [117] also investigated the evolution of cell voltage during the steady state electrolysis test ON and the voltage drop is about 3.8 mV/kh (Figure 1.21).

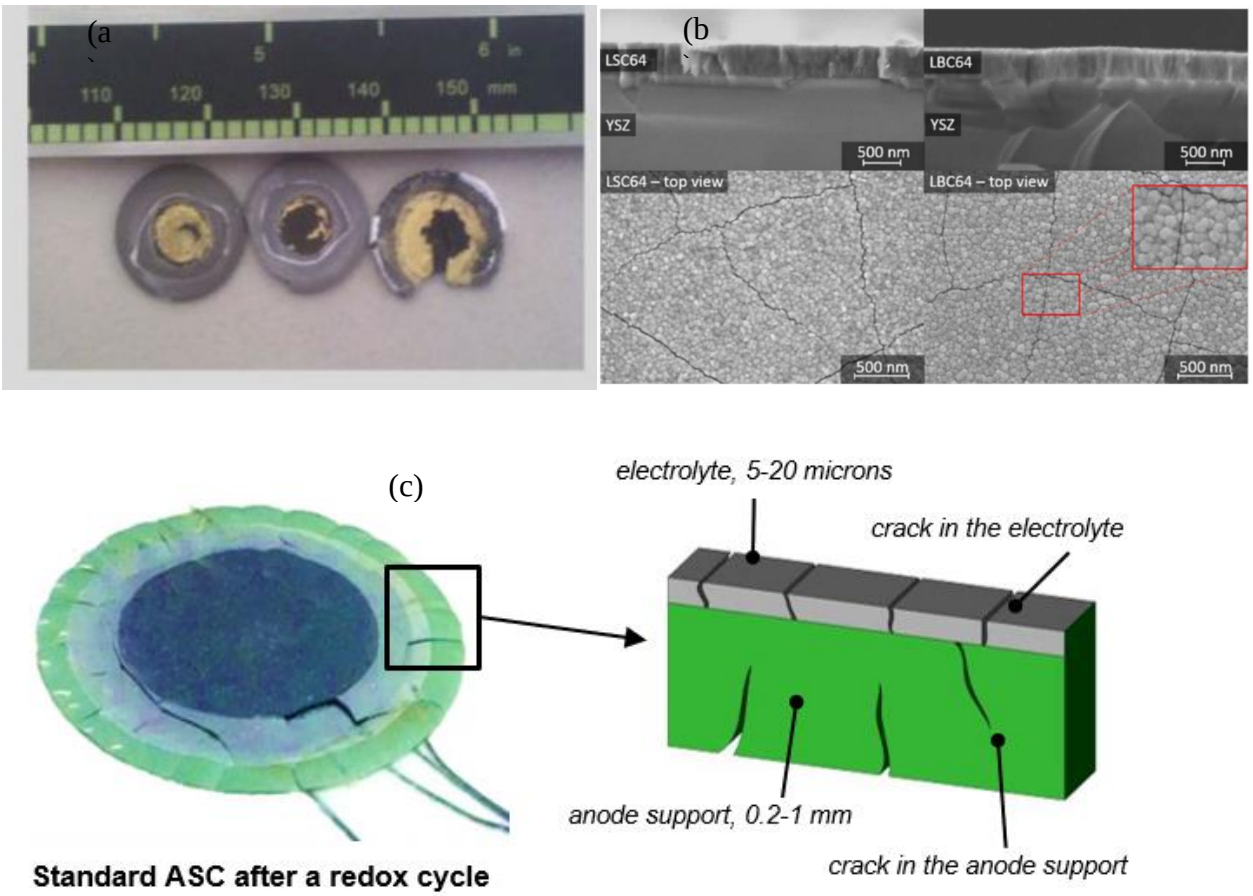

Figure 1.19. (a) Ni-YSZ|YSZ|LSM anode supported button cell after 120 h of operation in 50 ppm H_2S sour fuel. Reprinted from Cao et al., [118] Copyright 2020. Royal Society of Chemistry (b) SEM images of LSC crack formation driven by different thermal expansion coefficient [119], (LSC_{64} = 20.5 · 10^{-6} K^{-1}[120], and (YSZ = 10.8 10^{-6} K^{-1}[40]) (c) Illustration of the component failures of SOFCs from Fiaxell fuel cell technology[121].

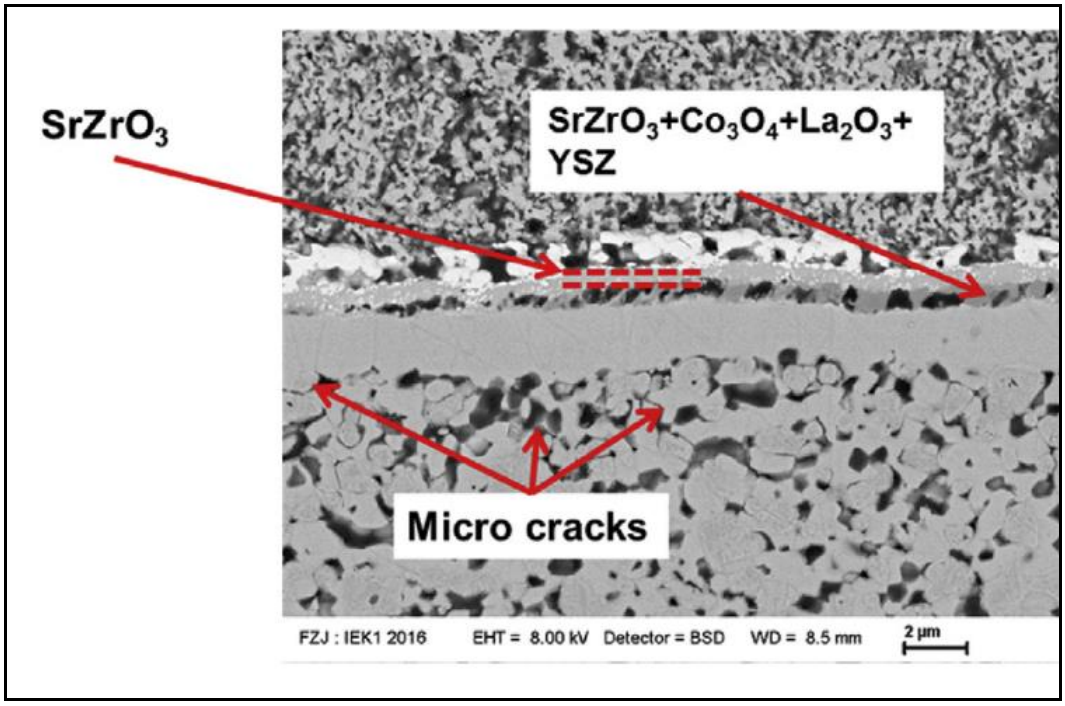

Figure 1.20. Representation of Backscattered Electron Detector mages of the degradation of the cells by nickel coarsening, formation of microcracks and $SrZrO_3$ layers, delamination of the air electrode and GDC (taken form Yan et al.[113]).

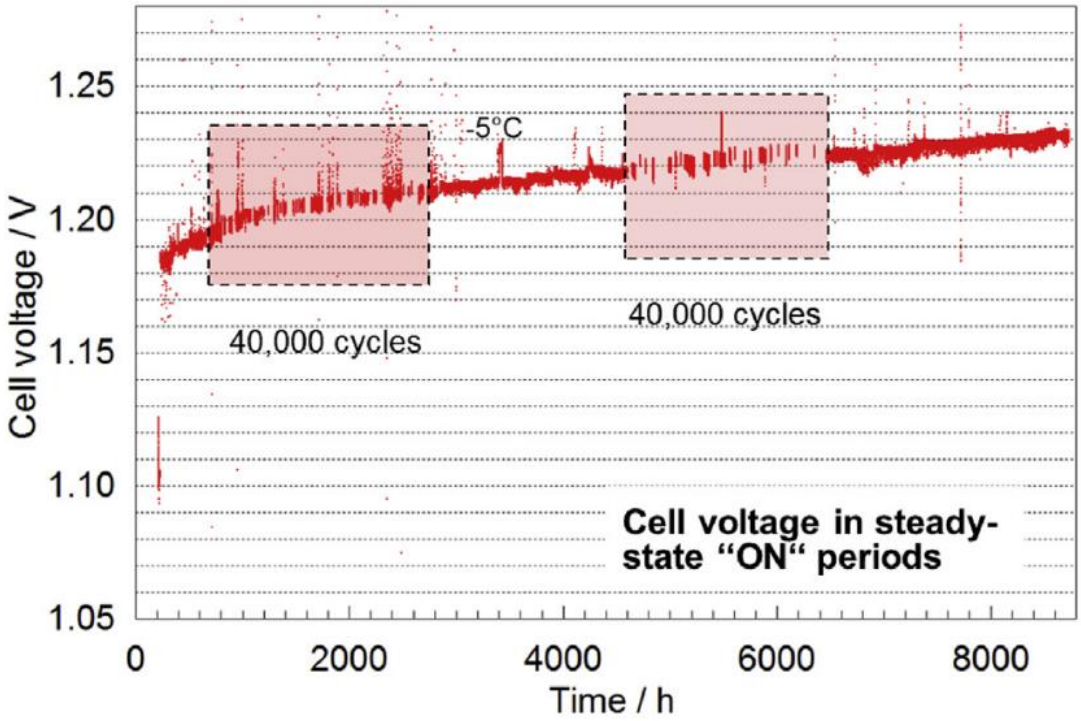

Figure 1.21 Cell-voltage evolution during the electrolysis test in the steady state ON periods [117].

1.3.2 The need for waste reduction and end-life product managements of SOCs

The primary solution to reduce production waste may be for example, to increase process efficiency, select high-purity materials, and avoid overproduction. The second method of waste reduction is effective recycling and recovery of products.

Even if few studies have been published on the environmental effects of SOFCS, their production contribute to the emission associated to the energy sector. The first study was conducted by Zapp et al. in 1996 [122] and pointed out the need for waste management of SOFCs after operation and disassembly. Five years later, Karakoussis et al. (2001) [123] pointed out the need to invest in recycling and reusing materials at the end of their life in order to reduce the environmental impacts associated with material supply. Pint et al. studied the end life scenario of fuel cell materials [124].

Four years later, after Karakoussi's work, Baratto et al. (2005) [125] reported that a full life cycle assessment was not possible due to lack of data. Wincewicz and Cooper, in 2005 [126] studied the alternative material and manufacturing of SOFC stack, for future Life Cycle Assessment (LCA) studies.

In 2011, Ellen focused on the end life management of SOFCs materials[127]. Valente et al.[128] reviewed the overall existing technologies for the recycling of valuable materials from solid oxide fuel cell, but there is no end life process available for SOFCs. Férriz et al.[129] proposed an overall classification of Fuel Cells and Hydrogen (FCH) materials based on related hazardousness, scarcity and cost. Kamiya et al.[130] also studied the possibilities of the disintegration of pure YSZ-based sintered ceramics to recover the fine zirconia powders. In 2022, the group of N.H. Menzler from Julich (Germany) [50] has published an interesting review paper giving a comprehensive overview of possible recycling routes for solid oxide cells.

Khalid et.al [97] studied LCA for the fabrication of SOFCs. According to the materials inventory of this study, for 1MW of SOFC, about 1136 kg of nickel (70 wt.% of fuel electrode is nickel), 411kg of YSZ and 98 kg of LSM, corresponding to respective percentages of 69 wt.%, 25wt.%YSZ, 6 wt.% of LSM are used (Table 1. 3). In general, most commercially available SOFCs materials contain about 50 wt.% of NiO.

Table 1. 3. Lists of the material inventory for the fabrication of SOFC single cell (without bi-polar plates and sealings) and quantity required to generate a SOFC equivalent to 1 MW [97].

Materials description	Materials Weight (Kg/MW)
Ni from anode (Ni 70% wt)	1116
YSZ from anode (YSZ 30% wt)	332
YSZ from electrolyte (YSZ)	39
LSM from cathode (LSM)	78
Anode/electrolyte interlayer (NiO 50% vol)	20
Anode/electrolyte interlayer (YSZ 50% vol)	20
Electrolyte/cathode interlayer (LSM 50% vol)	20
Electrolyte/cathode interlayer (YSZ 50% vol)	20

For the giga size production and after the end of life of SOC, large amounts of waste are expected. At the same time, mineral resources are depleted. Major issues in terms of waste landfills and compliance with future regulations for end-of-life disposal of SOC products must be considered prior to commercialization [131] [132] [133].

1.3.3 End of life product regulation and circular economy

The concept of Extended Producer Responsibility (EPR) is a legislation that makes producers responsible of their end-of-life products. It includes recovery of end-of-life materials, removal of components containing hazardous substances (de-pollution) and wastes treatment [134] [135] [136] [137] [138].

According to studies, EU produce 6.5 Million tons per year of waste electrical and electronic equipment (WEEE) [139] are generated and a strict EPR policies is employed for this sector products . Up to now, there is currently no specific policy framework regulating the End-of-Life (EoL) of SOCs [140] [127].

Nevertheless, considering the future regulation in advances is important. Stationary power plants are considered to be very large and require large investments requiring a minimal lifetime of about 20-25 years[141]. However, due to material deterioration or failure, the life expectancy of large stationary power plant is less than 25 years. In contrast to these regulations, current SOCs are also designed for a 40,000 hrs lifetime and need consequent repair or/and replacement every 4 to 5 years. These failures, repairs and maintenance of device result in more critical raw material

consumption and landfill waste. However, the wise use of limited resources and environmental protection are current issues.

1.3.4 Recycling of end life products of solid oxide fuel and electrolyzers cells materials

Wastes of SOCs component materials contain critical raw materials. Major sources of waste in the SOFC industry include: End-of-life product waste[142], industrial waste (during manufacturing), or cell failure during operation. As said previously, nickel is one of the major component of SOFC's industry, whereas most nickel-bearing minerals (laterite accounts for 60-70%[143] is the world's nickel reserves) have only a low nickel content of 0.6-1.8% Ni[144] [145] [146]. However, there is high demand of Nickel or in compound form for many industrial applications such as surface finishing, automotive, aerospace, electronics, glass and ceramics, batteries, catalysts, fertilizers, pigments etc. [147].

Zirconium-bearing mineral is zircon sand, which is limited in occurrence and found mainly in Australia and South Africa [148]. The mineral reserves of Murray Zircon, South Australia, contain 3.1% valuable Heavy Minerals (HM), containing itself only 17.4% zircon ($ZrSiO_4$). Overall, the total concentration of zircon in the mineral reserves represents only 0.5 wt.% of zircon [149]. If the chemical content of zircon in the valuable heavy metal from the South African zircon mining projects of Southern Mining Corporation is higher, it represents nevertheless only 9 wt.% [150].

Zirconium or in its compound form is also applicable in many areas such as in nuclear power generation applications which account for more than 90% of commercial zirconium production. Other application in the form of compound or in alloy form include surgical appliances, explosive primers, rayon spinneret, lamp filaments, low temperature superconducting magnets, gemstones, laboratory crucibles, furnace linings for metallurgical, ceramics and glass refractory applications [151].

One of the most critical raw materials applied in SOCs is cobalt. The Democratic Republic of the Congo supplies about 70% of the world's cobalt requirements. The cobalt bearing ore content of less than 0.5% and often less than 0.1% [152] [153] [154]. Nevertheless, there is still a high demand for cobalt for catalysts, batteries, supperalloys, magnets, steel alloys, carbides and tools.

As Khalid et.al [97] noted in their inventory of SOFC component composition using nickel as an example (Table 1. 3), the Ni content of final SOFC end life products would be about 25 to 40 times higher than that of primary nickel-bearing minerals. Because of the high Ni content of SOFC waste, the processes of mining, concentration, and beneficiation can be skipped (Figure 1.22 and Figure *1.23*). Due to this advantage of reducing the mining steps, the use of these end life products of SOCs could consume less energy and be more cost effective than the extraction of primary materials. The cost of extracting primary materials is increased by the difficulties of mining, inaccessible mining sites, geopolitical concerns, and geographic hazards [155].

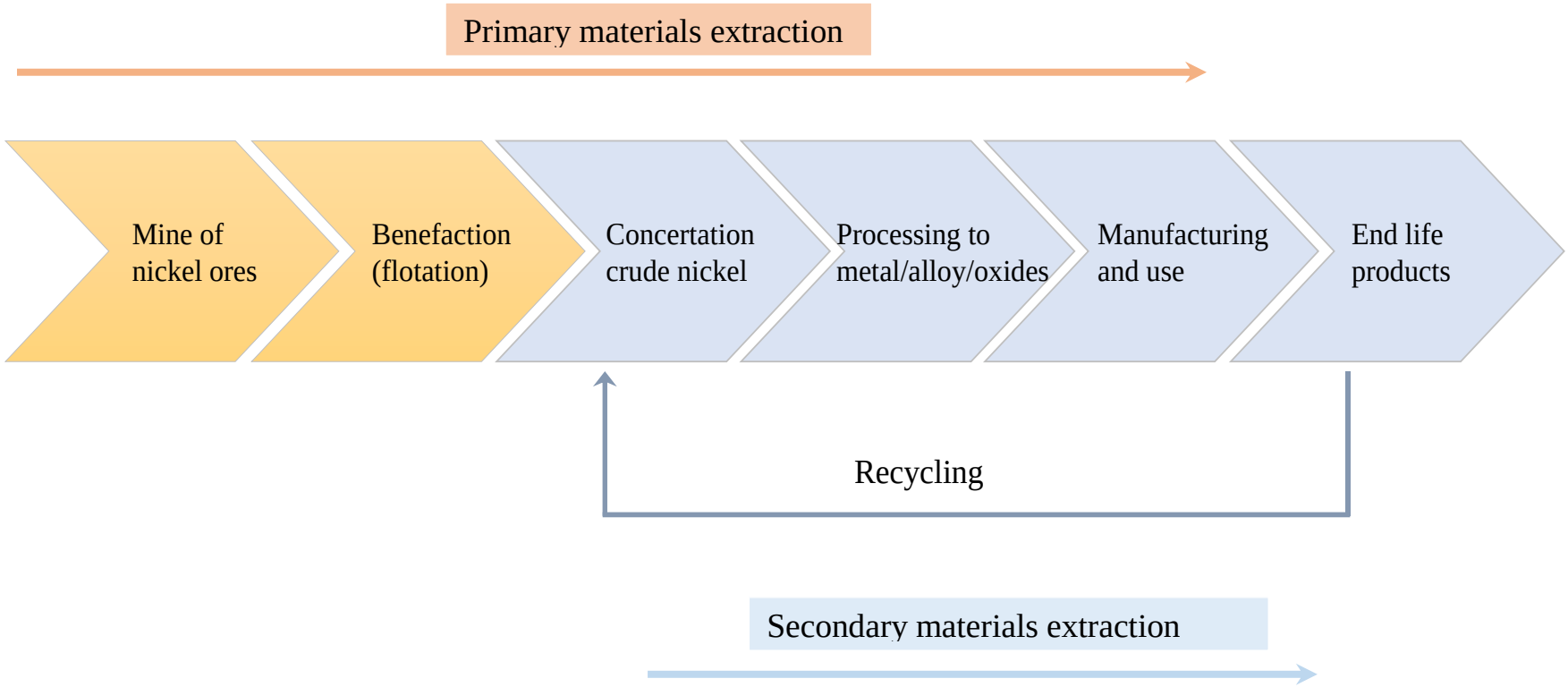

Figure 1.22. Illustration of comparison of primary nickel mining and recycling from end life products of SOCs.

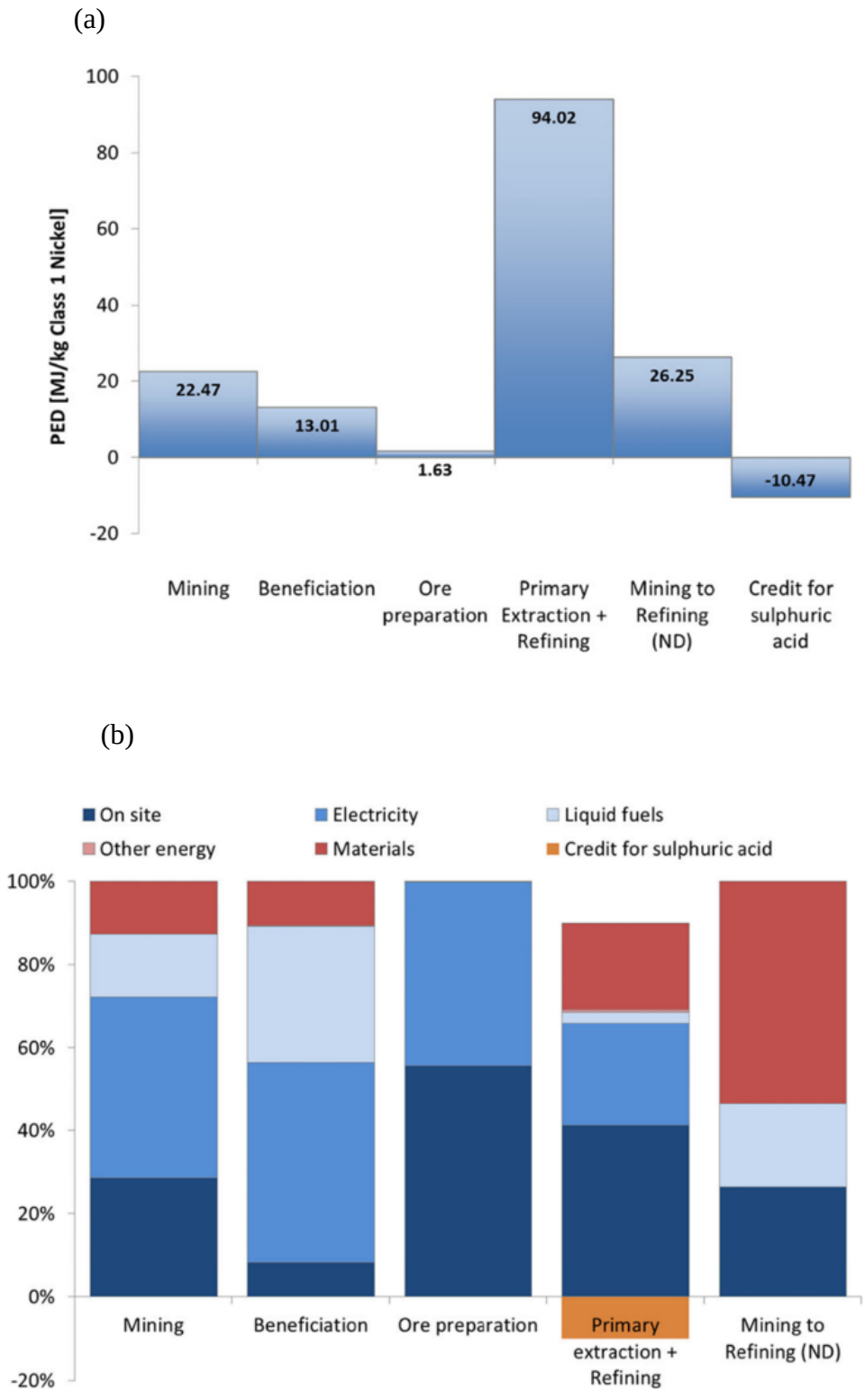

Figure 1.23. (a) Primary energy demand (PED) of 1 kg nickel mining, (b) relative contribution of consumption sources to the primary energy demand (PED) of nickel mining (adapted from Mistry et al. [155].

Comprehensive studies of life cycle assessment (LCA) for SOFC has been done by S. Sarneret.al [50]. Table 1.4 shows advantages of reducing the environmental impact of manufacturing a 150-kW SOEC using recycled material compared to non-recycled material. Depending on the environmental impact category, the most important conclusions are that savings range from 32% to 83%. Indeed, the Ecotoxicity and human toxicity has notable reductions of 83 and 80% respectively. Recycling materials on the resource use, mineral and metals impact category has also a significant benefit of 64% over non recycled one. Reducing the need for additional raw materials by using recycled materials reduces environmental impact and saves materials and energy, which in turn reduces costs.

Table 1.4 Environmental impacts of 150-kW SOEC construction without and with material recycling (avoided burden approach) [50].

Impact category	Abbreviation	Unit	Impact w/o recycling (I^n)	Impact with use of recycled material (I^m)	Benefit through recycling [%] $= \left(\frac{1 - I^m}{I^n}\right)$
Acidification	AP	mole of H^+ eq.	79.6	18.3	77
Climate change – total	GWP	kg CO_2 eq.	6.76	3.02	55
Ecotoxicity, freshwater – total	$ET_{f.w.}$	CTUe	1780000	311000	83
Eutrophication, freshwater	$EP_{f.w.}$	kg P eq.	4.94	3.34	32
Eutrophication, marine	EP_{marine}	kg N eq.	14.5	3.77	74
Human toxicity, cancer – total	HTP_{cancer}	CTUh	$4.41E^{-05}$	$8.66E^{-06}$	80
Ozone depletion	ODP	kg CFC-11 eq.	$3.80E^{-04}$	$1.40E^{-04}$	64
Particulate matter	PM	disease incidences	$5.70E^{-04}$	$1.20E^{-04}$	80
Photochemical ozone Formation, human health	$POC_{Phuman\ health}$	kg NO_x eq.	30.4	16.7	45
Resource use, fossil	FD	[MJ]	113000	50800	55
Resource use, mineral and metals	ADP	kg Sb eq.	0.151	0.0548	64
Water use.	Water	m^3 world eq.	3.35	1.19	64

Conclusions and Objectives of the thesis

This chapter is devoted to introducing the context of the hydrogen economy. Hydrogen as a chemical energy carrier can be produced from water using decarbonized electricity and will play an important role in decarbonizing transportation (especially heavy vehicles), homes, and buildings. It can also be used to decarbonize industry by replacing carbonaceous hydrogen as a chemical feedstock.

Among different electrochemical systems solid oxide based electrolysers and fuel cells (SOEC and SOFC)s, are the efficient way of high hydrogen utilization. The principle of operation, the state of the art in electrode materials and design, and the physical phenomena of SOCs system are presented.

SOCs system contains significant amounts of critical raw materials. In this regard, the technology will face the major challenge of mass production of feedstock and waste landfills. However, the mineral resources on our planet are limited. This leads to a rapid depletion of minerals, which requires a wise management of materials. The extraction of ore minerals is expensive and requires a lot of energy. It also leads to severe soil degradation, deforestation, erosion and pollution. Recycling materials can avoid the geographical dependence of mining and reduce the mining steps, as the end products have higher chemical grade than the primary minerals.

Therefore, the main objective of this work is to develop practical methods for separating and recovering the ceramic components of SOCs waste products. In particular, it is in our interest to:

a) Find an effective strategies for recycling anode-supported SOC ceramic materials with the air electrode ($La_{1-x}Sr_xCoO_3$), nickel oxide (NiO) which accounts for about 50% of the cell weight, and yttrium-stabilized zirconia (YSZ) coming from both the fuel electrode and the electrolyte.
b) Characterize the recovered ceramic powder materials from end life solid oxide cells.
c) Compare the properties of these recovered powders with those of powders from the industrial shelves and establish possible correlations.
d) Investigate the influence of the presence of impurities.
e) Analyse the cost estimation and the environmental impacts of proposed recycling protocols.

References

[1] J. Laurencin and J. Mougin, "High-temperature steam electrolysis," *Hydrog. Prod.*, vol. 1, 2015, [Online]. Available: https://onlinelibrary.wiley.com/doi/epdf/10.1002/9783527676507.ch1

[2] L. Duclos *et al.*, "Closing the loop: life cycle assessment and optimization of a PEMFC platinum-based catalyst recycling process," *Green Chem.*, vol. 22, no. 6, pp. 1919–1933, 2020.

[3] R. Granados-Fernández, M. A. Montiel, S. Díaz-Abad, M. A. Rodrigo, and J. Lobato, "Platinum Recovery Techniques for a Circular Economy," *Catalysts*, vol. 11, no. 8, p. 937, Jul. 2021, doi: 10.3390/catal11080937.

[4] A. Züttel, "Introduction," in *Hydrogen as a Future Energy Carrier*, 1st ed., A. Züttel, A. Borgschulte, and L. Schlapbach, Eds. Wiley, 2008, pp. 1–6. doi: 10.1002/9783527622894.ch1.

[5] "Hydrogen from renewable power: Technology outlook for the energy transition," p. 52.

[6] D. Slanger, "Run on Less with Hydrogen Fuel Cells," *RMI*, Oct. 02, 2019. https://rmi.org/run-on-less-with-hydrogen-fuel-cells/ (accessed Aug. 17, 2022).

[7] M. Hirscher, Ed., *Handbook of Hydrogen Storage: New Materials for Future Energy Storage*. Weinheim, Germany: Wiley-VCH Verlag GmbH & Co. KGaA, 2010. doi: 10.1002/9783527629800.

[8] S. Li, Q. Kang, J. Baeyens, H. L. Zhang, and Y. M. Deng, "Hydrogen Production: State of Technology," *IOP Conf. Ser. Earth Environ. Sci.*, vol. 544, no. 1, p. 012011, Jul. 2020, doi: 10.1088/1755-1315/544/1/012011.

[9] D. Cecere, E. Giacomazzi, and A. Ingenito, "A review on hydrogen industrial aerospace applications," *Int. J. Hydrog. Energy*, vol. 39, no. 20, pp. 10731–10747, Jul. 2014, doi: 10.1016/j.ijhydene.2014.04.126.

[10] R. Ramachandran, "An overview of industrial uses of hydrogen," *Int. J. Hydrog. Energy*, vol. 23, no. 7, pp. 593–598, Jul. 1998, doi: 10.1016/S0360-3199(97)00112-2.

[11] H. Zhang, L. Wang, J. Van herle, F. Maréchal, and U. Desideri, "Techno-economic comparison of green ammonia production processes," *Appl. Energy*, vol. 259, p. 114135, Feb. 2020, doi: 10.1016/j.apenergy.2019.114135.

[12] P. Galindo Cifre and O. Badr, "Renewable hydrogen utilisation for the production of methanol," *Energy Convers. Manag.*, vol. 48, no. 2, pp. 519–527, Feb. 2007, doi: 10.1016/j.enconman.2006.06.011.

[13] A. K. Sayah and A. K. Sayah, "Wind-hydrogen utilization for methanol production: An economy assessment in Iran," *Renew. Sustain. Energy Rev.*, vol. 15, no. 8, pp. 3570–3574, Oct. 2011, doi: 10.1016/j.rser.2011.05.013.

[14] D. Bellotti, M. Rivarolo, L. Magistri, and A. F. Massardo, "Feasibility study of methanol production plant from hydrogen and captured carbon dioxide," *J. CO2 Util.*, vol. 21, pp. 132–138, Oct. 2017, doi: 10.1016/j.jcou.2017.07.001.

[15] G. Zang, P. Sun, A. Elgowainy, and M. Wang, "Technoeconomic and Life Cycle Analysis of Synthetic Methanol Production from Hydrogen and Industrial Byproduct CO_2," *Environ. Sci. Technol.*, vol. 55, no. 8, pp. 5248–5257, Apr. 2021, doi: 10.1021/acs.est.0c08237.

[16] N. Monnerie, P. G. Gan, M. Roeb, and C. Sattler, "Methanol production using hydrogen from concentrated solar energy," *Int. J. Hydrog. Energy*, vol. 45, no. 49, pp. 26117–26125, Oct. 2020, doi: 10.1016/j.ijhydene.2019.12.200.

[17] "Renewable Methanol," *METHANOL INSTITUTE*. https://www.methanol.org/renewable/ (accessed Sep. 26, 2022).

[18] W. Liu, H. Zuo, J. Wang, Q. Xue, B. Ren, and F. Yang, "The production and application of hydrogen in steel industry," *Int. J. Hydrog. Energy*, vol. 46, no. 17, pp. 10548–10569, Mar. 2021, doi: 10.1016/j.ijhydene.2020.12.123.

[19] A. Toktarova, L. Göransson, and F. Johnsson, "Design of Clean Steel Production with Hydrogen: Impact of Electricity System Composition," *Energies*, vol. 14, no. 24, p. 8349, Dec. 2021, doi: 10.3390/en14248349.

[20] A. Bhaskar, R. Abhishek, M. Assadi, and H. N. Somehesaraei, "Decarbonizing primary steel production : Techno-economic assessment of a hydrogen based green steel production plant in Norway," *J. Clean. Prod.*, vol. 350, p. 131339, May 2022, doi: 10.1016/j.jclepro.2022.131339.
[21] R. R. Wang, Y. Q. Zhao, A. Babich, D. Senk, and X. Y. Fan, "Hydrogen direct reduction (H-DR) in steel industry—An overview of challenges and opportunities," *J. Clean. Prod.*, vol. 329, p. 129797, Dec. 2021, doi: 10.1016/j.jclepro.2021.129797.
[22] J. Astier, J. Krug, and Y. Depressigny, "Technico-economic potentialities of hydrogen utilization for steel production," *Int. J. Hydrog. Energy*, vol. 7, no. 8, pp. 671–679, 1982, doi: 10.1016/0360-3199(82)90192-6.
[23] J. Gretz, W. Korf, and R. Lyons, "Hydrogen in the steel industry," *Int. J. Hydrog. Energy*, vol. 16, no. 10, pp. 691–693, 1991, doi: 10.1016/0360-3199(91)90193-M.
[24] L. Forsythe, "Hydrogen Applications in Industry," *WHA International, Inc.*, Sep. 29, 2020. https://wha-international.com/hydrogen-in-industry/ (accessed Nov. 02, 2022).
[25] I. Ghosh, "A Global Breakdown of Greenhouse Gas Emissions by Sector." November, 2020.
[26] "IPCC issues Special Report on Global Warming of 1.5 °C," Nov. 14, 2018. https://public.wmo.int/en/resources/bulletin/ipcc-issues-special-report-global-warming-of-15-%C2%B0c (accessed Sep. 08, 2022).
[27] R. Newell, D. Raimi, S. Villanueva, and B. Prest, "Global Energy Outlook 2021: Pathways from Paris," p. 46.
[28] "EHB_Analysing-the-future-demand-supply-and-transport-of-hydrogen_June-2021_v3.pdf."
[29] International Energy Agency, *Global Hydrogen Review 2021*. OECD, 2021. doi: 10.1787/39351842-en.
[30] S. C. Ameta and R. Ameta, Eds., "Organic Photovoltaic Cells," in *Solar Energy Conversion and Storage*, 0 ed., CRC Press, 2015, pp. 68–97. doi: 10.1201/b19148-9.
[31] A. Besha, M. T. Tsehaye, G. Tiruye, A. Gebreyohannes, A. Assayie, and R. A. Tufa, "Deployable Membrane-Based Energy Technologies: the Ethiopian Prospect," *Sustainability*, vol. 12, p. 8792, Oct. 2020, doi: 10.3390/su12218792.
[32] K. G. dos Santos *et al.*, "Hydrogen production in the electrolysis of water in Brazil, a review," *Renew. Sustain. Energy Rev.*, vol. 68, pp. 563–571, Feb. 2017, doi: 10.1016/j.rser.2016.09.128.
[33] N. A. Kelly, "Hydrogen production by water electrolysis," in *Advances in Hydrogen Production, Storage and Distribution*, Elsevier, 2014, pp. 159–185. doi: 10.1533/9780857097736.2.159.
[34] "Green hydrogen supply: A guide to policy making," p. 64.
[35] A. Ursua, L. M. Gandia, and P. Sanchis, "Hydrogen Production From Water Electrolysis: Current Status and Future Trends," *Proc. IEEE*, vol. 100, no. 2, pp. 410–426, Feb. 2012, doi: 10.1109/JPROC.2011.2156750.
[36] A. Brisse, J. Schefold, and M. Zahid, "High temperature water electrolysis in solid oxide cells," *Int. J. Hydrog. Energy*, vol. 33, no. 20, pp. 5375–5382, Oct. 2008, doi: 10.1016/j.ijhydene.2008.07.120.
[37] M. Ni, M. Leung, and D. Leung, "Technological development of hydrogen production by solid oxide electrolyzer cell (SOEC)," *Int. J. Hydrog. Energy*, vol. 33, no. 9, pp. 2337–2354, May 2008, doi: 10.1016/j.ijhydene.2008.02.048.
[38] n-tv NACHRICHTEN, "Aus Wind, Wasser und CO2 wird Öko-Sprit," *n-tv.de*. https://www.n-tv.de/auto/Aus-Wind-Wasser-und-CO2-wird-Oko-Sprit-article13979336.html (accessed Oct. 24, 2022).
[39] H. Koide, "Properties of Ni/YSZ cermet as anode for SOFC," *Solid State Ion.*, vol. 132, no. 3–4, pp. 253–260, Jul. 2000, doi: 10.1016/S0167-2738(00)00652-4.
[40] A. J. Jacobson, "Materials for Solid Oxide Fuel Cells," *Chem. Mater.*, vol. 22, no. 3, pp. 660–674, Feb. 2010, doi: 10.1021/cm902640j.
[41] M. Hubert *et al.*, "Role of microstructure on electrode operating mechanisms for mixed ionic electronic conductors: From synchrotron-based 3D reconstruction to electrochemical modeling," *Solid State Ion.*, vol. 294, pp. 90–107, Oct. 2016, doi: 10.1016/j.ssi.2016.07.001.

[42] C. Sun, R. Hui, and J. Roller, "Cathode materials for solid oxide fuel cells: a review," *J. Solid State Electrochem.*, vol. 14, no. 7, pp. 1125–1144, Jul. 2010, doi: 10.1007/s10008-009-0932-0.
[43] A. J. Jacobson, "Materials for Solid Oxide Fuel Cells," *Chem. Mater.*, vol. 22, no. 3, pp. 660–674, Feb. 2010, doi: 10.1021/cm902640j.
[44] F. Tietz, "Components manufacturing for solid oxide fuel cells," *Solid State Ion.*, p. 9, 2002.
[45] G. Kaur, "Solid Oxide Fuel Cell Components," *Switz. Springer*, 2016.
[46] R. M. Ormerod, "Solid oxide fuel cells," *Chem. Soc. Rev.*, vol. 32, no. 1, pp. 17–28, Dec. 2003, doi: 10.1039/b105764m.
[47] N. Laosiripojana, W. Wiyaratn, W. Kiatkittipong, A. Arpornwichanop, A. Soottitantawat, and S. Assabumrungrat, "Reviews on Solid Oxide Fuel Cell Technology," *Eng. J.*, vol. 13, no. 1, pp. 65–84, Feb. 2009, doi: 10.4186/ej.2009.13.1.65.
[48] C. Song, "Fuel processing for low-temperature and high-temperature fuel cells Challenges, and opportunities for sustainable development in the 21st century," *Catal. Today*, p. 34, 2002.
[49] N. Mahato, A. Banerjee, A. Gupta, S. Omar, and K. Balani, "Progress in material selection for solid oxide fuel cell technology: A review," *Prog. Mater. Sci.*, vol. 72, pp. 141–337, Jul. 2015, doi: 10.1016/j.pmatsci.2015.01.001.
[50] S. Sarner, A. Schreiber, N. H. Menzler, and O. Guillon, "Recycling Strategies for Solid Oxide Cells," *Adv. Energy Mater.*, p. 2201805, Jul. 2022, doi: 10.1002/aenm.202201805.
[51] C. Lenser *et al.*, "Solid oxide fuel and electrolysis cells," in *Advanced Ceramics for Energy Conversion and Storage*, Elsevier, 2020, pp. 387–547. doi: 10.1016/B978-0-08-102726-4.00009-0.
[52] J.-C. Njodzefon, D. Klotz, A. Kromp, A. Weber, and E. Ivers-Tiffée, "Electrochemical modeling of the current-voltage characteristics of an SOFC in fuel cell and electrolyzer operation modes," *J. Electrochem. Soc.*, vol. 160, no. 4, p. F313, 2013.
[53] S. Biswas, S. S. Rathore, A. P. Kulkarni, S. Giddey, and S. Bhattacharya, "A Theoretical Study on Reversible Solid Oxide Cells as Key Enablers of Cyclic Conversion between Electrical Energy and Fuel," *Energies*, vol. 14, no. 15, Art. no. 15, Jan. 2021, doi: 10.3390/en14154517.
[54] F. Coutelieris, "The importance of the fuel choice on the efficiency of a solid oxide fuel cell system," *J. Power Sources*, vol. 123, no. 2, pp. 200–205, Sep. 2003, doi: 10.1016/S0378-7753(03)00559-7.
[55] A. B. Stambouli and E. Traversa, "Solid oxide fuel cells (SOFCs): a review of an environmentally clean and efficient source of energy," *Renew. Sustain. Energy Rev.*, vol. 6, no. 5, pp. 433–455, Oct. 2002, doi: 10.1016/S1364-0321(02)00014-X.
[56] Q. Fang, L. Blum, and D. Stolten, "Electrochemical Performance and Degradation Analysis of an SOFC Short Stack Following Operation of More than 100,000 Hours," *J. Electrochem. Soc.*, vol. 166, no. 16, pp. F1320–F1325, Jan. 2019, doi: 10.1149/2.0751916jes.
[57] J. L. Sheean, "The beginnings of electrochemical activities," *J. Chem. Educ.*, vol. 7, no. 1, p. 33, 1930.
[58] J. T. Stock, "THE PATHWAY TO THE LAWS OF ELECTROLYSIS," Bulletin for the History of Chemistry, pp. 86–92, 1991.
[59] J. Wisniak, "Historical Notes: Electrochemistry and Fuel Cells: The Contribution of William Robert Grove," *Indian J. Hist. Sci.*, vol. 50, no. 4, Aug. 2015, doi: 10.16943/ijhs/2015/v50i4/48318.
[60] "On the Gas Voltaic Battery. Voltaic Action of Phosphorus, Sulphur and Hydrocarbons," p. 13, 2022.
[61] F. Mödinger, "Is Hydrogen a Viable Fuel Alternative for a Traditional Tunnel Brick Kiln?," *Interceram - Int. Ceram. Rev.*, vol. 70, no. 1, pp. 32–37, Apr. 2021, doi: 10.1007/s42411-020-0436-6.
[62] F. Scholz, "Wilhelm Ostwald's role in the genesis and evolution of the Nernst equation," *J. Solid State Electrochem.*, vol. 21, no. 7, pp. 1847–1859, 2017.
[63] N. Gupta and G. D. Yadav, "Solid Oxide Fuel Cell: A Review," vol. 03, no. 06, p. 7.
[64] P. Rane, R. Dubey, D. Rawal, and M. Mandake, "Critical review on fabrication of tubular solid oxide fuel cell," *Int Res J Eng Technol*, 2017.
[65] O. Yamamoto, "Solid oxide fuel cells: fundamental aspects and prospects," *Electrochimica Acta*, vol. 45, no. 15–16, pp. 2423–2435, May 2000, doi: 10.1016/S0013-4686(00)00330-3.

[66] J. H. Joo and G. M. Choi, "Rapid Thermal-Cycling Test Using Thick-Film Electrolyte-Supported Solid Oxide Fuel Cells," *Electrochem. Solid-State Lett.*, vol. 13, no. 3, p. B17, 2010, doi: 10.1149/1.3276698.

[67] S. de Souza, S. J. Visco, and L. C. De Jonghe, 'Reduced-Temperature Solid Oxide Fuel Cell Based on YSZ Thin-Film Electrolyte', J. Electrochem. Soc., vol. 144, no. 3, pp. L35–L37, Mar. 1997, doi: 10.1149/1.1837484.

[68] K. A. Kuterbekov *et al.*, "Classification of Solid Oxide Fuel Cells," p. 22, 2022.

[69] M. Liu *et al.*, "High-performance cathode-supported SOFCs prepared by a single-step co-firing process," *J. Power Sources*, vol. 182, no. 2, pp. 585–588, Aug. 2008, doi: 10.1016/j.jpowsour.2008.04.039.

[70] X. Wang *et al.*, "Numerical modeling of ceria-based SOFCs with bi-layer electrolyte free from internal short circuit: Comparison of two cell configurations," *Electrochimica Acta*, vol. 248, pp. 356–367, Sep. 2017, doi: 10.1016/j.electacta.2017.07.130.

[71] J. D. McCullough and K. N. Trueblood, "The crystal structure of baddeleyite (monoclinic ZrO2)," *Acta Crystallogr.*, vol. 12, no. 7, pp. 507–511, Jul. 1959, doi: 10.1107/S0365110X59001530.

[72] S. Badwal, "Zirconia-based solid electrolytes: microstructure, stability and ionic conductivity," *Solid State Ion.*, vol. 52, no. 1–3, pp. 23–32, May 1992, doi: 10.1016/0167-2738(92)90088-7.

[73] G. M. Wolten, "Diffusionless Phase Transformations in Zirconia and Hafnia," *J. Am. Ceram. Soc.*, vol. 46, no. 9, pp. 418–422, Sep. 1963, doi: 10.1111/j.1151-2916.1963.tb11768.x.

[74] W. M. Kriven, "Possible Alternative Transformation Tougheners to Zirconia: Crystallographic Aspects," *J. Am. Ceram. Soc.*, vol. 71, no. 12, pp. 1021–1030, Dec. 1988, doi: 10.1111/j.1151-2916.1988.tb05786.x.

[75] H. G. Scott, "Phase relationships in the zirconia-yttria system," *J. Mater. Sci.*, vol. 10, no. 9, pp. 1527–1535, Sep. 1975, doi: 10.1007/BF01031853.

[76] C. Viazzi, J.-P. Bonino, F. Ansart, and A. Barnabé, "Structural study of metastable tetragonal YSZ powders produced via a sol–gel route," *J. Alloys Compd.*, vol. 452, no. 2, pp. 377–383, Mar. 2008, doi: 10.1016/j.jallcom.2006.10.155.

[77] J. Kelly and I. Denry, "Stabilized zirconia as a structural ceramic: An overview☆," *Dent. Mater.*, vol. 24, no. 3, pp. 289–298, Mar. 2008, doi: 10.1016/j.dental.2007.05.005.

[78] D. G. Lamas, "X-ray diffraction study of compositionally homogeneous, nanocrystalline yttria-doped zirconia powders," p. 5.

[79] J.-P. Brog, C.-L. Chanez, A. Crochet, and K. M. Fromm, "Polymorphism, what it is and how to identify it: a systematic review," *RSC Adv.*, vol. 3, no. 38, p. 16905, 2013, doi: 10.1039/c3ra41559g.

[80] A. Nakamura and J. B. Wagner, "Defect Structure, Ionic Conductivity, and Diffusion in Yttria Stabilized Zirconia and Related Oxide Electrolytes with Fluorite Structure," *J. Electrochem. Soc.*, vol. 133, no. 8, pp. 1542–1548, Aug. 1986, doi: 10.1149/1.2108965.

[81] J. Zhang, C. Lenser, N. H. Menzler, and O. Guillon, "Comparison of solid oxide fuel cell (SOFC) electrolyte materials for operation at 500 °C," *Solid State Ion.*, vol. 344, p. 115138, Jan. 2020, doi: 10.1016/j.ssi.2019.115138.

[82] Z. Pan, Q. Liu, L. Zhang, X. Zhang, and S. H. Chan, "Effect of Sr Surface Segregation of $La_{0.6}Sr_{0.4}Co_{0.2}Fe_{0.8}O_{3-\delta}$ Electrode on Its Electrochemical Performance in SOC," *J. Electrochem. Soc.*, vol. 162, no. 12, pp. F1316–F1323, 2015, doi: 10.1149/2.0371512jes.

[83] F. Wang *et al.*, "Sr and Zr diffusion in LSCF/10GDC/8YSZ triplets for solid oxide fuel cells (SOFCs)," *J. Power Sources*, vol. 258, pp. 281–289, Jul. 2014, doi: 10.1016/j.jpowsour.2014.02.046.

[84] A. Choudhury, H. Chandra, and A. Arora, "Application of solid oxide fuel cell technology for power generation—A review," *Renew. Sustain. Energy Rev.*, vol. 20, pp. 430–442, Apr. 2013, doi: 10.1016/j.rser.2012.11.031.

[85] S. Primdahl and M. Mogensen, "Oxidation of Hydrogen on Ni/Yttria-Stabilized Zirconia Cermet Anodes," *J. Electrochem. Soc.*, vol. 144, no. 10, pp. 3409–3419, Oct. 1997, doi: 10.1149/1.1838026.

[86] B. Shri Prakash, S. Senthil Kumar, and S. T. Aruna, "Properties and development of Ni/YSZ as an anode material in solid oxide fuel cell: A review," *Renew. Sustain. Energy Rev.*, vol. 36, pp. 149–179, Aug. 2014, doi: 10.1016/j.rser.2014.04.043.
[87] Y. Liu, Z. Shao, T. Mori, and S. P. Jiang, "Development of nickel based cermet anode materials in solid oxide fuel cells – Now and future," *Mater. Rep. Energy*, vol. 1, no. 1, p. 100003, Feb. 2021, doi: 10.1016/j.matre.2020.11.002.
[88] P. A. Connor *et al.*, "Tailoring SOFC Electrode Microstructures for Improved Performance," *Adv. Energy Mater.*, vol. 8, no. 23, p. 1800120, 2018, doi: 10.1002/aenm.201800120.
[89] F. Tietz, "Thermal expansion of SOFC materials," *Ionics*, vol. 5, no. 1–2, pp. 129–139, Jan. 1999, doi: 10.1007/BF02375916.
[90] Z. Cheng, J.-H. Wang, Y. Choi, L. Yang, M. C. Lin, and M. Liu, "From Ni-YSZ to sulfur-tolerant anode materials for SOFCs: electrochemical behavior, in situ characterization, modeling, and future perspectives," *Energy Environ. Sci.*, vol. 4, no. 11, p. 4380, 2011, doi: 10.1039/c1ee01758f.
[91] S. Zha, Z. Cheng, and M. Liu, "Sulfur Poisoning and Regeneration of Ni-Based Anodes in Solid Oxide Fuel Cells," *J. Electrochem. Soc.*, vol. 154, no. 2, p. B201, 2007, doi: 10.1149/1.2404779.
[92] S. Sun, O. Awadallah, and Z. Cheng, "Poisoning of Ni-Based anode for proton conducting SOFC by H2S, CO2, and H2O as fuel contaminants," *J. Power Sources*, vol. 378, pp. 255–263, Feb. 2018, doi: 10.1016/j.jpowsour.2017.12.056.
[93] H. Yokokawa, H. Tu, B. Iwanschitz, and A. Mai, "Fundamental mechanisms limiting solid oxide fuel cell durability," *J. Power Sources*, vol. 182, no. 2, pp. 400–412, Aug. 2008, doi: 10.1016/j.jpowsour.2008.02.016.
[94] F. Tietz, "Components manufacturing for solid oxide fuel cells," *Solid State Ion.*, p. 9, 2002.
[95] T. Setoguchi, K. Okamoto, K. Eguchi, and H. Arai, "Effects of anode material and fuel on anodic reaction of solid oxide fuel cells," *J. Electrochem. Soc.*, vol. 139, no. 10, p. 2875, 1992.
[96] Y. M. Park and G. M. Choi, "Mixed Ionic and Electronic Conduction in YSZ-NiO Composite," *J. Electrochem. Soc.*, vol. 146, no. 3, pp. 883–889, Mar. 1999, doi: 10.1149/1.1391696.
[97] K. Al-Khori, S. G. Al-Ghamdi, S. Boulfrad, and M. Koç, "Life Cycle Assessment for Integration of Solid Oxide Fuel Cells into Gas Processing Operations," *Energies*, vol. 14, no. 15, p. 4668, Aug. 2021, doi: 10.3390/en14154668.
[98] J. R. Wilson and S. A. Barnett, "Solid Oxide Fuel Cell Ni–YSZ Anodes: Effect of Composition on Microstructure and Performance," *Electrochem. Solid-State Lett.*, vol. 11, no. 10, p. B181, 2008, doi: 10.1149/1.2960528.
[99] H. Anderson, "Review of p-type doped perovskite materials for SOFC and other applications," *Solid State Ion.*, vol. 52, no. 1–3, pp. 33–41, May 1992, doi: 10.1016/0167-2738(92)90089-8.
[100] E. Maguire, "Cathode materials for intermediate temperature SOFCs," *Solid State Ion.*, vol. 127, no. 3–4, pp. 329–335, Jan. 2000, doi: 10.1016/S0167-2738(99)00286-6.
[101] F. Yadollahi Farsani, M. Jafari, E. Shahsavari, H. Shakeripour, and H. Salamati, "Investigation of structural, electrical and electrochemical properties of La0.6Sr0.4Fe0.8Mn0.2O3-δ as an intermediate temperature solid oxide fuel cell cathode," *Int. J. Hydrog. Energy*, vol. 45, no. 15, pp. 8915–8929, Mar. 2020, doi: 10.1016/j.ijhydene.2020.01.030.
[102] L. Z. Bian, L. J. Wang, N. Chen, F. S. Li, and K.-C. Chou, "Enhanced performance of La 0.7 Sr 0.3 Fe 0.9 Ni 0.1 O 3 cathode by partial substitution with Ce," *Ceram. Int.*, vol. 43, no. 1, pp. 982–987, Jan. 2017, doi: 10.1016/j.ceramint.2016.10.029.
[103] J. Wu and X. Liu, "Recent Development of SOFC Metallic Interconnect," *J Mater Sci Technol*, p. 13, 2010.
[104] F. Tietz, "Components manufacturing for solid oxide fuel cells," *Solid State Ion.*, p. 9, 2002.
[105] J. W. Fergus, "Metallic interconnects for solid oxide fuel cells," *Mater. Sci. Eng. A*, vol. 397, no. 1–2, pp. 271–283, Apr. 2005, doi: 10.1016/j.msea.2005.02.047.
[106] "Solid Oxide Fuel Cell [SOFC] Market Size | Growth Report, 2028." https://www.fortunebusinessinsights.com/industry-reports/solid-oxide-fuel-cell-market-101306 (accessed Jul. 20, 2022).

[107] R. Ihringer, "2R-Cell: A Universal Cell for an Easy and Safe SOFC Operation," *ECS Trans.*, vol. 35, no. 1, p. 393, Apr. 2011, doi: 10.1149/1.3570014.
[108] "Green hydrogen cost reduction: Scaling up electrolysers to meet the 1.5C climate goal," p. 106.
[109] M. M. Whiston, I. M. Lima Azevedo, S. Litster, C. Samaras, K. S. Whitefoot, and J. F. Whitacre, "Paths to market for stationary solid oxide fuel cells: Expert elicitation and a cost of electricity model," *Appl. Energy*, vol. 304, p. 117641, Dec. 2021, doi: 10.1016/j.apenergy.2021.117641.
[110] G. Haxel, *Rare earth elements: critical resources for high technology*, vol. 87. US Department of the Interior, US Geological Survey, 2002.
[111] K. W. Eichhorn Colombo, V. V. Kharton, F. Berto, and N. Paltrinieri, "Mathematical modeling and simulation of hydrogen-fueled solid oxide fuel cell system for micro-grid applications - Effect of failure and degradation on transient performance," *Energy*, vol. 202, p. 117752, Jul. 2020, doi: 10.1016/j.energy.2020.117752.
[112] M. S. Sohal, J. E. O'Brien, C. M. Stoots, V. I. Sharma, B. Yildiz, and A. Virkar, "Degradation Issues in Solid Oxide Cells During High Temperature Electrolysis," *J. Fuel Cell Sci. Technol.*, vol. 9, no. 1, p. 011017, Feb. 2012, doi: 10.1115/1.4003787.
[113] Y. Yan, "Performance and degradation of an SOEC stack with different cell components," *Electrochimica Acta*, p. 8, 2017.
[114] V. Miguel-Pérez *et al.*, "Degradation Studies and Sr Diffusion Behaviour in Anode Supported Cell after 3,000 h SOFC Short Stack Testing," *ECS Trans.*, vol. 68, no. 1, pp. 1803–1813, Jun. 2015, doi: 10.1149/06801.1803ecst.
[115] X. Yin, L. Bencze, V. Motalov, R. Spatschek, and L. Singheiser, "Thermodynamic perspective of Sr-related degradation issues in SOFCs," *Int. J. Appl. Ceram. Technol.*, vol. 15, no. 2, pp. 380–390, Mar. 2018, doi: 10.1111/ijac.12809.
[116] N. Menzler, D. Sebold, S. Zischke, J. Zurek, D. Naumenko, and S. Gross-Barsnick, "Post-Operational Characterization of a Long-Term Operated Solid Oxide Fuel Cell Stack," *ECS Trans.*, vol. 103, no. 1, p. 1047, 2021.
[117] J. Schefold, A. Brisse, A. Surrey, and C. Walter, "80,000 current on/off cycles in a one year long steam electrolysis test with a solid oxide cell," *Int. J. Hydrog. Energy*, vol. 45, no. 8, pp. 5143–5154, Feb. 2020, doi: 10.1016/j.ijhydene.2019.05.124.
[118] H. C. Erythropel *et al.*, "The Green ChemisTREE: 20 years after taking root with the 12 principles," *Green Chem.*, vol. 20, no. 9, pp. 1929–1961, 2018, doi: 10.1039/C8GC00482J.
[119] G. M. Rupp, A. Schmid, A. Nenning, and J. Fleig, "The Superior Properties of $La_{0.6}Ba_{0.4}CoO_{3-\delta}$ Thin Film Electrodes for Oxygen Exchange in Comparison to $La_{0.6}Sr_{0.4}CoO_{3-\delta}$," *J. Electrochem. Soc.*, vol. 163, no. 6, pp. F564–F573, 2016, doi: 10.1149/2.1061606jes.
[120] H. Ullmann, N. Trofimenko, F. Tietz, D. Stöver, and A. Ahmad-Khanlou, "Correlation between thermal expansion and oxide ion transport in mixed conducting perovskite-type oxides for SOFC cathodes," *Solid State Ion.*, vol. 138, no. 1–2, pp. 79–90, Dec. 2000, doi: 10.1016/S0167-2738(00)00770-0.
[121] "Fiaxell SOFC Technologies - Cells." https://fiaxell.com/products/specialty-inks-powders-and-cells/cells?fbclid=IwAR0X8LZh-A8Z7wvHNjCe6BnynsZMGuSX7OoqnhkhuTyNpKZqDpjivzPvl64 (accessed Aug. 18, 2022).
[122] P. Zapp, "Environmental analysis of solid oxide fuel cells," *J. Power Sources*, vol. 61, no. 1–2, pp. 259–262, Jul. 1996, doi: 10.1016/S0378-7753(96)02368-3.
[123] V. Karakoussis, N. P. Brandon, and M. Leach, "The environmental impact of manufacturing planar and tubular solid oxide fuel cells," *J. Power Sources*, p. 18, 2001.
[124] M. Pehnt, "Life Cycle Assessment of Fuel Cells and Relevant Fuel Chains," p. 10.
[125] F. Baratto, U. M. Diwekar, and D. Manca, "Impacts assessment and trade-offs of fuel cell-based auxiliary power units," *J. Power Sources*, vol. 139, no. 1–2, pp. 205–213, Jan. 2005, doi: 10.1016/j.jpowsour.2004.07.023.
[126] K. Wincewicz and J. Cooper, "Taxonomies of SOFC material and manufacturing alternatives," *J. Power Sources*, vol. 140, no. 2, pp. 280–296, Feb. 2005, doi: 10.1016/j.jpowsour.2004.08.032.

[127] Wright, Eileen I, "End-of-life Management of Solid Oxide Fuel Cell, phd thesis{wright2011end," p. 265, 2011.
[128] A. Valente, D. Iribarren, and J. Dufour, "End of life of fuel cells and hydrogen products: From technologies to strategies," *Int. J. Hydrog. Energy*, vol. 44, no. 38, pp. 20965–20977, Aug. 2019, doi: 10.1016/j.ijhydene.2019.01.110.
[129] A. M. Férriz, A. Bernad, M. Mori, and S. Fiorot, "End-of-life of fuel cell and hydrogen products: A state of the art," *Int. J. Hydrog. Energy*, vol. 44, no. 25, pp. 12872–12879, May 2019, doi: 10.1016/j.ijhydene.2018.09.176.
[130] M. Kamiya, Y. Mori, T. Kojima, R. Sasai, and H. Itoh, "Recycling process for yttria-stabilized tetragonal zirconia ceramics using a hydrothermal treatment," *J. Mater. Cycles Waste Manag.*, vol. 9, no. 1, pp. 27–33, Mar. 2007, doi: 10.1007/s10163-006-0168-3.
[131] E. I. Wright, S. Rahimifard, and A. J. Clegg, "Impacts of environmental product legislation on solid oxide fuel cells," *J. Power Sources*, vol. 190, no. 2, pp. 362–371, May 2009, doi: 10.1016/j.jpowsour.2009.01.069.
[132] A. M. Férriz, A. Bernad, M. Mori, and S. Fiorot, "End-of-life of fuel cell and hydrogen products: A state of the art," *Int. J. Hydrog. Energy*, vol. 44, no. 25, pp. 12872–12879, 2019.
[133] E. I. Wright, A. J. Clegg, S. Rahimifard, and L. Jones, "An investigation into end-of-life management of solid oxide fuel cells," p. 6.
[134] N. M. Sachs, "Planning the Funeral at the Birth: Extended Producer Responsibility in the European Union and the United States," *Harv. Environ. Law Rev.*, vol. 30, p. 49.
[135] D. S. Khetriwal, P. Kraeuchi, and R. Widmer, "Producer responsibility for e-waste management: Key issues for consideration – Learning from the Swiss experience," *J. Environ. Manage.*, vol. 90, no. 1, pp. 153–165, Jan. 2009, doi: 10.1016/j.jenvman.2007.08.019.
[136] S. Shokohyar, S. Mansour, and B. Karimi, "Simulation-based optimization of ecological leasing: a step toward extended producer responsibility (EPR)," *Int. J. Adv. Manuf. Technol.*, vol. 66, no. 1–4, pp. 159–169, Apr. 2013, doi: 10.1007/s00170-012-4315-9.
[137] Y. Gupt and S. Sahay, "Review of extended producer responsibility: A case study approach," *Waste Manag. Res. J. Sustain. Circ. Econ.*, vol. 33, no. 7, pp. 595–611, Jul. 2015, doi: 10.1177/0734242X15592275.
[138] M. W. Toffel, A. Stein, and K. L. Lee, "Extending Producer Responsibility: An Evaluation Framework for Product Take-Back Policies," *SSRN Electron. J.*, 2008, doi: 10.2139/ssrn.1262335.
[139] N. Alavi, M. Shirmardi, A. Babaei, A. Takdastan, and N. Bagheri, "Waste electrical and electronic equipment (WEEE) estimation: A case study of Ahvaz City, Iran," *J. Air Waste Manag. Assoc.*, vol. 65, no. 3, pp. 298–305, Mar. 2015, doi: 10.1080/10962247.2014.976297.
[140] A. M. Férriz, A. Bernad, M. Mori, and S. Fiorot, "End-of-life of fuel cell and hydrogen products: A state of the art," *Int. J. Hydrog. Energy*, vol. 44, no. 25, pp. 12872–12879, May 2019, doi: 10.1016/j.ijhydene.2018.09.176.
[141] "Thesis-2011-Wright.pdf."
[142] E. I. Wright, A. J. Clegg, S. Rahimifard, and L. Jones, "An investigation into end-of-life management of solid oxide fuel cells," p. 6.
[143] C. R. M. Butt and D. Cluzel, "Nickel Laterite Ore Deposits: Weathered Serpentinites," *Elements*, vol. 9, no. 2, pp. 123–128, Apr. 2013, doi: 10.2113/gselements.9.2.123.
[144] H. L. Carpen and E. C. Giese, "Enhancement of nickel laterite ore bioleaching by Burkholderia sp. using a factorial design," *Appl. Water Sci.*, vol. 12, no. 8, p. 181, Aug. 2022, doi: 10.1007/s13201-022-01704-5.
[145] P. Meshram, Abhilash, and B. D. Pandey, "Advanced Review on Extraction of Nickel from Primary and Secondary Sources," *Miner. Process. Extr. Metall. Rev.*, vol. 40, no. 3, pp. 157–193, May 2019, doi: 10.1080/08827508.2018.1514300.
[146] K. Shibayama *et al.*, "Taganito HPAL Plant Project," *Miner. Eng.*, vol. 88, pp. 61–65, Mar. 2016, doi: 10.1016/j.mineng.2015.10.002.

[147] "Nickel - Base Metals," *Nickel - Base Metals*. https://fyers.in/school-of-stocks/chapter/commodities/nickel.html (accessed Nov. 02, 2022).
[148] "021738907.PDF."
[149] J. Keeling, A. Reid, B. Hou, and R. Pobjoy, "Provenance of zircon in heavy mineral sand deposits, western Murray Basin," p. 64, 2016.
[150] *An overview of South Africa's zircon industry and the role of BEE*. Pretoria: Department : Minerals and Energy, 2007.
[151] "Zirconium Market Update Zircomet Limited - Zirconium Based Materials." http://www.zircomet.com/sec/11189/Zirconium-Market-Update/ (accessed Nov. 02, 2022).
[152] E. Peek, T. Åkre, and E. Asselin, "Technical and business considerations of cobalt hydrometallurgy," *JOM*, vol. 61, no. 10, pp. 43–53, Oct. 2009, doi: 10.1007/s11837-009-0151-2.
[153] S. Horn *et al.*, "Cobalt resources in Europe and the potential for new discoveries," *Ore Geol. Rev.*, vol. 130, p. 103915, Mar. 2021, doi: 10.1016/j.oregeorev.2020.103915.
[154] Q. Dehaine, L. T. Tijsseling, H. J. Glass, T. Törmänen, and A. R. Butcher, "Geometallurgy of cobalt ores: A review," *Miner. Eng.*, vol. 160, p. 106656, Jan. 2021, doi: 10.1016/j.mineng.2020.106656.
[155] M. Mistry, J. Gediga, and S. Boonzaier, "Life cycle assessment of nickel products," *Int. J. Life Cycle Assess.*, vol. 21, no. 11, pp. 1559–1572, Nov. 2016, doi: 10.1007/s11367-016-1085-x.

Chapter 2: Experimental Techniques and Methodology

2.1 Introduction

This thesis proposes to answer scientific questions related to the fundamental end-of-life solution for solid oxide fuel and electrolyzer cells. The content of this chapter is mainly devoted to the overview of the chemicals, equipment and techniques used in the recycling process and the characterization methods used in this work. Further chapters describe the specific experiments and analytical methods for the particular material of interest.

2.2 Products and chemicals used

Fiaxell (Lausanne-Switzerland) and Elcogen (Tallin-Estonia) cells were used as starting material for the recycling of ceramic component materials. Other various materials, reagents and solvents come from various suppliers, such as Sigma-Aldrich, Alfa aesar, Acros organics, Labosi, Tosoh, Melox, Fuel cell materials, and are used without special purification.

Nitric acid (HNO_3) (CRALO ERBA, 65 wt.%) and Dimethylglyoxime ($C_4H_8N_2O_2$), (R.P NORMAPUR) were used for powder chemical treatment. Zirconium(IV) oxy-nitrate ($ZrO(NO_3)_2.6H_2O$, Acros organics, 99.5%), cerium(III) nitrate ($Ce(NO_3)_3.6H_2O$, thermo scientific, 99.5%), $Gd(NO_3)_3.6H_2O$, lanthanum(III) nitrate ($La(NO_3)_3.6H_2O$, Alfa aesar, 99.9%), strontium nitrate ($Sr(NO_3)_2$, Acros oragnics, 99+%), cobalt(II) nitrate ($Co(NO_3)_3.6H_2O$, Acros oragnics, 99+%), manganese(II) nitrate ($Mn(NO_3)_3.4H_2O$ (Labosi, 96%), sodium hydroxide (NaOH, Alfa aesar, 97.0%), gadolinium-doped ceria (GDC) (fuel cell materials) and Nickel Oxide (NiO, PHARMACIE CHEMICAL DE FRANCE S P R) and YSZ powder from Tosoh and Melox (Luxfer MEL Technologies) were used for synthesis or electrolyte support (GDC) or for comparison with recovered materials (YSZ) were used for comparison.

2.3 Experimental procedures

2.3.1 Mechanical scratching

The mechanical scratching technique is a gentle removal of the coated surface from the flat surface by abrasion (Figure 2.1). In this technique, the fine powders are transported by wear and abrasion. After abrasion, the fine powders are collected by brushing. This is a simple technique

done manually with sharp scratching material. Here we use a spatula as the scratching tool for illustration (Figure 2.1).

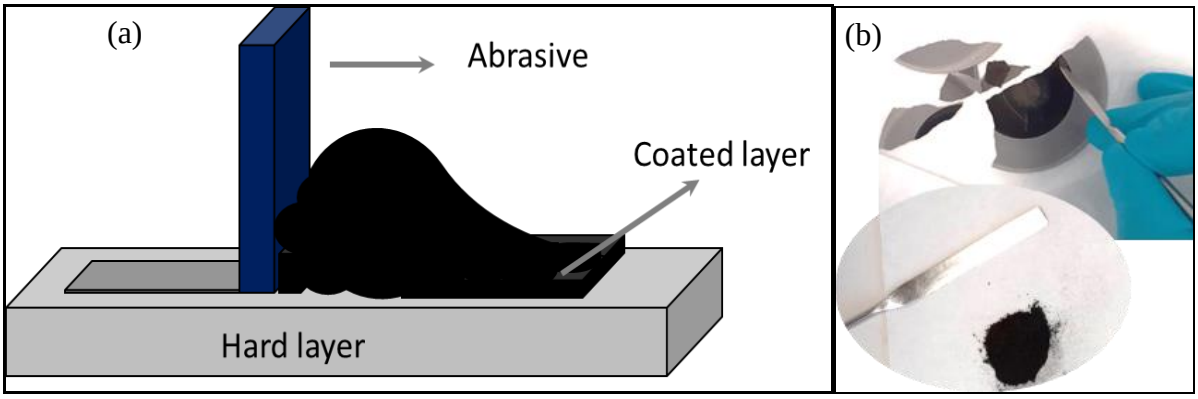

Figure 2.1. (a) Schematic representation of mechanical scratching of powder, (b) mechanical scratching techniques used for separating air electrode of solid oxide cells, and LSC powder collected after scratching.

2.3.2 Grinding with mortar and ball mill

The SOC waste was collected and manually crushed using an agate mortar (Figure 2.2a). After crushing, the particles were ground using a ball mill (with YSZ ball and jars) for further size reduction (Figure 2.2b). Absolute ethanol about 6 ml, 6 balls with a diameter of 10 mm, at 500 rpm for 5 hrs milling time were used to grind the materials into fine powder (FRITSCH Pulverisette abll miller), and the direction and speed of the rotating ball were changed frequently to allow effective grinding.

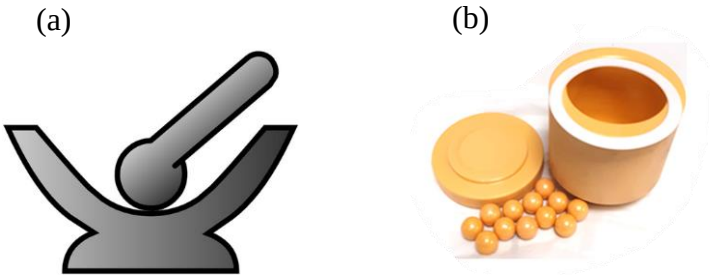

Figure 2.2.Representation of (a) mortal grinder and (b) ball miller.

2.3.3 Leaching and precipitation

In this section, the term "leaching step" refers to the ionic dissolution of the metal species from the air-dried powder obtained after ball milling. This is a crucial step in the hydrometallurgical process, where strong acids are generally used as leaching agents. This step uses the advantages of different solubility of components in acid.

Another chemical separation method is precipitation. During selective precipitation of metal ions from the a liquid phase, heterogeneous insoluble solid particles are formed (Figure 2.3). This selective precipitation is governed by the solubility constants of the various metals in the liquid phase.

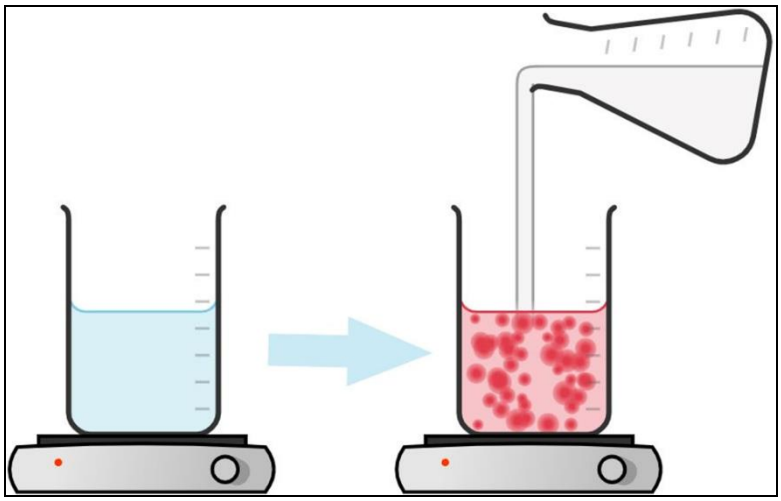

Figure 2.3. Representation of precipitation step.

2.3.4 Centrifugation

During centrifugation, particles that have a higher weight and density are thrown against the walls of the container or against the bottom of the centrifugation tube (Figure 2.4a). Centrifugation is used for solid (2.5 g) and liquid phase (about 35 ml) separation at 500 rpm for 10min. The solution and the solid phases are dried separately with a hot plate and furnace (Figure 2.4b) is used for further thermal degradation.

(a)  (b) 

Figure 2.4. Lab eauipment (a) Centrifuge (Sorvall Plus) and (b) furnace (carbolite)

2.4 Characterization techniques

2.4.1 Powder X-ray Diffraction (XRD)

X-ray Powder Diffraction (XRD) technique was performed at room temperature using a Bruker D8 Advance diffractometer in Bragg-Brentano geometry with a Cu-Kα1 radiation (λ = 1.5406 Å) (Figure 2.5a). Each scan was recorded using different parameters, but usually 2θ ranges from 10 to 80°, the step size is 0.0117 and scan time is 1hr. XRD was largely used for characterization: identification and quantification of phases, crystal structures, unit cell parameters and composition [1]. An example of diffraction pattern related to the interaction between X-Rays and the periodical arrangement of atoms is given (Figure 2.5b)[1] [2], and XRD of NiO is given in Figure 2.5c. A significant part of this PhD work was devoted to the analysis of XRD patterns of recovered products.

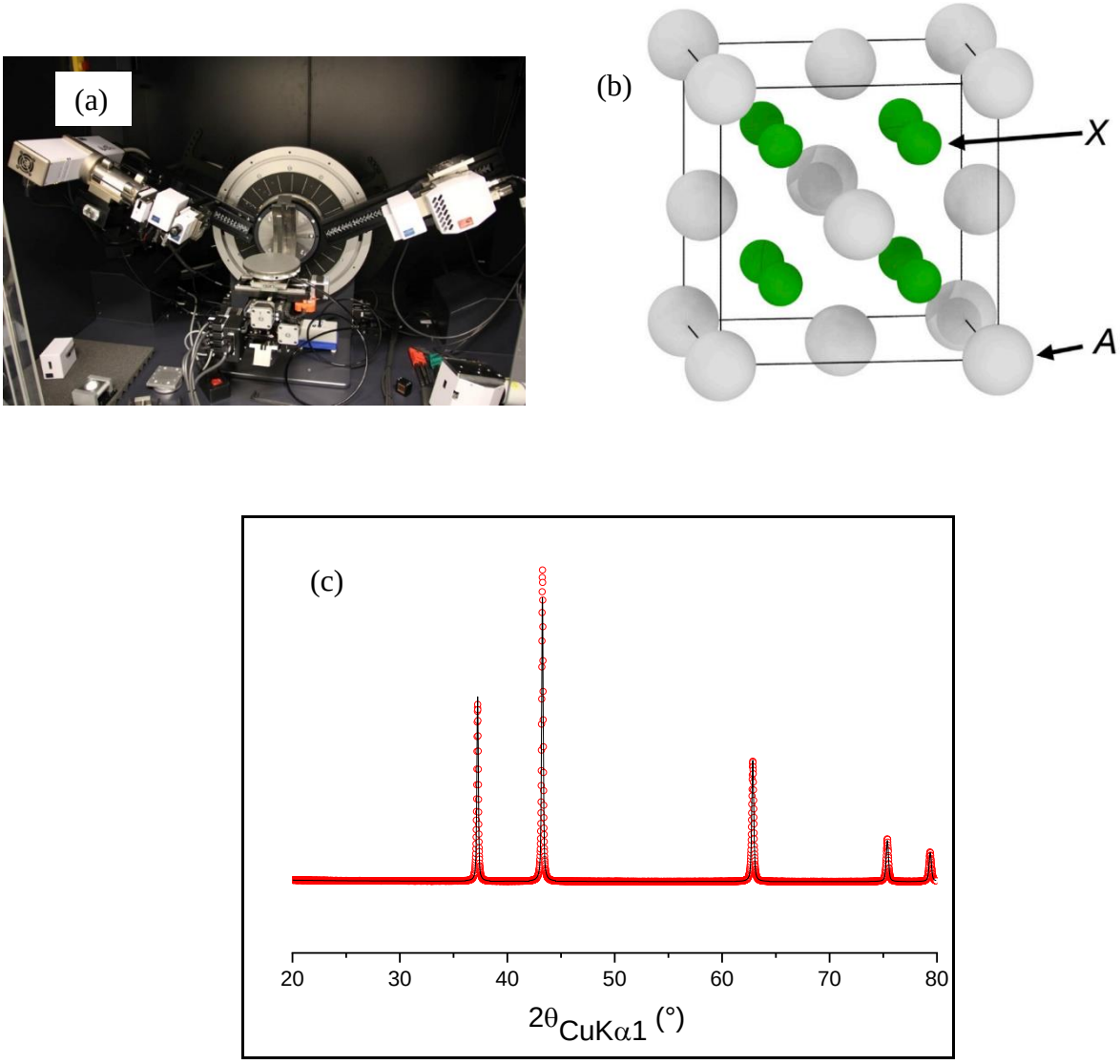

Figure 2.5. (a) Powder XRD diffractometer, (b) AX_2 type compound with space group Fm-3m, showing both A and X sub lattices and (c) experimental (red) and calculated (black) diffraction peaks of NiO powder.

The crystallite size (D) of the powder is calculated using the Scherer equation (Equation 2.1), taking into account the peak broadening of the diffraction peaks. K is the shape factor with a value of about 0.9, but varies with the actual shape of the crystallite, λ is the wavelength of XRD, β is width at half maximum (FWHM), and Θ is the peak position in the 2Θ axis. Smaller crystallite size induces an increase in peak broadening.

$$D = \frac{K\lambda}{\beta cos\theta}$$ Equation 2.1 [3]

2.4.1.1 High temperature X-ray diffraction (XRD)

In situ thermal X-ray powder diffraction (XRD) was used to study the phase evolution as a function of temperature, generally from room temperature to 1100°C in air, using a Bruker D8 Advance diffractometer in Bragg-Brentano geometry with Cu-Kα1 and Kα2 radiations (λ = 1.5406 Å and 1.5444 Å respectively). The ratio of Kα1 to Kα2 is 0.500. Each 2θ-scan was performed from 10 to 80 degrees with a step size of 0.012°.

2.4.1.2 Databases and Software's used for powder XRD pattern analysis

The Inorganic Crystal Structure Database (**ICSD**) is the world's largest database of fully identified inorganic crystal structures, containing unit cell, space group, complete atomic parameters, site occupancy factors, Wyckoff positions, molecular formula and weight, ANX formula, mineral group etc [4]. The **Bilbao** crystallographic server is a database and contains crystallographic programs available online [5]. Therefore, both ISCD and Bilbao crystallographic server are used as the main database for this study.

On the other hand, different crystallographic software were used. **FULLPROF** is a program for pattern matching analysis and Rietveld refinement using the **WinPLOTR** graphical interface [6]. Through this refinement, the crystallite size and microstrain of powder samples can be determined [7]. The quality of the refinement is given by various R factors, including the chi squared value (χ^2) which is equal to the ratio Rwp to Rexp squared, see below. The R factors measures the agreement between the calculated crystallographic model and the experimental data [8].

The phase quantification is performed using the computer program **TOPAS** [9]. The agreement between the calculated and experimental integral intensity is given by the goodness of fit (GOF) and the R-factors, which describe how well the model fits the experimental data. These are [3] (adapted from the Topas software manual): R-factors in Rietveld analysis, indicating the goodness of fit (GOF), RWP is the R-weighted pattern, Rp is the R pattern, RB is R Bragg, Rexp is R-expected, Yo,m and Yc,m are the observed and calculated data at data point m, respectively. Bkgm is the background at data point m, M is the number of data points, P is the number of parameters, and Wm is the weight of data point m.

R- Pattern R_p, $R_p = \frac{\sum|Y_{o,m} - Y_{c,m}|}{\sum Y_{o,m}}$

R- Pattern R_p (background corrected), $R'_p = \frac{\sum|Y_{o,m} - Y_{c,m}|}{\sum|Y_{o,m} - Bkg_m|}$

R-weight pattern, $R_{wp} = \sqrt{\frac{\sum w_m (Y_{o,m} - Y_{c,m})^2}{\sum w_m Y_{o,m}^2}}$

R-weight pattern (background corrected), $R'_{wp} = \sqrt{\frac{\sum w_m (Y_{o,m} - Y_{c,m})^2}{\sum w_m (Y_{o,m} - Bkg_m)^2}}$

$R_{exp} = \sqrt{\frac{M - P}{\sum w_m Y_{o,m}^2}}$

R- Expected R_{exp} (background corrected), $R'_{exp} = \sqrt{\frac{M-P}{\sum w_m (Y_{o,m} - Bkg_m)^2}}$

Goodness of fitting, $GOF = chi = \frac{R_{wp}}{R_{exp}} = \sqrt{\frac{\sum w_m (Y_{o,m} - Y_{c,m})^2}{M-P}}$

R-Bragg, R_B, $R_B = \frac{\sum|I"_o",k - I_{c,K}|}{\sum I"_o",k}$

A goodness of fit close to one shows that the calculated pattern is close to the observed pattern and that the crystallographic model is correct.

PowDLL was used for the data conversion software between different formats of powder X-ray files, e.g. from raw files to uxd or xy files etc. **EVA Interface** is a fast analysis software for XRD patterns with all relevant databases used for phase identification and composition information. **Diamond software** was also used for 3D molecular and crystal structure visualization.

2.4.2 Thermal Gravimetric Analysis (TGA)

Combined Thermal Gravimetric Analyzis (TGA) and Differential Scanning Calorimetry (DSC) of NETZSCH[10] (STA 449F5 STA449F5A-0150-M) were used to study thermal behavior of

powders at different heating and cooling rates in a flowing air atmosphere. Illustration of TGA and DSC curves are shown in Figure 2.6 [11].

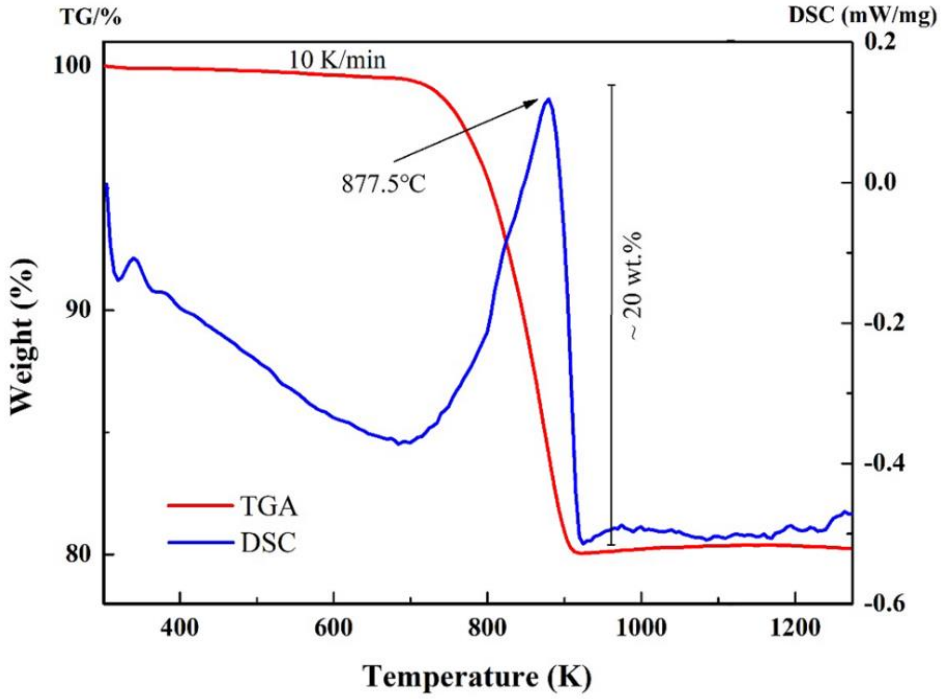

Figure 2.6. Illustration of thermogravimetric analysis (TGA) and differential scanning calorimetry (DSC) curves, taken from X. Li et.al [11].

2.4.3 Electron microscopy (SEM/EDX)

Scanning electron microscopy (SEM) (Figure 2.7a) is used for morphological and topographic information. Images of the sample surface are generated by scanning it with a beam of high energy electrons. The electrons interact with the atoms that make up the sample and generate signals that contain information about the microstructure, topography, and composition of the sample surface. Signals generated by a SEM include secondary electrons (SE), backscattered primary electrons (BSE), and characteristic X-rays (Figure 2.7b). The secondary electrons provide accurate images of the material, while the backscattered electrons shows a better resolution between the different elements present in the sample. The characteristic X-rays enable to obtain information about the nature of the elements constituting the sample [12] [13] [14]. The microstructure of the pellet was observed by scanning electron microscopy (JEOL 7600 SEM).

The composition was performed by SEM energy dispersive X-ray spectroscopy (EDX JEOL 5800).

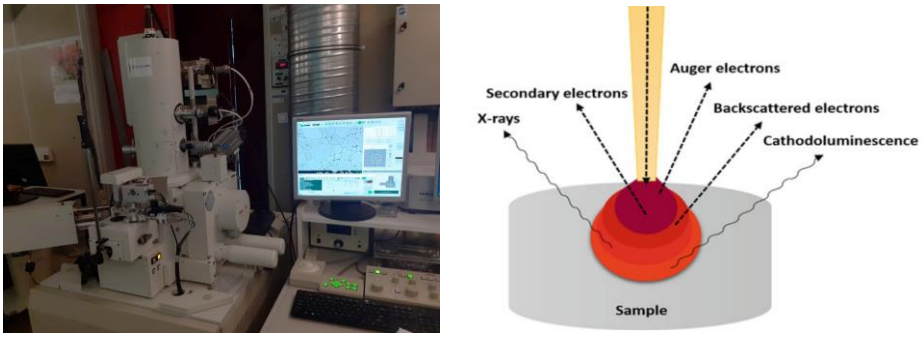

Figure 2.7. (a) SEM equipment (b) Representation of the interaction of electron beam with sample and of the emitted signals [15].

2.4.4 Inductively coupled plasma atomic emission spectrometry

Inductively coupled plasma atomic emission spectrometry (ICP-MS) allows high sensitivity multi-element analysis with lower detection limits in ppb order. Our experiments were realised at the Laboratoire de Planétologie et Géodynamique of Nantes University with a Thermo Scientific iCAP6300 Radial with RF power 1150W. Certified single element containing standard solutions from SODIPRO, France, at 1000µg/ml were used for calibration.

2.4.5 UV-visible absorption spectroscopy

UV visible spectroscopy (Absorption Perkin Elmer) (Figure 2.8a) is used to quantify nickel ion concentration. The analysis is done by accurately measuring the intensity of the light absorbed at each wavelength and using Beer-Lambert Law [16] [17]. The law states that the concentration of a chemical is directly proportional to the absorbance of light by the solution.

$$A = log_{10}\left(\frac{I_o}{I}\right) = \varepsilon C l \qquad \text{Equation 2.2 [17]}$$

Where A is absorbance (unit less), Io is the incident light (intensity of light before sample), I is the transmitted light (intensity of light after sample), C is concentration of the compound in solution (mole L), l is path length of the sample (cm) and ε molar absorptivity the absorbing species (L mole^{-1} cm^{-1}). A calibration curve was firstly obtained using standard solutions of Ni^{2+} by dissolution of NiO powder in 65 wt.% nitric acid (1.46g L^{-1} up to 12.0 g L^{-1}) (Figure

2.8c). For Ni^{2+}, the absorbance for the pic at ~400 nm (Figure 2.8b) was used to trace the calibration curve (Figure 2.8c) and to calculate the concentration.

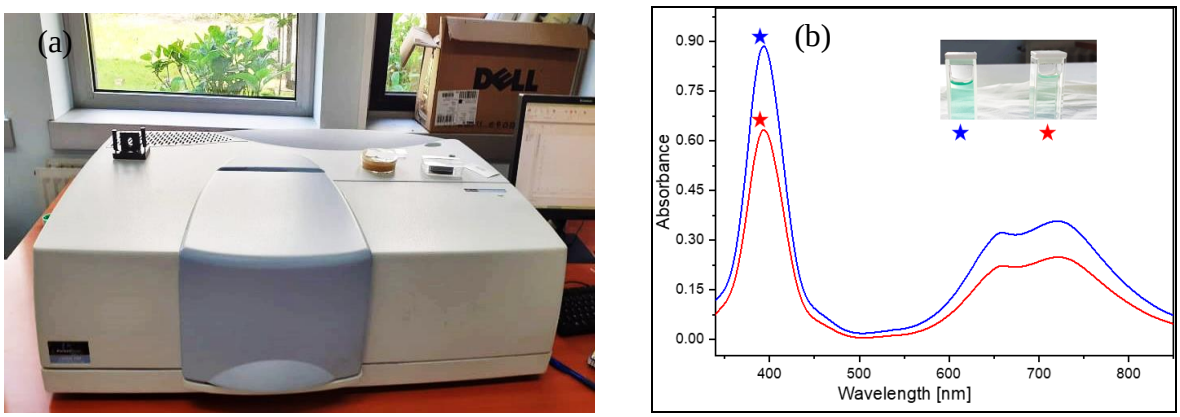

Figure 2.8. (a) UV visible spectroscopy instrument and (b) UV-Visible absorption spectrum of $NiNO_3$ solutions

2.4.6 BET (Brunauer, Emmett, and Teller) surface area

The specific surface area (m^2/g) of powders were determined using BET (Brunauer, Emmett, and Teller) surface area measurement techniques. (Figure 2.9a). The powder (1.5 g) is first cooled to cryogenic temperature (with liquid nitrogen) under vacuum. Then nitrogen gas (as a typical adsorbate) is added in controlled steps (Figure 2.9b). After each step, the relative pressure (P/P_0) is equalized and the layer of adsorbed nitrogen is determined (Figure 2.9b) using BET theory [18]

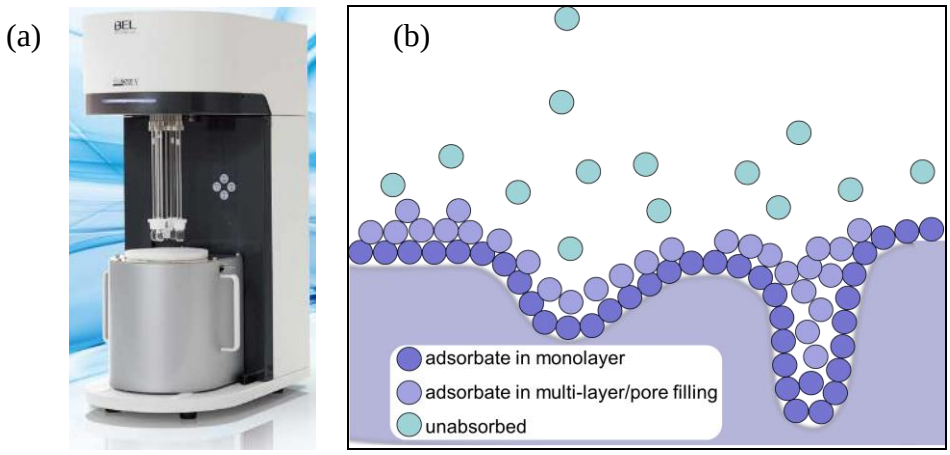

Figure 2.9. (a) BET surface area measurement equipment and (b) illustration of gas adsorption process layer.

2.4.7 Particle size analysis

LASER granulometer (Malvern Mastersizer 3000) was used to determine the statistical distribution of particles sizes (PSD) of the powders [19]. The laser diffraction technique is based on the principle that particles passing through a laser beam scatter light at an angle directly related to their size: large particles scatter at a small angle, while small particles scatter at a large angle (Figure 2. 10). It is used to measure the particle size of powder suspensions, emulsions and slurries, as well as aerosols and sprays.

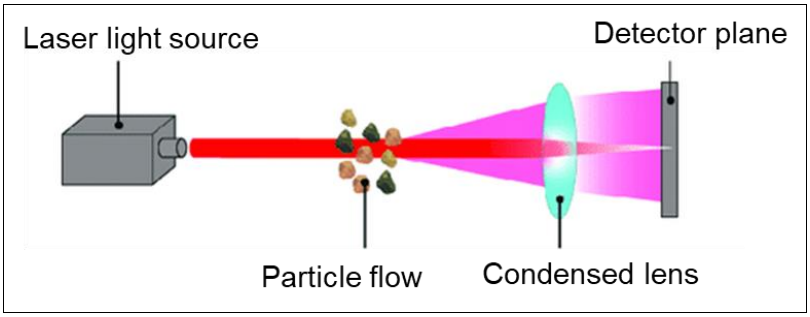

Figure 2. 10. Laser light particle size measuring setup [20].

2.4.8 Electrochemical impedance spectroscopy

Electrochemical impedance spectroscopy (EIS) is an experimental method for characterizing electrochemical systems. It is realized by applying an AC voltage to an electrochemical cell and then measuring the resulting current through the cell and the corresponding impedance. Results are interpreted by modelling the cell with an equivalent electrical circuit, in which each element correspond to a physical phenomenon occurring in a part of the cell [21]. It is an important tool for studying the characteristic behavior of electrochemical systems in terms of their ohmic and polarization resistance, their time constants under different conditions, and their changes with time. The EIS measurement is done by a frequency response analyzer Solartron 1260 and using Ec-Lab software.

For conductivity measurements, YSZ powders were uniaxially pressed (Figure 2.11a) into pellets (Ø = 10mm) and sintered at 1450°C for 10 hours. $La_{0.8}Sr_{0.2}MnO_3$ (LSM) paint was applied to both sides of the pellet and sintered at 1100°C for 2 hour. The symmetrical LSM/YSZ/LSM cell was carefully pressed between two gold meshes, which were used as current collection contacts.

For the LSC electrode test, a GDC electrolyte was used as the support and an ink was prepared from recovered LSC. LSC /GDC/ LSC a symmetrical cell was fabricated. A gold mesh was pressed into the outside of the cell as a current collecting contact. Samples are then placed in home-made support which is then inserted into a cylindrical furnace (Figure 2.11b)

EIS was recorded with a frequency response analyzer in a frequency range from 10 MHz to 0.1 Hz at 50 mV amplitude of the interfering signal were used to see realistic current and distinic features of all frequency ranges. Spectra were recorded from 250°C to 750°C; temperature was measured with a thermocouple placed near the symmetric cell.

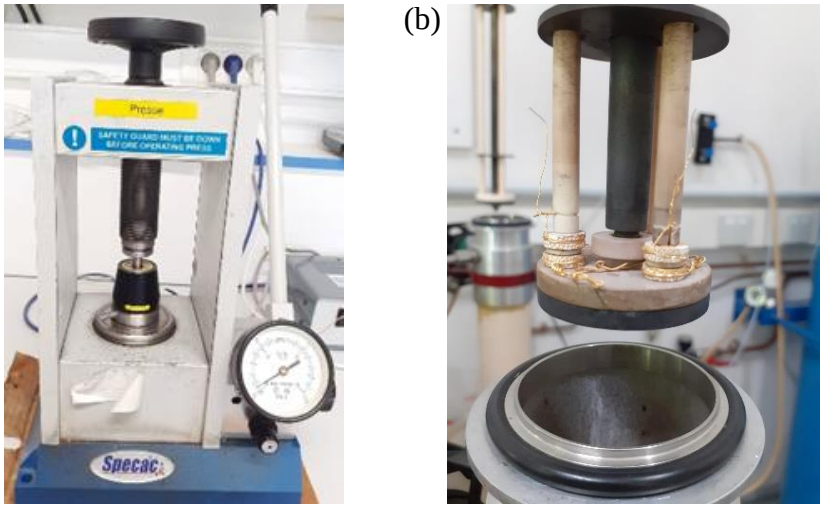

Figure 2.11. (a) Photos of the uniaxial press used for sample preparation, and (b) EIS set up.

2.4.9 Cross-section polishing

The cross-sectional preparation (CSP) is used for surface preparation of samples before scanning electron microscopy. Flat and smoot surface can be prepared as shown in Figure 2.12b. The system operates in a low vacuum environment about $1x10^{-4}$atm. The CSP uses the ion etching process (model of equipment) (Figure 2.12). The ion used in polishing is Argon. The accelerating voltage and current, adjusted for optimum operation, are of 6.0kV and 140mA. The time required depends on the thickness and hardness of the sample.

(a) (b)

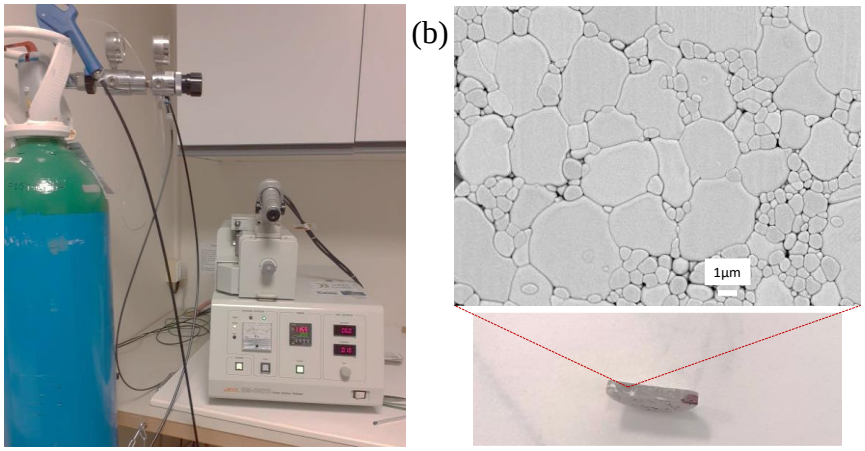

Figure 2.12. Illustration of (a) cross-sectional preparation by Ar ion milling, (b) samples prepared by CSP.

2.4.10 Screen printing

Screen-printing uses a mesh to transfer ink or slurry onto a substrate. The ink was formulated with active materials, pore former additive, plasticizer, and solvent. The blade is moved across the screen, the slurry is then poured onto the electrolyte surface using the screen printing process.

Reference

[1] A. Chauhan, "Powder XRD Technique and its Applications in Science and Technology," *J. Anal. Bioanal. Tech.*, vol. 5, no. 6, 2014, doi: 10.4172/2155-9872.1000212.

[2] A. A. Chernyshov, A. A. Veligzhanin, and Y. V. Zubavichus, "Structural Materials Science end-station at the Kurchatov Synchrotron Radiation Source: Recent instrumentation upgrades and experimental results," *Nucl. Instrum. Methods Phys. Res. Sect. Accel. Spectrometers Detect. Assoc. Equip.*, vol. 603, no. 1–2, pp. 95–98, May 2009, doi: 10.1016/j.nima.2008.12.167.

[3] "TOPAS 5 Technical Reference.pdf."

[4] G. Bergerhoff, R. Hundt, R. Sievers, and I. D. Brown, "The inorganic crystal structure data base," *J. Chem. Inf. Comput. Sci.*, vol. 23, no. 2, pp. 66–69, May 1983, doi: 10.1021/ci00038a003.

[5] M. I. Aroyo *et al.*, "Bilbao Crystallographic Server: I. Databases and crystallographic computing programs," *Z. Für Krist. - Cryst. Mater.*, vol. 221, no. 1, pp. 15–27, Jan. 2006, doi: 10.1524/zkri.2006.221.1.15.

[6] J. Rodríguez-Carvajal, "Introduction to the Program FULLPROF: Refinement of Crystal and Magnetic Structures from Powder and Single Crystal Data," p. 15.

[7] J. Rodríquez-Carvajal and T. Roisnel, "Line broadening analysis using FullProf*: determination of microstructural properties," in *Materials Science Forum*, 2004, vol. 443, pp. 123–126.

[8] L. B. McCusker, R. B. Von Dreele, D. E. Cox, D. Louër, and P. Scardi, "Rietveld refinement guidelines," *J. Appl. Crystallogr.*, vol. 32, no. 1, pp. 36–50, Feb. 1999, doi: 10.1107/S0021889898009856.

[9] A. A. Coelho, "*TOPAS* and *TOPAS-Academic*: an optimization program integrating computer algebra and crystallographic objects written in C++," *J. Appl. Crystallogr.*, vol. 51, no. 1, pp. 210–218, Feb. 2018, doi: 10.1107/S1600576718000183.

[10] "NETZSCH Simultaneous Thermal Analyzer," *Shared Instrumentation Network*, Jul. 27, 2016. https://www.colorado.edu/sharedinstrumentation/instruments-deptinstitutecampus/netzsch-simultaneous-thermal-analyzer (accessed Jul. 26, 2022).

[11] X. Li, Y. Liu, H. Song, Q. Zhang, and X. Wu, "Thermal stability and compressibility of bastnaesite," *Phys. Chem. Miner.*, vol. 47, no. 3, p. 13, Mar. 2020, doi: 10.1007/s00269-020-01084-9.

[12] W. Zhou, R. P. Apkarian, Z. L. Wang, and D. Joy, "Fundamentals of Scanning Electron Microscopy," p. 40.

[13] D. M. Kannan, "Scanning Electron Microscopy: Principle, Components and Applications," p. 13.

[14] M. Abd Mutalib, M. A. Rahman, M. H. D. Othman, A. F. Ismail, and J. Jaafar, "Scanning Electron Microscopy (SEM) and Energy-Dispersive X-Ray (EDX) Spectroscopy," in *Membrane Characterization*, Elsevier, 2017, pp. 161–179. doi: 10.1016/B978-0-444-63776-5.00009-7.

[15] K. Akhtar, S. A. Khan, S. B. Khan, and A. M. Asiri, "Scanning Electron Microscopy: Principle and Applications in Nanomaterials Characterization," in *Handbook of Materials Characterization*, S. K. Sharma, Ed. Cham: Springer International Publishing, 2018, pp. 113–145. doi: 10.1007/978-3-319-92955-2_4.

[16] A. Das, "Portable UV–VISIBLE Spectroscopy – Instrumentation, Technology, and Applications," in *Portable Spectroscopy and Spectrometry*, 1st ed., R. Crocombe, P. Leary, and B. Kammrath, Eds. Wiley, 2021, pp. 179–207. doi: 10.1002/9781119636489.ch8.

[17] T. G. Mayerhöfer, S. Pahlow, and J. Popp, "The Bouguer-Beer-Lambert Law: Shining Light on the Obscure," *ChemPhysChem*, vol. 21, no. 18, pp. 2029–2046, Sep. 2020, doi: 10.1002/cphc.202000464.

[18] M. Naderi, "Surface Area," in *Progress in Filtration and Separation*, Elsevier, 2015, pp. 585–608. doi: 10.1016/B978-0-12-384746-1.00014-8.

[19] "Manual: Mastersizer 3000 User Manual (MAN0474-2.1)," p. 182.

[20] "Particle Size Analysis with Laser Diffraction," *Sympatec*. https://www.sympatec.com/en/particle-measurement/sensors/laser-diffraction/ (accessed Oct. 12, 2022).

[21] G. Constantin, "Interfaces et durabilité d'un coeur de pile à combustible à oxyde solide fonctionnant à température intermédiaire," p. 191.

Chapter 3: Recycling via "mechanical scratching" route

This part concerns the recovery of the ceramic component materials of the solid oxide cells, the full characterization and elucidation of structural and morphological properties, conductivity, and chemical purity of recovered materials. The name "mechanical scratching" route is given to this process because of the process used to recover the air electrode material. Since all the study is published in journal of Resources, Conservation & Recycling, this chapter is a copy of the paper.

Publication: Recycling and characterization of end-of-life solid oxide fuel/electrolyzer ceramic material cell components

Autours: Gudaysew Tsegaye YENESEW, Eric QUAREZ, Annie LE GAL LA SALLE*,

Clément NICOLLET, Olivier JOUBERT

Nantes Université, CNRS, Institut des Matériaux de Nantes Jean Rouxel, IMN, F-44000 Nantes, France

Journal: Resources, Conservation & Recycling

Published: March 2023

Contribution

Contribution Gudaysew Tsegaye Yenesew acquired and processed the experimental data, and wrote this article. Eric QUAREZ, Annie LE GAL LA SALLE, Clément NICOLLET, Olivier JOUBERT contributed to the interpretation of the results and corrected the different versions of the article.

***Corresponding author:** annie.legal@cnrs-imn.fr (Annie LE GAL LA SALLE)

Abstract

In this work, a strategy for recycling and recovery of anode supported Solid Oxide Cell (SOC) ceramic components is presented. From commercial cells, electrodes and electrolyte are separated by mechanical scratching and grinding, followed by thermal and chemical treatments. Air electrode ($La_xSr_{1-x}CoO_3$), nickel oxide (NiO), which accounts for about 50% of the cell weight, and yttria-stabilized zirconia (YSZ), which is coming from both the fuel electrode and the electrolyte, were successfully separated, and 90-92% of the total weight of initial Ni and YSZ can be collected. The recovered materials are characterized by X-ray diffraction, scanning electron microscopy, (thermal, chemical) analysis and BET surface area measurement, and impurity amount never excess 1 At.%. The conductivity level of the recycled YSZ materials was measured in ambient air by electrochemical impedance spectroscopy and is found comparable with commercial YSZ material, with a total value exceeding 6.4 10^{-3} S cm^{-1} at 700°C. The contributions of grain and grain boundary conductivities to the total conductivity are clearly distinguishable at lower temperatures.

Keywords: Recycling wastes; Solid Oxide Cells; YSZ; Ionic conductivity; Phase separation.

Highlights

Successful separation, recycling and recovering of solid oxide cells component

Air electrode $La_xSr_{1-x}CoO_3$ (x = 0.6), nickel oxide, and $Zr_{1-x}Y_xO_{(2-x)/2}$ (x = 0.08) recovered at high purity level

Physical and electrochemical characterizations of recycled compounds

Total recovered YSZ conductivity is close to commercial product.

90-92% of the total weight of initial NiO and YSZ recovered

1. Introduction

There is a high intention of using renewable energies to tackle the question of global warming and recent acceleration of global CO_2 emissions. Shifting from a fossil fuel energy system to a renewable energy system must be considered. Unlucky, renewable energy is inherently intermittent, costly, and location-dependent [1] [2] [3]. The use of hydrogen is a current solution to reduce CO_2 emissions in transport [3] [4] and in industry, especially in the production of steel [5], ammonia and fertilizers [6]. Therefore, hydrogen must be produced in large quantities and without CO_2 emissions. Currently, the cleanest way to produce hydrogen is water electrolysis with renewable or carbon-free electricity [7] [8].

Numerous electrolysis technologies can be used to achieve this goal, each with drawbacks and advantages. Among them high-temperature solid oxide electrolyzers (SOEs) present the advantage, if operated with waste heat available in industry, of their high efficiency. Produced hydrogen can therefore be converted, always with high efficiency, into electricity by Solid Oxide Fuel Cells (SOFCs), are closely related to SOEs, with similar electrode and electrolyte ceramic components.

A SOEs or SOFCs stack is made of various materials such as metals and ceramics. A planar SOEs /SOFCs stack consists of repeating single cells connected in series with metallic interconnectors. A single cell is a superposition of multiple layers, as shown in Figure 3. 1 for an anode-supported SOFC. State-of-the-art materials are yttria-stabilized zirconia (YSZ) for the electrolyte layer, a cermet made of Ni and YSZ for the fuel electrode, and perovskite-based ceramic such as doped lanthanum manganites or cobaltites for the air electrode [9] [10] [11].

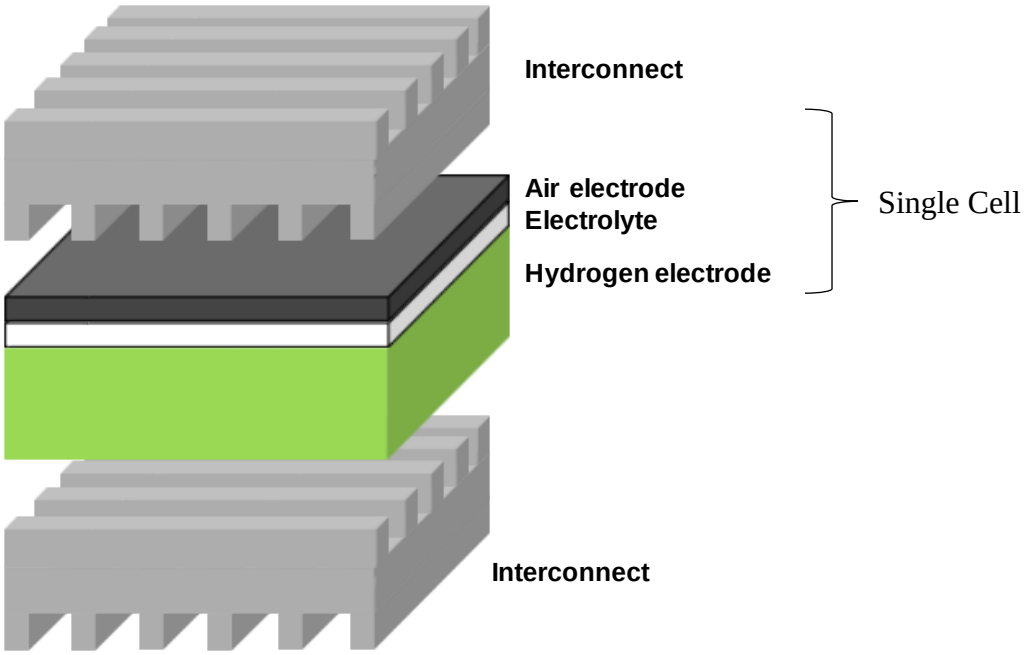

Figure 3. 1 Scheme of a planar fuel-cell supported SOFC, with electrodes and electrolyte sandwiched between metallic interconnects.

The current research challenges for SOEs and SOFCs are mainly focused to increase the lifetime and reduce the cost. In addition to the good performance of SOEs and SOFCs, it should be noted that solid oxide stacks are likely to generate waste during manufacturing (scrap, cutting or punching, and after quality control) and at the end of life. Taking into account the expected large development of the electrolysis technology, including SOE, in a near future, this also requires large-scale production of electrolysers. In this respect, the technology will face the major challenge of mass production of raw materials, dependence on commercial products, and production of waste for the environment [12]. For example, 1MW of SOFC stack uses than 1 ton of valuable ceramic materials [13].

As Waste Electrical and Electronic Equipment (WEEE) directive, the recycling and reuse of end-of-life electronic products should be encouraged [14] [15] [16]. As described by Sarner et al. in their extensive review of solid oxide cells recycling strategies [11], there are only few studies dealing with practical ways to recover separately cells components. The decomposition of sintered tetragonal zirconia polycrystals (3Y-TZP) by hydrothermal treatment into powder particles was studied by Kamiya et.al [17]. Coman et.al [18] have carried out a comprehensive study on nickel recovery from industrial waste. Ferreira et.al [19] briefly studied a 3D

manufacturing technology for SOFC production and its environmental impact compared to conventional manufacturing. The concern for the end products [12] and recycling of materials contained in the SOFC electrolyte and using these wastes to produce new compounds is thoroughly highly desirable.

In this paper, we conducted a practical study on the recovery and reuse of SOFCs components. This study does not address the disassembly of a planar SOFC stack, but focusses on the ceramic part, which contains a mixture of potentially valuable materials. This work addresses the separation and characterization of the unit cell ceramic materials. In order to limit the energy required to separate and recycle materials for solid oxide cells, the goal of this original work is not to obtain pure and simple oxide materials, but to obtain materials and compounds that serve as new starting materials for the fabrication of new SOCs (*Figure S3.11*). Surface treatment of individual plates, either by mechanical or chemical processing, has the potential to separate the materials present in the fuel cell anode, electrolyte, cathode and current collectors from the bulk ceramic substrate.

In this paper, we describe a simple way to separate solid oxide single cell materials present in the electrode and electrolyte parts. Systematic methods of dissolution of waste product and investigating the techniques to separate and characterize the mixture of recycled products were applied to commercial solid oxide single cells. Finally, solid oxide electrolyte made from recycled products is studied and its conductivity performance is measured and compared to that of commercial YSZ powders.

2. Experimental

Planar commercial Fiaxell and Elcogen cells about ~400 µm were chosen to perform this study. Before recycling, these cells were tested in the laboratory under standard conditions, that is between 700 and 850°C, with air on cathode side and H_2/Ar mixtures on anode side.

The only reagents necessary for recycling were HNO_3 from Fischer Scientific, ethanol and deionized water. In order to evaluate conductivity of the recycled YSZ, commercial 3YSZ and 8YSZ powders provided by Melox Company and commercial 8YSZ powder provided by Tosoh Company.

Combined Thermal Gravimetric Analyzer (TGA) and Differential Scanning Calorimetry (DSC) (NETZSCH STA 449F5 STA449F5A-0150-M) were performed with a heating rate of 5°C/min in air atmosphere from room temperature to 400°C. Collection of Powder X-ray Diffraction (XRD) data was done at room temperature using a Bruker D8 Advance diffractometer in Bragg-Brentano geometry with a Cu Kα radiation (ʎ = 1.5406 Å). Each 2θ scan was performed from 10 to 80 degrees with a step size of 0.012°. The refinement of the lattice parameters was performed using the program FULLPROF with the interface WinPLOTR whereas phase quantification was performed with the computer program TOPAS [20]. The specific surface area (m^2/g) of the recovered YSZ and NiO powder were determined by physical adsorption of nitrogen gas at 77.3 K using BET measurement (Brunauer, Emmett, and Teller). The adsorbed gas P/P^o from 0.05 to 0.27 was used as standard measurement points and the calculation was based on BET theory.

The microstructure of the pellet was studied by Scanning Electron Microscopy (JEOL 7600 SEM) and the composition by SEM energy dispersive X-ray spectroscopy (JOEL 5800 SEM). Impurity concentration was obtained using Inductively Coupled Plasma Mass Spectrometry ICP-MS (Thermo Scientific iCAP6300 Radial with RF power 1150 W) with an auxiliary gas flow rate 0.5L/min, a mist gas flow rate 0.65 L/min and an observation height of 12 mm. Calibration was done using certified single element standard solutions from SODIPRO(France), concentrated at 1000 µg/ml. The samples in solution form were evaporated on a hot plate and then transferred to an argon plasma.

For conductivity measurements, YSZ powders (recovered and commercial) were uniaxially pressed into pellets (Ø = 10mm,) and sintered at 1450°C for 10 hours. In order to determine recovered YSZ conductivity without interference due to electrode effects, commercial $La_{0.8}Sr_{0.2}MnO_3$ (LSM) ink was applied to both sides of the pellet and sintered at 1100°C for two hours, leading to final LSM coverage of 0.524 cm^2. Resulting symmetrical LSM/YSZ/LSM cells, 0.13 cm thick are gently pressed between two gold meshes, used as current collection contacts. Electrochemical Impedance Spectroscopy (EIS) was recorded in ambient air with a frequency response analyzer Solartron 1260 in a frequency range from 10 MHz to 0.1 Hz at 50 mV amplitude of the interfering signal. Spectra were recorded from 250°C to 750°C with a step of 50°C after a stabilization plateau of 30 min; temperature was measured with a thermocouple placed near the symmetric cell. It has been checked that the amplitude of the perturbation signal

is small enough to meet the linearity requirement of the transfer function [21]. The data were analyzed and modeled using ZView® software [22].

3. Results and discussion

3.1. Methodology for recycling the components of used solid oxide cells

Figure 3. 2 (a-b) shows an image of the fracture cross-section of untested cells (Fiaxell [23] and Elcogen [24]) (Appendix 1 and Appendix 2). Both are fuel electrode supported cells and based on same materials: the thick and porous fuel electrode substrate is made of a cermet NiO-3YSZ, the thin functional layer of NiO-8YSZ, the dense electrolyte of 8YSZ, a thin barrier layer of GDC separating the electrolyte and the air electrode made of LSC ($La_{1-x}Sr_xCoO_{3-\delta}$). As clearly shown in Figure 3. 2, differences are found in the thickness of each layer, the microstructure and the composition of the cermet. For example, the fuel electrode in the Fiaxell cells contains about 32.1wt. % NiO, while in the Elcogen cell, it is about 69.0wt. %.Figure 3. 2b shows used cells after testing in solid oxide fuel cell setup. This is the type of cells employed in the present study.

The methodology to recycle components from used solid oxide cells is detailed in Figure 3. 2d. First, the air electrode material containing LSC is removed by a simple mechanical scratching. To avoid any further contamination from the air-electrode, the electrolyte surface is carefully washed with concentrated nitric acid (65 wt. %). Then, the remaining hard part of the cell which contains the fuel electrode/electrolyte assembly, is roughly crushed by hand with a mortar and pestle and ball milled for 5h in absolute ethanol. The powder is dried at 70°C until stabilization of weighted mass. After drying, the powder is dissolved and leached with HNO_3 (65 wt. %), in order to dissolve nickel. Indeed, the solution becomes green, in accordance with the presence of nickel ions, whereas a white sediment appears at the bottom of the container. Finally, a centrifugation process is used to separate the green solution and sediment. After drying the solution at 75°C overnight, a green powder is obtained. Characterizations of the three powders are presented below.

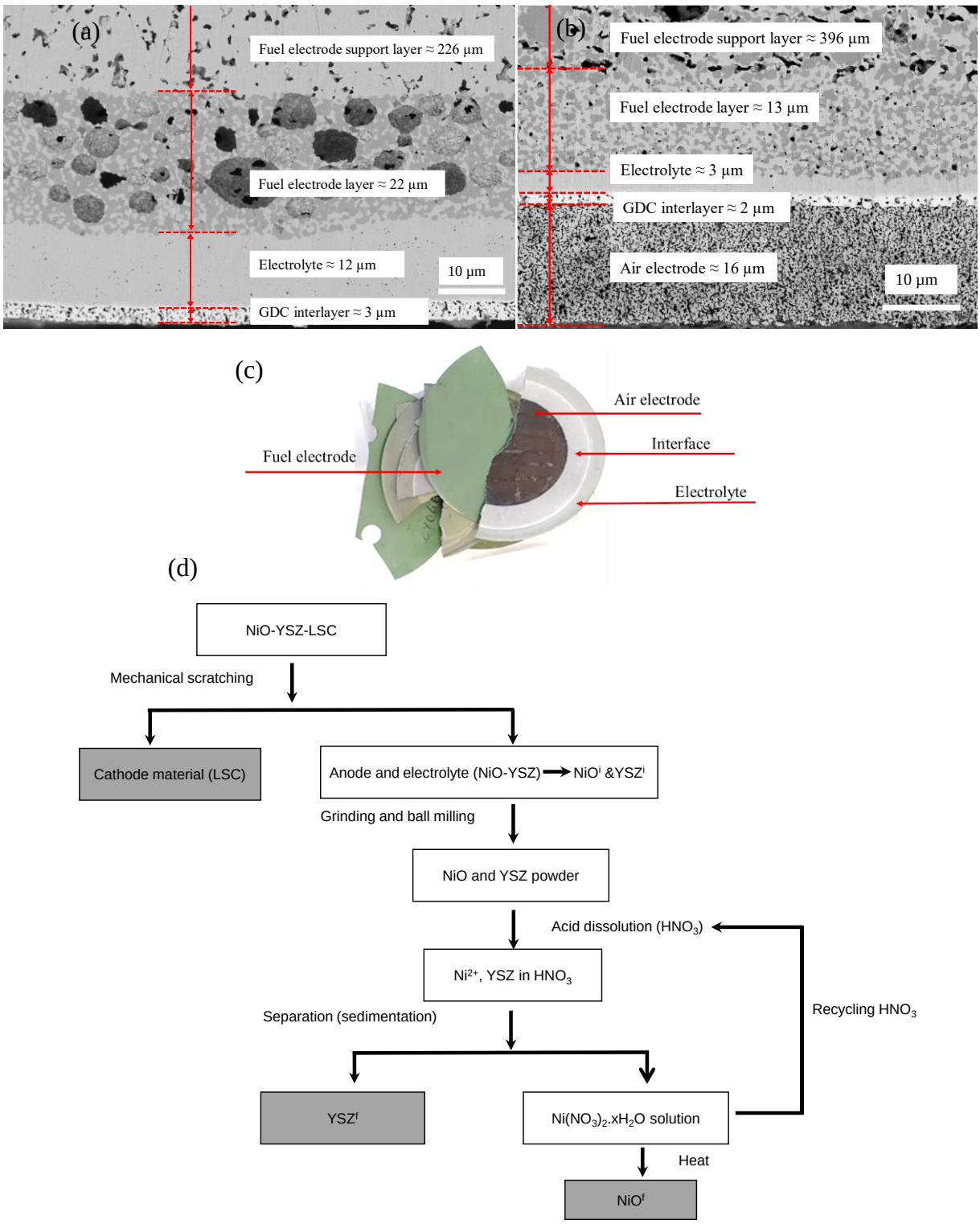

Figure 3. 2 Cross section of unused SOFCs from (a) Fiaxell, (b) Elcogen, (c) Used cells employed and (d) Recovery scheme of the solid oxide cell components. Superscript i and f in NiO and YSZ stand for initial and final, respectively, used later for the yield calculation, see section 3.2.3.

3.2. Recovered materials characterization

3.2.1. Recovery of LSC:

The raw air electrode material obtained by a simple mechanical scratching was characterized by X-ray diffraction (XRD).

Figure 3. *3* (a) shows the XRD pattern of the recovered air electrode powder from Fiaxell and Elcogen cell technology. A single crystallized phase appears. As expected, the cell parameters and cell volume after Rietveld refinement are close to those of $La_{0.6}Sr_{0.4}CoO_{3-\delta}$ from database (ICSD 237871: a = 5.4367(4) Å, c = 13.2142(1) Å, V = 338.25(5) $Å^3$, R-3c space group)

The Rietveld refinement plot of the XRD data of (bottom) the recovered air electrode material from Fiaxell is presented in Figure 3.3 a. The final R values are Rexp = 4.59 %, Rwp = 7.19 %, Rp = 5.11 % and GOF = 1.57, (top) recovered from Elcogen cell, the final R values are Rexp = 6.85 %, Rwp = 9.5 %, Rp = 7.31 % and GOF = 1.39. Figure 3.3 a. shows the Rietveld refinement plot of the XRD data of the recovered hydrated nickel nitrate from Fiaxell crystallizing in triclinic P-1 space group with a = 7.69665(12) Å, b = 11.9019(2) Å, c = 5.80508(12) Å, α = 101.8314(14)°, β = 102.2849(15)°, γ = 106.0323(11)°, V = 479.281(17) Å3. The final R-values are Rexp = 9.28 %, Rwp = 14.75 %, Rp = 11.57 % and GOF = 1.59. The recovered hydrated nickel nitrate (Elcogen cells) which is crystallized in triclinic P-1 space group has a = 7.7015(9) Å, b = 11.9003(5) Å, c = 5.80493(4) Å, α = 101.824(1)°, β = 102.2880(8)°, γ = 106.0323(11)°, V = 479.281(17) Å3. The final R-values are Rexp = 5.09 %, Rwp = 17.32 %, Rp = 12.90 % and GOF = 3.40.

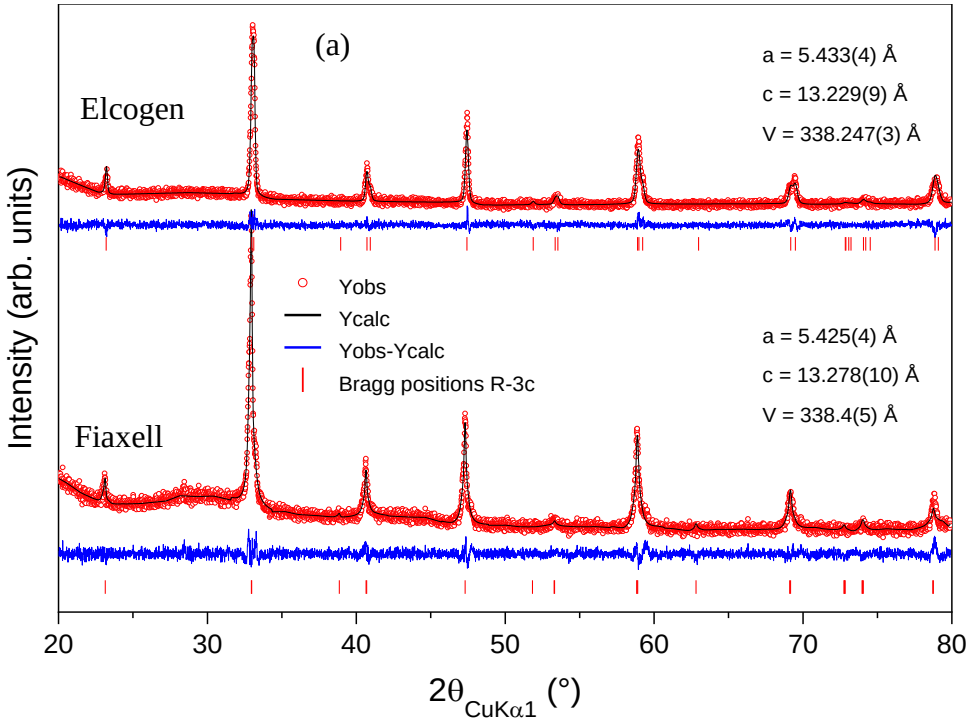
(a)
Elcogen
a = 5.433(4) Å
c = 13.229(9) Å
V = 338.247(3) Å
Yobs
Ycalc
Yobs-Ycalc
Bragg positions R-3c
Fiaxell
a = 5.425(4) Å
c = 13.278(10) Å
V = 338.4(5) Å
Intensity (arb. units)
20
30
40
50
60
70
80
2θCuKα1 (°)

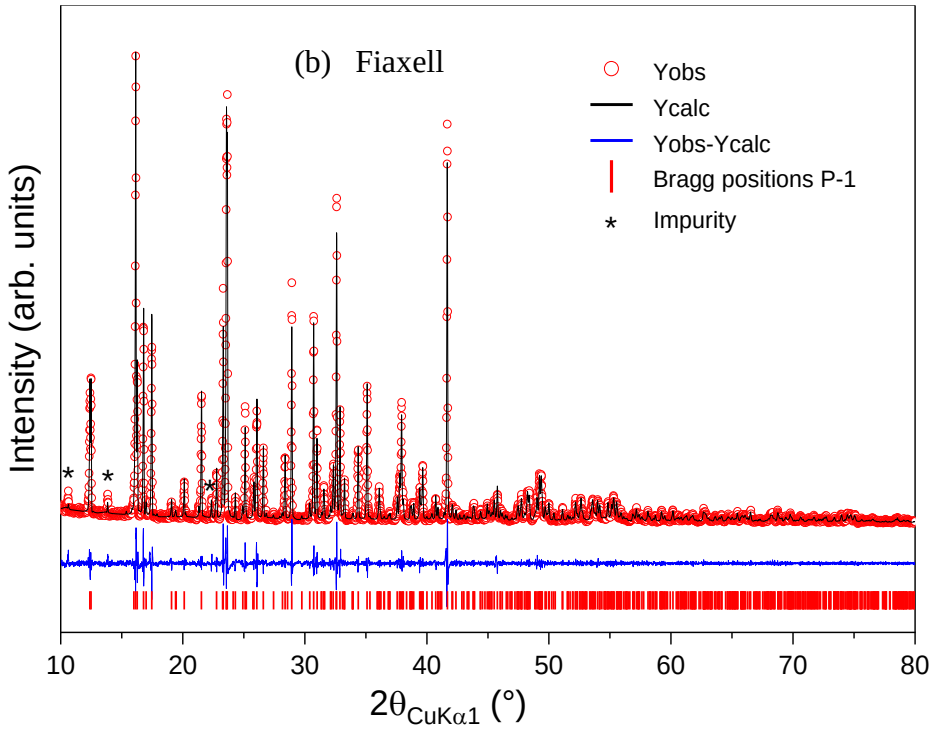
(b) Fiaxell
Yobs
Ycalc
Yobs-Ycalc
Bragg positions P-1
Impurity
Intensity (arb. units)
10
20
30
40
50
60
70
80
2θCuKα1 (°)

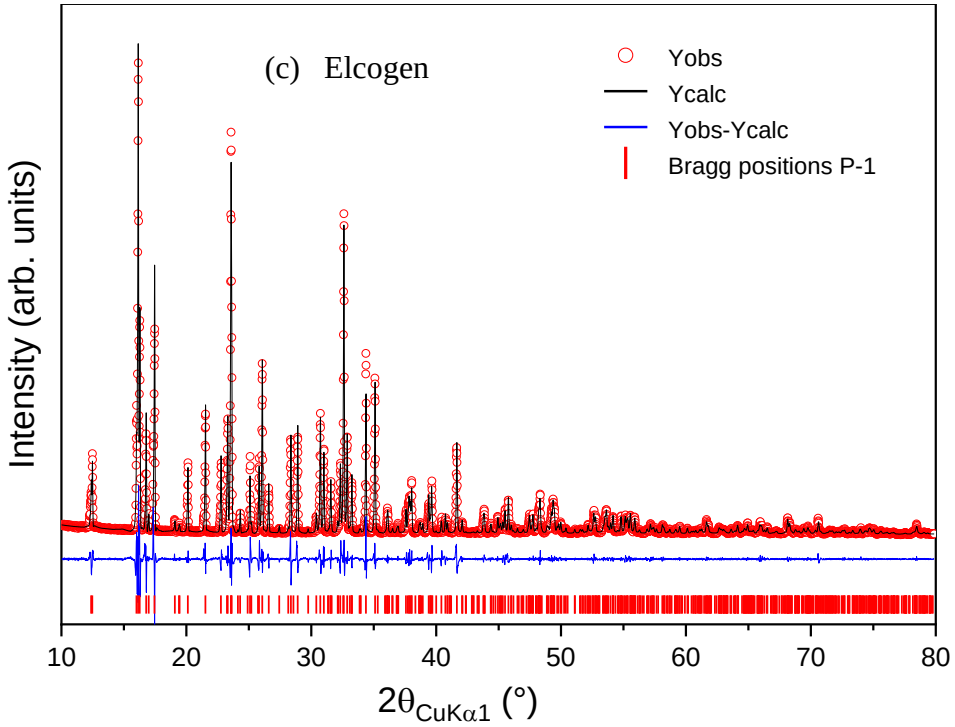

Figure 3. 3 (a) Rietveld refinement plot of the XRD data of (bottom) the recovered air electrode material from Fiaxell. (b) Rietveld refinement plot of the XRD data of the recovered hydrated nickel nitrate from Fiaxell, (c) the recovered hydrated nickel nitrate (Elcogen cells).

In order to verify whether elements from the neighboring layers (GDC and YSZ) are present in the air electrode, the compositions and trace elements of the recycled LSC (Fiaxell cell) are analyzed using an ICP-MS calibrated with mono-elemental solutions of La, Sr, Co, Ce, Fe, Gd, Si, Y, and Zr and compared to EDX data. Compositional studies of the recovered air electrode show good agreement between SEM/EDX, ICP data and expected values (Table 3. 1). As expected, the recovered air electrode is mainly composed with Co, La, and Sr. Ce and Gd are present in trace amounts, in accordance with the initial composition of the cells, and confirming that GDC interface has been scratched with the air electrode (Figure 3. 2 (a-b)). The most important impurity is Zr which could come from the electrolyte. The XRD refinement showed no significant variation of the cell parameters compared to the pure LSC, suggesting that these elements are not incorporated in the structure. Since these cells were not used in stacks but directly tested in our laboratory set-up, Si and Fe could be impurities issued from the raw materials used to synthesize the air electrode and it does not seem to affect electrochemical performance (Figure S3.1 and Figure S3.2).

Table 3. 1 EDX and ICP-AES compositional analysis of recovered LSC.

	Co	La	Sr	Ce	Gd	Zr	Si	Y	Fe
Expected value At. %	50.00	30.00	20.00	-	-	-	-	-	-
EDX At.%	51.34	28.35	19.82	0.47	0.024	-	-	-	-
ICP-MS At.%	52.56	28.66	17.77	0.07	0.02	0.65	0.13	0.06	0.06

3.2.2. Recovery of NiO

Nitric acid leaching and centrifugation allows the separation of a green solution (Figure S3.3) and a white powder. Concerning the green solution, after drying at 75°C overnight, a green powder is obtained (Figure S3.3). XRD analysis shows a well crystallized powder (

Figure 3. *3* (b and c)). After Rietveld refinement, the lattice parameters are comparable to those of $Ni(H_2O)_6(NO_3)_2$ (ICSD 9127) with a = 7.694(10) Å, b = 11.916(12) Å, c = 5.817(8) Å, α =102.3(2)°, β = 102.4(1)°, γ = 105.9(3)°, V = 479.5(153)Å^3), P-1 space group. An impurity not identified is present in small amount (0.60(11) wt. %) on Fiaxell XRD pattern while no impurity is observed on the Elcogen XRD pattern.

Thermal gravimetric analysis of recovered hydrated nickel nitrate from Fiaxell, Elcogen cells and Ni(H2O)6 (NO3)2 from literature are presented in Figure 3. 4a. The Rietveld refinement plot of the XRD data of the recovered NiO from Fiaxell (bottom) with the final R values are Rexp = 5.75 %, Rwp = 7.10 %, Rp = 5.28 % and GOF = 1.23 (Figure 3.4 b). NiO recovered from Elcogen cells (top) has R values Rexp = 5.56 %, Rwp = 9.14 %, Rp = 6.72 % and GOF = 1.64 (Figure 3. 4b). The Rietveld refinement plot of the XRD data of the recovered YSZ from (Fiaxell) exhibiting three phases present in different amounts (Figure 3. 4 c.). The first phase is monoclinic P21/c space group (a = 5.169(2) Å, b = 5.209(2) Å, c = 5.320(2) Å, β = 98.679(6)°, V = 141.58(10) Å^3). The final R values are Rexp = 6.71 %, Rwp = 10.20 %, Rp = 7.67 % and GOF = 1.52. The second is .tetragonal phase P42/nmc space group (a = 3.634(5) Å, c = 5.141(14) Å, V = 67.9(3) Å^3). The third is cubic phase Fm-3m space group (a = 5.141(2) Å, V = 135.84(16) Å^3).

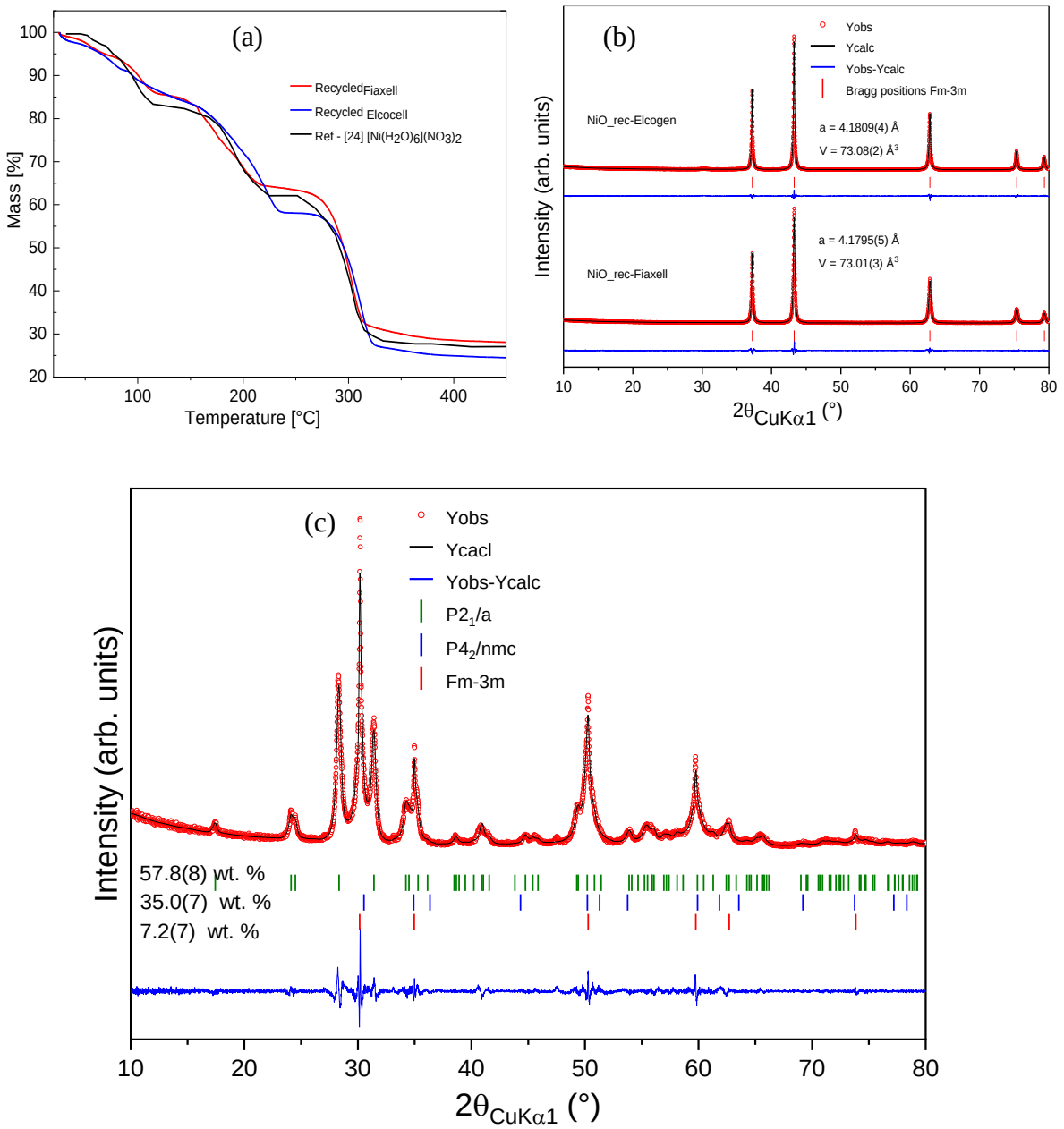

Figure 3. 4 *(a) Thermal gravimetric analysis of recovered hydrated nickel nitrate from Fiaxell, Elcogen cells and $Ni(H_2O)_6$ $(NO_3)_2$ from literature [25], (b) Rietveld refinement plot of the XRD data of the recovered NiO from Fiaxell (bottom).(c) Rietveld refinement plot of the XRD data of the recovered YSZ (Fiaxell.*

Figure 3. 4 (a) shows the thermal decomposition profile of the green powder. Whatever the cell provider, TGA traces are similar and are in agreement with that of the hydrated nickel nitrates reported in the literature [25]. The mass losses occurring between RT and 350°C correspond to the dehydration and decomposition of the nitrate. These processes take place in four main

separate steps (Figure 3.4 a). The first three stages involve the departure of water molecules from the structure and the fourth stage involves the decomposition of the nitrate. The first dehydration occurred at ~50°C and the second dehydration started at ~80°C. The final dehydration occurred at ~155°C and continues up to ~230°C. After complete evaporation of water, the decomposition of nitrate starts at ~270°C and finally the non-decomposable product NiO is collected above ~350°C. All this corresponds to the global reaction of $Ni(NO_3)_2$. xH_2O = NiO + NO_x + xH_2O. From the TGA curve (Figure 3.4 a)**Erreur ! Source du renvoi introuvable.**, it is possible to identify the water content of the nickel nitrate, which was $Ni(NO_3)_2$ $4.4H_2O$ for Fiaxell cell and $Ni(NO_3)_2$ $6.4H_2O$ for Elcogen cell, i.e. consistent with usual water content for commercial products stored at ambient air and room temperature.

The green powder obtained from the thermal decomposition of $Ni(NO_3)_2$. xH_2O is subsequently characterized by X-Ray diffraction. The Rietveld refinement in Figure 3. 4b indicates that the crystalline phase of the powder has cell parameters and cell volume close to those of NiO from database (ICSD 61324: a = 7.1771(2) Å, V = 72.88(1) $Å^3$, Fm-3m space group). For both types of solid oxide cells analyzed, EDX and ICP-MS analysis showed that the green powder is pure nickel oxide of commercial grade (> 99 At. %) with low Y and Si contents, this latter coming probably from the starting YSZ powder. The BET surface area of recovered NiO from Fiaxell and Elcogen products show 8.1 (3) m^2/g and 13.9(3) m^2/g respectively. The particle size of recovered NiO from Fiaxell has 0.13 µm (Figure S3.4), which in the range of commercial powder particle size.

3.2.3. Recovery of Yttrium Stabilized Zirconia (YSZ)

The white sediment left by centrifugation is carefully washed with distilled water and dried at 120ºC for a few hours. The recovered powder was first examined by XRD (Figure 3.4 c). It shows a 3-phase mixture corresponding to YSZ polymorphs. With phase quantification performed using Rietveld refinement, the resulting YSZ powder crystallized mainly in the monoclinic space group $P2_1/a$ and accounted for 57.8(8) wt.% of the total weight. The second most present phase adopted the cubic space group Fm-3m with 7.2(7) wt.%. Finally, the least present phase crystallizes in the tetragonal space group $P4_2/nmc$ with 35.0(7) wt.%. Phase mixing can occur due to various reasons such as manufacturing processes, uneven mixing of

dopant ions and host cations or insufficient amount of dopant, incomplete phase reaction, and thermal history of the material and other phase transformation parameters. The commercial 3YSZ powder provided by Melox Company presents a phase mixture, which resembles to the recovered material.

To confirm that the acid dissolution process does not introduce a new phase, commercial 8YSZ (Tosoh) was treated with concentrated HNO_3 at 75°C. The acid treatment was performed for an extended period of time and the result showed no change in phase type.

An important parameter for a powder, which is useful to produce a dense electrolyte, is the surface area measured by the BET method. The specific surface area of the recovered YSZ powder is determined by adsorption of nitrogen at 77.3 K. BET surface area of recovered YSZ from Fiaxell and Elcogen cells are 3.77 m^2/g and 4.5 m^2/g, respectively. This is in good agreement with the range of BET surface area of commercial YSZ powders with different yttrium concentrations provided by the supplier Melox, which varies from 3 to 5 m^2/g. It can therefore may be used as starting material for fuel cell fabrication. The particle size of the recovered YSZ measured by laser diffraction is 0.39µm (Figure S3.5).

3.2.3. Recycling efficiency of NiO and YSZ: The recovery performance of NiO and YSZ was investigated by a combination of EDX, XRD techniques and TGA analysis. The yield was calculated from a defined quantity (2.5 g) of the powder obtained after scratching the air electrode. The GDC layer is very thin compared to other layers and consequently, it was not taken into account in the recovery calculation. From the EDX quantification of elements in At. %, the percentage of NiO and YSZ phases can be evaluated in wt.%. The percentage phases of NiO and YSZ in wt.% is also given from the XRD pattern studied by Rietveld refinement. Quantification Rietveld refinement and EDX analysis show good agreement. Thus, from the total mass of the used commercial Ni-YSZ/YSZ assembly, the mass of NiO and YSZ can be determined and they will be considered as initial masses in the recovery calculation (m_i NiO and m_i YSZ).

After dissolution and separation, the mass of the recovered YSZ white powder (m_f YSZ) is simply measured with a precision scale. Based on the amount of nickel nitrate hydrate recovered

after recycling and the percentage of nickel oxide obtained at 400°C, as reported in the TGA study, the mass of NiO can be calculated (m_f NiO). Then, the recovery performance of NiO and YSZ is calculated considering the initial and the final masses (Table 3. 2). The yield of NiO recovery is calculated ((m_i NiO / m_f NiO) * 100) and is about 91% for Fiaxell cells and about 92% for Elcogen cells. On the other hand, the yield of YSZ is calculated ((m_i YSZ / m_f YSZ) * 100) and 92% of YSZ was successfully recovered from Fiaxell products and 89% of YSZ is recovered from Elcogen cells. The composition of YSZ given by the relative At. % ratio of yttrium and zirconium (Y/Zr), was also studied and shows that the Y/Zr ratio of recovered YSZ and the original waste material agrees well (see next section 3.3). This indicates that almost no loss of yttrium occurs during the recycling stages.

Table 3. 2 Calculated yield based on initial and final mass of NiO and YSZ materials for Elcogen and Fiaxell cells. The yield was calculated from the EDX data.

Products	Stages	Measured by	Wt. % NiO	Wt. % YSZ	m NiO (g)	m YSZ (g)
Elcogen cells	Initial 2.5g	EDX	48.92	51.08	1.223	1.277
		XRD (TOPAS)	48.95(3)	51.05	1.2237	1.276
	Final	TGA	-	-	1.14(3)	-
		precision scale	-	-	-	1.142(6)
	Yield				NiO 91.8(8)%	YSZ 89.4(5)%
Fiaxell cells	Initial 2.5g	EDX	15.31	84.69	0.3828	2.1175
		XRD	14.52(14)	85.48	0.363	2.137
	Final	TGA	-	-	0.35(1)	-
		precision scale	-	-	-	1.96(4)
	Yield				NiO 91(3)%	YSZ 92(2)%

Concerning concentrated nitric acid (65% HNO_3) used for Ni dissolution, HNO_3 can be recollected back by careful drying system. We managed to collect the HNO_3 vapor by simple distillation and 93.48 vol% of used HNO_3 is recovered. The concentration of recovered HNO_3 is 97.77% of the initial concentration of HNO_3 used. The total yield of HNO_3 recovery including the volume of HNO_3 wasted is about 88%. It is possible to recover back high quality HNO_3 that

can be used repeatedly. The part HNO_3 that is lost is that which is used to make the nickel nitrate complex.

3.3. Densification of the recovered YSZ

Recovered YSZ powders are uniaxial pressed into pellets (Ø = 10mm) and sintered at 1450°C for 10 hours. The density of the sintered samples is determined using sample dimensions and weight (and lattice volume). The densities of sintered pellets from Fiaxell and Elcogen cells are 95.5 % and 96.30 % of their theoretical values, respectively. The morphology and detailed compositional analysis of the sintered, then polished and thermally etched surfaces of the pellets are analyzed using SEM (Figure 3.5). The microstructures are well developed and show a well crystallized and dense structure, separated by visible grain boundaries, consisting of micrometric grains.

Grain-size measurements were obtained from micrographs recorded from the polished and thermally etched samples. The grain size of the YSZ pellet recovered from Elcogen and Fiaxell cells are 1.8 µm and 1 µm, respectively. YSZ recovered from Elcogen cells has clean topography as seen in *Figure 3. 5*b, grains with different topographic features (dark grains in*Figure 3. 5*a) surrounded by YSZ grains are visible with SEM in the case of Fiaxell cells. The compositional study of these dark grains analyzed by EDX shows they are zirconium (IV) silicate phase ($ZrSiO_4$). The segregation of silica through grain boundaries are also observed by EDX elemental mapping. The distribution of the siliceous phase is not homogeneous (Appendix 3). They are more concentrated in some areas of YSZ and sparsely distributed in the other areas. Silica-free grains and grain boundaries are also clearly observed. In addition to Si element, aluminum element was also detected by SEM in Fiaxell product. As we have used zirconia jars and grinding balls instead of Si_3N_4 in the recycling process, and Teflon beaker instead of glass beaker for the dissolution process, these impurities may possibly come from the original commercial precursor of YSZ or from the manufacturing process specific to Fiaxell cells. The fact that these impurities are not present in the case of Elcogen cells confirms this assertion.

The deduced chemical composition of YSZ from EDX analysis is ($Zr_{0.92}Y_{0.08}O_{1.96}$ (~4YSZ)). In the solid oxide cells examined in this study, the fuel electrode is mainly based on 3YSZ while the electrolyte and fuel electrode functional layer are based on 8YSZ. By taking into account the

thickness of each part, it is expected to obtain a YSZ powder with an intermediate composition close to 3YSZ. Since the recovered YSZ is ~4YSZ, it is in the range of expected composition. Regarding the gadolinium-doped ceria (GDC) barrier layer, Gd and Ce are detected in very small amounts in the recovered NiO and YSZ. This is expected since they represent a very small proportion compared to the other elements in the complete cell (*Figure 3. 2*a and b).

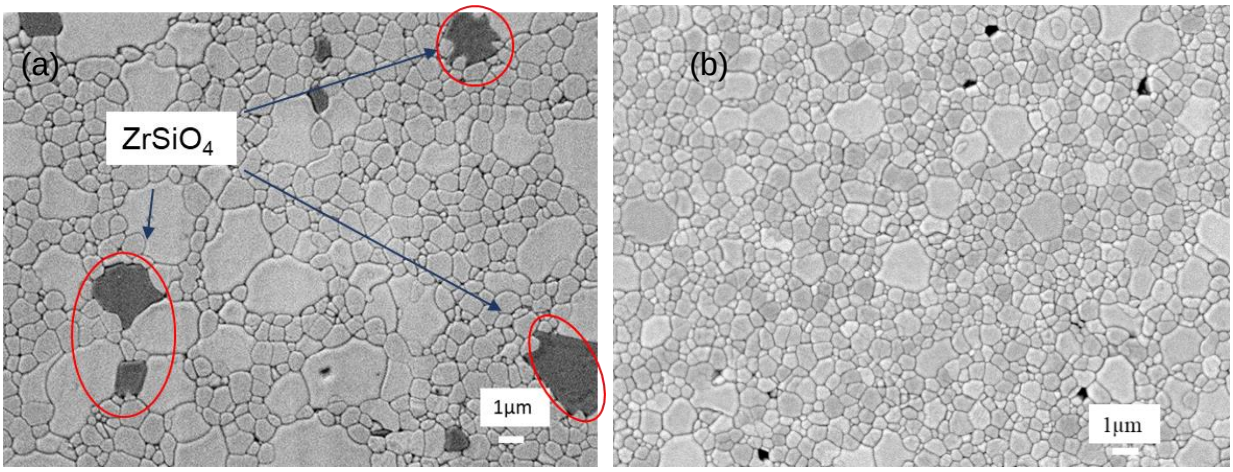

Figure 3. 5 Back scattered SEM images of recycled YSZ from (a) Fiaxell fuel cell technology, (b) Elcogen cell technology. Dark spots seen on (b) are voids.

3.4. Ionic conductivity of recovered YSZ

The conductivities of dense YSZ electrolyte pellets made from recycled materials are measured by electrochemical impedance spectroscopy (EIS). As shown on Figure 3. 6a, at low temperatures, Nyquist plots of LSM/YSZ/LSM symmetrical cells show three depressed semicircles and can be fitted by the electrical equivalent circuit R0 + (R1//CPE1) + (R2//CPE2) + (R3//CPE3). The impedance formula of a Constant Phase Element (CPE) is $1/Q(j\omega)^n$, and the associated real capacitance C is determined from impedance diagrams by the formula $(RC)^n = RQ$ [26], [27]. Figure 3.4 (b) shows the C1 and C2 capacitance values of YSZ recovered from Elcogen and Fiaxell products plotted as a function of temperatures. According to literature [28], they correspond to the bulk capacitance and the grain boundary capacitance whereas C3, always higher than 10^{-3} F cm^{-2} corresponds to the electrode contribution (LSM). Consequently R1, R2 and R3 can be assigned to the resistances of YSZ bulk conductivity ($R1 = R_b$), YSZ grain boundary insulating pahse conductivity contribustion ($R2= R_{gb}$), and electrode contribustion ($R3 = R_{el}$)[29] [30]. Conductivity of YSZ, with grain and grain boundary contribution, can

therefore be calculated without being affected by LSM contribution. As the temperature increases all three contributions are shifted to higher frequencies. Thus, the contribution corresponding to the bulk conductivity disappears above 450°C, and the diagram can be fitted with the equivalent circuit R_b + (R_{gb}//CPE_{gb}) + (R_{el}//CPE_{el}). Above 650°C, the contribution corresponding to the grain boundary disappears, and it is no longer possible to separate bulk and grain boundary contributions. Therefore, the diagram is fitted with the equivalent circuit (R_b + R_{gb}) + (R_{el}//CPE_{el}). The temperature dependence of the total conductivity of samples prepared with recycled YSZ is shown in Figure 3. 6c.

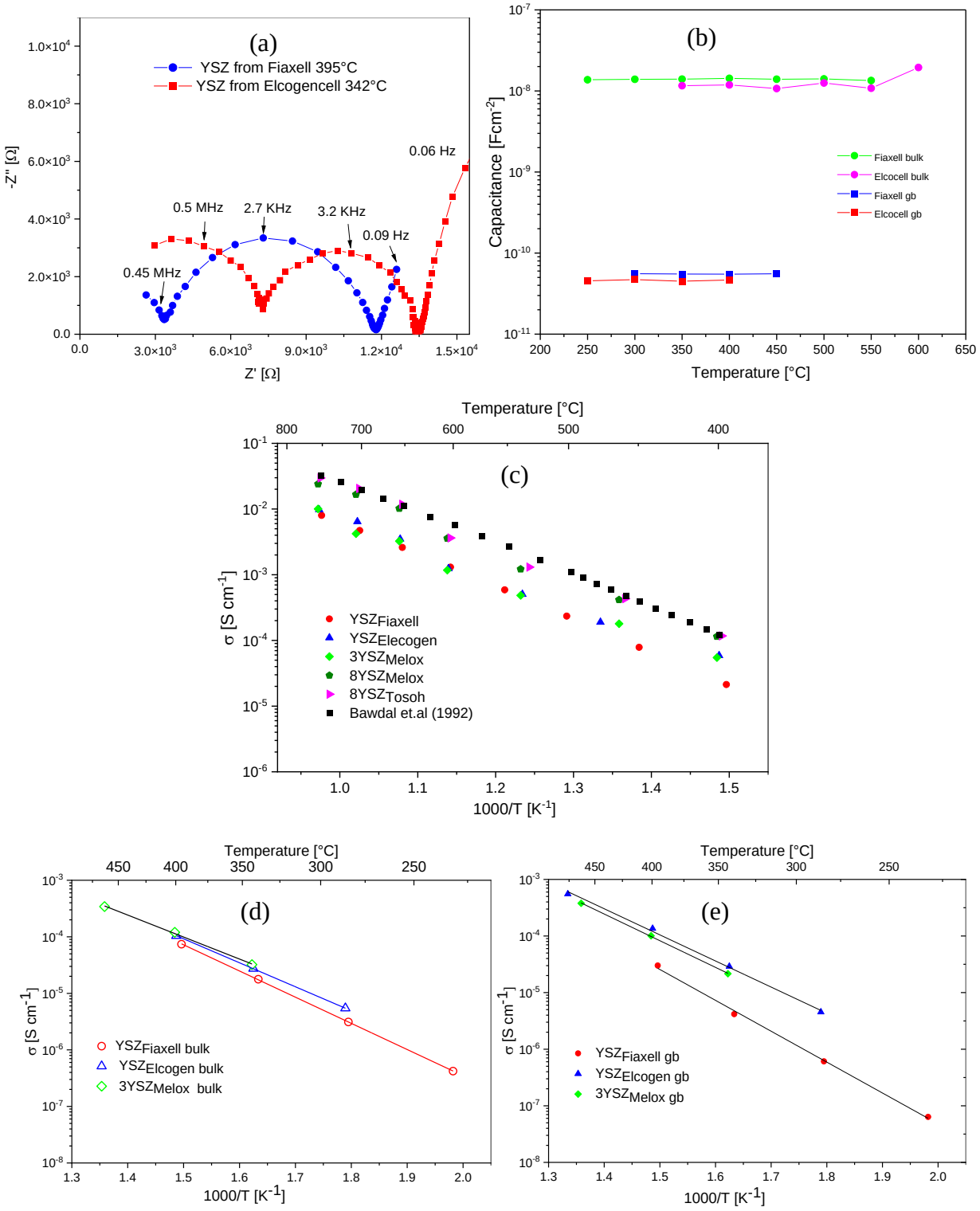

Figure 3. 6. Nyquist plot of recovered YSZ electrolyte from Elcogen cell at 342°C,(b) capacitance values of YSZ recovered from Fiaxell and Elcogen cells as function of temperature (c), comparison of conductivities of recovered YSZ with original precursors and with literature values, and (d) bulk and (e) grain boundary conductivities of recovered YSZ at low temperatures.

The activation energy of conduction as calculated from the plot of natural logarithm as a function of inverse temperature is given in Table 3. 3. The activation energy of recovered YSZ from both products are in the range of activation energy reported on literature [31] [32]. In the 250°C - 550°C range, it is then possible to quantify the different contributions of the total YSZ conductivity as *shown in* Figure 3.6 *d and* e. For the two samples, the activation energy for diffusion of O^{2-} through grain boundary is higher than in the bulk because the space charge layer at those interfaces adds an additional barrier to the diffusion [31- 33]. In the case of YSZ recovered from Fiaxell, the grain boundary resistance is 2 to 6.5 times higher than the bulk, which could be assigned to the presence of significant amount of Si impurities in this sample, as mentioned before. Indeed, previous reports have shown that SiO_2 can segregate to the grain boundaries and block the diffusion of O^{2-} [35]. As the bulk conductivities of the YSZ issued from Elcogen and Fiaxell cells are the same, the lower grain boundary conductivities for YSZ issued from Fiaxell, resulting from the purity level of recovered powders, explain the slightly higher total conductivity values obtained for YSZ recovered from Elcogen.

Table 3. 3 The activation energies for the bulk and grain boundary (E_a^{bulk} and E_a^{gb}) from 250°C to 450°C and for the total conductivities (E^{tot}) from 450°C to 750°C in [eV]

Products	E_a^{bulk} (eV)	E_a^{gb}(eV)	E_a^{tot} (eV)	Products	E_a^{tot} (eV)
4YSZ recovered from Fiaxell	0.92	1.08	0.98	8YSZ prepared from Melox	0.92
4YSZ recovered from Elcocell	0.84	0.91	0.89	8YSZ prepared from Tosoh	0.954
3YSZ prepared from Melox	0.77	0.93	0.85	8YSZ from Badwal [36]	0.95

Figure 3.6 (c) compares the conductivity values of YSZ pellets prepared with the recycled powders and with commercial TOSOH 8YSZ, commercial Melox 8YSZ and commercial Melox 3YSZ. Comparison with 8YSZ studied by Badwal et al. [36] is also presented. The conductivity of the recycled YSZ is lower than that of 8YSZ from Badwal from Melox and Tosoh original materials. The most relevant comparison, both for activation energy and conductivity, is with the 3YSZ from Melox, in accordance with is nearly similar dopant concentration.

An increase of the yttrium content, a stabilization of the single-phase phase as well as an improvement of the conductivity are possible by upcycling with Y_2O_3 (S3.2, Figure S3. *6*, Figure S3. 7, Figure S3 *8*, Figure S3.9 and Figure S3.10).

Conclusion

In this work we succeeded to separate the 3 materials which constitute two types of solid oxide cells. These cells are representative of commercials cells. Using mechanical scratching and grinding, followed by thermal and chemical treatments, components were successfully separated. More than 92% of Nickel oxide and YSZ are recovered. NiO powder is close to commercial product. YSZ was recovered as a 4YSZ powder of micrometer range size, with less than 0.5 At% Si impurities, and presenting, after sintering, a conductivity level close to the primary products' values. As this conductivity is highly dependent on presence of impurities in grain boundary, additional effort should be considered to avoid them from the recycled YSZ. Another suggestion would be to use the recycled YSZ powder only for the preparation of fuel electrode support. Indeed, recovered YSZ would provide good mechanical support at which the ionic conductivity is not as critical as for the functional layer and the electrolyte layer. Future work will consider both strategies.

Reference

[1] S. M. Moosavian, M. Modiri-Delshad, N. A. Rahim, and J. Selvaraj, 'Imperialistic competition algorithm: Novel advanced approach to optimal sizing of hybrid power system', *Journal of Renewable and Sustainable Energy*, vol. 5, no. 5, p. 053141, Sep. 2013, doi: 10.1063/1.4824977.

[2] S. Putt del Pino and World Resources Institute, *Switching to green: a renewable energy guide for office and retail companies*. Washington, D.C.: World Resources Institute, 2006. Accessed: Oct. 08, 2020. [Online]. Available: http://pdf.wri.org/switching_to_green.pdf

[3] Pietzcker, R. C., Longden, T., Chen, W., Fu, S., Kriegler, E., Kyle, P., Luderer, G., 'Long-term transport energy demand and climate policy: Alternative visions on transport decarbonization in energy-economy models', *Energy*, vol. 64, pp. 95–108, Jan. 2014, doi: 10.1016/j.energy.2013.08.059.

[4] O. Tlili, C. Mansilla, D. Frimat, and Y. Perez, 'Hydrogen market penetration feasibility assessment: Mobility and natural gas markets in the US, Europe, China and Japan', *International Journal of Hydrogen Energy*, vol. 44, May 2019, doi: 10.1016/j.ijhydene.2019.04.226.

[5] W. Liu, H. Zuo, J. Wang, Q. Xue, B. Ren, and F. Yang, 'The production and application of hydrogen in steel industry', *International Journal of Hydrogen Energy*, vol. 46, no. 17, pp. 10548–10569, Mar. 2021, doi: 10.1016/j.ijhydene.2020.12.123.

[6] M. Rivarolo, G. Riveros-Godoy, L. Magistri, and A. F. Massardo, 'Clean Hydrogen and Ammonia Synthesis in Paraguay from the Itaipu 14 GW Hydroelectric Plant', *ChemEngineering*, vol. 3, no. 4, p. 87, Nov. 2019, doi: 10.3390/chemengineering3040087.

[6] S. E. Hosseini, and M. A. Wahid, 'Hydrogen production from renewable and sustainable energy resources: Promising green energy carrier for clean development', *Renewable and Sustainable Energy Reviews*, *57*, 850-866, 7 Jan 2016, http://dx.doi.org/10.1016/j.rser.2015.12.112

[8] A. Pandiyan, A. Uthayakumar, R. Subrayan, S. W. Cha, and S. B. Krishna Moorthy, 'Review of solid oxide electrolysis cells: a clean energy strategy for hydrogen generation', *Nanomaterials and Energy*, vol. 8, no. 1, pp. 2–22, Jun. 2019, doi: 10.1680/jnaen.18.00009.

[9] K. P, S. Bm, W. Bn, and R. Pvb, 'Review on Different Components of Solid Oxide Fuel Cells', *J Powder Metall Min*, vol. 06, no. 03, 2017, doi: 10.4172/2168-9806.1000181.

[10] N. Mahato, A. Banerjee, A. Gupta, S. Omar, and K. Balani, 'Progress in material selection for solid oxide fuel cell technology: A review', *Progress in Materials Science*, vol. 72, pp. 141–337, Jul. 2015, doi: 10.1016/j.pmatsci.2015.01.001.

[11] S. Sarner, A. Schreiber, N. H. Menzler, and O. Guillon, 'Recycling Strategies for Solid Oxide Cells', *Advanced Energy Materials*, p. 2201805, Jul. 2022, doi: 10.1002/aenm.202201805.

[12] E. I. Wright, S. Rahimifard, and A. J. Clegg, 'Impacts of environmental product legislation on solid oxide fuel cells', *Journal of Power Sources*, vol. 190, no. 2, pp. 362–371, May 2009, doi: 10.1016/j.jpowsour.2009.01.069.

[13] K. Al-Khori, S. G. Al-Ghamdi, S. Boulfrad, and M. Koç, 'Life Cycle Assessment for Integration of Solid Oxide Fuel Cells into Gas Processing Operations', *Energies*, vol. 14, no. 15, p. 4668, Aug. 2021, doi: 10.3390/en14154668.

[14] R. Hischier, P. Wäger, and J. Gauglhofer, 'Does WEEE recycling make sense from an environmental perspective?', *Environmental Impact Assessment Review*, vol. 25, no. 5, pp. 525–539, Jul. 2005, doi: 10.1016/j.eiar.2005.04.003.

[15] S. N. M. Menikpura, A. Santo, and Y. Hotta, 'Assessing the climate co-benefits from Waste Electrical and Electronic Equipment (WEEE) recycling in Japan', *Journal of Cleaner Production*, vol. 74, pp. 183–190, Jul. 2014, doi: 10.1016/j.jclepro.2014.03.040.

[16] K. Parajuly, K. Habib, and G. Liu, 'Waste electrical and electronic equipment (WEEE) in Denmark: Flows, quantities and management', *Resources, Conservation and Recycling*, vol. 123, pp. 85–92, Aug. 2017, doi: 10.1016/j.resconrec.2016.08.004.

[17] M. Kamiya, Y. Mori, T. Kojima, R. Sasai, and H. Itoh, 'Recycling process for yttria-stabilized tetragonal zirconia ceramics using a hydrothermal treatment', *J Mater Cycles Waste Manag*, vol. 9, no. 1, pp. 27–33, Mar. 2007, doi: 10.1007/s10163-006-0168-3.

[18] V. Coman, B. Robotin, and P. Ilea, 'Nickel recovery/removal from industrial wastes: A review', *Resources, Conservation and Recycling*, vol. 73, pp. 229–238, Apr. 2013, doi: 10.1016/j.resconrec.2013.01.019.

[19] V. J. Ferreira *et al.*, '5 kW SOFC stack via 3D printing manufacturing: An evaluation of potential environmental benefits', *Applied Energy*, vol. 291, p. 116803, Jun. 2021, doi: 10.1016/j.apenergy.2021.116803.

[20] A. A. Coelho, 'TOPAS and TOPAS-Academic: an optimization program integrating computer algebra and crystallographic objects written in C++', *J Appl Cryst*, vol. 51, no. 1, Art. no. 1, Feb. 2018, doi: 10.1107/S1600576718000183.

[21] Q.-A. Huang, R. Hui, B. Wang, and J. Zhang, 'A review of AC impedance modeling and validation in SOFC diagnosis', *Electrochimica Acta*, vol. 52, no. 28, pp. 8144–8164, Nov. 2007, doi: 10.1016/j.electacta.2007.05.071.

[22] D. Johnson, 'ZView and ZPlot: a Software Program for IES Analysis, Version 2.8, Scribner Associates', *Inc., Southern Pines, NC*, 2002.

[23] R. Ihringer, '2R-Cell: A Universal Cell for an Easy and Safe SOFC Operation', *ECS Trans.*, vol. 35, no. 1, p. 393, Apr. 2011, doi: 10.1149/1.3570014.

[24] M. Noponen *et al.*, 'Status of Solid Oxide Fuel Cell Development at Elcogen', *ECS Transactions*, vol. 68, no. 1, pp. 151–156, Jul. 2015, doi: 10.1149/06801.0151ecst.

[25] W. Brockner, C. Ehrhardt, and M. Gjikaj, 'Thermal decomposition of nickel nitrate hexahydrate, Ni(NO3)2·6H2O, in comparison to Co(NO3)2·6H2O and Ca(NO3)2·4H2O', *Thermochimica Acta*, vol. 456, no. 1, pp. 64–68, May 2007, doi: 10.1016/j.tca.2007.01.031.

[26] K. S. Cole and R. H. Cole, 'Dispersion and Absorption in Dielectrics I. Alternating Current Characteristics', *The Journal of Chemical Physics*, vol. 9, no. 4, pp. 341–351, Apr. 1941, doi: 10.1063/1.1750906.

[27] J. ROSS Macdonald, 'Impedance spectroscopy', *Impedance Spectroscopy*, p. 17.

[28] J. Nielsen and J. Hjelm, ‘Impedance of SOFC electrodes: A review and a comprehensive case study on the impedance of LSM:YSZ cathodes’, *Electrochimica Acta*, vol. 115, pp. 31–45, Jan. 2014, doi: 10.1016/j.electacta.2013.10.053.

[29] M. Gerstl, E. Navickas, G. Friedbacher, F. Kubel, M. Ahrens, and J. Fleig, ‘The separation of grain and grain boundary impedance in thin yttria stabilized zirconia (YSZ) layers’, *Solid State Ionics*, vol. 185, no. 1, pp. 32–41, Mar. 2011, doi: 10.1016/j.ssi.2011.01.008.

[30] X. Guo and J. Maier, ‘Grain Boundary Blocking Effect in Zirconia: A Schottky Barrier Analysis’, *J. Electrochem. Soc.*, vol. 148, no. 3, p. E121, 2001, doi: 10.1149/1.1348267.

[31] C. Ahamer, A. K. Opitz, G. M. Rupp, and J. Fleig, ‘Revisiting the Temperature Dependent Ionic Conductivity of Yttria Stabilized Zirconia (YSZ)’, *J. Electrochem. Soc.*, vol. 164, no. 7, pp. F790–F803, 2017, doi: 10.1149/2.0641707jes.

[32] X. Guo and Y. Ding, ‘Grain Boundary Space Charge Effect in Zirconia’, *J. Electrochem. Soc.*, vol. 151, no. 1, p. J1, 2004, doi: 10.1149/1.1625948.

[33] M. J. Verkerk, B. J. Middelhuis, and A. J. Burggraaf, ‘Effect of grain boundaries on the conductivity of high-purity ZrO2□ Y2O3 ceramics’, *Solid State Ionics*, vol. 6, no. 2, pp. 159–170, 1982.

[34] X. Guo, ‘Role of space charge in the grain boundary blocking effect in doped zirconia’, *Solid State Ionics*, vol. 154–155, pp. 555–561, Dec. 2002, doi: 10.1016/S0167-2738(02)00491-5.

[35] M. C. Martin and M. L. Mecartney, ‘Grain boundary ionic conductivity of yttrium stabilized zirconia as a function of silica content and grain size’, *Solid State Ionics*, p. 13, 2003.

[36] S. Badwal, ‘Zirconia-based solid electrolytes: microstructure, stability and ionic conductivity’, *Solid State Ionics*, vol. 52, no. 1–3, pp. 23–32, May 1992, doi: 10.1016/0167-2738(92)90088-7.

Supplementary information

S3.1 Supplementary characterisation of recovered products

The Area Specific Resistance (ASR) of the recovered air electrode is investigated by EIS. The commercial $Gd_{0.1}Ce_{0.9}O_2$ (GDC) electrolyte is used as the support material, and symmetrical LSC/commercial GDC/LSC are studied under ambient air and results are shown in Figure S3.1a. At studied temperatures (>600°C) the total measured impedance includes the inductive contribution of wire (L), the electrolyte (GDC) resistance (Ro), and R_{ct}//CPE_{ct} and R_{diff}//CPE_{diff} elements associated to charge transfer and gas diffusion reactions at electrodes.

The following equation was used to compute area-specific resistance (ASR): ASR is equal = (R_pxA)/2, where R_p is the resistance or polarization resistance at the air electrode-electrolyte interface and A is a specific area of the active air electrode. ASR for LSC recovered from Fiaxell is 0.08 Ωcm^2 at 700℃ and 1.42 Ωcm^2 at 600℃. Whereas ASR for LSC recovered from Elcogen is 0.144 Ωcm^2 at 700℃ and 2.24 Ωcm^2 at 600℃.

ASR values obtained for recovered LSC from Elcogen cells are slightly higher than LSC recovered from Fiaxell, probably related to slight differences in composition [1] [2].

These values are compared with internal reference from our group at a composition of $La_{0.6}Sr_{0.4}CoO_3$ and shows slightly lower ASR (Figure S3.1b).

The microstructure studied by SEM shows a porous structure as expected and required. The topography of the air electrode is well crystallized in both samples (Figure S3.2).

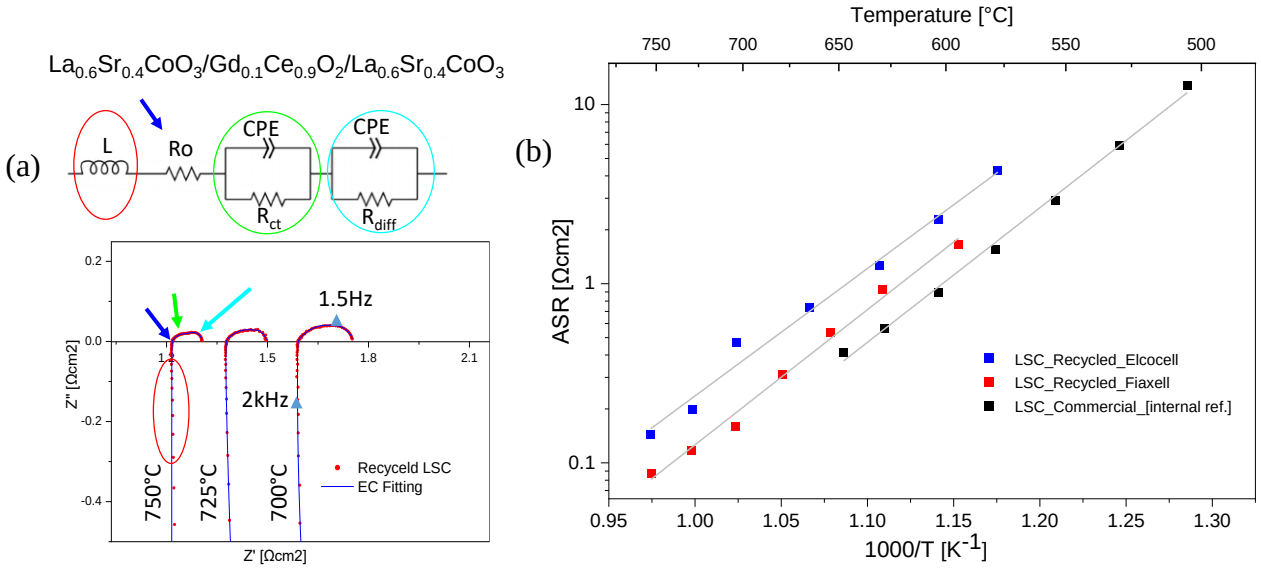

Figure S3.1 (a) Nyquist plot of EIS spectra of the electrode response of made from recovered LSC from Fiaxell. (b) ASR measurement of recovred LSC from Elcogen and Fiaxell in comparsion with internal refrence of commercial powder $La_{0.6}Sr_{0.4}CoO_{3.}$

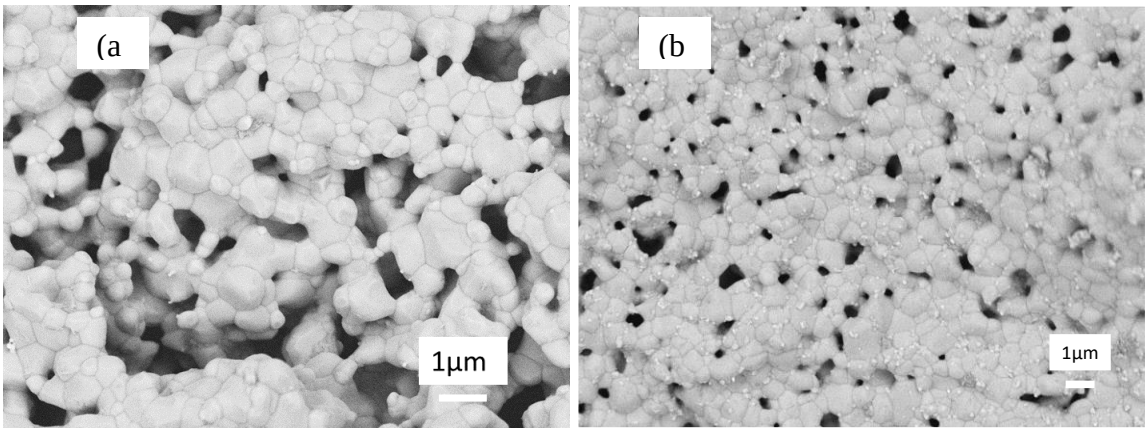

Figure S3.2 The SEM microstruture of post EIS analysis of recovered LSC from (a) by mechanical scratching from Fiaxell and (b) Elcogen cells.

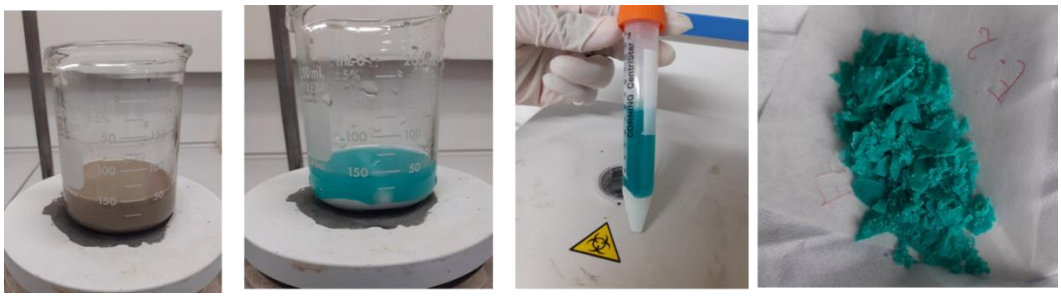

Figure S3.3 Illustration of leaching and recovery of green solution of Ni^{2+} cations, and final hydrated nickel nitrate obtained after drying the solution at 70°C.

The microscopic images of recovered NiO powders recovered from Fiaxell and Elcogen products show micro and sub-micro particles (Figure S3.4a and b).

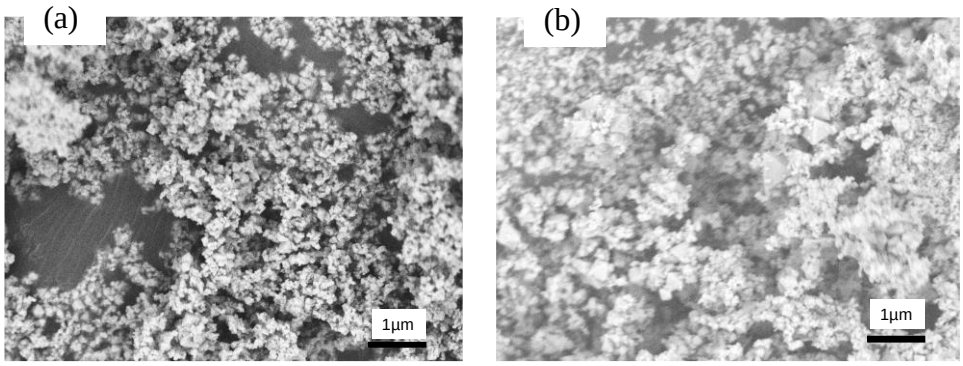

Figure S3.4 SEM images of NiO powders recovered by mechanical scratching from (a) Fiaxell and (b) Elcogen cell.

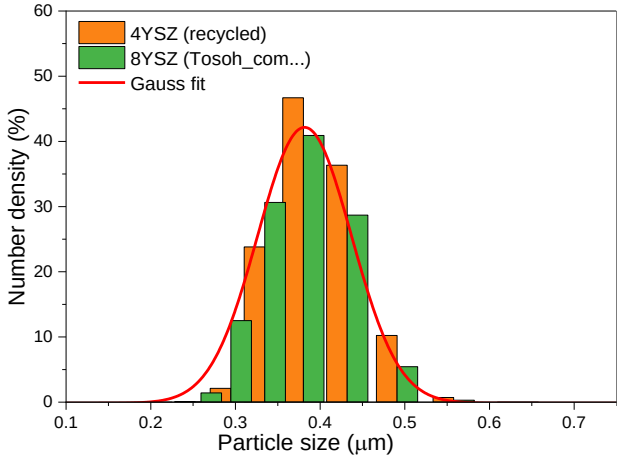

Figure S3.5 Histograms of particle size distribution of YSZ from Fiaxell obtained by mechanical scratching.

S3.2 Upgrading of YSZ recovered materials

The recovered YSZ has a composition of about 4YSZ and is a mixture of three polymorphs of zirconia, i.e. tetragonal, cubic, and monoclinic. 8YSZ, generally used for the electrolyte, shows a conductivity level about 10^{-2} S cm^{-1} at 700°C and adopts a cubic structure with Fm-3m space group. The main objective of "upgrading" the recovered YSZ material is to obtained new compositions such as 8YSZ through the introduction of Y_2O_3.

In situ thermal X-ray diffraction of recovered YSZ

The phase transformation as a function of temperature is studied with in situ thermal X-ray powder diffraction (XRD) using Bruker D8 Advance diffractometer in Bragg-Brentano geometry with a Cu-$K_{\alpha1}$ and $K_{\alpha2}$ radiation (λ = 1.5406 Å) and (1.544390 Å) respectively. The ratio of $K_{\alpha1}$ to $K_{\alpha2}$ is 0.500. Each 2θ-scan was performed from 10 to 80 degrees with a step size of 0.012° (Figure S3. 6).

With increasing temperature at the rate of 0.1℃/sec, the recovered YSZ tends to undergo a progressive phase transformation, i.e., the cubic and monoclinic phases changes into the tetragonal phase (Figure S3. 7). At 1100°C, the tetragonal phases represents about 79.5(7) wt.%, the cubic phase accounts for only 18.9(7) wt.%, and the monoclinic phase accounts for only 1.62(16) wt.% . After cooling to 30°C at the same rate, the cubic phase amount decreases and accounts for 12.3(10) wt.%, while the tetragonal phase increases to 85.6(10) wt.%, whereas no change is observed for the monoclinic phase. The amount of each phase is relatively constant with the main phase being the tetragonal phase (~80- 85 wt.%), the cubic phase is present at about ~12-18 wt. % and the monoclinic phase is almost no represented (Figure S3. 7).

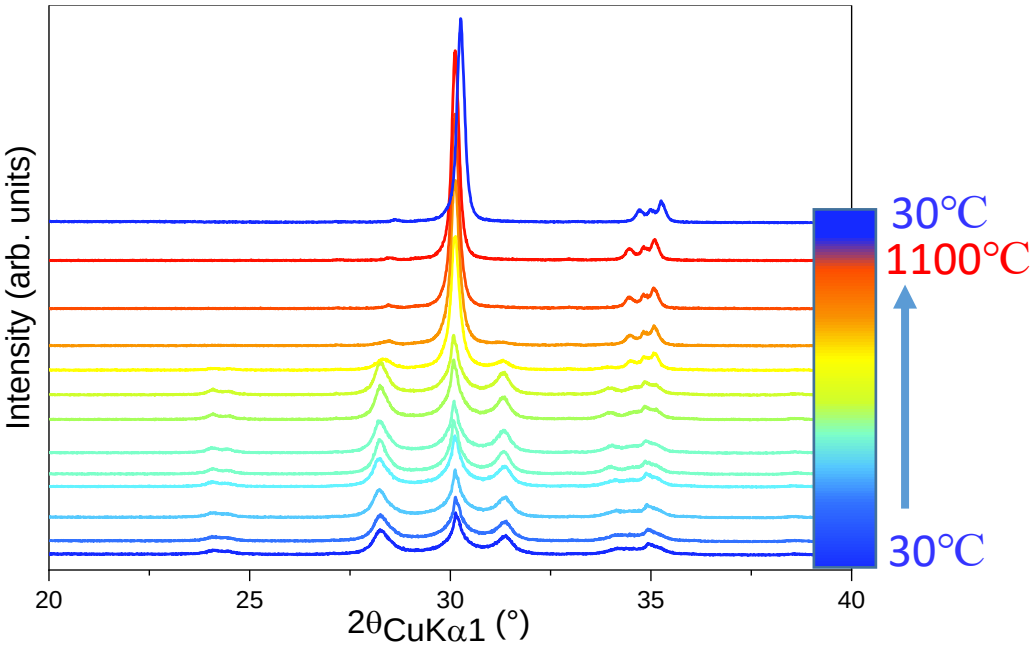

Figure S3. 6 XRD patterns of in situ diffraction of recovered YSZ from RT to 1100°C at 0.2°C/sec heating and cooling rate, with temperature steps of 100°C.

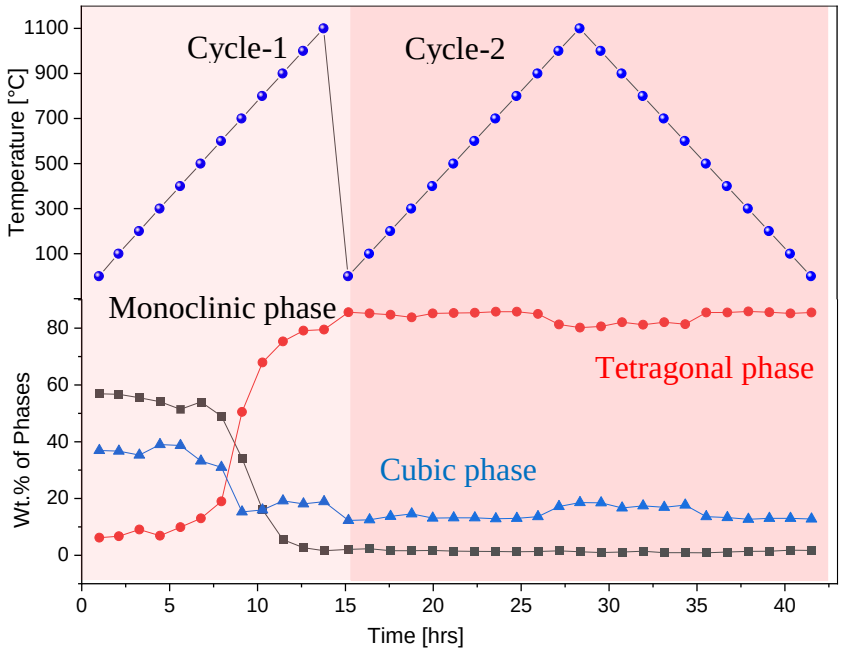

Figure S3. 7 Weight fraction of phases as a function of temperature. Cycle-1: heating from 30°C to 1100°C and cooling to 30°C. Cycle-2: heating from 30°C to 1100°C and cooling to 30°C.

Optimization of yttrium content of recovered YSZ

Recovered YSZ powder was carefully weighed and mixed with commercial Y_2O_3 (Sigma Aldrich). Before mixing, the amount of Y_2O_3 required to increase the yttrium content from 4YSZ to 6YSZ, 8YSZ and 10YSZ is calculated. The mixture was ground in absolute ethanol for 6 hours using zirconia jars and balls in a planetary ball mill. After drying, the powder was uniaxially pressed at 125 MPa into pellets (10 mm diameter) without any pre-thermal treatment. Then the pellet was sintered at 1450°C for 10 hours with 300°C/h heating and 100°C/h cooling rates.

XRD characterization of adapted YSZ

Quantification analysis of the 6YSZ powder after sintering gives a mixture of 69.3(3) wt.% of a tetragonal phase ($P4_2$/nmc space group) with a = 3.60465(12) Å and c = 5.1826(2) Å and 0.7(3) wt.% of a cubic phase (Fm-3m space group) with a = 5.14000 Å (Figure S3.10a). On the other hand, 8YSZ stabilizes in a single cubic phase (Fm-3m space group), with a= 5.14001(1) Å, in accordance with ICSD 238379 database [6] (Figure S3.10). The amount of yttrium in 8YSZ is sufficient to stabilize the cubic phase, as studied in the literature, e.g., [7]. Finally, 10YSZ with lattice parameter a= 5.145(2) agrees well with the values of 10YSZ from the ICSD_181236 database [8] (Figure S3.10c).

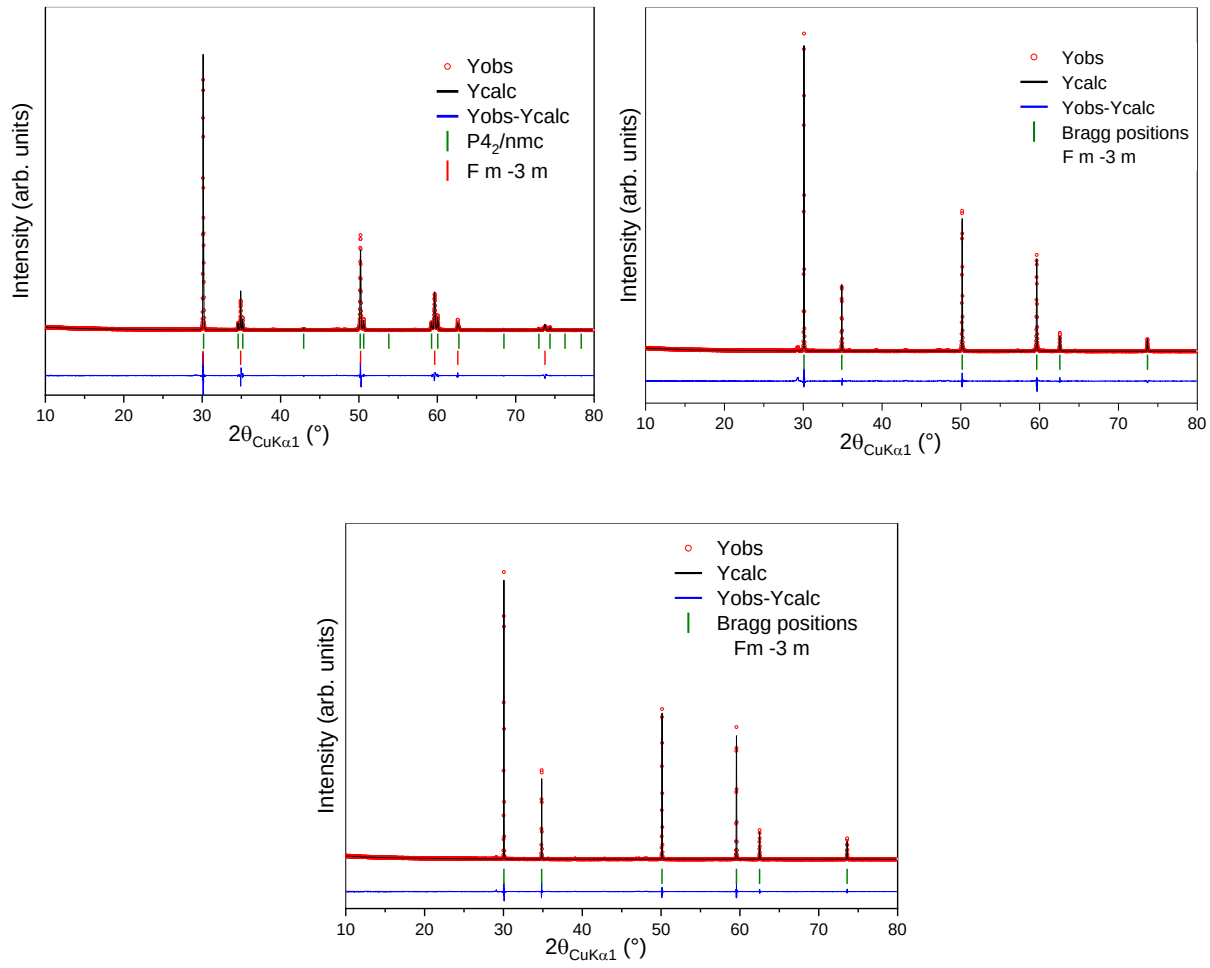

Figure S3 8 XRD of YSZ_{rec}+Y_2O_3 = (a) 6YSZ, (b) 8YSZ and (c) 10YSZ ball milled for 6h with zirconia jar and sintered at 1450°C for 10hrs.

Microstructure and density of optimized YSZ

The relative density of 6YSZ, 8YSZ and 10YSZ pellets are 97.2%, 96.7%, and 94.9% respectively, i.e. convenient for assuming gas tightness and being used as electrolyte [9]. The cross-sectional structure of the sintered and thermally etched pellets is shown in Figure S3.9. Rare pores appearing between the grains could have been created by removal of small grains induced by Ar ion during cross-section preparation. Dark silica grains (zircon (ZrSiO4)) are visible between YSZ grains. As shown in Table S3.1, YSZ grain size increases with the yttrium content increases, as reported in literature [10].

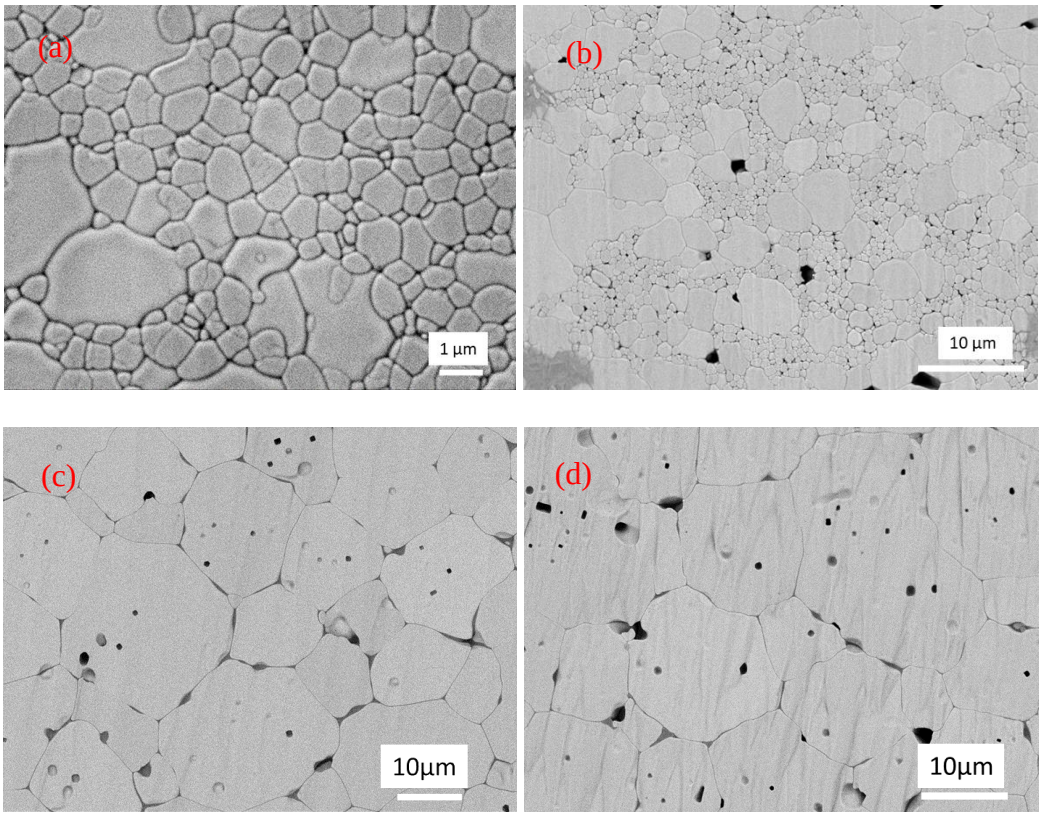

Figure S3.9 SEM images of recycled YSZ modified to (a) 4YSZ (as recovered), (b) 6YSZ, (c) 8YSZ and (d) 10YSZ.

Table S3.1 Relative density and grain sizes of various compositions of modified YSZ after sntering at 1450°C during 10h.

Sample	Time (h)	Density (%)	Grain size (µm)
4YSZ(as recovered)	10	97.2	1.0
6YSZ	10	97.2	1.5
8YSZ	10	96.7	5.7
10YSZ	10	94.9	31

Ionic conductivity of optimized YSZ

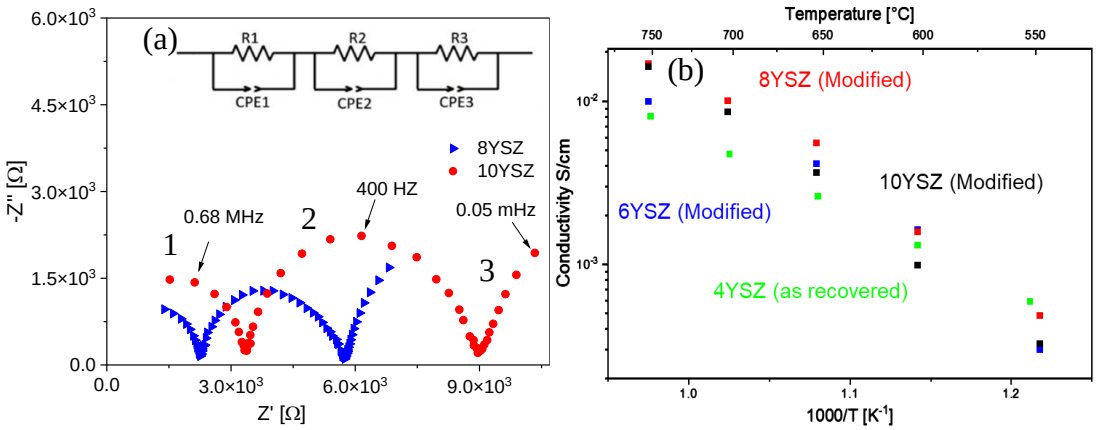

Figure S3.10 (a) Typical impedance spectra of Nyquist plot YSZ plots of 8YSZ and 10YSZ t 400°C (b) variation of conductivity of recycled and modified YSZ with temperature.

EIS analysis shows that better ionic conductivities are obtained after optimization, and decreased in the order 8YZ > 10YSZ > 6YSZ > 4YSZ (i.e. as recovered) (Figure S3.10). The grain boundary resistance was assumed to be in series with the lattice one, and an equivalent circuit was proposed (Figure S3.10a), in which the three R//CPE elements correspond respectively to bulk, grain boundary and electrode contributions, as explained above. At high temperatures, 8YSZ and 10YSZ have almost the same conductivity. However, below 700°C, the conductivity of 8YSZ is slightly higher than that of 10YSZ. This lower conductivity values for modified 10YSZ are due to over doping and defect association of charge carriers, as explained in literature [11] [12].

S3.3 Direct recovery of Y_2O_3 and ZrO_2 from recovered YSZ

YSZ is known as stable ceramic material that cannot be dissolved in usual media. The goal of this section is to recover ZrO_2 and Y_2O_3. Na_2ZrO_3 [1] can be used as intermediate since its solubility in HNO_3 is high. This compound can be easily formed by reacting YSZ and Na_2CO_3.

[1] Na_2ZrO_3 is an intermediary compound in zirconium mining obtained from zircon, according to the reaction: ZrSiO4 + 4NaOH = Na2ZrO3 + Na2SiO3 + 2H2O

For practical demonstration, 8YSZ (Tosoh) is mixed with Na_2CO_3 and thermal treatment is carried out at 900°C for 4h and 1000°C for 20h. Resulting Na_2ZrO_3 is characterized by XRD (Figure S3.10).

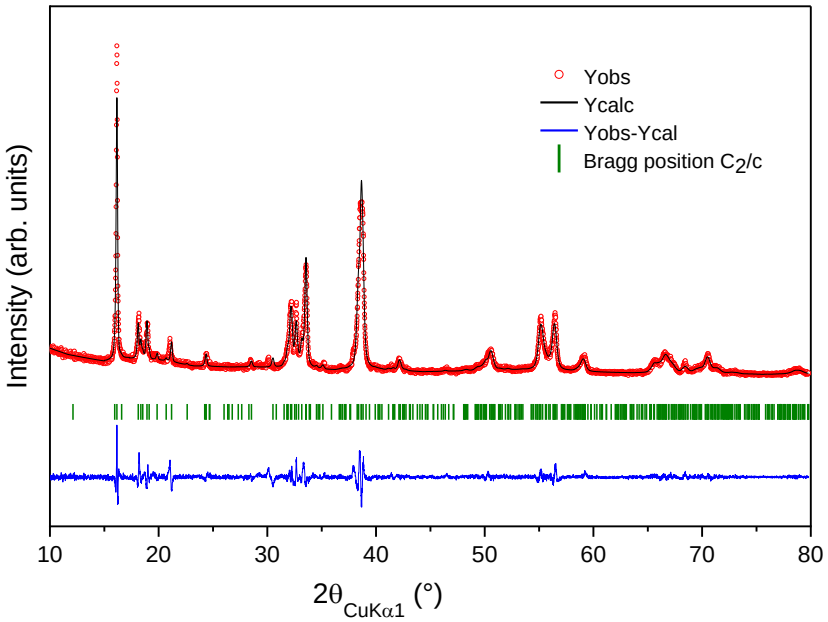

Figure S3.11 The refinement plot of the Na_2ZrO_3 crystallizing in monoclinic C2/c space group with a = 5.6409(7) Å, b = 9.7535(10) Å, c = 11.0884(13) Å, β = 99.354(9)° and V = 601.96(12) Å^3. The final R-values are Rexp = 7.89 %, Rwp = 17.65 %, Rp = 12.75 % and GOF = 2.24.

Reference

[1] Z. Zhu, Y. Shi, C. Aruta, and N. Yang, 'Improving Electronic Conductivity and Oxygen Reduction Activity in Sr-Doped Lanthanum Cobaltite Thin Films: Cobalt Valence State and Electronic Band Structure Effects', *ACS Appl. Energy Mater.*, p. acsaem.8b00931, Oct. 2018, doi: 10.1021/acsaem.8b00931.

[2] J. Hwang *et al.*, 'Study on the Electrode Reaction Mechanism of Pulsed-Laser Deposited Thin-Film $La_{1-x}Sr_xCoO_{3-\delta}$ (x = 0.2. 0.4) Cathodes', *J. Electrochem. Soc.*, vol. 159, no. 10, pp. F639–F643, 2012, doi: 10.1149/2.038210jes.

[3] G. M. Wolten, 'Diffusionless Phase Transformations in Zirconia and Hafnia', *Journal of the American Ceramic Society*, vol. 46, no. 9, pp. 418–422, Sep. 1963, doi: 10.1111/j.1151-2916.1963.tb11768.x.

[4] J. Kelly and I. Denry, 'Stabilized zirconia as a structural ceramic: An overview☆', *Dental Materials*, vol. 24, no. 3, pp. 289–298, Mar. 2008, doi: 10.1016/j.dental.2007.05.005.

[5] W. M. Kriven, 'Possible Alternative Transformation Toughening to Zirconia: Crystallographic Aspects', *J American Ceramic Society*, vol. 71, no. 12, pp. 1021–1030, Dec. 1988, doi: 10.1111/j.1151-2916.1988.tb05786.x.

[6] T. Itoh *et al.*, 'Effect of Annealing on Crystal and Local Structures of Doped Zirconia Using Experimental and Computational Methods', *J. Phys. Chem. C*, vol. 119, no. 16, pp. 8447–8458, Apr. 2015, doi: 10.1021/jp5117118.

[7] D. G. Lamas, 'X-ray diffraction study of compositionally homogeneous, nanocrystalline yttria-doped zirconia powders', p. 5.

[8] M. Ando *et al.*, 'High field O-17 NMR study of defects in doped zirconia and ceria', *Solid State Ionics*, vol. 192, no. 1, pp. 576–579, Jun. 2011, doi: 10.1016/j.ssi.2010.04.024.

[9] D. Panthi, N. Hedayat, and Y. Du, 'Densification behavior of yttria-stabilized zirconia powders for solid oxide fuel cell electrolytes', *J Adv Ceram*, vol. 7, no. 4, pp. 325–335, Dec. 2018, doi: 10.1007/s40145-018-0282-4.

[10] J. Kondoh, H. Shiota, K. Kawachi, and T. Nakatani, 'Yttria concentration dependence of tensile strength in yttria-stabilized zirconia', *Journal of Alloys and Compounds*, vol. 365, no. 1–2, pp. 253–258, Feb. 2004, doi: 10.1016/S0925-8388(03)00640-6.

[11] X. Guo and Z. Wang, 'Effect of niobia on the defect structure of yttria-stabilized zirconia', *Journal of the European Ceramic Society*, vol. 18, no. 3, pp. 237–240, Jan. 1998, doi: 10.1016/S0955-2219(97)00123-4.

[12] J. P. Goff, W. Hayes, S. Hull, M. T. Hutchings, and K. N. Clausen, 'Defect structure of yttria-stabilized zirconia and its influence on the ionic conductivity at elevated temperatures', *Phys. Rev. B*, vol. 59, no. 22, pp. 14202–14219, Jun. 1999, doi: 10.1103/PhysRevB.59.14202.

[13] S. P. S. Badwal, 'Electrical conductivity of single crystal and polycrystalline yttria-stabilized zirconia', *J Mater Sci*, vol. 19, no. 6, pp. 1767–1776, Jun. 1984, doi: 10.1007/BF00550246.

[14] M. Gödickemeier *et al.*, 'Effect of intergranular glass films on the electrical conductivity of 3Y-TZP', *J. Mater. Res.*, vol. 9, no. 5, pp. 1228–1240, May 1994, doi: 10.1557/JMR.1994.1228.

[15] X. Guo and J. Maier, 'Grain Boundary Blocking Effect in Zirconia: A Schottky Barrier Analysis', *J. Electrochem. Soc.*, vol. 148, no. 3, p. E121, 2001, doi: 10.1149/1.1348267.

[16] X. Guo, ‘Role of space charge in the grain boundary blocking effect in doped zirconia’, *Solid State Ionics*, vol. 154–155, pp. 555–561, Dec. 2002, doi: 10.1016/S0167-2738(02)00491-5.
[17] A. Hughes and S. Badwal, ‘Impurity and yttrium segregation in yttria-tetragonal zirconia’, *Solid State Ionics*, vol. 46, no. 3–4, pp. 265–274, Jul. 1991, doi: 10.1016/0167-2738(91)90225-Z.
[18] R. Raj, ‘Morphology and Stability of the Glass Phase in Glass Ceramic Systems’, *J American Ceramic Society*, vol. 64, no. 5, pp. 245–248, May 1981, doi: 10.1111/j.1151-2916.1981.tb09596.x.
[19] V. Subotić and C. Hochenauer, ‘Analysis of solid oxide fuel and electrolysis cells operated in a real-system environment: State-of-the-health diagnostic, failure modes, degradation mitigation and performance regeneration’, *Progress in Energy and Combustion Science*, vol. 93, p. 101011, Nov. 2022, doi: 10.1016/j.pecs.2022.101011.

Chapter 4: Alternative scalable recycling route using Dimethylglyoxime

4.1. Introduction

In Chapter 3, the recycling by "mechanical scratching" route and characterizations of the recycled ceramic materials were presented. The recovery of the air electrode materials was performed by mechanical scratching. The remaining part of the cell was crushed and undergo ball milling followed by leaching for preferential leaching of nickel. This recovery route was successful and has the advantage of being less prone to contamination of the air electrode components. It also has the advantage of not requiring additional chemical input other than HNO_3, making it an economical and simple route.

Nevertheless, the disadvantage associated with mechanical scratching is that it is not easily applicable at industrial scale. Especially in the case of broken cells. Indeed, the recovery efficiency of the air electrode is low, about 64 wt.%, probably associated with the dispersion of very fine powders. Moreover, after scratching, significant amounts of deposit remain on the surface of the electrolyte, and are only removed during the HNO_3 washing step applied before the fuel electrode /electrolyte crushing.

Another possibility is to dissolve a maximum of cations and to use chemicals to separate these cations. In this route, leaching using HNO_3 and nickel preferential precipitation using Dimethylglyoxime $C_4H_8N_2O_2$ (DMG) are performed directly after the grinding and milling of entire cell components together. For this study, planar cells from Elcogen (Elcogen AS, Tallin, Estonia) [1]) were selected. Details of Elcogen products are presented in chapter 3.

This chapter will present the study of "Dimethylglyoxime (DMG)" route of recycling techniques. First, DMG, its history and application in the chemical industry are introduced, focusing on its end life management. Then, the established recovery of ceramic components of solid oxide cells are described in detail. Simple nitric acid-assisted leaching and nickel Dimethylglyoxime (DMG) complexation are used to recover SOC waste products from a solution comprising nickel, cobalt, strontium, and lanthanum ions. The physical and chemical characterizations of the recovered materials are highlighted in this part. A thorough crystallographic study will be presented to explain the identification and quantification of the phases.

Second, the study will mainly focus on understanding the effects of parameters i.e. pH and cation to DMG ratio, on the recovery of the components. In addition, chemical, and morphological characterizations are shown. Third, the recyclability of the reagents used, namely DMG, is investigated. Finally, mechanical scratching and DMG recycling routes are compared. The differences and preference of the two processes are discussed in terms of chemical purity, cost, and ease of scalability.

4.2 Structure, properties and applications of Dimethylglyoxime

For a century, Dimethylglyoxime (DMG) is widely used in analytical chemistry as a detection, precipitation and photometric reagent for various metal ions such as platinum, palladium, nickel, and others [2] [3]. In the case of nickel, the precipitation from an ammoniacal nickel solution takes the form of a bright red voluminous compound. DMG also allows the detection of nickel in in our skin, when it is released from a watch or a jewelry [4] [5] [6] [7] [8]. In various countries, dimethylglyoxime tests are even available over-the-counter in pharmacies.

Finally, one of the main applications of DMG is in the sustainable recycling of discarded lithium-ion batteries, which are considered as environmentally hazardous substances. The hydrometallurgical process used to leach lithium, cobalt and nickel from the spent cathode materials of these batteries requires precipitation by dimethylglyoxime [9] [10].

In addition, several works have shown that DMG can be recycled and reused in several steps, which would significantly reduce the overall cost and environmental impact of the recycling process [9] [11]. It has even been demonstrated that Ni precipitation performance of fresh DMG (98.75%) and recycled DMG (97.6%) were nearly the same [9].

Dimethylglyoxime (DMG) is a white crystalline powder of chemical formula $C_4H_8N_2O_2$. DMG has a molecular weight of Mw: 116.12 g/mole and a density of 1.37 g/cm³. It has low solubility in water and is soluble in acids, bases and alcohols. The toxicity level of DMG is unknown, but it is toxic if swallowed (Appendix 4). Figure 4.1a represent the structure of DMG.

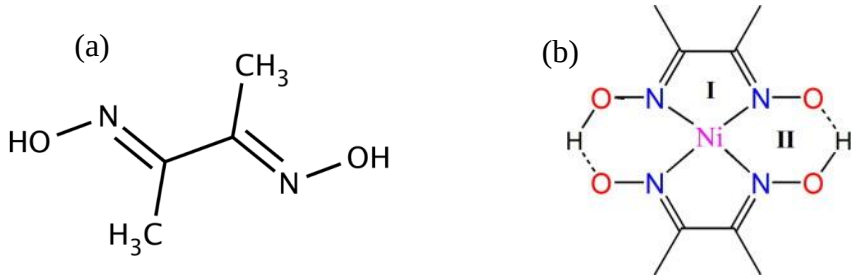

Figure 4.1. Representation of structure of (a) Dimethylglyoxime (DMG), (b) Ni Dimethylglyoxime complex.

In this study, we applied DMG to complex nickel ions in the process of recovering the ceramic components of solid oxide cells. The scalable approaches for the recycling of solid oxide cell component materials and characterization of recovered materials will be described below.

4.3. Result and discussions

Solid oxide cells were collected and manually crushed and ball-milled for five hours into a fine black powder (Figure 4.2). This is the first step of recycling for DMG route.

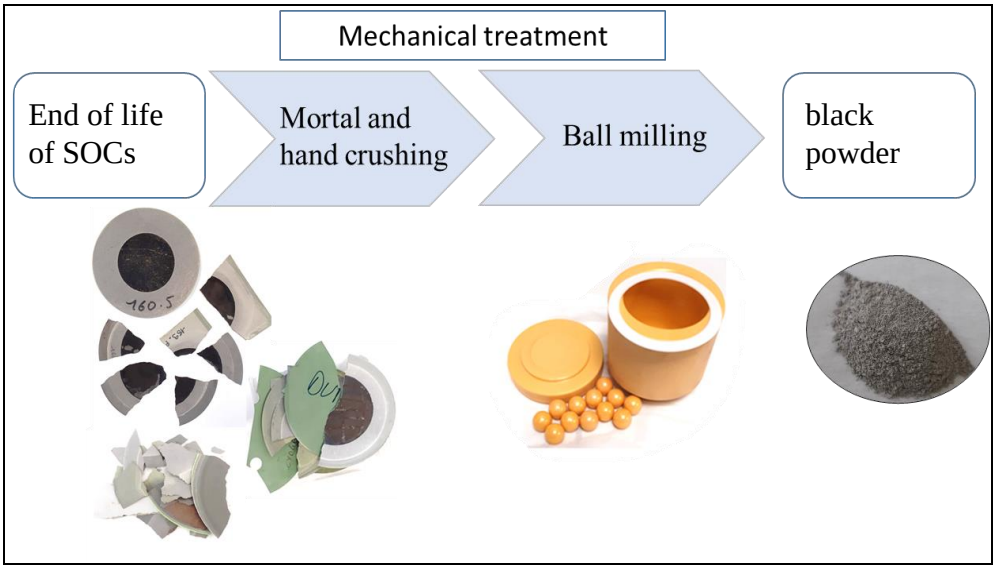

Figure 4.2. Mechanical grinding of ceramic component of solid oxide cells

Characterization of the black powder: X-Ray diffraction pattern reveals a mixture of five crystallized phases (Figure 4.3): NiO, $La_xSr_{1-x}CoO_3$ (LSC), and three $Zr_{1-x}Y_xO_{2-x/2}$ (YSZ) zirconia polymorphs. These are Tetragonal P42/nmc, cubic Fm-3m, and monoclinic $P2_1a$. The

two others correspond to the cubic Fm-3m NiO phase and the rhombohedral R-3c LSC phase. The relative proportion of each phase as quantified by Rietveld refinement are 27.4(4) wt.% of monoclinic YSZ, 17.3(4) wt.% of tetragonal YSZ, 6.2(1) wt.% of cubic YSZ, 46.1(17) wt.% NiO, and 2.18(7) wt.% LSC. Total amount of YSZ is about 50.9 wt. %.

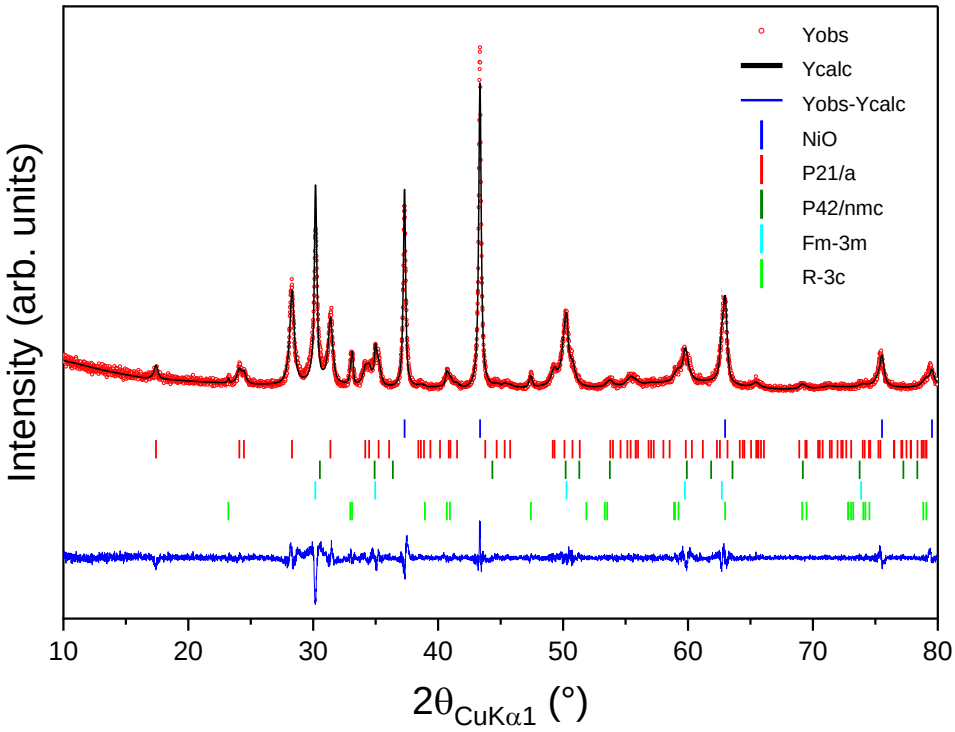

Figure 4.3. Rietveld refinement plot of the XRD data of the ceramic powder containing the air electrode-fuel electrode and electrolyte ($La_xSr_{1-x}CoO_3$ -NiO-$Y_yZr_{1-y}O_2$) powder. The final R-values are Rexp = 10.30 %, Rwp = 12.37 %, Rp = 9.71 % and GOF = 1.20.

The weight percentage of each phase is in good agreement with the relative thickness of the SOFC components (Figure 4. 4). Because the fuel electrode accounts for the largest part of the cell volume, the black powder has large amount of NiO and YSZ. On the other hand, XRD quantification of LSC yields 2.18(7) wt. %, which is consistent with the electrode thickness, porosity and area of LSC. The GDC layer roughly accounts about 0.42 % of the cell thickness. Including the consideration of porosity of this layer, it might be below the detection limit of the XRD quantification. This can be treated as trace impurities in YSZ.

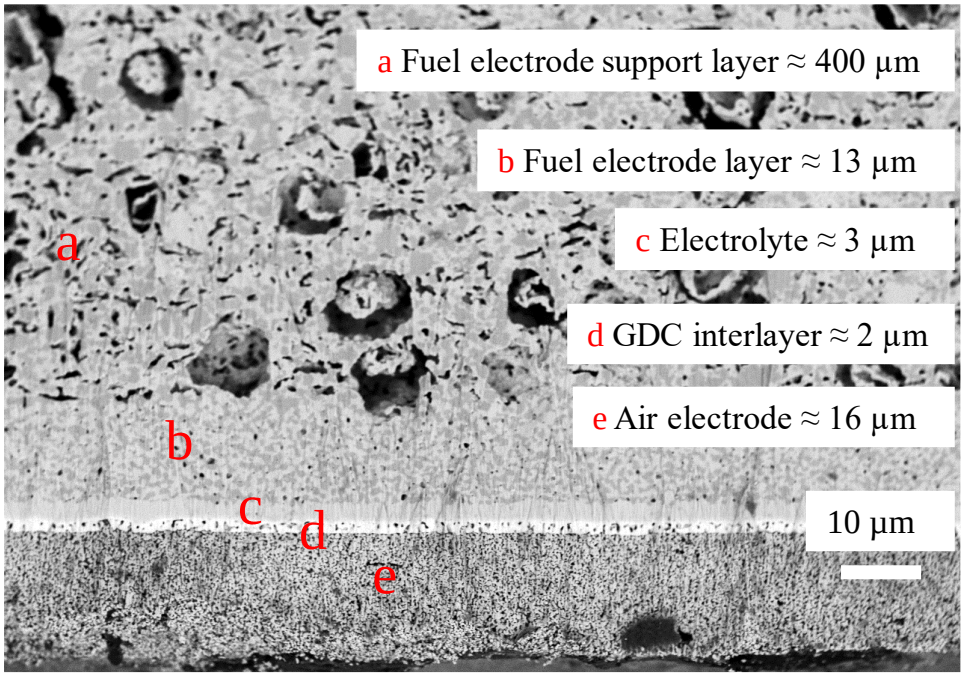

Figure 4. 4 Illustration of thickness of the cross section of SOFCs from Elcogen cell

The elemental analysis of the black powder is performed by SEM via energy dispersive X-ray spectroscopy (EDX JOEL 5800) is given in Table 4.1. The phase quantification performed by XRD through Rietveld refinement and the compositional analysis performed by EDX are in good agreement with each other (Figure 4.3 and Table 4.1).

Table 4.1. EDX elemental analysis of ball-milled black powder of SOCs.

Black mass	Co	Ni	Sr	Y	Zr	La	Ce	Gd
Composition in At. %	1.16	60.97	0.79	3.13	33.08	0.6	0.2	0.06

The XRD pattern of the black powder shows that it contains a substantial quantity of NiO and YSZ (47% and 51% respectively). The information previously provided in the literature that is the waste components of SOFCs have higher chemical grades than their metal-bearing minerals is supported here by the composition of black powder. For example, Ni-Laterite contains from 0.6-1.8% Ni[12], cobalt mining less than 0.5 most often less than 0.1wt.% [13], zirconium mining 0.5394 % [14]. Due to the high chemical grade of the black mixture, the processes of mining, concentration, and beneficiation could be skipped. Because of this advantage of decreasing the mining steps, it might be less energy consuming and less expensive to use this powder than to extract primary materials.

The recycling process combines a multi-step process, including acid leaching, precipitation and centrifugation followed by drying as shown in **Figure 4.5**.

4.3.1 Recovery of YSZ

A) General presentation of the method

Following mechanical treatment shown in Figure 4.2, the second step of the recycling process consists in separating YSZ from the other compounds (

Figure 4.5). It is based on the high stability of YSZ material in acidic medium whereas other metal oxide are soluble.

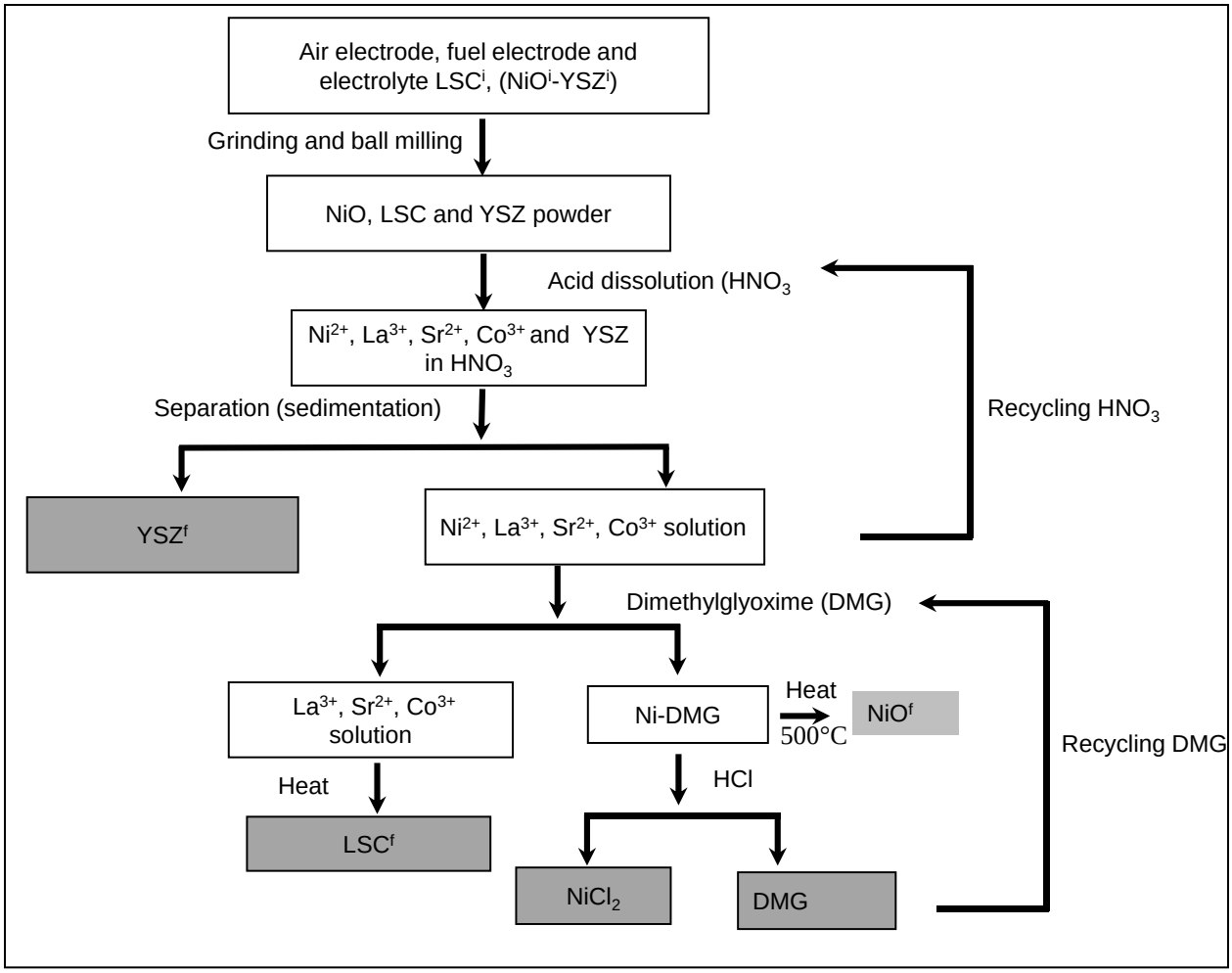

Figure 4.5 *The recovery scheme of the solid oxide ceramic cell component materials. Superscript i and f in LSC, NiO and YSZ stand for initial and final, respectively, as used later for the yield calculation.*

B) Leaching

A 2.5 g of the initial black mixture was mixed with 50 ml of HNO_3 (65 wt.%),heated at 75°C and stirred continuously during one day (Figure 4.6). Centrifugation 500 rpm was used to separate the green filtrate from the solid white residue. The solid was then repeatedly washed in water to avoid contamination. After a few hours of drying in a 100°C oven, it was weighed in order to estimate the recovery yield.

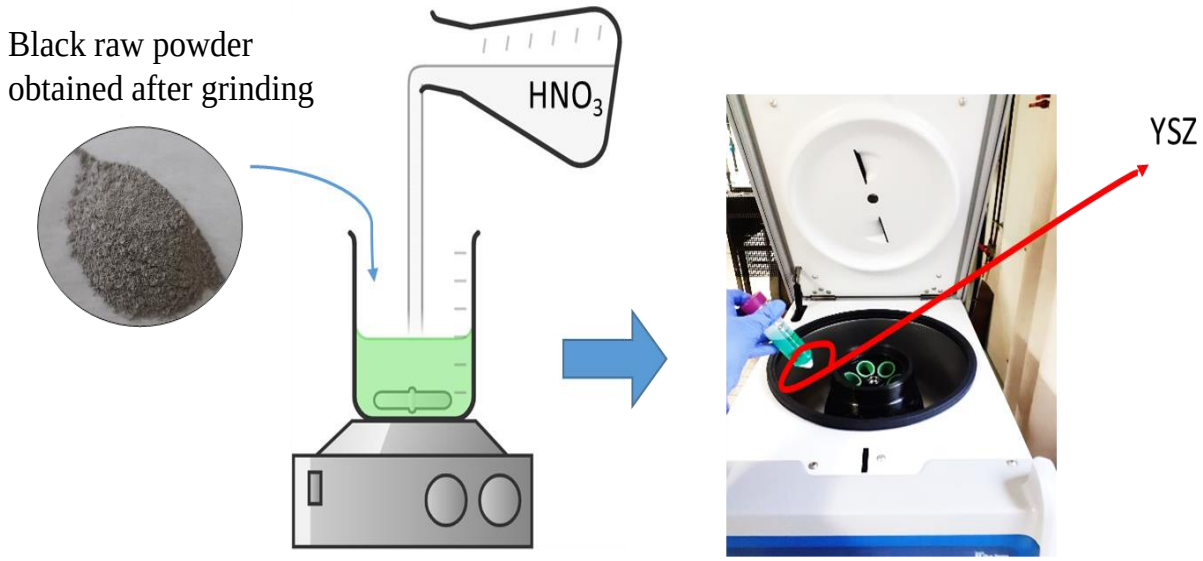

Figure 4.6. Schematic representation of the leaching process.

Yield of recovery: The recovery yield was calculated from the following equation.

$$Y_r = \frac{(m_i - m_f)}{m_i} x\ 100 \qquad \textit{Equation 4. 1}$$

In which m_i and m_f represent the mass of the YSZ in the black powder and after filtration in the residue respectively.

C) Characterization

XRD analysis of the white residue powder shows that it is composed of 3 crystalized phases attributed to YSZ polymorphs: tetragonal $P4_2/nmc$, cubic Fm-3m, and monoclinic $P2_1a$ (Figure 4.7). Using Rietveld technique, the phase quantification shows 23.4(16) wt. % of tetragonal accounting for, 14.0(3) wt. % of cubic, and 62.0(2) wt. % of monoclinic (Table 4.2)

Table 4.2 gathers the relative quantities of these YSZ polymorphs before and after leaching. Globally, we still observe a highest ratio for the monoclinic, higher than tetragonal and cubic. However, monoclinic and cubic phase amounts increase while tetragonal phase level decrease. This can be due to either a small energy exchange or to the crystal size variation which can happen during dissolution nitric acid leaching.

According to SEM/EDX, the white powder has a composition of yttrium and zirconium elements higher than 97 At.% and certain minor elements like Ni, La, Sr, and Co are detected (Table 4.3). From the relative quantity of Y/Zr, the recovered YSZ has composition equivalent to 4YSZ.

The yield of YSZ recovery, calculated by equation:

$$Y_r = \frac{(YSZ_i - YSZ_f)}{YSZ_i} \; x \; 100 \qquad \textit{Equation 4. 2}$$

In which m_i and m_f represent the mass of the YSZ in the black powder and after filtration in the residue respectively. The yield is of about 90%.

For economical perspective of recycling, to make it as cheap as possible, the high concentrated HNO_3 can be recycled and reused again with particular distillation method. It is explained in detail in chapter 5.

Table 4.2. Comparison of phase quantification of YSZ before and after leaching.

Phases	Monoclinic (Wt.%)	Tetragonal (Wt. %)	Cubic (Wt. %)
YSZ before leaching	53.8(4)	34.0(4)	12.18(1)
YSZ after leaching	62.0(2)	23.4(16)	14.0(3)

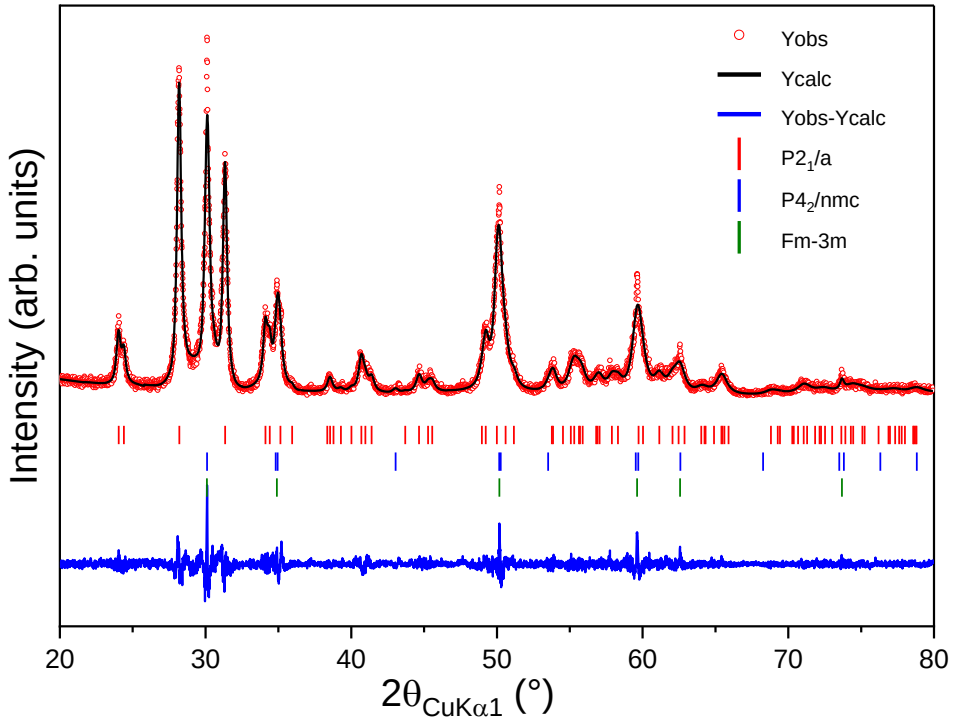

Figure 4.7. Rietveld refinement plot of the XRD data of the YSZ powder recovered from fuel electrode and electrolyte. The final R-values are Rexp = 10.05%, Rwp = 13.15 %, Rp = 9.96% and GOF = 1.3.

Table 4.3. EDX compositional analysis of recovered YSZ.

Elements	Co	Ni	Sr	Y	Zr	La	Ce	Gd
Recovered YSZ composition (At. %)	0.38	1.23	0.28	7.82	89.3	0.07	0.6	0.31

After successful separation of YSZ, the main objective of the next step is the recovery of nickel mixed with cobalt, strontium and lanthanum ions in the filtrate.

4.3.2 Recovery of Ni/NiO

A) Precipitation

As stated section 4.2, Dimethylglyoxime (DMG) is largely used to complex selectively nickel ions. The process is illustrated in Figure 4.8. 2 ml green solution containing 0.0063 mole of Ni was mixed with 0.0126 mole of DMG (at 0.2 mole/l in ethanol) and stirred at room temperature. The Ni to DMG ratio was fixed as stoichiometric (Equation 4.2, Ni/DMG = 0.5). The pH of the solution was adjusted with ammonium hydroxide and maintained at 5.5. After 10 minutes of

reaction, the precipitate was separated from the solution by centrifugation and filtration. The solid was then washed several times with ethanol.

$$Ni^{2+}_{(aq]} + 2C_4H_8N_2O_{2(aq]} \rightarrow Ni(C_4H_7N_2O_2)_{2(s]} \downarrow + 2H^{+}_{(aq]}$$ *Equation 4. 3*

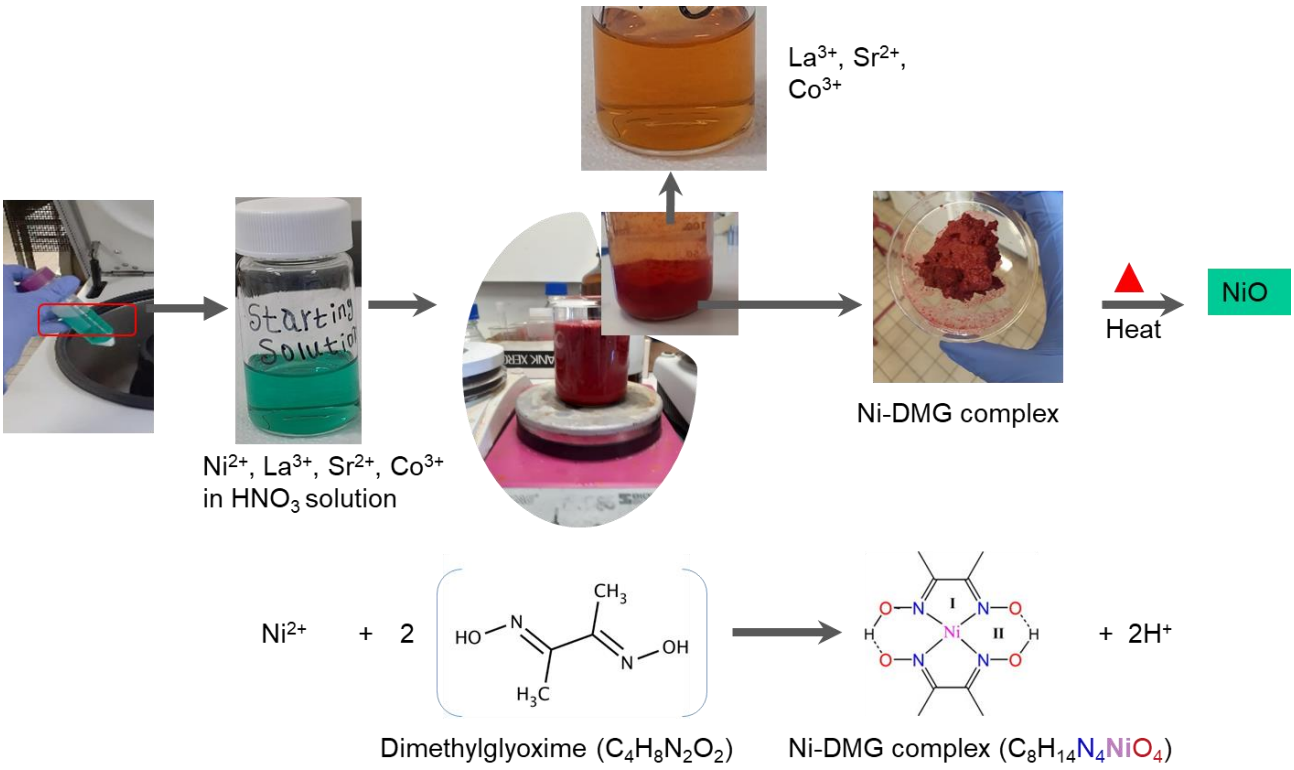

Figure 4.8. Illustration of the precipitation of Nickel, Nickel complexation with DMG, sedimentation and separation of the precipitate.

B) Drying and heating

The solid was then dried on the hot plate for overnight at 75 °C (Figure 4.9). Then the powder was heated at the temperature of 500°C for 3hrs.

Figure 4.9. Photo of the Ni-DMG complex powder obtained by precipitation.

C) Characterizations

The quantitative characterization of the Ni-DMG powder was performed by ICP-MS (Table 4.4) showing that more than 99 At.% of nickel is present. Co, Sr, La, Ce and Gd were detected only in trace amounts.

Table 4.4. ICP-MS compositional analysis of the recovered Ni/(NiO)

Elements	Co	Ni	Sr	La	Ce	Gd
Composition ICP-MS in At.%	0.2	99.71	0	0.06	0.2	0.017

XRD analysis of the precipitated powder (Figure 4.9) and confirms the presence of nickel oxide. No other impurities were detected in the XRD analysis as all peaks correspond to the cubic phase of nickel oxide. According to the Rietveld refinement (Figure 4.10), cell parameters and volume are similar to those of NiO (ICSD 61324: a = 4.177(3), V = 72.90(3), Fm-3m space group) [15]. The Rietveld method yielded a crystallite size of 49.3 (11) nm for the recovered NiO.

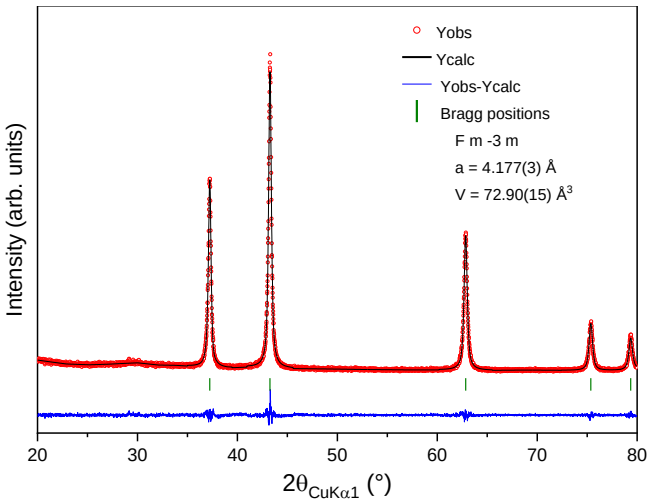

Figure 4.10. Rietveld refinement plot of the XRD data of the DMG complex after drying and calcination.

Scanning electron microscopy (SEM) images of the recovred NiO from mechanical scratching and DMG routes of recycling are shown in Figure 4.11. With mechanical scratching routes of recyceling, the recvred NiO shows nano particles morphology (Figure 4.11a). On the other hand, with DMG routes, the recovered NiO powder displays Nanoflakes morphology (Figure 4.11b), This type of NiO with a loosely packed anisotropicmorphology can be useful for energy storage applications [16].

The yield of recovery, calculated by using Equation 4.1, is about 90 %. Indeed, to extract more nickel while avoiding precipitation of other metals, the influence of pH and nickel to DMG ratio were studied.

(a)

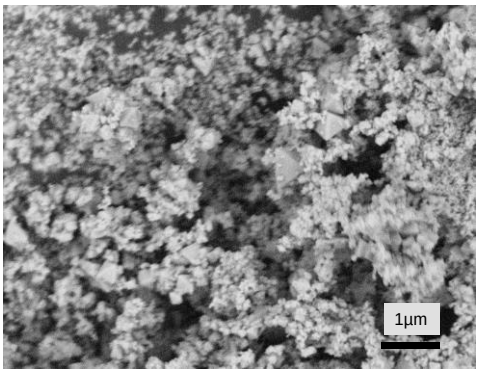

(b)

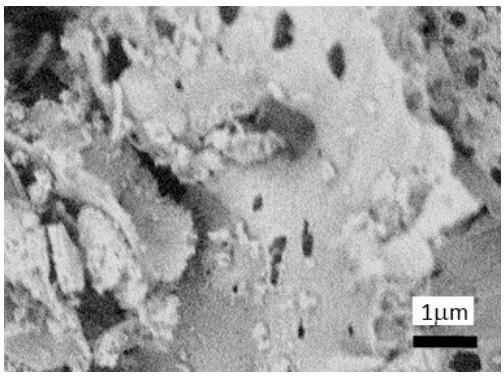

Figure 4.11. Comparison of (a) mechanical scratching and (b) DMG routes of recycling on recovred NiO powder morphology (SEM topography of backscattering mode)

4.3.2.1 Effects of pH on nickel recovery

Selective precipitation of the nickel was tested using different pH values. Indeed, NiO (or Ni $(OH)_2$ in its hydrated form) precipitates for pH ≳ 5.0 [17]. The effects of pH on the preferential recovery of nickel from a solution containing nickel, cobalt, strontium, and lanthanum were investigated, in the 1-12.7 range whereas the ratio Ni-DMG remains of 0.5. After each experiment, the liquid part was analyzed by ICP-MS. Results presented in **Erreur ! Source du renvoi introuvable.** showed that the nickel content of the solution decreases when the pH increases, especially above pH 6. When the pH increases, additional elements present in the aqueous solution can precipitate into hydroxides as Ni^{2+}. As shown in Pourbaix diagram of Figure 4.13, whereas, Ni^{2+} precipitates above pH~5 [17] , Co above pH~6 [13], La above pH ~7 [18] and Sr above pH ~ 12[19].

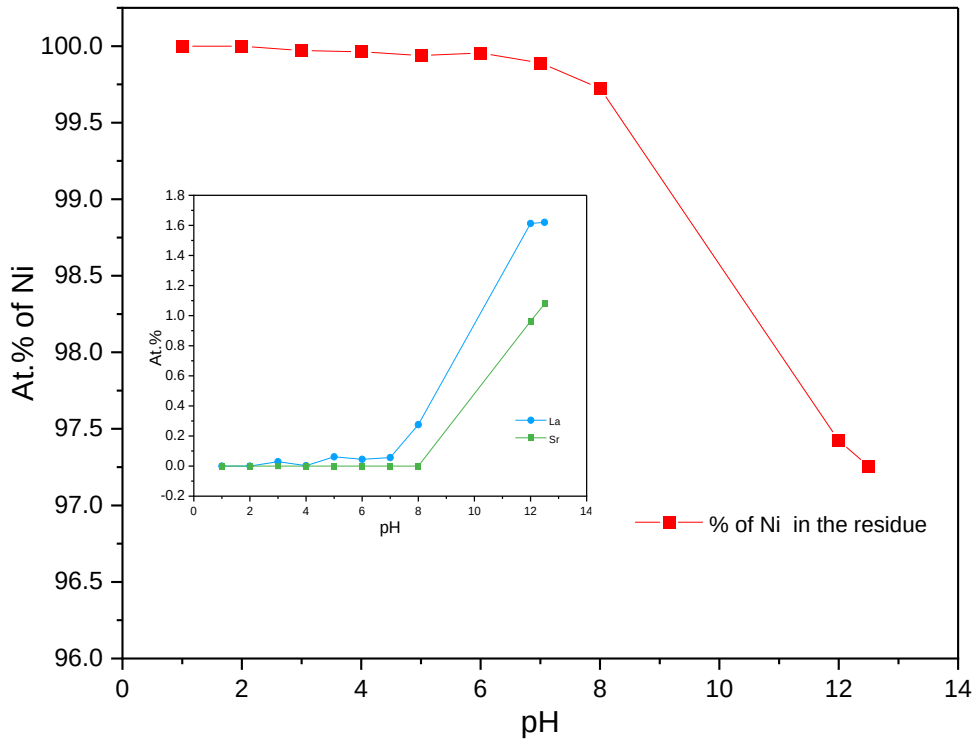

Figure 4. 12 *Quantitative analysis of Ni, La and Sr in the solution after addition of DMG, versus pH.*

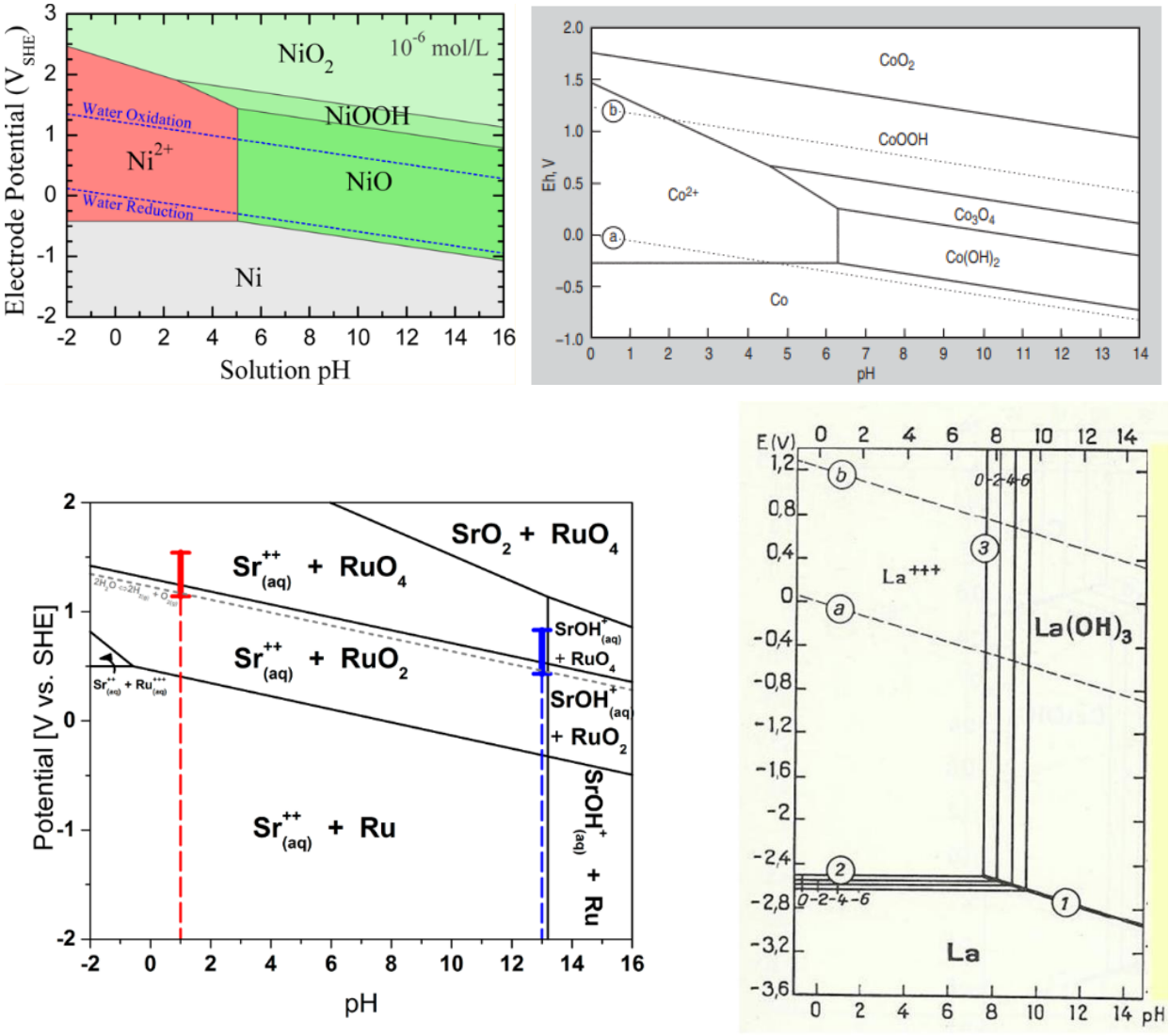

Figure 4.13. Pourbaix diagrams of elements present in the filtrate: (a Ni [17], (b) Co [13], (c), Sr [19] (d), La [18].

In accordance with these diagrams, there are traces of Co and La at pH = 6 and above. This may due to the similarities of the precipitation conditions of Ni-DMG complex and La and Co hydroxides. After studying the effects of pH on nickel recovery efficiency, the second parameter studied was the ratio Ni/DMG. Therefore, pH at 5.5 is reasonably chosen for better recovery of nickel via Ni-DMG complexation.

4.3.2.2. Effects of Ni to DMG ratio on nickel recovery

Different solutions were prepared with Ni/DMG ratio varied from 0.1 to 2. During experiment, the solution was studied at pH 5 at room temperature, and under constant stirring.

When Ni/DMG ratio is below 0.5, Ni is the limiting reactant, and all Ni^{2+} cations precipitate as Ni-DMG complex. On the other hand, for Ni/DMG ratio larger than 0.5, DMG becomes the limiting reactant and Ni remains in excess in the solution. In accordance with the color of the solution, which becomes greener as the Ni/DMG ratio increases to 2 (from left to right) (Figure 4.14). The Ni/DMG ratios of 0.1 and 0.3 yields total recovery of Nickel from the solution. Nonetheless, Ni/DMG = 0.5 was chosen due to economic considerations.

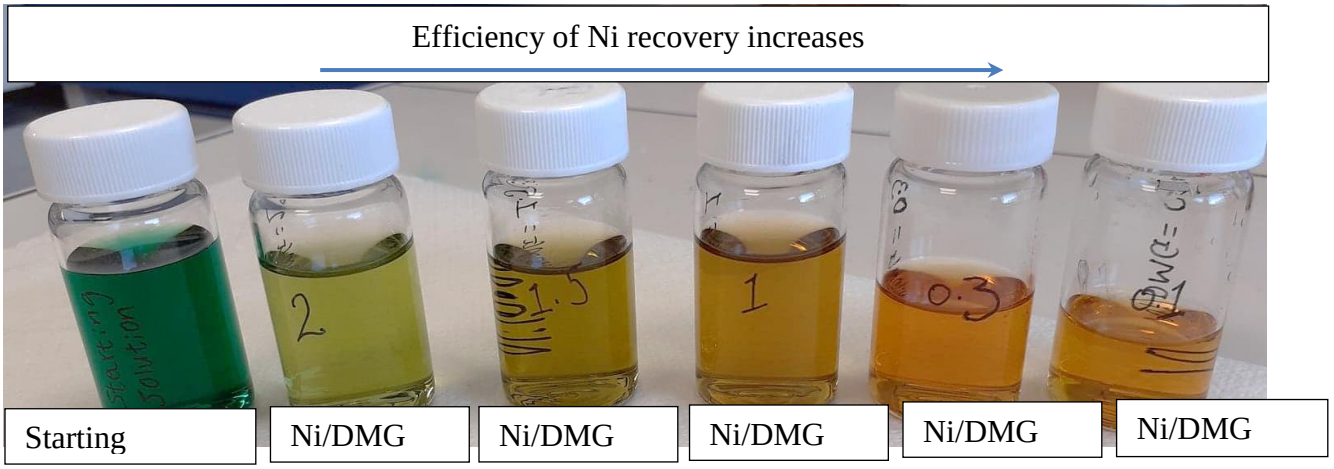

Figure 4.14.Illustration of the effect of variation of Ni/DMG ratios (at pH 5) on the color of the filtrate.

4.3.3. Recovery of LSC (air electrode)

Considering a pH = 5.5 and a Ni/DMG = 0.5, centrifugation and filtration steps were able to separate the solid part (Ni-DMG complex) and the liquid containing un-precipitated Co, Sr, and La ions. This "filtrate" was collected, then dried and heated at 500°C for 3hours. The XRD analysis of the powder recovered indicates LSC type compound (Figure 4.1). The compositional analysis of the recovered LSC powder is about 96% with Ni as the main impurity (Table 4.5). Since this LSC is acid soluble, it can be used as a starting material for the production of fuel electrode powder (Appendix 5).

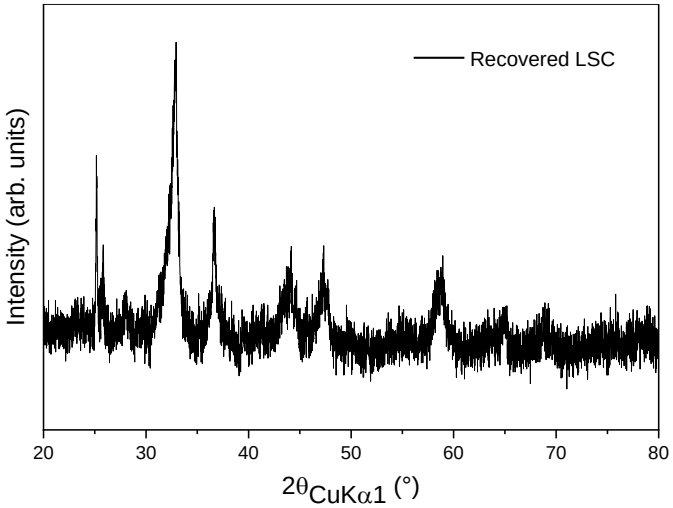

Figure 4. 15 Plot of the XRD data of the recovered LSC.

Table 4.5 ICP-MS compositional analysis of the recovered LSC

Elements	Co	Ni	Sr	La	Ce	Gd
Composition of LSC ICP-MS (At.%)	48.29	2.86	23.6	24.46	0.73	0.05

4.3.3.1 Effects of pH on the recovery of LSC

Figure 4.16 shows the ICP-MS elemental analysis (in At.%) of the filtrate after recovering the Ni-DMG complex, for different pH values. The filtrate solution has a bright green color at pH 1 and a pale yellow color at pH 2, indicating the presence of Ni in the solution, in accordance with the analysis' results. According to literature, the Ni-DMG complexation is optimal in the 6 to 8 pH range, explaining the absence of Ni in the solution in this pH range [20].

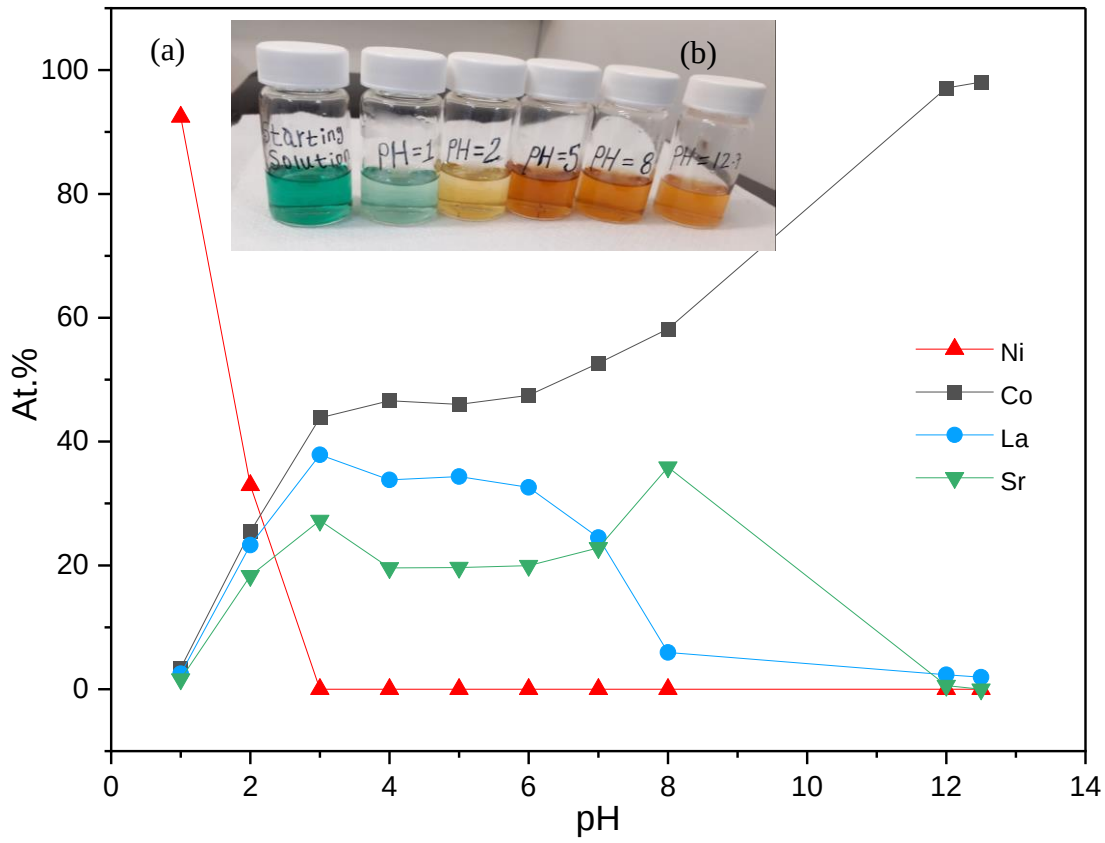

Figure 4.16. (a) ICP-MS elemental analysis of effects of pH on the composition of the filtrate towards the, the composition is given in At.%, (b) illustration of filtrate color variation with pH.

When pH is higher than 6, La and Sr hydroxides precipitate, Therefore, to obtain optimal precipitation of Ni into the Ni-DMG complex, and optimal dilution of La, Sr and Co as cations in the solution, the pH must be comprised between 4 and 6. In our study, we choose pH at 5.5.

4.3.3.2 Effects of Ni/DMG ratio on the recovery of LSC

The excess DMG left did not precipitate Co or other elements from the solution. As can be seen in Figure 4.17, the relative quantities of Co, La and Sr in the filtrate are consistent though different Ni/DMG ratios. The excess Dimethylglyoxime (DMG) in the solution (Ni/DMG < 0.5) do not lead to Ni in the filtrate but only Co, La and Sr. Above Ni/DMG = 0.5 Ni^{2+} is present in the filtrate, indicating the absence of reaction of Ni^{2+} with DMG. This indicates that whether or not there is an excess of DMG present, the DMG reaction only happens with nickel.

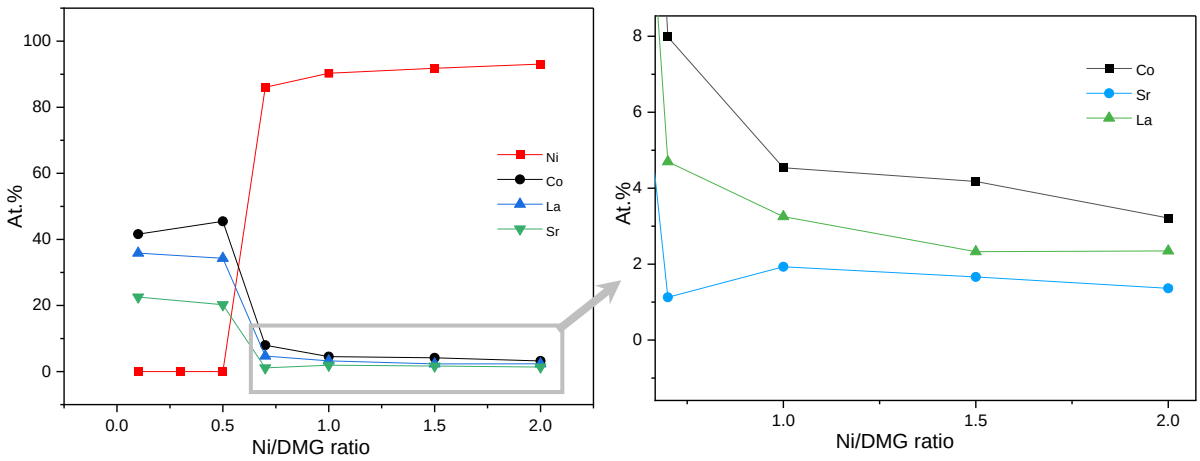

Figure 4.17. ICP-MS elemental analysis of effects of Ni/DMG ratio on the composition of the filtrate towards the recovery of LSC.

4.4.4 Recycling of Dimethylglyoxime

It is important to minimize quantities of products necessary for recycling, and even to be able to reuse them. Then, $Ni(C_4H_7N_2O_2)_2(s)$ after drying step is taken as a starting sample for DMG recycling. This was dissolved (10 mg/ml) in 0.2mol/L HCl (pH=2) at room temperature. The solution was stirred for 5h.

In this condition, Ni-DMG precipitates reacts as follows:

$$2H^+ + Ni(C_4H_7N_2O_2)_{2(s]} \longrightarrow Ni^{2+} + +2(C_4H_8N_2O_2)s \quad \textit{Equation 4. 4}$$

Leading to Ni^{2+} ions formation. XRD pattern of recovered DMG is shown in Appendix 6, and is similar to the fresh DMG.

4.5 Comparison of mechanical scratching and DMG routes

Mechanical scratching routes give higher purity of recovered materials with lower materials and energy input. DMG routes on the other hand require more numerous steps and DMG and ethanol use. The cost of recycling, the purity of recovered products and the scalability the process for mechanical scratching and DMG routes are compared in Table 4.6. The details of the cost and impact analysis of each route are examined in detail in Chapter 5. The yield is affected by several parameters, such as how the experiments were handled, and how it can be improved by large-scale recycling.

Table 4.6. Comparison of Mechanical scratching and DMG routes of recycling on the ceramic components of SOCs

Recovered materials	Parameters	Mechanical routes	DMG routes	Remarks
YSZ	Purity	+	-	Possible contamination with air electrode materials with DMG
	Cost	-	+	Equivalent cost, or may be less expensive in DMG routes
	Scalability	-	+	Mechanical scratching is possible with a certain techniques of scratching or large size cells
NiO	Purity	+	-	Possible contamination with air electrode materials
	Cost	-	+	Higher with DMG
	Scalability	-	+	Impossible with mechanical route
LSC	Purity	+	-	Possible contamination with Ni and all GDC interlayer material, i.e. Ce and Gd in DMG routes
	Cost	-	+	Higher with DMG
	Scalability	-	+	Mechanical scratching route is scalable on large size and unbroken cells

Conclusion

In this chapter, we practiced an affordable recycling process that can be directly applied at the industrial level. This process combines mechanical and hydrometallurgical processes with acid leaching followed by organic complexation, allowing recovery of ceramic component of solid oxide cell waste materials at high purity level. Three ceramic components of SOCs, NiO, YSZ and LSC are recovered with high purity. A Ni/DMG ratio of 0.5 and a pH of 5.5 are chosen for better production. Further studies will look at extending DMG route recycling for other fuel electrode compositions such as LSCF and LSM.

Reference

[1] M. Noponen *et al.*, 'Status of Solid Oxide Fuel Cell Development at Elcogen', *ECS Transactions*, vol. 68, no. 1, pp. 151–156, Jul. 2015, doi: 10.1149/06801.0151ecst.

[2] J. Wang and K. Varughese, 'Determination of traces of palladium by adsorptive stripping voltammetry of the dimethylglyoxime complex', *Analytica Chimica Acta*, vol. 199, pp. 185–189, 1987, doi: 10.1016/S0003-2670(00)82813-5.

[3] K. Burger and D. Dyrssen, 'On the complex formation of palladium with dimethylglyoxime', *Acta chem. scand.*, vol. 17, p. 1489, 1963.

[4] A. E. García-Rabasco, V. Zaragozá-Ninet, R. García-Ruíz, and J. de la Cuadra-Oyanguren, 'Allergic Contact Dermatitis due to Nickel: Descriptive Study in a Tertiary Hospital, 2000-2010', *Actas Dermo-Sifiliográficas (English Edition)*, vol. 105, no. 6, pp. 590–596, Jul. 2014, doi: 10.1016/j.adengl.2014.05.017.

[5] N. B. Silverberg *et al.*, 'Nickel Allergic Contact Dermatitis: Identification, Treatment, and Prevention', *Pediatrics*, vol. 145, no. 5, p. e20200628, May 2020, doi: 10.1542/peds.2020-0628.

[6] J. P. Thyssen, T. Menné, and J. D. Johansen, 'Nickel release from inexpensive jewelry and hair clasps purchased in an EU country — Are consumers sufficiently protected from nickel exposure?', *Science of The Total Environment*, vol. 407, no. 20, pp. 5315–5318, Oct. 2009, doi: 10.1016/j.scitotenv.2009.06.034.

[7] R. Darlenski, J. Kazandjieva, and K. Pramatarov, 'The many faces of nickel allergy: Faces of nickel allergy', *International Journal of Dermatology*, vol. 51, no. 5, pp. 523–530, May 2012, doi: 10.1111/j.1365-4632.2011.05233.x.

[8] A. Tosti, Torres, and Melo, 'Management of contact dermatitis due to nickel allergy: an update', *CCID*, p. 39, Apr. 2009, doi: 10.2147/CCID.S3693.

[9] X. Chen, Y. Chen, T. Zhou, D. Liu, H. Hu, and S. Fan, 'Hydrometallurgical recovery of metal values from sulfuric acid leaching liquor of spent lithium-ion batteries', *Waste Management*, vol. 38, pp. 349–356, Apr. 2015, doi: 10.1016/j.wasman.2014.12.023.

[10] R.-C. Wang, Y.-C. Lin, and S.-H. Wu, 'A novel recovery process of metal values from the cathode active materials of the lithium-ion secondary batteries', *Hydrometallurgy*, vol. 99, no. 3–4, pp. 194–201, Nov. 2009, doi: 10.1016/j.hydromet.2009.08.005.

[11] M. Rath, L. P. Behera, B. Dash, A. R. Sheik, and K. Sanjay, 'Recovery of dimethylglyoxime (DMG) from Ni-DMG complexes', *Hydrometallurgy*, vol. 176, pp. 229–234, Mar. 2018, doi: 10.1016/j.hydromet.2018.01.014.

[12] H. L. Carpen and E. C. Giese, 'Enhancement of nickel laterite ore bioleaching by Burkholderia sp. using a factorial design', *Appl Water Sci*, vol. 12, no. 8, p. 181, Aug. 2022, doi: 10.1007/s13201-022-01704-5.

[13] E. Peek, T. Åkre, and E. Asselin, 'Technical and business considerations of cobalt hydrometallurgy', *JOM*, vol. 61, no. 10, pp. 43–53, Oct. 2009, doi: 10.1007/s11837-009-0151-2.

[14] J. L. Keeling, A. J. Reid, R. Pobjoy, and B. Hou, *Provenance of Zircon in Heavy Mineral Sands Deposits, Western Murray Basin*. Department of State Development, 2016.

[15] N. G. Schmahl and G. F. Eikerling, 'Über Kryptomodifikationen des *Cu* (II)-Oxids', *Zeitschrift für Physikalische Chemie*, vol. 62, no. 5_6, pp. 268–279, Dec. 1968, doi: 10.1524/zpch.1968.62.5_6.268.

[16] J.-W. Lang, L.-B. Kong, W.-J. Wu, Y.-C. Luo, and L. Kang, 'Facile approach to prepare loose-packed NiO nano-flakes materials for supercapacitors', *Chem. Commun.*, no. 35, p. 4213, 2008, doi: 10.1039/b800264a.
[17] L.-F. Huang, M. J. Hutchison, R. J. Santucci, J. R. Scully, and J. M. Rondinelli, 'Improved Electrochemical Phase Diagrams from Theory and Experiment: The Ni–Water System and Its Complex Compounds', *J. Phys. Chem. C*, vol. 121, no. 18, pp. 9782–9789, May 2017, doi: 10.1021/acs.jpcc.7b02771.
[18] P. Garnier, V. Joseph, and R. Krachewski, 'Lanthanum interaction with surface preparations', *ECS Transactions*, vol. 58, no. 6, p. 119, 2013.
[19] B.-J. Kim *et al.*, 'Unraveling Thermodynamics, Stability, and Oxygen Evolution Activity of Strontium Ruthenium Perovskite Oxide', *ACS Catal.*, vol. 7, no. 5, pp. 3245–3256, May 2017, doi: 10.1021/acscatal.6b03171.
[20] B. Ebrahimi, S. Bahar, and S. E. Moedi, 'Cold-Induced Aggregation Microextraction Technique based on Ionic Liquid for Preconcentration and Determination of Nickel in Food Samples', *Journal of the Brazilian Chemical Society*, 2013, doi: 10.5935/0103-5053.20130228.

Chapter 5: Comparison, selection and life cycle assessment of optimized recycling protocols

5.1 Introduction

Recycling of waste materials has become more important for economic reasons [1]. Recycling should be less energy intensive and produce fewer emissions than primary production of materials [2]. The first part of Chapter 5 presents the different processes tested in this thesis. The nature of the grinding and leaching media, the type of leaching chemicals used with different concentrations, the leaching time and temperature etc. are investigated, compared and optimized. The second part of the chapter is dedicated to the cost and life cycle assessment of the two main processes used in this thesis for separating the ceramic components of solid oxide cells. This chapter addresses the selection of techniques and methods considering effectiveness in terms of purity, economic and environmental benefits.

5.2 Ball milling medium

a) Silicon nitride based balls and jars

Several laboratory-scale ball mills materials have been tested for the grinding process. First, a silicon nitride-based ball mill (Figure 5.1a) was used. Characterization of the fine powder collected after grindings detected Al and Si contaminations in the powder. To investigate this contamination, the composition as a function of grinding time was studied. From the EDX study, the Al and Si concentration increases with milling time (Figure 5.2). YSZ-based mill was also used. Since, the composition is nearly the same as the ceramic solid oxide cell products, no contamination by other element was expected.

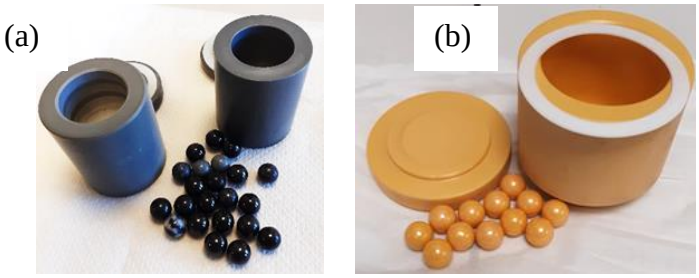

Figure 5.1. Milling jar and balls made of (a) silicon nitride, (b) YSZ-based

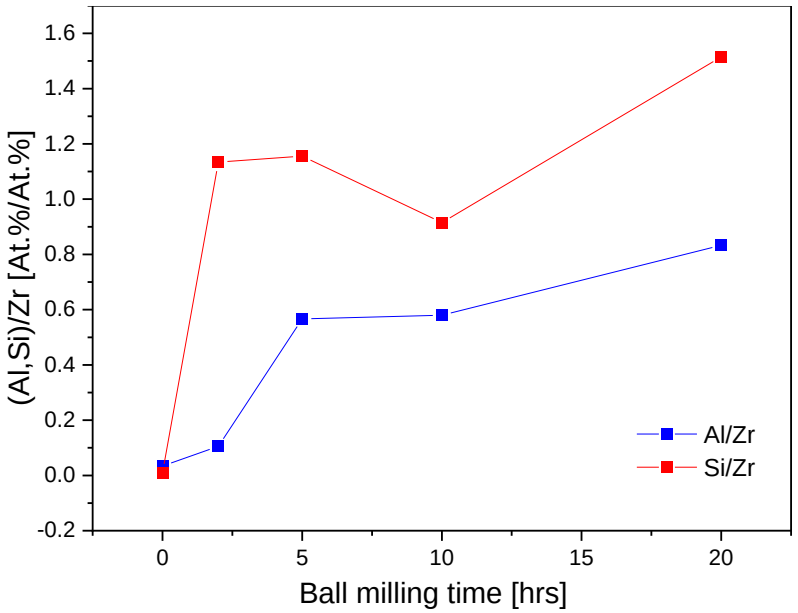

Figure 5.2. Effect of ball milling time using Si_3Ni_4 based jar and balls on Al and Si contamination.

b) YSZ based balls and jars

Both the milling jar and the balls were made of YSZ (Figure 5.1b). The effects of Si and Al concentration were studied as a function of milling time, and no change was observed over time (Figure 5.3). Based on these findings, we use YSZ balls and jars for the entire recycling experiment and for the results presented in Chapters 3 and 4.

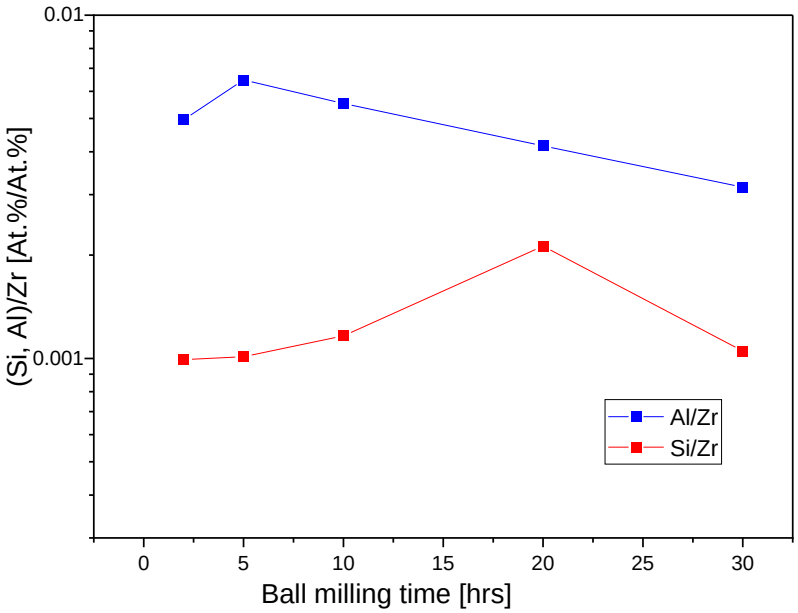

Figure 5.3. Al and Si contents of recycling products as a function of ball milling time when YSZ jar and balls are used.

5.3 Leaching medium

The leaching step was performed with laboratory beakers on a hot plate. For more information on this step, see Chapter 2, Leaching Step. The valuable metal cations are put into solution during the leaching step. In this process, the constituents of the leaching medium can have a significant influence on the contamination of the samples.

Two leaching media, i.e. laboratory beakers, are used for the recycling of ceramic components of solid oxide cell.

a) Glass beaker

This study is performed by leaching the powder in a glass beaker for an extended period of time and examining the evolution of Si and Al concentrations with time by EDX (Figure 5.4). As the leaching time increases, the Si concentration in the sediment (i.e. recovered YSZ) increases, while the Al content has no significant change with the leaching time (Figure 5.4a). Over time, the Si from the glass component begins to leach out and contaminates the recovered powder. Since Elcogen cells do not contain Si initially in the waste cell, the effect of leaching time on the change in composition shows a more visible evolution (Figure 5.4b). The Elcogen product is used as a representative sample to study the effect of leaching time on Si contamination and Ni removal.

The glass is expected to be resistant to wear and corrosion [3]. However, when exposed to a high concentration of acid at high temperatures (75 °C), the glass may degrade. It is known that laboratory glassware is mainly composed of silica (with a composition of 69-74% SiO_2, 5-12% CaO, 12-16% Na_2O, 0-6% MgO and 0-6% Al_2O_3) [4]. Various research teams have studied the release of Si from the vessels used to store water samples, reagents, and standard solutions. For example, Zhang et al. highlighted that the dissolution of silicate from glass vessels can lead to the contamination of the samples they contain [5]. Elmer et al. also studied the solubility of SiO_2 in nitric acid and concluded that the solubility is more favorable at low acid concentrations [6]. Therefore, Si contamination during leaching is expected from the glass-based beaker.

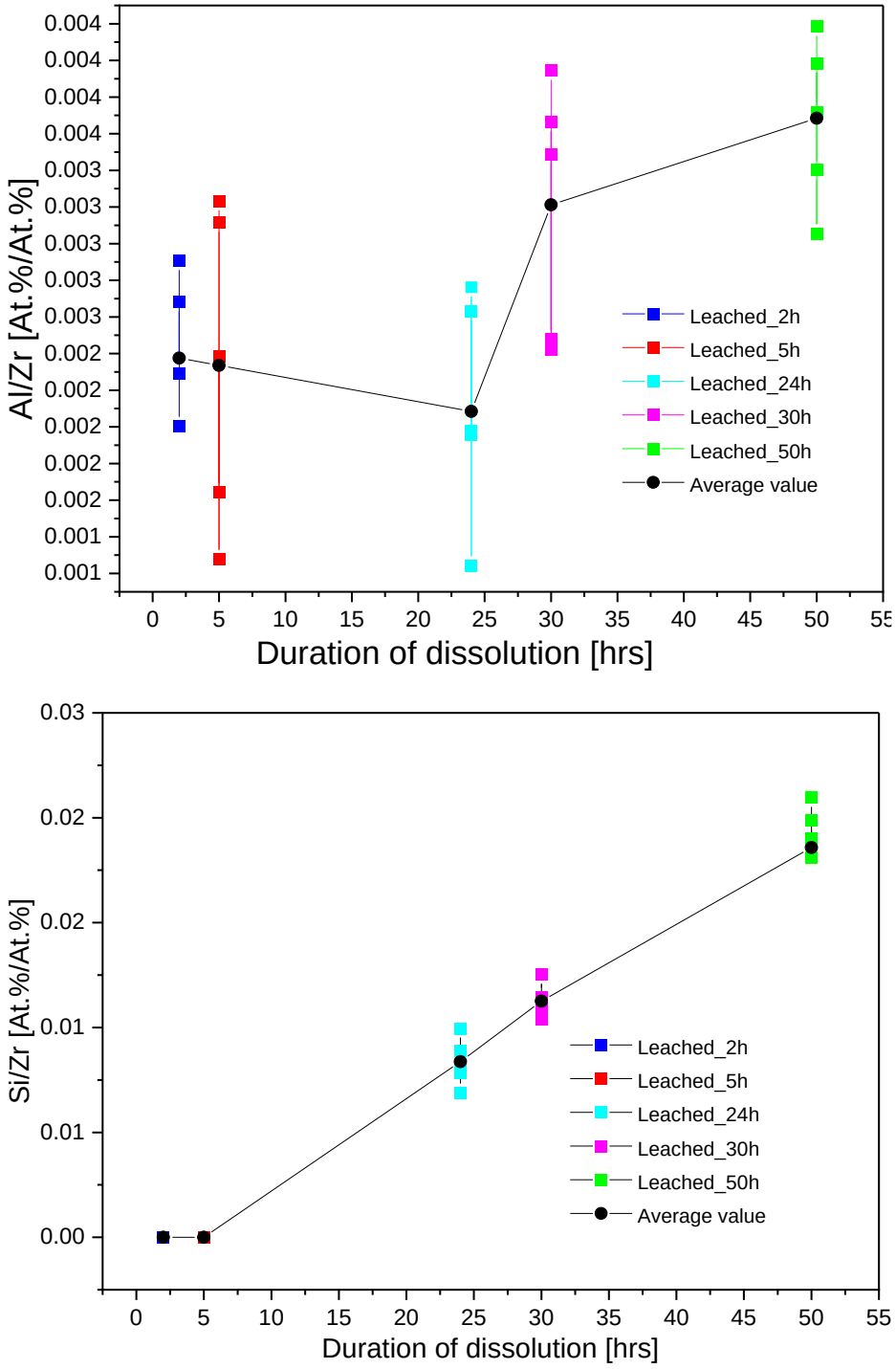

Figure 5.4. Effect of Si contamination as a function of leaching time of Elcogen ceramic cell components with glass beaker.

b) Teflon beaker

To avoid contamination of the glass beaker with Si, a Teflon beaker based on PTFE polymer (polytetrafluoroethylene) was used. The effect of leaching ceramic cell components using

Teflon beaker was studied on Fiaxell products. The results showed no change in the Al and Si content of the recovered YSZ. This proves that the Teflon beaker composition cannot be the source of impurities in the recovered powder. The composition, especially the content of Si and Al impurities, does not vary with leaching time. This shows us that the Teflon beaker is recommended for processing the materials leaching.

In addition to the beaker type, the type of solvent used has an effect on the efficiency and cost of recycling. To find the most cost-effective solvent, the dissolution of ceramic components of SOCs product in different acids is studied.

5.4 Comparison of leaching solvents

According to the leaching protocol explained in Chapter 2, the leaching step was performed with different acids at different concentrations. After each experiment, the product was analyzed by UV spectroscopy (see Chapter 2) in order to measure the concentration of dissolved metals. The results of this study are intended to select a suitable acid with an adequate concentration for the development of economical and environmental recycling routes.

Before getting into the details studies of the effect of acid type on dissolution, it is clearly known that dissolution rate can be affected by several factors. Among these factors, we find the particle size, which may be related to the ball milling step, the presence of Ni or NiO in the waste cells, and the relative ratio of Ni to YSZ in the electrode-electrolyte assembly.

Although the recycling studies were performed on both Fiaxell and Elcogen products, we chose the Elcogen product for the solvent comparison (section 5.4 of this chapter). The reason we chose Elcogen over Fiaxell is the NiO content in the waste cell. In Fiaxell, the NiO content in the SOFC component is relatively lower than in Elcogen. Thus, the Elcogen product contains about 50 wt. % NiO, which can be considered representative of other SOFC products.

Nitric acid HNO_3, hydrochloric acid HCl, sulfuric acid H_2SO_4 and phosphoric acid H_3PO_4 are investigated as leaching chemicals for ceramic material cell components of SOCs.

5.4.1 HNO_3

The waste cell ceramic powder was leached with HNO_3 at a ratio of 1g per 20ml acid at 75°C. Then, the concentration of metals in the solution was measured by UV spectroscopy to measure (see Chapter 2 for technical details). The leaching parameters, which include the HNO_3 concentration and the duration of leaching, were investigated. Different HNO_3 concentrations were tested: 65, 50, 40, 30, 20% HNO_3. Typical UV spectra of the green solution is given on Figure 5.5a showing different absorbance peaks. HNO_3 effectively leaches Ni/NiO from the electrode and electrolyte wastes: as the leaching time increases, the leaching efficiency increases and the absorption peak increases, as shown in Figure 5.5a. The concentration of Ni in the solution is directly proportional to the relative absorbance by applying the Beer-Lambert law (A = K x C). The intensity of peak at ~394 nm was used. It is therefore possible to correlate the concentration of an unknown solution with this calibration line.

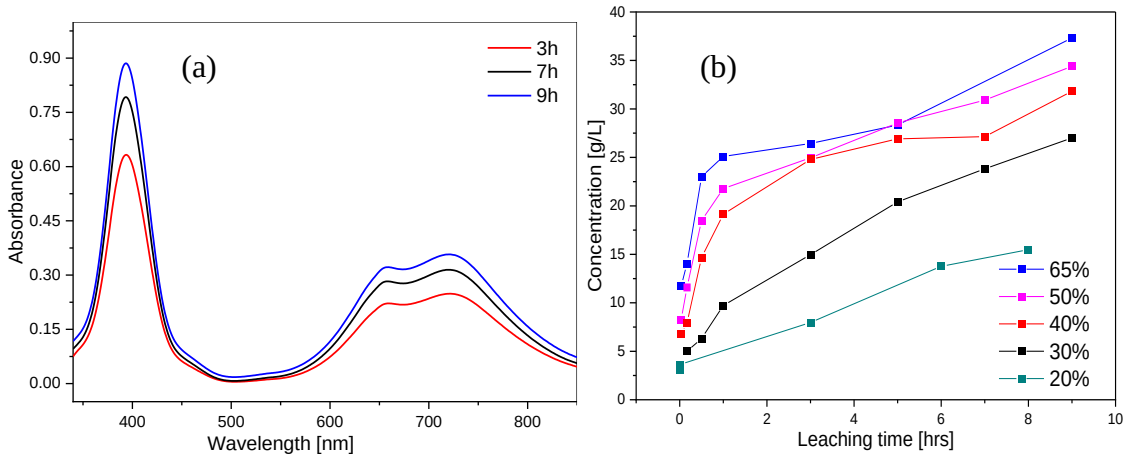

Figure 5.5. (a) UV visible spectrum peaks with different leaching time (b) calibration curve of NiO dissolution in HNO_3, (c) Ni ion concentration in solution as a function of leaching time for different HNO_3 concentrations (wt.%)

With a short leaching time, between half an hour and an hour, a high concentration, about 40% - 65% of HNO_3, is clearly more effective than lower concentrations. For longer leaching time, the Ni concentration increases slightly with leaching time for all concentrations (Figure 5.5b). With 20% HNO_3, it takes a long time to dissolve a small amount of NiO. The high concentration of 65 % HNO_3 is the most efficient to perform leaching.

After the selection of 65% HNO_3 at 75°C, the effect of leaching time on Ni/NiO dissolution is investigated. EDX studies of the recovered YSZ after different leaching times showed that the Ni/Zr ratio did not change after 24 hours of leaching (Figure 5.6). As detailed in chapters 3 and 4, leaching was therefore performed at 75°C for 24hrs.

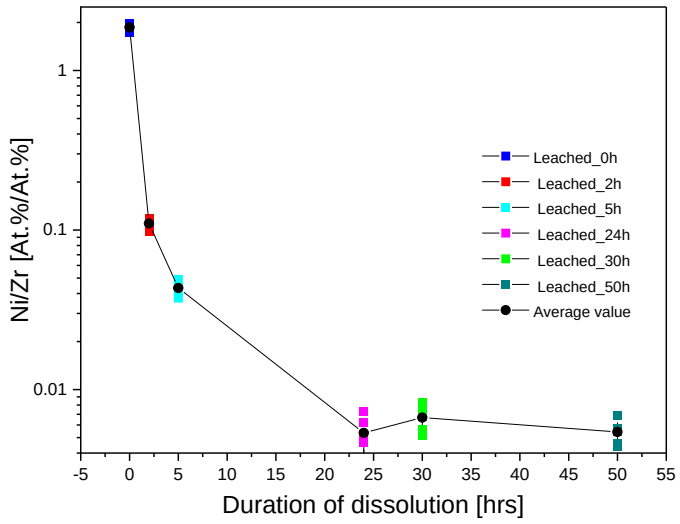

Figure 5.6. Effect of leaching time on Ni concentration in recovered YSZ.

5.4.2 Other acids (H_2SO_4, HCl, H_3PO_4)

Other acids were also tested but compared to HNO_3 they did not succeed:

- Only a small amount of Ni was detected in the solution with Sulfuric acid after leaching whatever the leaching time and temperature.

-Concerning hydrochloric acid (37 wt.%), the effect of leaching was studied at 50°C because of the evaporation of the HCl at temperature higher than 50°C. Ni UV peak intensity is almost null, indicating that HCl has no leaching effect.

- Phosphoric acid H_3PO_4 was also tested and is not as effective as HNO_3.

In summary, among the four acids tested, HNO_3 is the best leaching chemical for recycling SOFC waste. Leaching at 75°C for 24 hours is an optimal condition to remove Ni/NiO from the cell waste.

In order to reduce the leaching cost, we tried to recycle the spent HNO_3. Recycling protocols, purity of recovered HNO_3, concentration of recovered HNO_3, and yield of HNO_3 recovery are discussed in the following section.

5.5 Recycling of HNO_3

Recycling and recovery of ceramic components of SOFCs/SOECs consumes a relatively large amount of concentrated HNO_3. For every 2.5 g of waste powder, nearly 50 ml of concentrated HNO_3 (65 wt.%) is consumed (Figure 5.7). From the environmental point of view the recovery and reuse of HNO_3 is obvious.

The leaching to recover Ni or NiO from the NiO-YSZ electrode-electrolyte assembly was performed in a semi-closed system using a distillation mechanism or in an open system (Figure 5. 8). After a 24 h leaching at 75°C in a semi-closed system, 48.3 ml is recovered from 50 ml of HNO_3 as initial solution. On average, 96 vol. % of the initial HNO_3 solution is recovered from the original HNO_3 after leaching. The concentration of the recovered HNO_3 measured by acid-base titration (with diluted NaOH) is about 13.8M, which corresponds to a weight concentration of 63.5% HNO_3 (equation 5.1). Originally, the concentration of HNO_3 was 65%. Thus, with the 63.5/65%, about 97.77% of HNO_3 concentration is recovered. The total efficiency of HNO_3 recovery considering the loss of volume and concentration during all steps of dissolution is about 88%.

On the other hand, there is a major problem with the evaporation of HNO_3 in the open system. Due to the evaporation, the volume of the recovered green solution is smaller in the open system than in the semi-closed system. The concentration of recovered HNO_3 is also lower in the open system than in the semi-closed system because nitro products evaporate in the open system. The recovered HNO_3 from the open system has a concentration of 9.06M or 44.5%. Of the HNO_3 originally used (65%), 44.5% is recovered. This corresponds to a concentration of 68.4% of the HNO_3 initially used. Leaching in a semi-closed system has the great advantage of obtaining a large volume of green solution and preventing evaporation of the nitro products.

The molarity unit is converted to a unit of percentage using the following equation.

$$C_P = \frac{C_M x 100\% x M}{d} \qquad \text{Equation 5.1}$$

C_P = concentration in percent
C_M = concentration in molarity
M = molar mass of HNO_3
d = density of the solution

Figure 5.7. Green solutions of Ni or NiO in HNO_3

Figure 5. 8. HNO_3 recovery after Ni/NiO leaching from the electrode electrolyte assembly of SOFCs (a) semi-closed system (b) open system.

The net efficiency of HNO_3 recovery is about 88%. Thus, this recovery of HNO_3 is very useful for cost-benefit analysis of recycling protocols. The more valuable products are recovered, the greater the benefit. Conversely, the more material and energy consumption, the more drawbacks the recycling protocol has. Using less material and consuming less energy is highly recommended.

5.6 Life cycle assessment

5.6.1 Cost analysis of recycling

The feasibility of any industrial process depends on the economics of the process [7] [8]. Laboratory-scale processes are rarely adopted by industry unless the economic benefits are good. Therefore, the aim of this section is to give a brief study the economic of feasibility. In order to determine if the material recovery strategy described in this thesis is economically

feasible, A simple cost-benefit analysis is performed using optimized process parameters for lab scale recycling based on a 2.5 g of solid oxide cell ceramic component waste.

A cost-benefit analysis of recycling is performed by comparing the estimated costs of recycling with the benefits of the recovered products. It consists of examining the electricity bills for the equipment and chemicals used. Electricity bills for the ball mill, the hot plate for leaching and drying, the centrifuge for separation, and the furnace for heating are considered as inputs to recycling (for more details of the process used in recycling, see chapter 2). Chemicals used for leaching, precipitation, and washing are also considered inputs for recycling.

On the other hand, the cost of the recovered products are estimated. In this study, a cost-benefit analysis was conducted to monetize the input costs and benefits of the recycling process to calculate the economic feasibility of recycling waste solid oxide cells.

The cost-benefit analysis is performed for both the mechanical scratching route and the DMG route to compare the two routes. Waste collection and transportation costs are not included in this study. Only treatment costs are considered in this analysis (Figure 5.9). Manual crushing and labour costs are also not included. All recycling and recovered products costs are monetized in a common euro price currency.

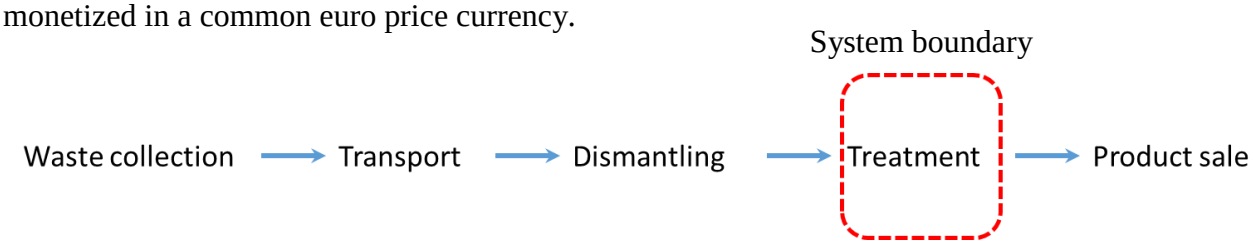

Figure 5.9. The recycling process of waste solid oxide cells, and considered steps (red mark) in this assessment.

For the foreground cost analysis, specific data is collected from various sources:

- Products cost collected using specific spreadsheets of suppliers.
- Recycled product own calculations based on weighing the single parts of each product.
- Energy consumption was monetized using French electricity bills.

Table 5.1. The economic analysis of the recycling process developed in mechanical scratching route

Equipment's used			Cost
Process	Equipment	equipment's (electric bill) (€)	Total cost (€) of recycling
Milling	Ball miller	0.3784	0.7370
Leaching	Hot plate	0.002167	
Centrifugation	Centrifuge	0.002031	
Drying-2	Hot plate_HNO_3 recovery	0.09632	
Drying-3	Furnace_ NiO recovery	0.000699	
Total cost of bills		0.479617	
Reagents used			
Process		Cost of reagents	
Ball milling	Ethanol	10 ml = 0.00782	
Ni-precipitation	HNO_3	6 ml = 0.25742	
Total cost of reagent		0.25742	
Products recovered			
Products recovered	Products recovered (g)	Price of recovered products (€)	Total cost recovered products (€)
YSZ	1.114	0.7688	1.519
NiO	1.070	0.678	
LSC	0.057	0.1244	

The average standard price of reagents used in the analysis and the cost of electricity are shown in Table 5.1 for the mechanical scratching route. Based on this study, the result shows that the recycling cost is about 50% lower than recycled product. In this regard, the cost of recycling using mechanical scratching route is about 2.0 times lower than the cost of recycled products. This results total investment costs of 0.74 €, which generate recycling products of 1.52 €. Expanding to 100 times, the result shows that an investment of about 74 € yields a product that costs about 152 €. Table 5.1 shows that the process developed in this study is economically viable with an estimated profit margin of about 314 € per Kg of waste solid oxide cells. It is likely that this profit margin can be further increased if it is exploited on a large recycling scale.

A similar cost study is conducted for the DMG route (Table 5. 2). In this study, the DMG reagent can be recycled and re used with small investment cost and can be reused is considered [9] [10]. Different authors studied the yield of DMG recovery from Ni-DMG complex as yield higher than 50%. Here to we select the minimum the yield as 50% to be recovered to avoid over estimation of cost.

Table 5. 2. The economic analysis of the recycling process developed in DMG route

Equipment's used			Cost
Process	Equipment	equipment's (electric bill) (€)	Total cost (€) of recycling
Milling	Ball miller	0.3784	1.300
Leaching	Hot plate	0.002167	
Centrifugation	Centrifuge	0.002031	
Drying-1			
Drying-2	Hot plate HNO_3 recycling	0.0963	
Drying-3	Furnace_ NiO recovery	0.000699	
Drying-4	Furnace _LSC recovery	0.004889	
Total cost of bills		0.4845	
Reagents used			
Process		Cost of reagents	
Ball milling	Ethanol	165 ml = 0.129	
Ni, Co, Sr, La-precipitation	HNO_3	6 ml = 0.2496	
Ni-precipitation	DMG	0.4192	
For DMG recovery	HCl	0.01849	
Total cost of reagent		0.7978	
Products recovered			
Products recovered	Products recovered (g)	Price of recovered products (€)	Total cost recovered products (€)
YSZ	1.11	0.7665	1.426
NiO	1.03	0.578	
LSC	0.037	0.0808	

The cost of recycling by DMG route is about 10% lower than the cost of recycled product. The cost of the recycling process is two time higher for the DMG route. However, this cost can be expected to be reduce on a large scale recycling. The grinding, leaching, precipitation and separation method used in the laboratory can also be directly applied to large-scale recycling. A new equipment design may be required for nitric acid recovery. It is possible to build such a facility for rapid distillation. In this context, the economics of recycling waste ceramic components need to be further investigated.

5.6.2 Environmental impact analysis

5.6.2.1 Introduction

Environmental impact of recycling YSZ, LSC and NiO is investigated using open LCA software (LCA 1.11.0 from greendelta) [11]. It complies with the framework set out in ISO 14040 and 14044 for LCA. The life cycle assessment tool and multi-criteria analysis are used to evaluate the environmental impact of recycling. Due to the significant amount of air pollutants emitted, environmental pollution is one of the major issues. Addressing emission sources and methods to eliminate or reduce emissions is now critical. Intensive life cycle analysis of SOC system is a long and hard work that will necessitate at least 3 years of PhD. Here, we will focus on the simple LCA for material recovery.

Following cost-benefit analysis methods, LCA has been successfully studied for recycling ceramic components of SOC. In this study, the two alternative "mechanical scratching route" and "DMG route" are investigated [12]. Using the Environmental Footprint 3.0 (EF 3.0) impact assessment method, different impact categories were identified. The decision-making process will also take into account engineering, economic and environmental indicators.

5.6.2.2 Methodology

Original laboratory data were used. No effort was made to produce theoretical inventory data sets for this investigation.

5.6.2.3 System boundary

System boundaries are where the contents of the system being analysed are located for the purposes of LCA. For both mechanical scratching and the DMG route, products are modelled from gate to grave. Recycling of waste materials is taken into account, and the recovered ceramic powder can be used directly to remanufacture SOC components. System boundaries considered in this study are shown in Figure 5.10.

To better frame the scope of the study and analysis, the following assumptions were made.

- ✓ The solid oxide ceramic components are brought and recycled in Nantes, France.
- ✓ Electricity consumed in the recycling process is considered as energy input in MJ.
- ✓ Storage, transportation, disassembly and labour were not considered.
- ✓ The amount of recycled HNO_3 and DMG was considered.
- ✓ No waste materials were generated during the recycling process.
- ✓ The selected system boundaries are consistent with the scope and objectives of this LCA.

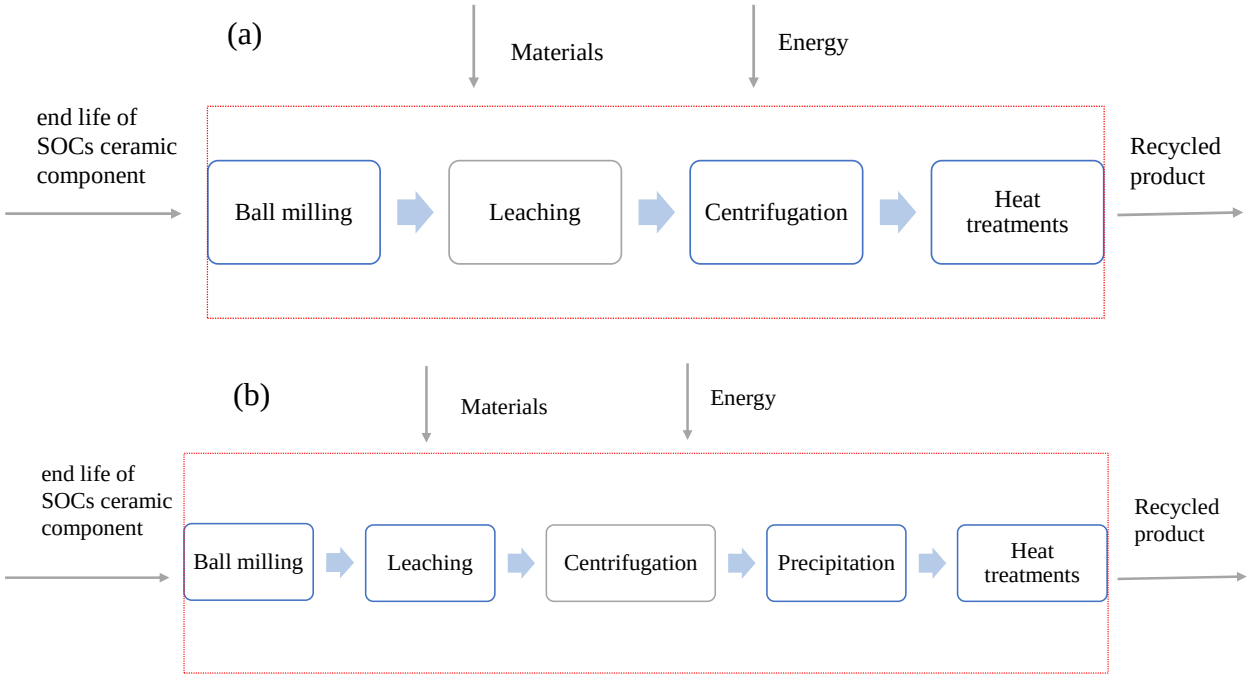

Figure 5.10. Illustration of the process flow for recycling and the system boundaries considered in this study via (a) the mechanical scratching route (b) the DMG route.

5.6.2.4 Inventory

The collected data are entered into the LCA software to create the product models and perform the impact assessment. Both routes were modelled for laboratory scale recycling using 2.5 g ceramic components of solid oxide cells. **Inventory processes used:** Electricity consumption for the ball mill, hot plate for leaching, centrifugation, drying, and furnace for heat treatment of the product were considered and added. **Inventory chemicals used:** nitric acid (HNO_3), ethanol (C_2H_6O) and the ceramic components of the solid oxide cell are used

for mechanical scratching route. The DMG route, on the other hand, uses DMG in addition to the above materials. All inventories are listed in Table 5.3. As mentioned above, the recycling of HNO_3 and DMG as well as the electricity consumption for the recovery of these reagents were considered. The main differences are in material use and treatment steps. For example, recycling via the DMG route has a larger share of ethanol consumption and DMG reagent.

Table 5.3. Flow inventories for the use of recycling solid oxide cell ceramic components.

Mechanical scratching route			DMG route		
NO.	Input	Quantity	NO.	Input	
1	HNO_3	6 ml	1	HNO_3	6 ml
2	Ethanol	10 ml	2	Ethanol	165 ml
3	Ceramic waste	2.5 g	3	Ceramic waste	2.5 g
4	Electricity	10 MJ	4	Electricity	10.1 MJ
			5	DMG	1.75 g

Based on this study for laboratory-scale recycling, the energy required to recycle 2.5 g of ceramic waste is about 10 MJ (Table 5.3) for both the mechanical scratching and DMG route. The other inventory materials are small quantities due to the small scale in practice. The LCIA give null values, and it is difficult to determine the environmental impact of the parallel products for this scale. Therefore, the assessment is adapted for this study to evaluate the environmental impact of ceramic recycling for thousand times.

5.6.2.5 Analysis

The impact analysis for mechanical scratching and DMG route is conducted using the EF 3.0 assessment method based on 28 impact indicators. The EF 3.0 database is compatible with the open LCA software used which is retrieved from Nexus [13]. The method translates emissions and resource materials and converts them into environmental indicators based on specific characterization factors. In this section, the impact assessment results (LCIA) for the two alternatives routes are reported (Table 5.4).

Table 5.4. Environmental impact categories of the EF 3.0 method results for the mechanical scratching and DMG route for the treatment of 2.5 kg of ceramic components of SOCs.

Impact categories	**Units**	**Mechanical scratching route**	**DMG route**
Acidification	mol H+ eq	2.12E-01	3.39E+00
Climate change	kg CO_2 eq	1.07E+01	1.71E+02
Climate change - Biogenic	kg CO_2 eq	4.14E-03	6.63E-02
Climate change - Fossil	kg CO_2 eq	1.07E+01	1.70E+02
Climate change - Land use and LU change	kg CO_2 eq	6.00E-03	9.60E-02
Ecotoxicity, freshwater	CTUe	5.81E+02	8.42E+03
Ecotoxicity, freshwater - inorganics	CTUe	9.56E+01	4.34E+02
Ecotoxicity, freshwater - metals	CTUe	2.71E+02	4.34E+03
Ecotoxicity, freshwater - organics	CTUe	2.15E+02	3.66E+03
Eutrophication, freshwater	kg P eq	3.41E-03	5.45E-02
Eutrophication, marine	kg N eq	1.46E-01	2.34E+00
Eutrophication, terrestrial	mol N eq	9.28E-01	1.48E+01
Human toxicity, cancer	CTUh	1.48E-08	1.52E-06
Human toxicity, cancer - metals	CTUh	8.36E-09	1.34E-07
Human toxicity, cancer - organics	CTUh	6.48E-09	1.39E-06
Human toxicity, non-cancer	CTUh	3.07E-05	4.98E-06
Human toxicity, non-cancer - inorganics	CTUh	3.06E-05	3.33E-06
Human toxicity, non-cancer - metals	CTUh	4.14E-08	6.63E-07
Human toxicity, non-cancer - organics	CTUh	1.14E-08	9.90E-07
Ionising radiation	kBq U-235 eq	1.16E+00	1.86E+01
Land use	Pt	1.91E+03	3.05E+04
Ozone depletion	kg CFC11 eq	1.13E-06	1.81E-05
Particulate matter	disease inc.	1.37E-06	2.19E-05
Photochemical ozone formation	kg NMVOC eq	4.85E-02	7.76E-01
Resource use, fossils	MJ	9.62E+01	1.54E+03
Resource use, minerals and metals	kg Sb eq	1.98E-05	3.17E-04
Water use	m^3 depriv.	5.68	90.92

Life cycle analysis of the recycling has high level of uncertainty. In some cases, variables could only be estimated and values of similar products had to substitute for missing data, which affects the results. Although mainly nitric acid consumed and electricity costs are crucial for the impact assessment, individual steps that are not considered also affect the results. As shown in Table 5.3, 28 environmental impact categories are displayed for the mechanical scratching and DMG route.

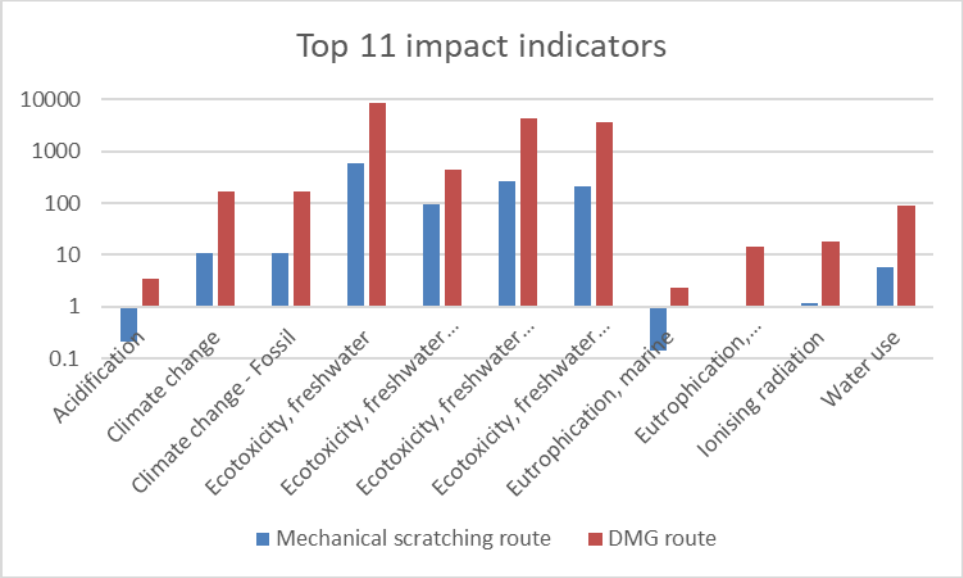

Figure 5.11. Normalized results of 11 impacts with highest rate results of the respective products via mechanical scratching and DMG route.

5.6.2.6 Interpretation

Environmental impact indicators reveal the environmental impact of the products and the main processes contributing (Figure 5.11). The comparison of mechanical scratching with DMG processes shows that recycling by mechanical scratching has lower environmental impacts for almost all impact potentials analyzed.

The Mechanical scratching routs investigated show about 16 times lower in Acidification, Climate change, Ecotoxicity, Eutrophication and Ionising radiation than DMG routes (Figure 5.11). The Ozone Depletion Potential (ODP) is the only potential impact that is similar for both routes. Therefore, the mechanical scoring route, on the other hand, proves to be the best choice in impact category.

Indeed, it is generally recommended to use recycling protocols via the DMG route against mechanical scratching to implement the system on an industrial scale. However, in our lab-scale recycling, the impact of mechanical scratching is very low.

To compare impact associated with these recycling process with mining and extraction of the same product, there is a lack of data. However, much work has been done on the mining of zircon sand ($ZrSiO_4$) and nickel. Compared to the data reported for zircon sand, the impact indicators for these recycling protocols are reasonable [14]. For nickel, the impact is not comparable. Since the environmental impacts are correspondingly higher [15] due to the fact that purification in metallic form is an intensive process.

Conclusion

In this chapter, various recycling alternatives were investigated and effective recycling protocols were selected in terms of purity, economic and environmental benefits. The costs of recycling for two optimized routes were determined. Then, the environmental impacts of categories for recycling solid oxide ceramic components were analyzed. Recycling via mechanical scratching is generally associated with lower environmental impacts than DMG. The efforts made to develop technologies with low environmental impacts and low costs are still challenging in terms of large-scale recycling. In general, the mechanical route over DMG route is advantageous in recovered chemical purity and cost of involved recycling. On the other hand, DMG routes is advantageous for large scale recycling. To improve the efficiency of recycling, more research is needed to find a better ecological alternative.

Reference

[1] T. Shevchenko, K. Laitala, and Y. Danko, "Understanding Consumer E-Waste Recycling Behavior: Introducing a New Economic Incentive to Increase the Collection Rates," *Sustainability*, vol. 11, no. 9, p. 2656, May 2019, doi: 10.3390/su11092656.

[2] J. B. Dunn, L. Gaines, J. C. Kelly, C. James, and K. G. Gallagher, "The significance of Li-ion batteries in electric vehicle life-cycle energy and emissions and recycling's role in its reduction," *Energy Environ. Sci.*, vol. 8, no. 1, pp. 158–168, 2015, doi: 10.1039/C4EE03029J.

[3] DWK LIFE SCIENCE DURAN WHEATON KIMBLE Glass Types & Properties." https://www.dwkltd.com/en/technical/glass-types-properties (accessed Aug. 10, 2022).

[4] "Laboratory Glassware - Specimen Lab | ConductScience," *Conduct Science*. https://conductscience.com/specimen-lab/glassware/ (accessed Aug. 10, 2022).

[5] J.-Z. Zhang, C. J. Fischer, and P. B. Ortner, "Laboratory glassware as a contaminant in silicate analysis of natural water samples," *Water Res.*, vol. 33, no. 12, pp. 2879–2883, Aug. 1999, doi: 10.1016/S0043-1354(98)00508-9.

[6] T. H. Elmer and M. E. Nordberg, "Solubility of Silica in Nitric Acid Solutions," *J. Am. Ceram. Soc.*, vol. 41, no. 12, pp. 517–520, Dec. 1958, doi: 10.1111/j.1151-2916.1958.tb12907.x.

[7] C. Koopmans and N. Mouter, "Cost-benefit analysis," in *Advances in Transport Policy and Planning*, vol. 6, Elsevier, 2020, pp. 1–42. doi: 10.1016/bs.atpp.2020.07.005.

[8] H. M. Gunatilake, *Cost-benefit analysis for development: a practical guide*. Mandaluyong City, Metro Manila, Philippines: Asian Development Bank, 2013.

[9] X. Chen, Y. Chen, T. Zhou, D. Liu, H. Hu, and S. Fan, "Hydrometallurgical recovery of metal values from sulfuric acid leaching liquor of spent lithium-ion batteries," *Waste Manag.*, vol. 38, pp. 349–356, Apr. 2015, doi: 10.1016/j.wasman.2014.12.023.

[10] M. Rath, L. P. Behera, B. Dash, A. R. Sheik, and K. Sanjay, "Recovery of dimethylglyoxime (DMG) from Ni-DMG complexes," *Hydrometallurgy*, vol. 176, pp. 229–234, Mar. 2018, doi: 10.1016/j.hydromet.2018.01.014.

[11] "openLCA.org | openLCA is a free, professional Life Cycle Assessment (LCA) and footprint software with a broad range of features and many available databases, created by GreenDelta since 2006." https://www.openlca.org/ (accessed Nov. 05, 2022).

[12] E. Sanyé-Mengual *et al.*, "Linking inventories and impact assessment models for addressing biodiversity impacts: mapping rules and challenges," *Int. J. Life Cycle Assess.*, pp. 1–21, 2022.

[13] "openLCA Nexus: The source for LCA data sets." https://nexus.openlca.org/ (accessed Nov. 05, 2022).

[14] J. Gediga, A. Morfino, M. Finkbeiner, M. Schulz, and K. Harlow, "Life cycle assessment of zircon sand," *Int. J. Life Cycle Assess.*, vol. 24, no. 11, pp. 1976–1984, Nov. 2019, doi: 10.1007/s11367-019-01619-5.

[15] M. Mistry, J. Gediga, and S. Boonzaier, "Life cycle assessment of nickel products," *Int. J. Life Cycle Assess.*, vol. 21, no. 11, pp. 1559–1572, Nov. 2016, doi: 10.1007/s11367-016-1085-x.

[16] S. Sarner, A. Schreiber, N. H. Menzler, and O. Guillon, "Recycling Strategies for Solid Oxide Cells," *Adv. Energy Mater.*, p. 2201805, Jul. 2022, doi: 10.1002/aenm.202201805.

General conclusion and perspectives

The work carried out during this thesis concerns the recovery of the ceramic component materials of the solid oxide cells, full characterization and elucidation of structural and morphological properties, conductivity, and chemical purity of recovered materials. This project focused on recycling and the use of recovered materials as a potential ceramic powder for the re manufacturing of components materials.

We put forward two new techniques to enable the recycling process in practice. One is the "mechanical scratching route" named after the air electrode recovery technique. The other technique is the "Dimethylglyoxime (DMG) route", named after the use of DMG as a precipitation reagent. The recycling strategies by mechanical scratching routes investigated in this work can be summarized as follows:

Mechanical scratching route

The powder of air electrode material was successfully recovered by the simple mechanical scratching techniques. The composition of the recovered air electrode material was determined by EDX and ICP-MS and showed good agreement with each other and with the expected values. The La, Sr and Co were the main components whereas Ce, Gd, Y, Zr, Si and Fe were present in trace amounts. These recovered powders has purity above 99 at. % and were in line with commercial grade which could be used for the production of new air electrodes materials.

Recycling protocols, such as grinding and leaching media, leaching and precipitation chemicals have been optimized to achieve the best recovery yield. Various acids were tested, and concentrated nitric acid was found to be the best leaching solvent.

The remaining fuel electrode and electrolyte layers were further treated by ball milling for 5 hours and leaching with HNO_3 (65 wt.%) at 75°C for 24 hours. One important feature of Ni/YSZ is the high stability of YSZ in various solvents which enable a solid/liquid phase separation. The leaching resulted in the recovery of nickel in a liquid phase, and the solid residue was found to contain YSZ oxide.

The recovery yields of NiO and YSZ from the two commercial are above 90%. The purity of recovered NiO is over 99 at.% with low Y and Si content. For both products (Fiaxell and Elcogen) NiO showed good agreement in BET surface area (8.1 m^2/g and 13.9 m^2/g, respectively) and composition. These results prove that it is possible use the recovered NiO as a new feedstock for the solid oxide cell industry without further modification.

The recovered YSZ was fully characterized using X-Ray powder diffraction showing that a mixture of different polymorphs is present at room temperature. The phase stability of recovered YSZ was investigated by in situ high temperature XRD. It shows successive phase transformation up on heating and cooling.

YSZ recovered powder from Fiaxell and Elcogen cells has BET surface area of 3.77 m^2/g and 4.50 m^2/g, respectively. These values are in the range of the BET surface areas of commercial YSZ powders with different yttrium concentrations. The YSZ recovered from the Fiaxell products has a particle size of 0.387 µm, which is similar to that of the commercial powder from the supplier Tosoh.

Conductivity of recovered YSZ has been characterized by Electrochemical Impedance Spectroscopy (EIS). First, small (ø < 10mm) dense pellets have been obtained after a sintering step at 1450°C for 10 hours (relative density > 95 %). SEM analysis showed a well-developed, crystallized, dense structure separated by visible grain boundaries. 1.8 µm and 1 µm, grain size were obtained for YSZ recovered from Elcogen and Fiaxell products, respectively. The deduced chemical composition of YSZ from EDX analysis is ($Zr_{0.92}Y_{0.08}O_{1.96}$ (~4YSZ)). The 4YSZ composition is expected since 8YSZ and 3YSZ are used in electrolyte and fuel electrode materials respectively. As for the barrier layer, gadolinium-doped ceria (GDC), Gd and Ce were detected in very small amounts in the recovered NiO and YSZ. EDX elemental mapping showed a zirconium silicate phase ($ZrSiO_4$) distributed at the grain boundaries.

The ionic conductivity of recovered YSZ from Fiaxell and Elcogen products are quite similar, 4.7 10^{-3} $S.cm^{-1}$ and 6.4 10^{-3} $S.cm^{-1}$ respectively at 700°C. Whereas, bulk conductivities of both cells are similar, the grain boundary conductivity of YSZ from Fiaxell is slightly lower

than that of YSZ from Elcogen. This is due to the presence of trace silica impurities in the recovered products.

As expected from their composition, the conductivity of recycled YSZ was found to be above but close to that of commercial 3YSZ. Therefore, recovered YSZ (which is 4YSZ) can be used to replace 3YSZ in the fabrication of fuel electrode. Other techniques should have to be used to characterize the mechanical properties of this material.

Higher yttrium compositions have been obtained using recovered 4YSZ mixed with commercial Y_2O_3. Pure 6YSZ, 8YSZ and 10YSZ powders have been fully characterized. EIS analysis of dense pellets showed that an expected order of ionic conductivity 8YSZ > 10YSZ > 6YSZ > 4YSZ (as recovered) is obtained. In such a way, we have shown that the recovered 4YSZ can be used as a basic powder to produce other compositions used for instance for electrolyte fabrication.

Dimethylglyoxime route

The recycling via DMG route was done by combining mechanical grinding and hydrometallurgical processes with acid leaching and organic complexation.

The entire ceramic cell components, including the electrolyte, fuel and air electrodes were first crushed and ball milled. The resulted fine powder was analyzed by X-Ray diffraction showing a mixture of mainly NiO (46.9(6) wt. %) and YSZ (50.9 wt. %) along with traces of $La_xSr_{1-x}CoO_3$ (LSC).

Nitric acid was used to solubilize nickel, cobalt, strontium, and lanthanum ions. Centrifugation allowed to collect the YSZ solid phase which was carefully analyzed by X-ray powder diffraction. As for the mechanical scratching route, a mixture of monoclinic, tetragonal and cubic phases is observed. The deduced chemical composition of YSZ from EDX analysis is also the same close to 4YSZ and purity is about 97.12 at.%.

The liquid phase, containing other metal ions, was treated with Dimethylglyoxime ($C_2H_8N_2O_2$ (DMG)). The main advantage of DMG is a selective precipitation of nickel. An optimization of the pH on the preferential recovery of nickel was investigated. Pure NiO was

recovered after a thermal treatment of the "Ni-DMG complex" at 500°C for 3 hours showing nanoflakes type particles. After evaporation of the solvent, LSC (and Ni as a trace impurity) was recovered. The purity level is at commercial grades.

This is the first time that DMG process has been applied to the recycling of ceramic components of oxide cells.

With regard to the cost of recycling, it is important to minimize the amount of products required for recycling and even to be able to reuse them. To this end, HNO_3 and DMG can be recycled and reused. The amount of HNO_3 used in recycling is not small, not cheap, not healthy and not environmentally friendly. Therefore, the recovery and reuse of HNO_3 with a distillation mechanism is proposed and practiced. About 88% of the HNO_3 originally used is recovered. DMG has been recycled with little investment.

The mechanical scratching and the DMG route have been compared. In our study, it is found that mechanical scratching is advantageous in terms of the purity of the recovered product, cost and environmental impact of recycling. On the other hand, the purity of the materials recovered by the DMG route is lower than that of the materials recovered by mechanical scratching. This due to possible contamination with air electrode materials with DMG route. The environmental impact of recycling via DMG route is higher than mechanical scratching route. Nevertheless, the DMG route is advantageous when used on a large scale. A lab scale recycling process possibly adopted to industrial scale is investigated for ceramic component of solid oxide cells that is technically and financially sustainable.

Perspectives

A full Solid oxide could be done using recycling materials. Before, symmetrical fuel electrode/YSZ/fuel electrode can be done in order to characterize the the catalytic performance of recovered NiO.

YSZ is not only used for high temperature cells. Other possible applications of recycled can be tested. Since IMN lab is also working on proton ceramic fuel cells based perovskite type proton conducting electrolyte, recovered YSZ can be converted into a proton-conducting electrolyte (BaCe1-xZrxO3) by reacting with BaCO3. NiO is also not only used for high temperature cells, but in stainless steel manufacturing and alloy production, electroplating, or

various batteries manufacturing. Indeed, further work must be carried out to optimize the final use of recycled nickel.

It is expected that this recycling protocol will be extended to other types of ceramic components of SOCs and the efficiency will be further improved. This method will therefore be the subject of several developments in the laboratory in the coming years. Initially, it will be used in the framework of the thesis of Valentin Brard, which started at the end of 2022, as a part of the European project NOUVEAU.

As we have also mentioned, our cost analysis of the recycling routes is incomplete. The two proposed routes are time consuming, and it will be interesting to compare the staff costs associated to each protocol. Moreover, it would be interesting to refine the evaluation of economic viability of the process by taking into account the cost of waste treatment, which will probably increase in the coming years.

Appendixes

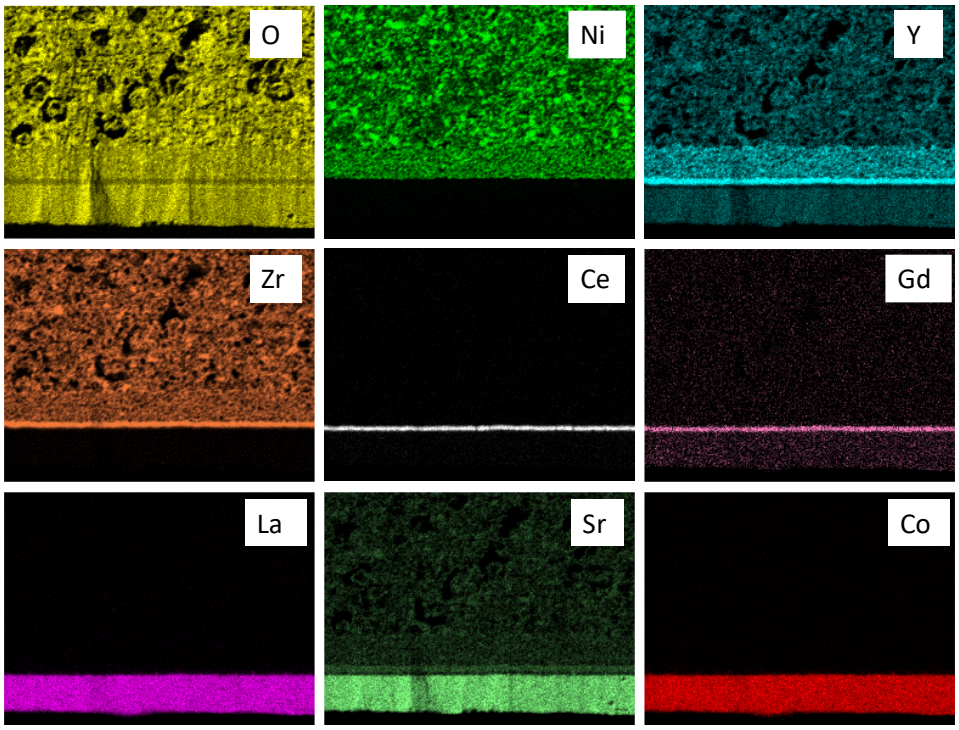

Appendix 1. The Elcogen cell employed in this study SEM cross section Elemental mapping by energy dispersive X-ray spectroscopy shows the composition of each layer.

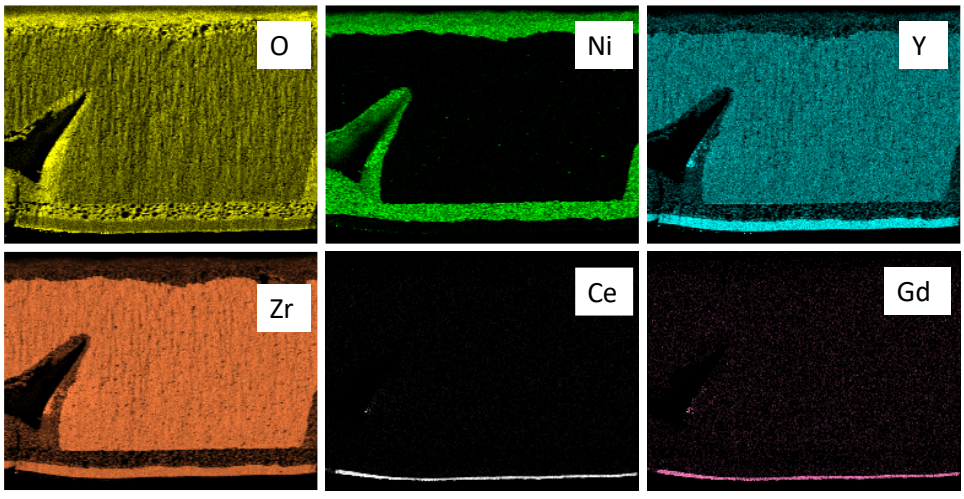

Appendix 2. The Fiaxell cell employed in this study SEM cross section Elemental mapping by energy dispersive X-ray spectroscopy shows the composition of each layer.

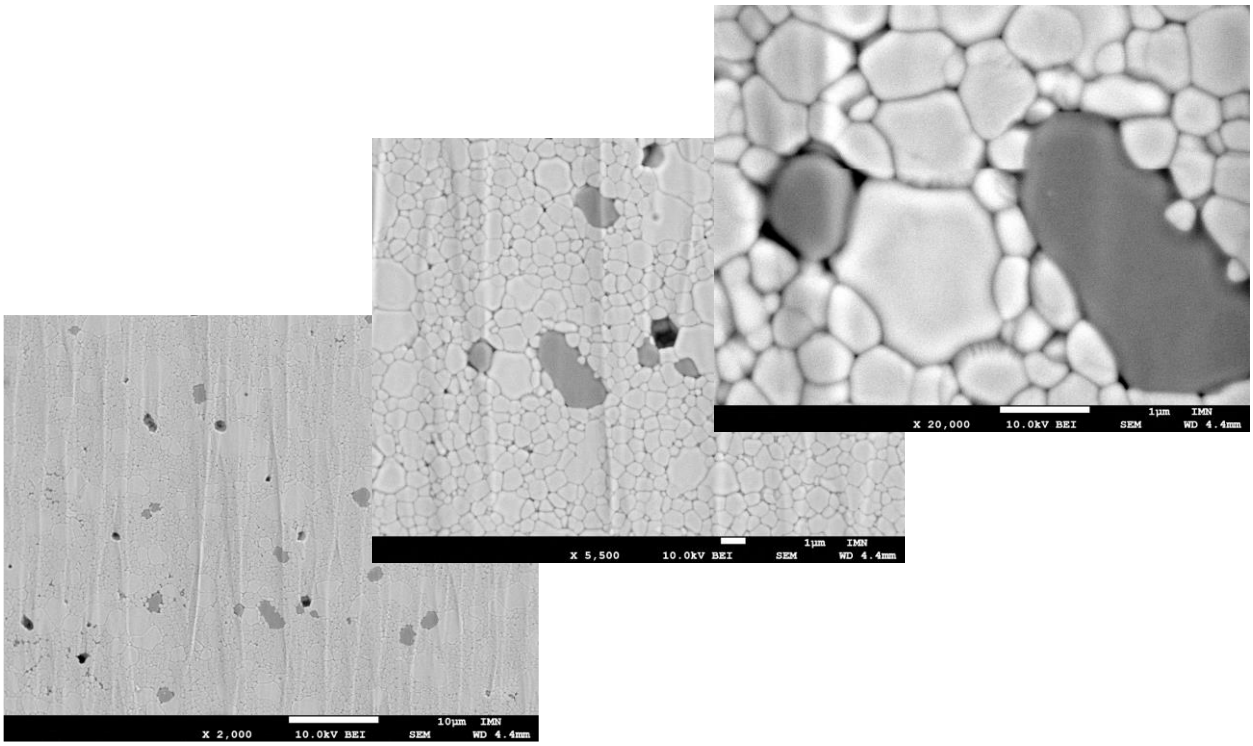

Appendix 3. SEM micrographs of polished and thermally etched sample of recovered YSZ from Fiaxell, illustration of the spatial distribution of dark grain ($ZrSO_4$).

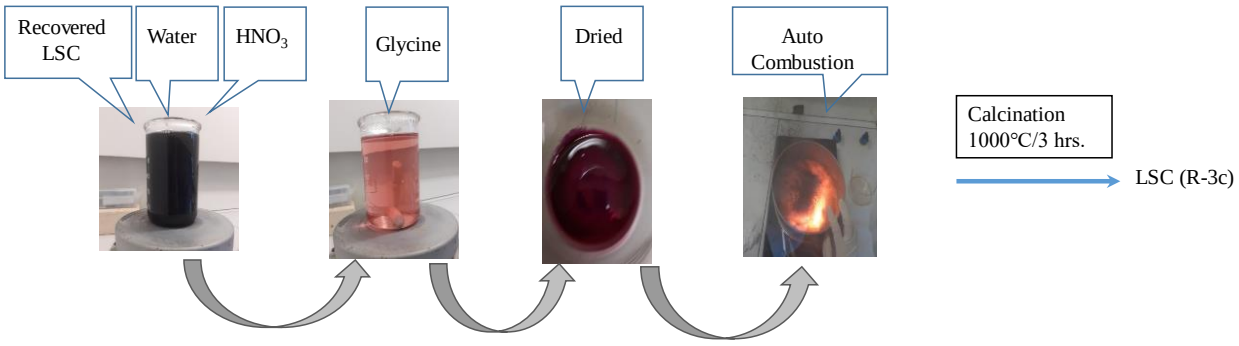

Appendix 4. Illustration of the possibility of LSC dissolution, the ability to make gel of it and auto-combustion for the formation of well-crystallized LSC ready for use.

LabChem
performance through chemistry

Dimethylglyoxime, ACS
Safety Data Sheet
according to Federal Register / Vol. 77, No. 58 / Monday, March 26, 2012 / Rules and Regulations
Date of issue: 11/18/2013 Revision date: 07/30/2019 Supersedes: 05/03/2017 Version: 2.0

SECTION 11: Toxicological information

11.1. Information on toxicological effects

Acute toxicity (oral)	:	Toxic if swallowed.
Acute toxicity (dermal)	:	Not classified
Acute toxicity (inhalation)	:	Not classified
ATE US (oral)		100 mg/kg body weight
Skin corrosion/irritation	:	Not classified pH: Not applicable
Serious eye damage/irritation	:	Not classified pH: Not applicable
Respiratory or skin sensitization	:	Not classified
Germ cell mutagenicity	:	Not classified
Carcinogenicity	:	Not classified
Reproductive toxicity	:	Not classified
Specific target organ toxicity – single exposure	:	Not classified
Specific target organ toxicity – repeated exposure	:	Not classified

Appendix 5.Material Safety Data Sheet for Dimethylglyoxime

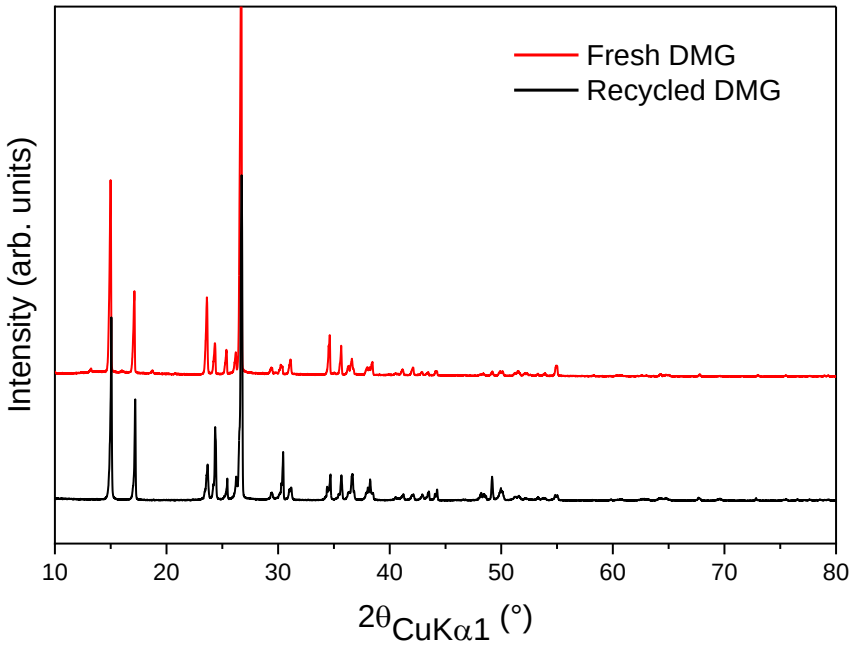

Appendix 6. X-ray diffraction (XRD) of fresh DMG and recovered DMG.

Titre : Recyclage des électrolyseurs ou des piles à combustible à oxydes solides fonctionnant à haute température et valorisation des déchets

Mots clés : Piles à combustible, Electrolyseurs, Oxydes solides, Fin de vie, Recyclage, Séparation de phase, Lixiviation sélective, Précipitation sélective

Résumé : La décarbonation de la production d'hydrogène est l'enjeu majeur actuel pour réduire les émissions de CO_2 dans les transports et les bâtiments autonomes équipés d'une pile à combustible et l'industrie. L'hydrogène vert peut être produit par le procédé d'électrolyse, en utilisant de l'électricité décarbonée. L'électrolyseur et les piles à combustible à oxydes solides (SOEC et SOFC) fonctionnant à haute température et basés sur des matériaux céramiques ont des rendements électriques les plus élevés parmi les convertisseurs électrochimiques. Cependant, l'adoption massive attendue de ces systèmes se heurte au défi du recyclage et de la réutilisation des déchets de matériaux céramiques.
Dans ce travail, nous proposons des stratégies efficaces concernant le recyclage des électrodes et de l'électrolyte : $Y_xZr_{1-x}O_2$, NiO et $La_{1-x}Sr_xCoO_3$. Un processus en plusieurs étapes impliquant le concassage et le broyage, la lixiviation assistée par acide et la précipitation des constituants a été réalisé.Après le recyclage, les matériaux récupérés ont été soigneusement caractérisés en termes de propriétés structurales et morphologiques, de conductivité et de pureté chimique. Ce procédé de recyclage rentable et directement applicable au niveau industriel pourrait ouvrir de nouvelles perspectives pour l'utilisation de ces matériaux récupérés dans le retraitement des SOEC/SOFC. Le potentiel économique et environnemental est évalué, soulignant les avantages significatifs du recyclage par rapport à l'utilisation de ressources minérales primaires.

Title : Recycling of high temperature solid oxide electrolyzers or fuel cells and recovery of waste materials

Keywords: Solid oxide fuel cells, Electrolyzers, Solid oxides, End of life, Recycling, Phase separation, Selective leaching, Selective precipitation.

Abstract: Decarbonizing hydrogen production is the actual major issue to reduce CO_2 emissions in transport, autonomous buildings equipped with a fuel cell and industries. Green hydrogen can be produced by the electrolysis process, using decarbonized electricity. High temperature solid oxide electrolysis (SOEC) and Fuel Cell (SOFC) based on ceramic materials have the highest electrical efficiency among electrochemical converters. However, the expected massive adoption of these systems faces the challenge of recycling and reuse ceramic materials waste. In this work, we propose effective strategies concerning electrodes and electrolyte recycling: $Y_xZr_{1-x}O_2$, NiO and $La_{1-x}Sr_xCoO_3$. A multi-step process involving crushing and grinding, acid-assisted leaching and precipitation of the constituents was performed. After recycling, the recovered materials were carefully characterized in terms of structural and morphological properties, conductivity and chemical purity. This cost-effective recycling process that can be directly applied at the industrial level could open new perspectives for the use of these recovered materials in SOEC/SOFC reprocessing. The economic and environmental potential is evaluated, highlighting the significant advantages of recycling over using the primary product.